Kumulative Dissertation

Organisation neuronaler Netzwerke zur Raumorientierung im Gehirn der Madeiraschabe *Rhyparobia maderae* und der indischen Riesengottesanbeterin *Hierodula membranacea*

Organization of neural networks for orientation in the brain of the Madeira cockroach *Rhyparobia maderae* and the Giant Asian mantis *Hierodula membranacea*

Zur Erlangung des Doktorgrades der Naturwissenschaften (Doctor rerum naturalium)

des Fachbereichs Biologie der Philipps-Universität Marburg

vorgelegt von

Vanessa Althaus geboren in Siegen

Marburg an der Lahn, Januar 2024

Die vorliegende Dissertation wurde in der Zeit vom Februar 2019 bis Januar 2024 am Fachbereich Biologie an der Philipps-Universität Marburg (Fachgebiet Tierphysiologie, Abteilung Neuroethologie) unter Leitung von Prof. Dr. Uwe Homberg angefertigt.

Vom Fachbereich Biologie der Philipps-Universität Marburg (Hochschulkennziffer 1180) als Dissertation angenommen am:

Erstgutachter: Prof. Dr. Uwe Homberg

Zweitgutachter: Prof. Dr. Monika Hassel

Tag der Disputation: 23.04.2024

Erklärung über Autorenschaft

Ich versichere hiermit, dass ich, Vanessa Althaus, die Dissertation mit dem Titel "Organisation neuronaler Netzwerke zur Raumorientierung im Gehirn der Madeiraschabe *Rhyparobia maderae* und der indischen Riesengottesanbeterin *Hierodula membranacea*" selbständig und ohne unerlaubte Hilfe angefertigt habe. Es wurden keine, außer die ausdrücklich erwähnten, Quellen und Hilfsmittel verwendet.

Ich versichere weiterhin, dass diese Dissertation weder in der vorliegenden noch in ähnlicher Form an einer anderen Hochschule vorgelegt wurde und bisher noch keinem Prüfungszweck gedient hat.

Marburg, den

22.01.2024

Vanessa Althaus

Erklärung zum Eigenanteil an den vorgelegten Publikationen/Manuskripten

Der folgende Abschnitt listet die eigenen Beiträge an den veröffentlichten und zur Veröffentlichung vorgesehenen Teile der Arbeit auf. Gemäß der Allgemeinen Bestimmungen für Promotionsordnungen der Philipps-Universität Marburg vom 01.04.2022, § 9(2) müssen die Teilleistungen der Doktorandin an den beschriebenen Manuskripten und Veröffentlichungen dargelegt werden.

Im Folgenden werden die Publikationen/Manuskripte aufgelistet, die im Rahmen dieser kumulativen Dissertation verwendet werden. Der Eigenanteil für die jeweiligen Projekte wird dabei detailliert aufgelistet.

Kapitel 1   Organisation des Gehirns in dictyopterer Insekten

Projekt I: 3D-atlas of the brain of the cockroach *Rhyparobia maderae*

Dieses Projekt wurde in der hier vorliegenden Form beim *Journal of Comparative Neurology* als: Vanessa Althaus, Stefanie Jahn, Azar Massah, Monika Stengl, und Uwe Homberg (2022). 3D-atlas of the brain of the cockroach *Rhyparobia maderae,* eingereicht und veröffentlicht. https://doi.org/10.1002/cne.25396

Eigene Anteile:

- Konzeption des Projektes in Zusammenarbeit mit Prof. Dr. Uwe Homberg und Prof. Dr. Monika Stengl
- Backfills der Antennen aus Figure 11 g-i und Einzelinjektionen von Neuronen aus Figure 7b, c und 10b, c und e
- Die weiteren Experimente wurden von Dr. Azar Massah (Synapsin-GABA Doppelfärbung, welche als Grundlage diente), Stefanie Jahn (Serotonin Immunfärbung aus Figure 8e und 10f, Orcokinin/Synapsin Immunfärbung aus Figure 7e und PDF/Synapsin Immunfärbungen aus Figure 8d, d' und 11b). Weitere Daten stammten von ehemaligen Studentinnen der Arbeitsgruppe Homberg, Irina Bedoeva (Locustatachykinin-II Immunfärbung aus Figure 11e) und Clara Grigoriev (Einzelzellinjektion aus 9b, b').
- Durchführung aller bildgebenden Aufnahmen der Synapsin/PDH-, GABA-Färbungen, Backfills und der Einzelzellinjektionen am konfokalen Laserscan Mikroskop
- Auswertung aller Daten
- Vollständige Rekonstruktion des dreidimensionalen Atlanten mit der Software AMIRA 6.5

- Anfertigung aller Abbildungen, ausgenommen Teilabbildung 7e, welche durch Stefanie Jahn erstellt wurde
- Datenanalyse, Vergleich und Interpretation der Daten, unterstützt durch Stefanie Jahn, Prof. Dr. Uwe Homberg und Prof. Dr. Monika Stengl
- Anfertigung des Manuskripts mit Unterstützung von Prof. Dr. Uwe Homberg und Prof. Dr. Monika Stengl

Projekt II: Anatomical organization of the cerebrum of the praying mantis *Hierodula membranacea*

Dieses Manuskript wurde in der hier vorliegenden Form beim *Journal of Comparative Neurology* als: Vanessa Althaus, Gesa Exner, Joss von Hadeln, Uwe Homberg und Ronny Rosner (2023). Anatomical organization of the cerebrum of the praying mantis *Hierodula membranacea,* eingereicht und ist in Revision (Stand: Januar 2024).

Eigene Anteile:

- Konzeption des Projekts zusammen mit Dr. Ronny Rosner, Dr. Joss von Hadeln und Prof. Dr. Uwe Homberg
- Bildgebende Aufnahmen der Synapsin- und GABA-Immunfärbungen
- Betreuung und Anleitung der Studentin Gesa Exner, zusammen mit Dr. Ronny Rosner, Dr. Joss von Hadeln und Prof. Dr. Uwe Homberg, die während ihrer Bachelorarbeit die erste Version der dreidimensionalen Rekonstruktion anfertigte und darüber hinaus als wissenschaftliche Hilfskraft das Projekt weiterführte
- Vollständige Überarbeitung und Komplementierung der dreidimensionalen Rekonstruktion des Gehirnatlas
- Rekonstruktion von 3 der 7 Neurone, die restlichen 4 Neurone wurden durch Dr. Joss von Hadeln rekonstruiert
- Registrierung aller Neurone in den dreidimensionalen Gehirnatlas
- Analyse der Verzweigungsgebiete der rekonstruierten Neurone, sowie der zusätzlichen Neurone aus Tabelle 1
- Erstellung aller Abbildungen
- Datenanalyse, Vergleich und Interpretation in Zusammenarbeit mit Dr. Ronny Rosner, Prof. Dr. Uwe Homberg, Dr. Joss von Hadeln und Gesa Exner
- Anfertigung des Manuskripts in Zusammenarbeit mit Dr. Ronny Rosner und Prof. Dr. Uwe Homberg

Kapitel 2   Neuroarchitektur des Zentralkomplexes der Madeiraschabe *Rhyparobia maderae*

Projekt III: Neuroarchitecture of the central complex in the Madeira cockroach *Rhyparobia maderae*: pontine and columnar neuronal cell types

Dieses Projekt wurde in der hier vorliegenden Form beim *Journal of Comparative Neurology* als: Stefanie Jahn[†], Vanessa Althaus[†], Jannik Heckmann, Mona Janning, Ann-Kathrin Seip, Naomi Takahashi, Clara Grigoriev, Juliana Kolano und Uwe Homberg (2023). Neuroarchitecture of the central complex in the Madeira cockroach *Rhyparobia maderae*: pontine and columnar neurons, eingereicht und veröffentlicht.

https://doi.org/10.1002/cne.25535

[†] Stefanie Jahn und Vanessa Althaus waren zu gleichen Teilen an der Arbeit beteiligt.

Eigene Anteile:

- Konzeption des Projektes zusammen mit Stefanie Jahn und Prof. Dr. Uwe Homberg
- Durchführung von 42 der insgesamt 102 ausgewerteten und im Paper verwendeten Einzelzellfärbungen
- Betreuung und Anleitung der Studentinnen Saron Rotella, Gesa Exner und von Mona Janning, die Einzelzellfärbungen in 22 Fällen dazu beisteuerten
- Auswertung von Altdaten ehemaliger Studierender in Zusammenarbeit mit Stefanie Jahn
- Teilweise Ausführung der bildgebenden Aufnahmen am konfokalen Mikroskop zusammen mit Stefanie Jahn
- Identifizierung der innervierten Verzweigungsbereiche zusammen mit Stefanie Jahn
- Teilweise Durchführung von zwei- und dreidimensionalen Rekonstruktionen der Neurone zusammen mit Stefanie Jahn
- Unterstützend bei der Datenanalyse und Interpretation in Zusammenarbeit mit Stefanie Jahn und Prof. Dr. Uwe Homberg
- Unterstützend bei der Anfertigung und Korrektur des Manuskripts zusammen mit Stefanie Jahn und Prof. Dr. Uwe Homberg

Die oben genannten Publikationen sind kein Bestandteil einer weiteren wissenschaftlichen Qualifikationsarbeit

Inhaltsverzeichnis

Zusammenfassung

Insekten besitzen relativ einfache Nervensysteme, die sie trotz ihrer geringen Größe zu beeindruckenden Verhaltensweisen und Navigationsverhalten befähigen. Diese Tatsache macht sie zu attraktiven Forschungsobjekten, um neuronale Netzwerke zu erforschen und zu verstehen. Ihr Gehirn, das Oberschlundganglion, besteht aus verschmolzenen Ganglien und ist weiter unterteilbar in das Proto-, Deuto- und Tritocerebrum. Diese sind in verschiedenen Spezies unterschiedlich stark verschmolzen und ausgeprägt und weiter einteilbar in Neuropile. Neuropile sind abgrenzbare Bereiche, in denen Neurone ihre Synapsen ausbilden und reich an Synapsin sind. Synapsine bilden eine konservierte Gruppe der Proteine, welche im Gehirn exprimiert werden. Sie sind gehäuft an den Präsynapsen nachweisbar und involviert in die Regulation der Transmitterfreisetzung. Eine besonders prominente und evolutionär konservierte Neuropilgruppe im Insektengehirn ist der Zentralkomplex. Er liegt mittig im Gehirn und kontrolliert die räumliche Orientierung des Tieres basierend auf verschiedenen sensorischen Inputs. Der Aufbau dieser Neuropilgruppe aus Zentralkörper, Protozerebralbrücke und Noduli ist innerhalb der Insekten konserviert, unterscheidet sich aber im Feinbau und Form der einzelnen Neuropile, welche durch komplexe Systeme von Neuronen entsteht: kolumnäre, tangentiale und pontine Neurone. Zum Verständnis von neuronalen Netzwerken und deren Funktion ist deren zugrundeliegende Morphologie und Ausprägung unerlässlich.

Diese Doktorarbeit untersucht die anatomische Organisation der Gehirne zweier hemimetaboler Insekten, der Madeiraschabe *Rhyparobia maderae* und der Riesengottesanbeterin *Hierodula membranacea*, so wie in näherem Detail den Zentralkomplex der Schabe auf neuronaler Ebene. Im Folgenden werden diese Projekte kurz zusammengefasst:

Projekt I und **II** setzen den Fokus auf die neuroanatomischen Grundlagen des Oberschlundganglions der Madeiraschabe *R. maderae* und der indischen Riesengottesanbeterin *H. membranacea*. Beide Arbeiten konzentrieren sich auf die Charakterisierung von Neuropilen und erstellen vollständig dreidimensionale Atlanten ihrer Gehirne. Diese sind die Grundlage für zukünftige Forschungen, um ein besseres Verständnis zu ermöglichen, wie neuronale Netzwerke miteinander verbunden sind und spezifische Gehirnregionen funktionell einzuordnen sind. Die beiden Atlanten reihen sich in eine bisher kleinere Sammlung von entstandenen vollständigen anatomischen Untersuchungen von Insektengehirnen ein. Hierzu gehören die Taufliege *Drosophila melanogaster* und, als bisher einziges anderes hemimetaboles Insekt, die Wüstenheuschrecke *Schistocerca gregaria*. Zusätzlich gibt es vergleichbare Arbeiten zum Monarchfalter *Danaus plexippus,* den Pillendrehern *Scarabaeus lamarcki* und *Scarabaeus satyrus*, den Ameisen *Cardiocondyla obscurior* und *Cataglyphis nodus*, der Honigbiene *Apis mellifera*, sowie der Bogong Motte *Agrotis infusa*. Die vollständige anatomische Charakterisierung zweier hemimetaboler Insekten erweitert so eine wichtige Sammlung,

die dabei hilft, neuronale Netzwerke besser zu verstehen und zukünftig die Möglichkeit gibt, anhand von Verwandtschaftsgraden der Spezies evolutionäre Vergleiche zu ziehen. Es stellte sich heraus, dass sich viele Gemeinsamkeiten innerhalb der Polyneoptera zeigten, die in den holometabolen Insekten nicht zu finden waren. Trotz einiger Unterschiede, die oft durch eine unterschiedliche Neuroachse entstehen oder durch die Größe und Anordnung der Neuropile, zeigen alle bisher katalogisierten Gehirne erstaunliche Gemeinsamkeiten. Die Daten der Schabe *R. maderae* sind zudem Teil einer für alle zugänglichen und anwachsenden Bibliothek von anatomischen und physiologischen Daten von Insektengehirnen auf www.insectbraindb.org.

Aufbauend auf dem dreidimensionalen Atlas des Gehirns der Madeira Schabe wurde in **Projekt III** der Zentralkomplex der Madeiraschabe *R. maderae* im Detail betrachtet. Durch die Katalogisierung und Einteilung der Neuropile konnten neuronale Zelltypen bestimmt und die genauen Verzweigungsgebiete beschrieben werden. Das Interesse lag auf der konservierten Neuropilgruppe, dem Zentralkomplex. Diese Struktur wurde durch Immunfärbungen und Einzelzellfärbungen weiter analysiert und eingeteilt, dabei wurden besonders die allgemeine Neuroanatomie des Zentralkomplexes in Betracht gezogen sowie die Morphologie und Klassifizierung von pontinen und kolumnären Neuronen. Der Zentralkomplex der Schabe ähnelt der vieler andere Insekten und besteht aus dem Zentralkörper, mit unterer und oberer Einheit, der Protozerebralbrücke und den paarigen Noduli. Diese Neuropilgruppe ist stark vernetzt mit dem lateralen Komplex, in dem in der Schabe auch eine neue Struktur gefunden werden konnte, die durch kolumnäre Neurone innerviert wird. Auffällig bei *R. maderae* ist die untere Einheit des Zentralkörpers, welche aus Zapfen und Zähnen besteht und nicht, wie in anderen Insektenarten, in Schichten eingeteilt werden konnte. Die Neuroarchitektur der kolumnären Neurone zeigt viele Übereinstimmungen mit anderen Insekten, besonders mit der Wüstenheuschrecke *S. gregaria*, der Taufliege *D. melanogaster* und der Hummel *Bombus terrestris*. Es wurden jedoch sechs neue Zelltypen beschrieben, die bisher noch nicht in anderen Insektenarten nachgewiesen werden konnten. Eine Besonderheit bei diesen ist eine starke Vernetzung mit der anterioren Lippe (ALI), welche in der Schabe sehr prominent ausgeprägt ist und anterior zum Zentralkörper die Mittellinie des Gehirns überspannt. Auch diese Neurone sind Teil der Website www.insectbraindb.org und sollen in Zukunft mit physiologischen Daten der Einzelneurone ergänzt werden.

Die Katalogisierung kolumnärer und pontiner Neurone soll zukünftig durch die Charakterisierung von tangentialen Neuronen ergänzt werden und so die Grundlage bilden für nachfolgende physiologische Untersuchungen von Zentralkomplexneuronen. Darüber hinaus dienen die Daten als Grundlage für die Erarbeitung eines Konnektoms des Zentralkomplexes der Schabe *R. maderae*.

Abstract

Insects possess relatively simple nervous systems, which, despite their small size enable them to exhibit impressive navigational behaviors. These facts make them attractive subjects for research to explore and understand neural networks. Their brain consists of fused ganglia and is further divisible into the proto-, deuto-, and tritocerebrum. These components vary in their degree of fusion and prominence across different species and are further subdivided into neuropils. Neuropils are distinct areas where neurons form synapses, and so characterized by a high concentration of synapsin. Synapsins constitute a conserved group of proteins expressed in the brain. They are predominantly found at presynaptic sites, and are involved in the release of neurotransmitters. A particularly prominent and evolutionarily conserved neuropil group is the central complex. It is located centrally in the brain, and controls the spatial orientation of the animals based on multiple sensory inputs. The architecture of this neuropil group, consisting of the central body, protocerebral bridge, and noduli, is highly conserved among insects. It varies in the deeper structure and form of individual neuropils across different species, created by complex systems of central complex neurons: columnar, tangential, and pontine neurons. Understanding the morphology and expression of these structures is essential for comprehending neural networks and their functions.

This doctoral thesis focuses on the neuroanatomy of two dictypteran insects, the Madeira cockroach *Rhyparobia maderae* and the giant Asian mantis *Hierodula membranacea* with detailed examination of central complex of the cockroach at the neural level. The following projects are summarized:

Projects I and **II** focus on the neuroanatomical foundations of the supraesophageal ganglion of the Madeira cockroach *R. maderae* and the Indian giant mantis *H. membranacea* as study subjects. Both projects concentrate on characterizing neuropils and provide complete three-dimensional atlases of these insect brains. These atlases serve as a basis for future research for a better understanding how neural networks are interconnected and how specific brain regions are functionally categorized. The cockroach and mantis atlases join a smaller collection of detailed 3-dimensional reconstructions of insect brains, including the fruit fly *Drosophila melanogaster* and the only other hemimetabolous insect, the desert locust *Schistocerca gregaria*. Similar studies exist for the monarch butterfly *Danaus plexippus*, the dung beetles *Scarabaeus lamarcki* and *Scarabaeus satyrus*, the ants *Cardiocondyla obscurior* and *Cataglyphis nodus*, the honeybee *Apis mellifera*, and the Bogong moth *Agrotis infusa*. The comprehensive three-dimensional brain atlases of two hemimetabolous insects contributes to a growing library of anatomical and physiological data on insect brains, accessible at www.insectbraindb.org.

Building on the brain atlas of the Madeira cockroach, **Project III** examines the central complex of *R. maderae* in detail. Through cataloging and clear delineation of neuropils, individual cell types were identified, and precise branching areas were described. The focus was on the highly conserved neuropil group, the central complex. This structure was further analyzed and classified through immunostaining and single-cell staining, with a particular focus on the neuroanatomy of the central complex and the morphology and classification of pontine and columnar neurons. The cockroach's central complex resembles that of many other insects, consisting of the central body with upper and lower divisions, the protocerebral bridge, and paired noduli. This central complex is strongly connected to the lateral complex, where a new structure, innervated by columnar neurons, was discovered in the cockroach. Notably, the lower division of the central body in *R. maderae* consists of cones and teeth, unlike in other insect species, where the lower division is divided into columns and layers. The neuroarchitecture of columnar neurons show many similarities with that of other insects, especially the desert locust *S. gregaria*, the fruit fly *D. melanogaster*, and the bumble bee *Bombus terrestris*. However, six new cell types were described that have not been documented in other insect species. A distinctive feature of these neurons is their strong connectivity with the very prominent anterior lip (ALI), which is highly developed in the cockroach and spans the midline of the brain anterior to the central body. All described neurons of this work are also part of the website www.insectbraindb.org and, in the future, can shall be complemented with physiological data for individual neurons.

The catalof of columnar and pontine neurons is intended to be complemented in the future by the characterization of tangential neurons, forming the basis for subsequent physiological investigations of central complex neurons. The data will, moreover build the foundation for the development of a connectome in the central complex of the Madeira cockroach *R. maderae.*

Abkürzungverzeichnis

Abkürzung	english	deutsch
ABR	**a**nterior **br**idge	anteriore Brücke
ACAR	**a**ccessory **ca**lyx **r**ing	akzessorischer Calyxring
AFP	**a**nterior **f**iber **p**lexus	anteriores Fasergeflecht
AL	**a**ntennal **l**obe	Antennallobus
ALA	**a**ccessory **la**mina	akzessorische Lamina
ALI	**a**nterior **li**p	anteriore Lippe
ALO	**a**nterior **lo**be	anteriore Lobus
ALT	**a**ntennal **l**obe **t**ract	Antennallobustrakt
AME	**a**ccessory **me**dulla	akzessorische Medulla
AMMC	**a**ntennal **m**echanosensory and **m**otor **c**enter	antennales mechanosensorisches und motorisches Zentrum
AOT	**a**nterior **o**ptic **t**ract	anteriorer optischer Trakt
AOTU	**a**nterior **o**ptic **tu**bercle	anteriorer optischer Tuberkel
ASOC	**a**nterior **s**uperior **o**ptic **c**ommissure	anteriore superiore optische Kommissur
ATL	**a**n**tl**er	Geweih
AVLP	**a**nterior **v**entro**l**ateral **p**rotocerebrum	anteriores ventrolaterales Protocerebrum
BU	**bu**lb	Bulbus
CA	**ca**lyx	Calyx
CB	**c**entral **b**ody	Zentralkörper
CBL	**l**ower division of the **CB**	untere Einheit des CB
CBU	**u**pper division of the **CB**	obere Einheit des CB
CL	**cl**amp	Klammer
CO	**co**nes	Zapfen
CRE	**cre**pine	Crepine
CX	**c**entral comple**x**	Zentralkomplex
dALA	**d**orsal **ALA**	dorsale ALA
DAMMC	**d**orsal **AMMC**	dorsales AMMC
DLO	**d**orsal **lo**be	dorsaler Lobus
EPA	**ep**aulette	Schulter
GA	**ga**ll	Gall
GABA	**γ**-**a**mino**b**utyric **a**cid	γ-Aminobuttersäure

GC	**g**reat **c**ommissure	große Kommissur
GLO	**g**lomerular **lo**be	glomerulärer Lobus
GOR	**gor**get	Kragen
hVLPF	**h**orizontal **v**entro**l**ateral **p**rotocerebrum **f**ascicle	horizontales ventrolaterales Protocerebrum Faszikel
IB	**i**nferior **b**ridge	inferiore Brücke
IBC	**IB c**ap	Kappe der IB
ICA	**i**nner **CA**	innerer CA
ICL	**i**nferior **CL**	inferiore CL
IFS	**i**nferior **f**iber **s**ystem	inferiores Fasersystem
INP	**i**nferior **n**euro**p**ils	inferiore Neuropile
IT	**i**sthmus **t**ract	Isthmustrakt
LA	**la**mina	Lamina
LAL	**l**ateral **a**ccessory **l**obe	lateraler akzessorischer Lobus
LALC	**LAL c**ommissure	LAL Kommissur
lALT	**l**ateral **ALT**	lateraler ALT
LAMMC	**l**ateral **AMMC**	laterales AMMC
LCA	**l**ateral **CA**	lateraler CA
LEF	**l**ateral **e**quatorial **f**ascicle	laterales äquatoriales Faszikel
LH	**l**ateral **h**orn	laterales Horn
LLAL	**l**ower **LAL**	unterer LAL
LO	**lo**bula	Lobula
LOVT	**LO v**alley **t**ract	Lobulatal Trakt
LOX	**LO** comple**x**	Lobulakomplex
LU	**l**ower **u**nit of the AOTU	untere Einheit des AOTU
LX	**l**ateral comple**x**	lateraler Komplex
MAL	**m**edial **a**ccessory **l**obe	medialer akzessorischer Lobus
mALT	**m**edial **ALT**	medialer ALT
MAMMC	**m**edial **AMMC**	mediales AMMC
MB	**m**ushroom **b**ody	Pilzkörper
MBDL	**m**edian **b**un**dl**e	medianes Bündel
MC	**m**edian **c**rescent	medianer Halbmond
MCA	**m**edial **CA**	medialer CA

ME	**me**dulla	Medulla
MEF	**m**edial **e**quatorial **f**ascicle	mediales äquatoriales Faszikel
ML	**m**edial **l**obe	medialer Lobus
mlALT	**m**edio**l**ateral **ALT**	mediolateraler ALT
N	**n**eck	Hals
NO	**no**duli	Noduli
NOL	**l**ower unit of the **NO**	untere Einheit der NO
NOU	**u**pper unit of the **NO**	obere Einheit der NO
OCA	**o**uter **CA**	äußerer CA
OCN	**oc**ellar **n**erve	Ocellarnerv
OL	**o**ptic **l**obe	optischer Lobus
OLO	**o**uter **LO**	äußere LO
OR	**o**cellar **r**oot	Ocellenwurzel
PB	**p**rotocerebral **b**ridge	Protozerebralbrücke
PC	**p**roto**c**erebrum	Protocerebrum
PDF	**p**igment-**d**ispersing **f**actor	pigmentdispergierender Faktor
PDH	**p**igment-dispersing **h**ormone	pigmentdispergierendes Hormon
PED	**ped**unculus	Pedunkulus
PEDD	**PED d**ivide	PED Teilung
PENP	**pe**riesophageal **n**euro**p**ils	periösophageale Neuropile
PLF	**p**osterior **l**ateral **f**ascicle	posteriores laterales Faszikel
PLP	**p**osterior **l**ateral **P**C	posteriores laterales PC
POC	**p**osterior **o**ptic **c**ommissure	posteriore optische Kommissur
POTU	**p**osterior **o**ptic **tu**bercle	posteriorer optischer Tuberkel
pPLPC	**p**osterior **PLP c**ommissure	posteriore PLP Kommissur
PRO	**pro**ng	Zinken
PS	**p**osterior **s**lope	posteriore Schräge
PVLP	**p**osterior **v**entrolateral **P**C	posteriores ventrolaterales PC
PYF	**py**riform **f**ascicle	birnenförmiges Faszikel
RUB	**rub**us	Rubus
SCL	**s**uperior **CL**	superiore CL
SFS	**s**uperior **f**iber **s**ystem	superiores Fasersystem
SIP	**su**perior **i**ntermediate **P**C	superiores intermediäres PC

SLP	**s**uperior **l**ateral **P**C	superiores laterales PC
SMP	**s**uperior **m**edial **P**C	superiores mediales PC
SNP	**s**uperior **n**euro**p**ils	superiore Neuropile
SPU	**spu**r	Sporn
TC	**t**rito**c**erebrum	Tritocerebrum
TH	**t**eet**h**	Zahn
TUBUT	**tu**bercle-**bu**lb **t**ract	Tuberkel-Bulbus Trakt
ULAL	**u**pper **LAL**	oberer LAL
UU	**u**pper **u**nit of the AOTU	obere Einheit des AOTU
vALA	**v**entral **ALA**	ventrale ALA
VES	**ves**t	Weste
VFA	**v**entral area of **f**lagellar **a**fferents	ventrale Region der flagellaren Afferenzen
VL	**v**ertical **l**obe	vertikaler Lobus
VLNP	**v**entro**l**ateral **n**euro**p**ils	ventrolaterale Neuropile
VLP	**v**entro**l**ateral **P**C	ventrolaterales PC
VMNP	**v**entro**m**edial **n**euro**p**ils	ventromediale Neuropile
VX	**v**entral comple**x**	ventraler Komplex
WED	**wed**ge	Keil

Einleitung

Insekten

Insekten (Insecta) bilden zweifelslos die facetten- und artenreichste Klasse innerhalb der Tierwelt (Grimaldi & Engel, 2005; Stork, 2018). Diese bemerkenswerte Vielfalt ist das Resultat ihrer erstaunlichen Fähigkeit zur Anpassung, die sie zur erfolgreichsten rezenten Tierklasse macht. Im Verlauf der Evolution haben Insekten nahezu sämtliche ökologischen Nischen besiedelt, darunter sowohl terrestrische als auch einige wenige aquatische Lebensräume. Neben Vögeln und Fledermäusen gehören Insekten zu den wenigen flugfähigen Tieren (Grandcolas & Grandcolas, 1997; Dijkstra et al., 2014; Tihelka et al., 2021). Insekten erfüllen eine ubiquitäre Rolle in unserem Ökosystem, auch für die menschliche Zivilisation. Sie fungieren als bedeutende Destruenten, Bestäuber und dienen zugleich als Nahrungsquelle für Nutztiere (Zhang et al., 2007; Bernard, 2017; Scudder, 2017). Ein fundamentales Klassifikationsmerkmal für Insekten ist ihre Metamorphose. Grundsätzlich lassen sich zwei Hauptgruppen unterscheiden: die holometabolen Insekten und die hemimetabolen, zu denen auch die Polyneoptera zählen (Misof et al., 2014). Bei holometaboler Metamorphose durchläuft das Insekt eine vollständige Entwicklung von der Larve über die Puppe bis hin zur geschlechtsreifen Imago. Im Gegensatz dazu, vollziehen hemimetabole Insekten ihre Entwicklung graduell über verschiedene Häutungsstadien, wobei sich die juvenilen Formen in Bezug auf Größe, Flügelentwicklung und Geschlechtsreife von den adulten Formen unterscheiden (Kristensen, 1999; Truman, 2019). Im Rahmen dieser Arbeit werden die Versuchstiere, die Madeiraschabe *Rhyparobia maderae* und die indische Riesengottesanbeterin *Hierodula membranacea*, untersucht. Beide Arten sind der Polyneoptera zugehörig und spezifischer, den Dictyoptera (Misof et al., 2014).

Die Madeiraschabe *Rhyparobia maderae*

Die Madeiraschabe *R. maderae* (ehemals *Leucophaea maderae*; Abbildung 1), eine Schabe aus der Familie der Blaberidae, wurde als Hauptorganismus in dieser Studie untersucht. Erstmalig wurde sie auf der portugiesischen Insel Madeira beschrieben (Fabricius, 1781). Ähnlich wie viele andere Schabenarten wurde auch *R. maderae* wahrscheinlich durch menschliche Aktivitäten in verschiedene Regionen verschleppt und hat sich dort an die neuen Umweltbedingungen angepasst. Aufgrund ihrer Nachtaktivität und ihrer bevorzugten Umgebung in dunklen und engen Verstecken, verfügt die Madeiraschabe über lange (Abbildung 1) komplexe Antennen.

Abbildung 1: Fotografie einer weiblichen Madeira-schabe *Rhyparobia maderae* von oben frontal. Die Schabenart wird zwischen 4-4,5 cm groß, besonders auffällig sind ihre langen Antennen. (Foto: Chris Dlouhy)

Die Antennen erfüllen verschiedene Funktionen, einschließlich der räumlichen Orientierung (Okada & Toh, 2000; Baba et al., 2010) und bei der Chemorezeption zur Partner- und Nahrungssuche (Schafer, 1971; Sreng, 1984; Page, 2009; Fuscà & Kloppenburg, 2021).

Die Madeiraschabe *R. maderae* erfreut sich aufgrund ihrer Größe, den verhältnismäßig einfachen Haltungsbedingungen und ihrer hohen Reproduktionsrate in der wissenschaftlichen Forschung großer Beliebtheit. Sie wird bereits seit mehreren Jahrzehnten als Modellorganismus im Bereich der zirkadianen Forschung eingesetzt (Page, 1982; Homberg et al., 2003; Stengl et al., 2015; Stengl & Arendt, 2016). Tagesperiodische Rhythmen, wie die täglichen Schwankungen von Temperatur und Licht, beeinflussen das Verhalten aller Lebewesen auf der Erde. In Anpassung der Rhythmen haben sich innere biologische Uhren entwickelt, die durch eine zirkadiane Rhythmik viele Verhaltensweisen/Stoffwechselaktivitäten hervorrufen. Mit Hilfe von Läsions- und Transplantationsexperimenten in *R. maderae* konnte der zirkadiane Oszillator im optischen Lobus im Gehirn lokalisiert werden, der unter anderem den Schlaf-Wach-Rhythmus, abhängig vom Hell-Dunkel Zyklus steuert. Dieses Areal, die akzessorische Medulla (AME) (Stengl & Homberg, 1994; Reischig & Stengl, 2003), befindet sich ventroproximal zur Medulla und wird von einem Netzwerk aus weitverzweigten Neuronen innerviert. Immunzytochemische Studien haben spezifische Neurone, die ‚pigment-dispersing hormone' (PDH) immunreaktiv sind, innerhalb der AME identifiziert. Diese Neurone erstrecken sich weiter in die Medulla, Lamina und verschiedene Bereiche des Protocerebrums (Homberg et al., 2003; Wei et al., 2010; Stengl & Arendt, 2016; Arnold et al., 2020). Sie agieren als zirkadiane Schrittmacherneurone und tragen maßgeblich zur Steuerung des Aktivitäts- und Ruhezyklus der Tiere bei (Stengl & Homberg, 1994; Stengl & Arendt, 2016; Arnold et al., 2020). Hinsichtlich des Sehsystems zeigt die Madeiraschabe *R. maderae* eine eher basale Struktur und verfügt über vergleichsweise wenig Ommatidien, im Gegensatz zum Beispiel zur Wüstenheuschrecke *S. gregaria* oder der Mantis *H. membranacea*. Im Komplexauge der amerikanischen Küchenschabe *Periplaneta americana* und der Riesenschabe *Blaberus giganteus* wurden bis zu 2000 Ommatidien nachgewiesen (Wolken & Gupta, 1961), die meist der Kontrastwahrnehmung dienen (Heimonen et al., 2006). Erste elektrophysiologische Ableitungen von Neuronen aus den optischen Loben in *R. maderae* zeigten eine hohe Empfindlichkeit gegenüber Hell-Dunkel-Wechseln und erbrachten erste Kenntnisse darüber, dass die Schabe den Schwingungswinkel polarisierten Lichts wahrnehmen kann (Loesel & Homberg, 2001).

Die indische Riesengottesanbeterin *Hierodula membranacea*

H. membranacea gehört wie die Madeiraschabe zu den Dictyoptera und durchläuft einen hemimetabolen Entwicklungszyklus. Sie zählt zur Ordnung der Mantodea (Fangschrecken; Misof et al., 2014), ist ursprünglich in Asien beheimatet und ein geschickter Lauerjäger. Ihr Erfolg beim Fangen von Beute beruht auf der Ausführung eines beeindruckenden Fangschlags.

Dieser wird äußerst präzise ausgelöst und ausgeführt, um blitzschnell Beute greifen zu können. Verhaltenstudien an *H. membranacea* haben zudem erstaunliche Fähigkeiten bei der Beuteerkennung, Verteidigung und der Distanzwahrnehmung gezeigt (Prete, 1999; Nityananda et al., 2016a, 2019a; b). Um diese Aufgaben zu bewältigen, verfügen Riesengottesanbeterinnen über große Komplexaugen, die fast 4,5 mal so viele Ommatidien aufweisen wie die der Schaben (Kral & Prete, 1999). Das visuelle Feld erstreckt sich nicht nur auf die seitlichen Partien, sondern die Facettenaugen sind bemerkenswert groß und ermöglichen nahezu eine vollständige Rundumsicht mit Überlappung im frontalen Bereich (Rossel, 1979). Die optischen Loben, spezialisierte Hirnregionen für die Verarbeitung und Aufnahme von visuellen Informationen, sind dementsprechend größer und komplexer als die einiger anderer Insekten (Rosner et al., 2017). Die komplexe Struktur des Lobulakomplexes innerhalb des optischen Lobus bei *H. membranacea* könnte in Verbindung mit der räumlichen Tiefenwahrnehmung stehen. Beuteobjekte präzise zu erkennen und fangen zu können basiert auf der Auswertung von Bewegungsparallaxe und binokularer Disparität, was die Gottesanbeterin zu dem bisher einzig bekannten Insekt macht, welches Stereopsis, also die Fähigkeit zur Tiefenwahrnehmung, nutzen kann (Rossel, 1983; Prete, 1999; Nityananda et al., 2016a; b, 2019a; b; Rosner et al., 2019, 2020).

Neuroanatomie des Insektengehirns

Ein wesentliches Interessengebiet der heutigen Neurowissenschaften befasst sich mit der engen Verknüpfung zwischen funktionellen Eigenschaften einzelner Gehirnregionen/Neurone mit ihrer morphologischen Struktur. Die Visualisierung und Erforschung neuronaler Strukturen sollen zukünftig tiefere Einblicke in die Gehirnstrukturen und komplexen neuronalen Schaltkreise des Gehirns ermöglichen. Insekten sind besonders interessante Modelle zur Untersuchung neuronaler Netzwerke aufgrund ihrer vergleichsweisen einfach aufgebauten Nervensysteme, im Vergleich zu denen von Wirbeltieren. So können Wissenschaftler einzelne Neurone identifizieren und deren spezifische physiologische Funktionen genauer erforschen.

Insekten verfügen über ein sogenanntes Strickleiternervensystem, welches entgegen dem Nervensystem von Wirbeltieren, ventral im Körper liegt. Es besteht pro Körpersegment aus zwei segmentalen Ganglien, die je nach Insektenspezies unterschiedlich stark miteinander verschmolzen und durch
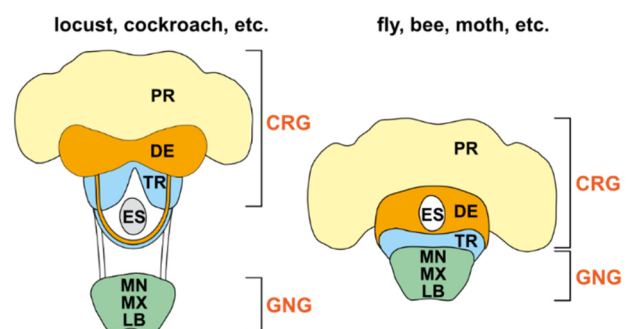

Abbildung 2: Schematische Darstellung der Verschmelzung der oberen Ganglien innerhalb hemimetaboler Insekten, wie der Heuschrecke, Schabe (links) und holometaboler Insekten, wie der Fliege oder der Biene (rechts). CRG, Cerebralganglion; DE, Deutocerebrum; ES, Ösophagus; GNG, Gnathalganglion; LB, labiale Neuromere; MN, mandibulare Neuromere; MX, maxillare Neuromere; PR, Protocerebrum; TR, Tritocerebrum. Verändert nach Ito et al. (2014)

Kommissuren verbunden sind. Diese Ganglienpaare sind wiederum mit dem jeweilig angrenzenden segmentalen Ganglienpaar durch Konnektive verknüpft. Im Kopfbereich verschmelzen die Ganglien zu einem Cerebral- und einem Gnathalganglion, wobei ersteres auch als Gehirn bezeichnet wird (Smith & Treherne, 1963; Strausfeld, 2012; Loesel et al., 2013; Schmidt-Rhaesa et al., 2016; Smarandache-Wellmann, 2016). Bei holometabolen Insekten, wie der Taufliege *D. melanogaster*, verschmilzt das Cerebralganglion mit dem Gnathalganglion, weshalb die Bezeichnung des Gehirns oft auch die Verschmelzung des Gnathalganglions miteinbezieht (Ito et al., 2014; Abbildung 2). Trotz Variationen in Größe und Form über die Insektenspezies hinweg weisen alle bisher untersuchten Insektencerebralganglien eine ähnliche Grundstruktur auf. Das Cerebrum, welches als Cerebralganglien ohne optischen Loben definiert wird, besteht dabei aus drei Hauptbereichen: dem Proto-, Deuto- und Tritocerebrum (Strausfeld, 2012; Abbildung 2).

Als caudalster Abschnitt der Cerebralganglien verarbeitet das Tritocerebrum sensorische Informationen und ist beteiligt an der Steuerung von Motorik. Innerhalb des Tritocerebrums verlaufen Nervenfasern, sowohl absteigende als auch aufsteigende, die aus den abdominalen, thorakalen und den gnathalen Ganglien entspringen. Zudem wird es von Nerven innerviert, die von den Mundwerkzeugen und dem stomatogastrischen System ausgehen. Das Tritocerebrum ist eng mit dem endokrinen System verbunden, das die Regulation von Hormonen im Körper steuert. Es interagiert unter anderem mit den Corpora allata, endokrinen Drüsen, die eine Schlüsselrolle bei der Kontrolle von Stoffwechselprozessen und Verhaltensweisen spielen (Aubele & Klemm, 1977; Rajashekhar & Singh, 1994; Farris, 2008).

Im weiter rostral gelegenen Deutocerebrum werden unter anderem sensorische Signale aus den Antennen empfangen und verarbeitet. Im antennalen mechanosenorischen und motorischen Zentrum werden Wahrnehmungen von Vibrationen, Berührungen und Bewegungen verarbeitet, was den Tieren bei der räumlichen Orientierung, der Partnersuche oder der Nahrungssuche hilft. Das oft größte Neuropil des Deutocerebrums, der Antennallobus, ist an der Chemorezeption beteiligt, einschließlich der Verarbeitung von Duftstoffen und Pheromonen. Obwohl das Deutocerebrum in verschiedenen Arthropodenarten ähnliche Funktionen auszufüllen scheint, variiert seine Anatomie und Organisation stark je nach Spezies. Es ist jedoch ein wesentlicher Bestandteil des Insektengehirns und trägt maßgeblich zur Informationsverarbeitung und Verhaltenssteuerung bei (Boeckh et al., 1987; Christensen & Hildebrand, 1987; Homberg et al., 1989; Hösl, 1990; Malun et al., 1993; Ignell et al., 2005; Fuscà & Kloppenburg, 2021).

Das Protocerebrum nimmt den Großteil des Insektengehirns ein, zu diesem gehören unter anderem prominente Neuropilgruppen wie der Zentralkomplex als mediale Neuropilgruppe und die paarigen Pilzkörper (Ito et al., 2014).

Die Hauptfunktionen des Protocerebrums bestehen in der Integration und Verarbeitung sensorischer Reize. Dazu gehört die Integrierung antennaler Reize, welche über den Antennallobus (deutocerebraler Ursprung) weitergeleitet werden und unter anderem an die Pilzkörper übertragen werden. Die Pilzkörper sind maßgeblich an der Prozessierung von olfaktorischen Reizen, der Gedächtnisbildung und Lernprozessen beteiligt (Heisenberg, 1998; Mizunami et al., 1998; Stopfer, 2014; Modi et al., 2020). Das Protocerebrum ist stark mit dem Trito- und Deutocerebrum vernetzt, nur so sind komplexe Verarbeitungen von Reizen und daraus resultierende Verhaltensweisen möglich. Alle drei Cerebralganglien wurden in der Schabe *R. maderae* und der Gottesanbeterin *H. membranacea* in dieser Arbeit genauer anatomisch unterteilt und als dreidimensionaler Atlas etabliert.

Neuropilgrenzen

Das Cerebrum der Insekten wird weiter in distinkte Bereiche separiert, die als Neuropile bezeichnet werden. Die Abgrenzung und dreidimensionale Rekonstruktion dieser Neuropile wurde erstmals vollständig in der Taufliege *D. melanogaster* durchgeführt (Ito et al., 2014). Ito et al. (2014) etablierte eine allgemeingültige Nomenklatur, die als Grundlage für die vorliegende Arbeit zur Gehirnanatomie diente. In der Vergangenheit führte das Fehlen klar definierter Neuropilgrenzen und einer einheitlichen Nomenklatur zu Verwirrung bei der Benennung und Definition der gleichen Gehirnareale, selbst innerhalb derselben Insektenspezies. Die Dokumentation der Nomenklatur und klar beschriebenen Neuropilgrenzen sollen zukünftig dazu beitragen diese Probleme zu minimieren oder auch zu lösen. In *D. melanogaster* konnten viele Neuropile anhand von synaptischen Markern und unterschiedlichen Antikörperfärbungen differenziert werden. Obwohl diese Methodik in anderen Insekten wegen fehlender Marker nur teilweise übernommen werden kann, bietet die von Ito et al. (2014) erstellte detaillierte Beschreibung von wichtigen Landmarken zur Einteilung von Neuropilen eine übertragbare Grundlage, die auch auf andere Insektengehirne angewendet werden kann. Auf diese Weise konnten auch bei der Schabe *R. maderae* (Althaus et al., 2022) und der Gottesanbeterin *H. membranacea* die Gehirnanatomie analysiert werden. Dies geschah unter Verwendung von diversen Immunfärbungen, Identifizierung von Trakten, Kommissuren, Faserbündeln und die Analyse von Projektionen einzeln markierter Neurone.

Zentralkomplex

Eine bemerkenswerte Region innerhalb des Protocerebrums ist der prominente und klar abgrenzbare Zentralkomplex (CX). Der CX nimmt eine zentrale Position im Insektengehirn ein und das nicht nur weil er sich über die Mittellinie des Gehirns erstreckt. Bei allen bisher untersuchten pterygoten Insekten, unabhängig von ihrer Ökologie, Größe und Lebensweise, besteht der CX aus dem Zentralkörper (CB), bestehend aus oberer (CBU; ‚fanshaped body' in *D. melanogaster)* und unterer Einheit (CBL; ‚ellipsoid body' in *D. melanogaster*), den paarigen Noduli (NO) und der

Protozerebralbrücke (PB) (Strausfeld, 2012; Pfeiffer & Homberg, 2014). Er spielt eine entscheidende Rolle in der Verarbeitung und Prozessierung manigfaltiger Informationen und gilt als Navigationszentrum im Insektengehirn (Pfeiffer & Homberg, 2014; Turner-Evans & Jayaraman, 2016; Pfeiffer, 2022; Heinze, 2023). Der CX bildet die Grundlage für viele wichtige Aufgaben, darunter die Ausrichtung des Tiers im Raum, wozu die Kodierung der Kopfrichtung (Seelig & Jayaraman, 2015) und die Verarbeitung von idiothetischen Informationen gehören. Zu idiothetischen Informationen gehören räumliche Informationen, die aus dem Tier selbst kommen und zur Bestimmung der Eigenlage im Raum relevant sind. Es kommt innerhalb des CX zu einer Integrierung zahlreicher sensorischer Informationen, wie die Verarbeitung von Himmelskompasssignalen (Homberg, 2004; Pfeiffer & Homberg, 2014; el Jundi et al., 2019; Homberg et al., 2022), sowie die Verarbeitung von antennalen Informationen zur Orientierung (Ritzmann et al., 2012; Turner-Evans & Jayaraman, 2016; Varga et al., 2017). Diese Informationen werden prozessiert und daraus Kommandos zur Steuerung und Motorik des Tieres weitergeleitet (Bender et al., 2010; Varga et al., 2017) für eine zielgerichteten Orientierung und Navigation. Auf diese Weise fungiert der CX als eine Art interner biologischer Kompass (Honkanen et al., 2019).
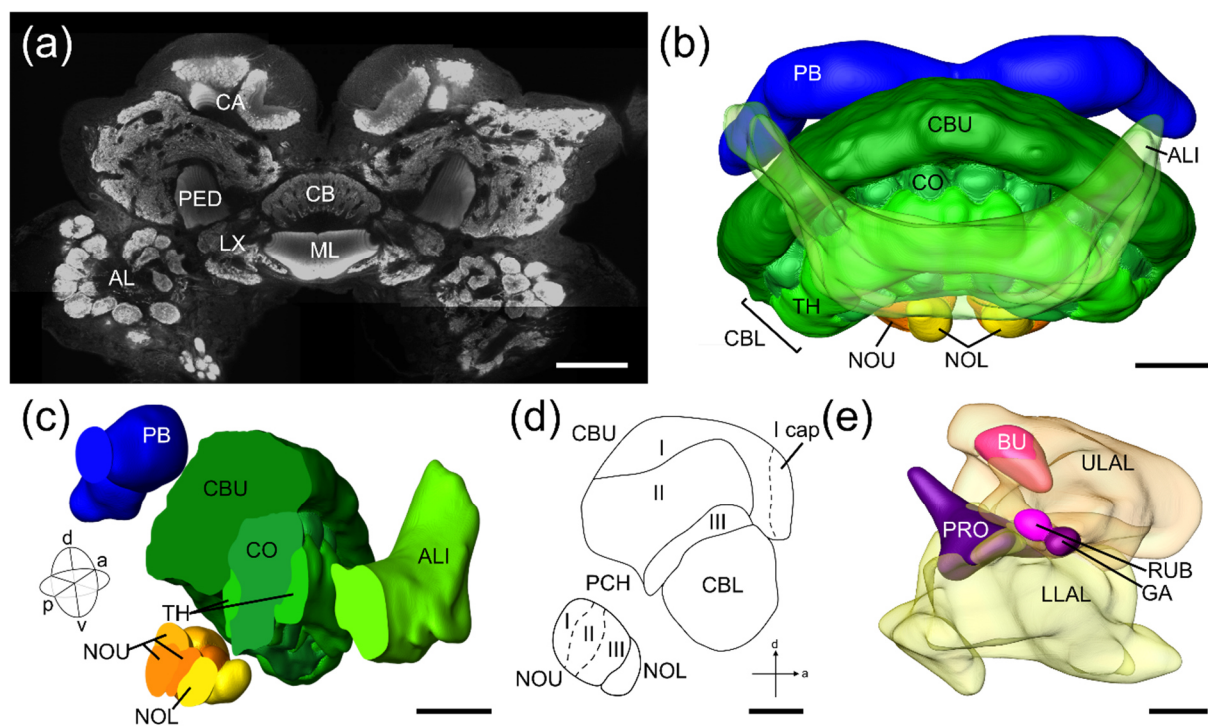

Abbildung 3: Organisation des Zentralkomplexes (CX), der anterioren Lippe (ALI) und des lateralen Komplexes (LX) in der Schabe *Rhyparobia maderae*. (a) Frontaler Schnitt einer Synapsin Immunfärbung zeigt die Position des Zentralkörpers (CB) und des LX innerhalb des Schabengehirns *R. maderae*. (b) Frontale Ansicht auf den drei-dimensional rekonstruierten CX mit transparentem ALI. (b) Schräge frontale Ansicht auf einen sagittalen Schnitt der Rekonstruktion des CX mit ALI. (d) Schematische Darstellung der sagittalen Ansicht auf den CX mit Organisation der einzelnen Schichten. (e) Frontale Darstellung der drei-dimensionalen Rekonstruktion des LX und angrenzendem Rubus (RUB). AL, Antennallobus; BU, Bulbus; CA, Calyx; CBL, untere Einheit des CB; CBU, obere Einheit des CB; CO, Zapfen; GA, Gall; LLAL, unterer lateraler akzessorischer Lobus; ML, medialer Lobus; NOL, untere Einheit der Noduli; NOU, obere Einheit der Noduli; TH, Zähne; ULAL, oberer lateraler akzessorischer Lobus; PB, Protozerebralbrücke; PED, Pedunkulus; PRO, Zinken. Maßstäbe = 50 μm (b-e), 200 μm (a). (b-e) aus Jahn et al. (2023)

Die Neuroarchitektur des CX wurde schon in mehreren Insekten ausführlich untersucht. Zu diesen gehören die besonders intensiv untersuchte Heuschrecke *S. gregaria* (Heinze & Homberg, 2008; von Hadeln et al., 2020), sowie die Taufliege *D. melanogaster* (Hanesch et al., 1989; Hulse et al., 2021), aber auch die Mistkäfer *S. satyrus* und *lamarcki* (el Jundi et al., 2018), und die Hummel *B. terrestris* (Sayre et al., 2021). Die bisherigen Daten zeigen, dass die Organisation des CX über die Insektenspezies hinweg konserviert, wenn auch nicht identisch, zu sein scheint (Strausfeld, 2012; Gillet et al., 2023). In Projekt III dieser Arbeit wird dieses Wissen mit der umfassenden Kartierung von CX Neuronen in der Schabe *R. maderae* erweitert.

Folgend wird die CX Anatomie mit besonderem Augenmerk auf den CX in der Madeiraschabe *R. maderae* beschrieben. Die PB ist das am posteriorsten gelegene Neuropil des CX. Es ist ein langgezogenes Neuropil, dessen laterale Enden nach posterior gebogen sind. Beide Hemisphären sind über ein Faserbündel über die Mittellinie miteinander verbunden. Die PB ist in einzelne vertikale Kolumnen (auch Scheiben oder Glomeruli genannt) eingeteilt. Die Anzahl der Kolumnen variiert geringfügig über die Insektenspezies hinweg. So hat *R. maderae* 9 Scheiben pro Hemisphäre (Jahn et al., 2023), übereinstimmend mit der PB in der Hummel *B. terrestris* (Sayre et al., 2021), der Fliege *D. melanogaster* (Wolff et al., 2015) und der Wüstenheuschrecke *S. gregaria* (Hensgen et al., 2022), während bei Mistkäfern und dem Monarchfalter bisher 8 Scheiben bekannt sind (el Jundi et al., 2018; Heinze et al., 2013). Auch innerhalb der CBL und CBU findet man eine vertikale Ordnung, wobei die CBU, CBL und die NO auch eine horizontale Unterteilung aufweisen. Die NO sind paarig angelegte Neuropile, ventral zum CB gelegen. Sie scheinen nur bei pterygoten Insekten vorzukommen und sind meist unterteilt in eine obere und untere Einheit, wobei die Obere oft in weitere Unterschichten unterteilt ist, wie in *S. gregaria* (Heinze & Homberg, 2008), *S. satyrus* und *lamarcki* (Immonen et al., 2017; Wolff et al., 2015; Hulse et al., 2021). Dies ist auch in der Schabe *R. maderae* zu beobachten, in der die obere Einheit in drei horizontale Schichten geteilt ist und die kleinere untere Einheit ungeteilt ventral dazu liegt (Althaus et al., 2022; Jahn et al., 2023).

Die CBU in der Schabe lässt sich in drei horizontale Schichten einteilen (Schulze et al., 2012; Homberg et al., 2018; Timm et al., 2021; Jahn et al., 2023), ähnlich wie in der Hummel *B. terrestris* (Sayre et al., 2021) und Heuschrecke *S. gregaria* (Heinze & Homberg, 2008), dagegen ist der ‚fan-shaped body' (äquivalent zur CBU) in der Fliege *D. melanogaster* in neun Schichten geteilt (Wolff et al., 2015). In *H. membranacea* konnte noch keine horizontale Schichtung identifiziert werden, dafür aber eine vertikale Einteilung in 5 Kolumnen pro Hemisphäre (Rosner et al., 2017). In der Schabe wurden zwei Systeme von kolumnären Neuronen identifiziert, die zwei Organisationen von vertikaler Schichtung herbeiführen, einmal in 8 Scheiben (4 pro Hemisphäre) über die gesamte CBU und einmal

9 Scheiben (Jahn et al., 2023). Es zeigt damit ein ähnliches System wie das in der Taufliege *D. melanogaster* (Hulse et al., 2021)*.*

Auch die CBL weist in vielen Insekten eine horizontale und vertikale Schichtung auf, wie in der Heuschrecke *S. gregaria* (Heinze & Homberg, 2008), der Taufliege *D. melanogaster* (Hulse et al., 2021) oder den Mistkäfern *S. lamarcki* und *satyrus* (el Jundi et al., 2018; Immonen et al., 2017). Die CBL der Schabe *R. maderae* scheint dagegen auffällig zu sein und zeigt hauptsächlich eine vertikale Aufteilung in stark abgegrenzte Unterteilungen. Diese sogenannten 8 Zähne und 9 Zapfen über die gesamte CBL hinweg konnten bisher nicht weiter in horizontale Schichten unterteilt werden (Homberg et al., 2018; Jahn et al., 2023).

Eine prominente Ausgangsregion für den CX in einigen Insekten, besonders in *R. maderae*, ist die anteriore Lippe (ALI; Jahn et al., 2023). Sie wird offiziell nicht zu den Neuropilen des CX gerechnet, ist aber eng mit diesen vernetzt. Der ALI liegt anterior zum CB und ist ein langgezogenes mittellinienüberspannendes Neuropil. Dieses in der Schabe sehr prominente Neuropil (Althaus et al., 2022), konnte bisher nicht in *D. melanogaster* (Ito et al., 2014) identifiziert werden, ist aber aus der Heuschrecke *S. gregaria* (Heinze und Homberg, 2008; von Hadeln et al., 2018) und Gottesanbeterin *H. membranacea* (Althaus et al., Projekt II) bekannt sowie weniger stark ausgeprägt, in der Honigbiene *A. mellifera* (Hensgen et al., 2021a).

Lateraler Komplex

Der laterale Komplex (LX) ist eine wichtige Eingangs- und Ausgangsregion für den CX. Er besteht aus dem lateralen akzessorischen Lobus (LAL) und dem Bulbus (BU), die bilateral zum CX gelegen sind. Der BU ist in verschiedenen Insektenarten unterschiedlich komplex aufgebaut. In der Schabe *R. maderae* scheint er ungeteilt zu sein (Homberg et al., 2018; Althaus et al., 2022), dagegen ist er in der Heuschrecke *S. gregaria* räumlich getrennt in medialen und lateralen BU (Träger et al., 2008; Hensgen et al., 2021b). Der BU ist spezies-übergreifend GABA-immunoreaktiv und ist innerviert von tangentialen Neuronen aus der CBL.

Der LAL ist unterteilt in den oberen (ULAL) und unteren (LLAL) Teil, was nicht nur in *R. maderae* (Althaus et al., 2022; Jahn et al., 2023) zu beobachten ist, sondern auch über andere Insektenspezies konserviert zu sein scheint (*D. melanogaster*: Ito et al., 2014; Hulse et al., 2021; *S. gregaria*: Hensgen et al., 2021b; *H. membranacea*: Althaus et al., Projekt II; *S. lamarcki* und *S. satyrus*: Immonen et al., 2017). Die beiden Untereinheiten werden maßgeblich durch drei prominente Trakte voneinander getrennt, den Isthmustrakt, die LAL Kommissur und den medialen Antennallobustrakt (Ito et al., 2014; Hensgen et al., 2021b; Althaus et al., 2022; Jahn et al., 2023). Der LAL ist nicht nur stark mit den Neuropilen des CX verknüpft, sondern bekommt auch eine Vielfalt an Informationen aus anderen

Gehirnbereichen, unter anderem bekommt er Eingang durch sensorische Neurone. Aus *D. melanogaster* ist bekannt, dass absteigende Neurone Informationen aus dem LAL weiterleiten und involviert sind in die Steuerung der Motorik des Tieres (Namiki et al., 2018).

Erstmalig in der *R. maderae* in Althaus et al. (2022) wurder der prong (PRO) beschrieben als zusätzliche Unterteilung des LALs. Dieser ist auffällig Synapsin-reich und beinhaltet die Verzweigungsregionen von kolumnären Neuronen aus der CBU. Ein der Crepine (CRE) zugeordnetes Neuropil, der Rubus (RUB), ist direkt an den LX anliegend. Er wurde bisher nur in der Taufliege *D. melanogaster* (Wolff et al., 2015; Hulse et al., 2021) und Schabe *R. maderae* (Althaus et al., 2022; Jahn et al., 2023) identifiziert und wird von kolumnären Neuronen der CBU innerviert. Seine funktionelle Einordnung ist bisher noch nicht weiter erforscht.

Zentralkomplexneurone

Die Neuroanatomie des CX ist geprägt durch unterschiedliche Neuronenklassen, die innerhalb des CX verzweigen, sogenannte Zentralkomplexneurone. Drei Haupttypen von Neuronen werden unterschieden: tangentiale, kolumnäre und pontine Neurone.

Tangentiale Neurone

Tangentiale Neurone liefern die Haupteingangssignale an den CX. Sie innervieren einzelne Schichten innerhalb der CX Neuropile, wodurch Informationen aus vielen unterschiedlichen Gehirnregionen in den CX gelangen (Hanesch et al., 1989; Honkanen et al., 2019; von Hadeln et al., 2020; Hulse et al., 2021; Abbildung 4).
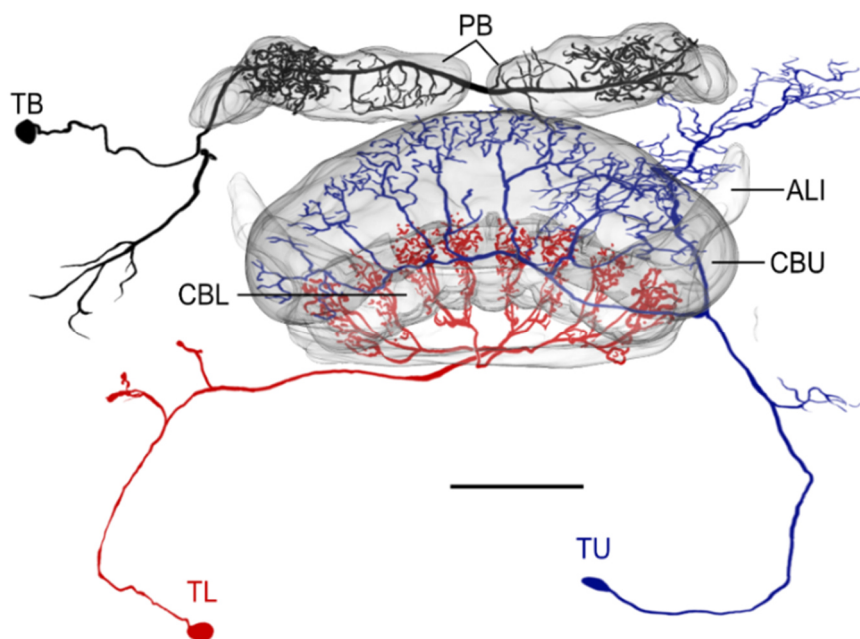

Abbildung 4: Beispiele tangentialer Neurone des Zentralkomplexes aus der Schabe Rhyparobia maderae. Posteriore Ansicht eines tangentialen Neurons der Protozerebralbrücke (TB Neuron), der oberen (TU Neuron) und unteren Einheit (TL Neuron) des Zentralkörpers, dargestellt in einer semi-transparenten dreidimensionalen Rekonstruktion des Zentralkörpers, der Protozerebralbrücke (PB) und der anterioren Lippe (ALI). CBL, untere Einheit des Zentralkörpers; CBU, obere Einheit des Zentralkörpers. Maßstab: 50 µm

Insbesondere tangentiale Neurone der CBU (TU Neurone; Abbildung 4) erhalten Eingang von einer Vielzahl unterschiedlicher Neuropile (von Hadeln et al., 2020; Hensgen et al., 2021a) und können dadurch Informationen aus unterschiedlichsten Bereichen in den CX transportieren und dort gebündelt weiter prozessieren. TU Neurone stellen somit eine der umfangreichsten und vielfältigsten Neuronengruppen innerhalb des CX dar (von Hadeln et al., 2021). Tangentiale Neurone der CBL (TL Neurone; Abbildung 4) liefern sensorische Informationen, aus dem LX in die CBL (Omoto et al., 2017; von Hadeln et al., 2021; Pfeiffer, 2023). Hierbei handelt es sich hauptsächlich um visuelle Informationen (Vitzthum et al., 2002; el Jundi et al., 2014), aber auch Informationen aus den Antennen, die an den CX weitergegeben werden (Okubo et al., 2020). Diese Neurone liefern Information über den Sonnenazimut und werden azimutabhängig, sowohl durch direktes Sonnenlicht, als auch indirekt durch das von der Sonne erzeugte Polarisationsmuster des Himmels erregt (Hardcastle et al., 2021; Takahashi et al., 2022; Nguyen et al., 2022). Durch die Verzweigungsmuster innerhalb der CBL bilden sie dort die horizontale Organisation des Neuropils (von Hadeln et al., 2020).

Tangentiale Neurone mit Projektionen in einzelnen Schichten des NO werden als TN Neurone bezeichnet (Müller et al., 1997; Stone et al., 2017; von Hadeln et al., 2020). Sie geben Informationen über Rotations- und Translationsgeschwindigkeiten an den CX weiter (Lyu et al., 2022). Input bekommen die Neurone aus unterschiedlichen Neuropilen innerhalb des Protocerebrums (Wolff & Rubin, 2018; von Hadeln et al., 2020; Hensgen et al., 2021a). Die letzte Kategorie der tangentialen Neurone bilden die TB Neurone, welche unterschiedliche Scheiben der PB innervieren und miteinander verbinden (Abbildung 4). Sie verzweigen zusätzlich im posterioren optischen Tuberkel (POTU) oder in anderen Bereichen des Protocerebrums (Pfeiffer & Homberg, 2014; von Hadeln et al., 2020). Bestimmte Subtypen von TB Neuronen (TB1 und TB2 Neurone) sind an der Etablierung einer topographischen Kodierung der Kopfrichtung relativ zum Sonnenazimut in den 18 Kolumnen der PB beteiligt. Dabei wird die unterschiedliche Ausrichtung des Polarisationswinkels und des Sonnenazimuts topographisch über die Scheiben der PB repräsentiert (Heinze & Homberg, 2007; Pegel et al., 2019; Homberg et al., 2022).

Weitere Neurone des CX, die auch zur vertikalen Organisation des CX beitragen, sind pontine und kolumnäre Neurone.

Pontine Neurone

Pontine Neurone (POU, oder in *D. melanogaster* hΔ Zellen) sind Neurone innerhalb der CBU, welche Scheiben über die Mittellinie hinweg miteinander verbinden. Eine Besonderheit, bisher nur identifiziert in *D. melanogaster* (Hulse et al., 2021) und jetzt auch durch eine Einzelzellfärbung in der Schabe *R. maderae,* sind vertikale POU Neurone (Jahn et al., 2023). Diese verbinden unterschiedliche Schichten innerhalb einer Scheibe miteinander.

In *R. maderae* konnten die POU Neurone in drei Gruppen unterteilt werden (POU 1-3; Jahn et al., 2023), ähnlich zu der Einteilung innerhalb der Wüstenheuschrecke *S. gregaria* (Heinze & Homberg, 2008). Als Kriterien zur Einteilung dieser Untergruppierungen wurden die unterschiedlichen Innervierungsregionen innerhalb der CBU, die Somaposition und der Verlauf des Hauptneurites genutzt. Die vermutete Funktion von pontinen Neuronen liegt im horizontalen Aktivitäts-Shift über die Mittellinie hinweg auf die andere Seite des CB. Sie sind Zielneurone von kolumnären Neuronen mit Innervierungen innerhalb des NO (CPU4/5; PFN in *D. melanogaster*), welche involviert sind in der Verarbeitung von Informationen der Kopfrichtung und Translationsgeschwindigkeit (Sayre et al., 2021).

Kolumnäre Neurone

Kolumnäre Neurone verknüpfen einzelne vertikale Scheiben der PB und/oder des CB mit den NO (Abbildung 5a, b) und anderen unterschiedlichen Neuropilen innerhalb des Protocerebrums, häufig innerhalb des LX. Sie bilden in der Regel ein Set aus acht oder neun Neuronen innerhalb einer Hemisphäre, welches sich auch in der vertikalen Schichtung des CB und der PB widerspiegelt (Heinze & Homberg, 2008; Sayre et al., 2021; Jahn et al., 2023).
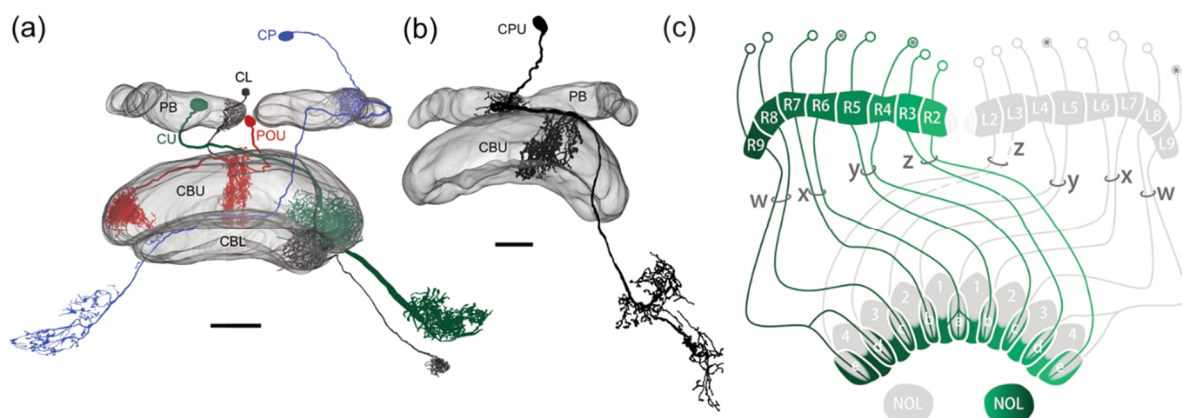

Abbildung 5: Darstellung kolumnärer und pontiner Neuronentypen im Zentralkomplex der Schabe *Rhyparobia maderae*. Dreidimensional rekonstruierte Neurone im semi-transparenten Zentralkomplex dargestellt. (a) Anteriore Ansicht eines pontinen Neurons (POU; rot) und kolumnäre Neurone der Protozerebralbrücke (CP Neuron; blau), der unteren (CBL) Einheit des Zentralkörpers (CL Neuron; schwarz) und der oberen (CBU) Einheit des Zentralkörpers (CU Neuron; grün). (b) Anteriore Ansicht des kolumnären Neurons der Protozerebralbrücke (PB) und der CBU (CPU Neuron; schwarz). Maßstäbe: 50 μm. (c) Schematische Darstellung der Verzweigungsmuster von CL2 Neuronen in der Madeiraschabe zur Darstellung der w-, x-, y- und z-Bündel (aus Jahn et al., 2023). NOL, untere Einheit der Noduli.

Die Somata der kolumnären Neurone befinden sich dorsal vom CX in der Pars intercerebralis. Von diesem Punkt aus erstrecken sich ihre Neurite ventral in Richtung PB, wobei sie sich teilweise in dieser verzweigen. Ventral zur PB bilden die Fasern acht Bündel, das w-, x-, y- und z-Bündel (Abbildung 5c), welche bilateral symmetrisch zur Mittellinie hin in Richtung CB verlaufen (Williams, 1975). Kolumnäre Neurone lassen sich in vier Kategorien einteilen, welche in den meisten untersuchten Spezies weitere Untergruppierungen besitzen.

Kolumnäre Neurone der CBL, auch als CL Neurone bezeichnet, verzweigen in der CBL und projizieren weiter in die PB, sowie den Gall (CL1 Neurone; E-PG in *D. melanogaster*) oder in die untere Einheit der NO (CL2 Neurone; PEN in *D. melanogaster*; Heinze & Homberg, 2008; Hulse et al., 2021; Jahn et al., 2023; Abbildung 6). CL1 Neurone empfangen Kopfrichtungssignale von TL Neuronen in der CBL und senden diese weiter in die PB. In *D. melanogaster* erzeugen Populationen von E-PG Neuronen (CL1 in anderen Insekten) ein einzelnes Aktivitätsmaximum („bump") innerhalb der CBL, dessen Position die Kopfrichtung und Rotation des Tieres repräsentiert, während es durch die Weiterleitung der Information an die PB dort zu zwei Aktivitätsmaxima kommt (Abbildung 7). Bei CL2 Neuronen geht man davon aus, dass sie Inputsignale in der PB und in den NO erhalten, und so Informationen über die Selbstrotation an die CBL weiterleiten, die von CL1 Neurone für die Bestimmung der Kopfrichtung des Tieres benötigt werden (Seelig & Jayaraman, 2015; Turner-Evans et al., 2017; Honkanen et al., 2019).
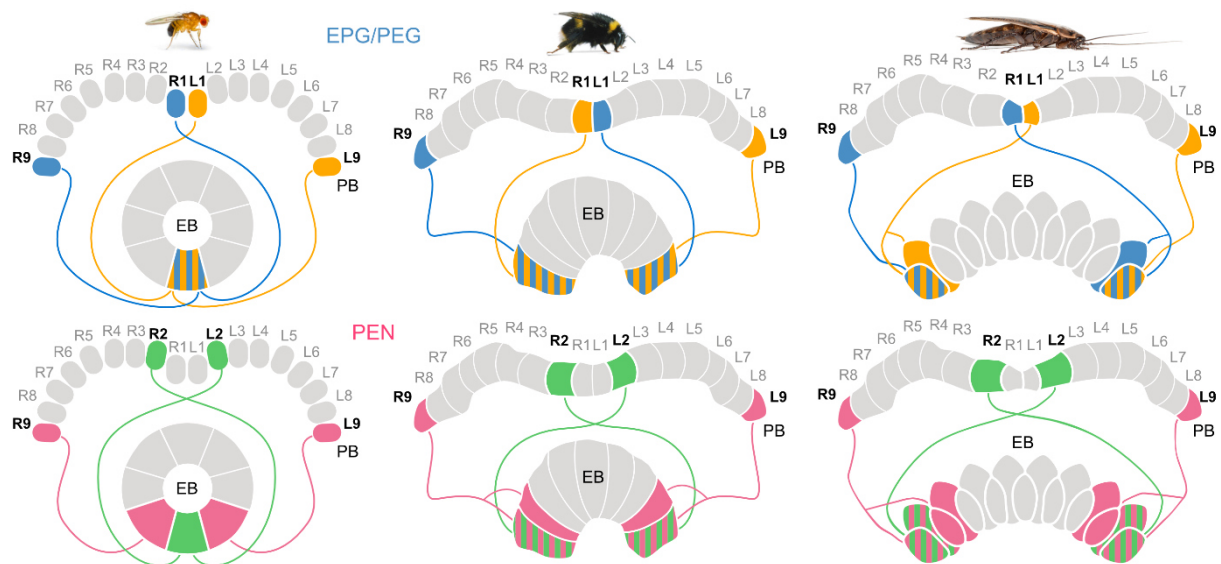

Abbildung 6: Verzweigungsmuster in drei unterschiedlichen Insektenspezies (*Drosophila melanogaster,* links; *Bombus terrestris*, Mitte; *Rhyparobia maderae*, rechts) von EPG/CL1 Neuronen (blau und gelb) und PEN/CL2 Neuronen (grün und magenta). Gestreifte Bereiche weisen auf überlappende Verzweigungsbereiche hin. CBL, untere Einheit des Zentralkörpers; EB, ellipsoid body; PB, Protozerebralbrücke (modifiziert nach Sayre et al., 2021).

Dreht die Fliege ihren Kopf, kommt es zu einer Verschiebung der Aktivität innerhalb der CBL und PB, deren Orientierung die Kopfrichtung widerspiegelt (Seelig & Jayaraman, 2015; Zittrell et al., 2023). CL1 und CL2 Neurone, die in der gleichen Scheibe der PB verzweigen, verzweigen in benachbarten Kolumnen der CBL (Abbildung 6). Dies führt zu einem Offset zwischen den Verzweigungspunkten der Neurone innerhalb der CBL und erlaubt damit einen Aktivitätsshift innerhalb des CX, der im und entgegen dem Uhrzeigersinn laufen kann, wenn das Insekt seinen Kopf dreht (Seelig & Jayaraman, 2015; Turner-Evans et al., 2017; Honkanen et al., 2019; Abbildung 7).
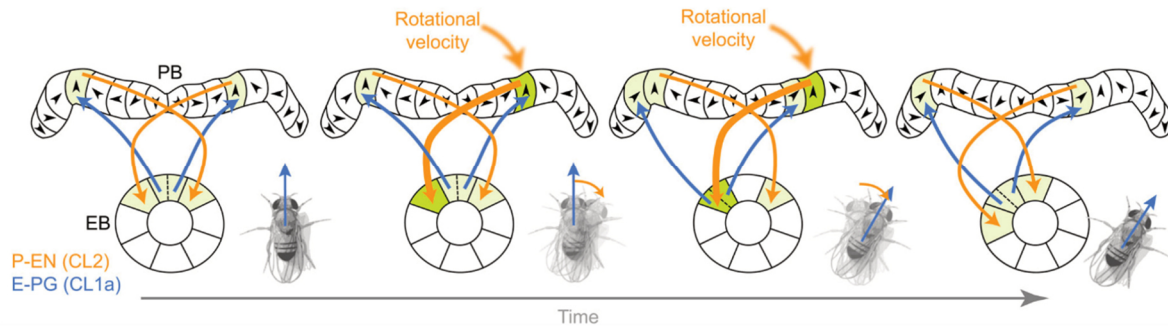
Abbildung 7: Schematische Darstellung der Aktivitätsmaxima innerhalb des Ellipsoidkörpers (EB) und der Protocerebralbrücke (PB) in der Fliege *Drosophila melanogaster*. P-EN Neurone senden Informationen zu Selbstrotations aus der PB (und den Noduli) in die EB. E-PG Neurone erzeugen ein einzelnes Aktivitätsmaximum innerhalb der EB, dessen Position die Kopfrichtung des Tieres repräsentiert und senden diese Informationen an die PB, wo es zu einem Aktivitätshoch innerhalb einer Kolumne pro Hemisphäre kommt. P-EN und E-PG die in der gleichen Scheibe der PB verzweigen, verzweigen in benachbarten Kolumnen der EB, dadurch kommt es zu einem Offset zwischen den Neuronen innerhalb der EB, dies erlaubt einen Aktivitätsshift innerhalb der EB. Dreht die Fliege ihren Kopf kommt es zu einer Verschiebung des Aktivitätshoch innerhalb des Zentralkomplexes in entgegengesetzter Richtung. (aus Honkanen et al., 2019)

CPU Neurone verbinden meist eine Kolumne der PB mit Kolumnen der CBU. Von dort aus zieht der Neurit weiter, entweder in Bereiche des LALs (CPU1 und 2 Neurone), den NO (CPU4 und 5 Neurone) oder ohne weitere Verzweigungen (CPU3 Neurone; Heinze & Homberg; 2008). CPU 1 und 2 Neurone (entsprechen PFL1 und 2 Neuronen in *D. melanogaster*; Hulse et al., 2021) sind Teil des Himmelskompass-Netzwerkes im CX (Heinze et al., 2009; el Jundi et al., 2015; Zittrell et al., 2020). Beide Neuronentypen in *R. maderae* haben breite Verzweigungen innerhalb des LALs (Jahn et al., 2023). CPU4 und 5 Neurone (entsprechen PFNv und PFNd Neuronen in *D. melanogaster*; Hulse et al., 2021) übernehmen zusammen mit hΔ-Zellen (POU Neurone in anderen Insektenarten) eine wichtige Funktion bei der Umwandlung von egozentrischen Bewegungen in einen räumlichen Kontext (Lu et al., 2020; Lyu et al., 2022).

Kolumnäre Neurone der CBU, auch als CU Neurone bezeichnet, verbinden die CBU mit unterschiedlichen Bereichen der CRE, Teile des LALs und dem ALI. Eine kleine Region der CRE, der Rubus (RUB) wurde bisher nur in der Fliege *D. melanogaster* (Hulse et al., 2021) beschrieben und von Jahn et al. (2023) erstmals auch in einem anderen Insekt, der Schabe, identifiziert (CU2c Neuron*). CU Neurone scheinen in *R. maderae* sehr umfangreich und vielfältig vorhanden zu sein (Jahn et al., 2023), während in der Honigbiene *A. mellifera* (Hensgen et al., 2021a), der Hummel *B. terrestris* (Sayre et al., 2021) oder im Mistkäfer *S. lamarcki* und *satyrus* (el Jundi et al., 2018) bisher keine CU Neurone bekannt sind. In *D. melanogaster* liefern CU Neurone (FC und FR Neurone in *D. melanogaster*) Eingangssignale an CPU Neurone. Aufgrund dessen vermutet Hulse et al. (2021), dass sie involviert sein könnten in die Anpassung von Verhalten zur Selbstausrichtung. CU Neurone in *R. maderae* sind, vergleichbar mit den anderen kolumnären Neuronen in der Schabe, oft stark mit dem ALI vernetzt (Jahn et al., 2023).

CP Neurone sind kolumnäre Neurone der PB ohne Verzweigungen im CB. Sie verbinden die PB mit Bereichen außerhalb des CX. In der Schabe innervieren die CP Neurone den Bereich um den Gall herum und der CP2-2 Typ mit zusätzlichen Verzweigungen in der CBL (Jahn et al., 2023). Während CP Neurone auch bei der Heuschrecke (Heinze & Homberg, 2008) und bei Mistkäfern vorkommen (el Jundi et al., 2018) sind in der Fliege *D. melanogaster* dagegen keine CP Neurone bekannt (Hulse et al., 2021). CP Neurone, CL1 und CL2, sowie CPU1 und CPU2 Neurone zählen zu den Hauptprozessierungsneuronen der Polarisationssehbahn von Heuschrecken (Heinze und Homberg, 2009).

Referenzen

Althaus, V., Jahn, S., Massah, A., Stengl, M., & Homberg, U. (2022). 3D-atlas of the brain of the cockroach *Rhyparobia maderae*. *Journal of Comparative Neurology 530*, 3126–3156. https://doi.org/10.1002/cne.25396

Arnold, T., Korek, S., Massah, A., Eschstruth, D., & Stengl, M. (2020). Candidates for photic entrainment pathways to the circadian clock via optic lobe neuropils in the Madeira cockroach. *Journal of Comparative Neurology 528*, 1754–1774. https://doi.org/10.1002/cne.24844

Aubele, E., & Klemm, N. (1977). Origin, destination and mapping of tritocerebral neurons of locust. *Cell and Tissue Research 178*, 199–219. https://doi.org/10.1007/BF00219048

Baba, Y., Tsukada, A., & Comer, C. M. (2010). Collision avoidance by running insects: antennal guidance in cockroaches. *Journal of Experimental Biology 213*, 2294–2302. https://doi.org/10.1242/jeb.036996

Bender, J. A., Pollack, A. J., & Ritzmann, R. E. (2010). Neural activity in the central complex of the insect brain is linked to locomotor changes. *Current Biology 20*, 921–926. https://doi.org/10.1016/j.cub.2010.03.054

Bernard, T., & Womeni, H. M. (2017). Entomophagy insects as food. *Insect Physiology and Ecology*, 233–249.

Boeckh, J., Ernst, K.-D., & Selsam, P. (1987). Neurophysiology and neuroanatomy of the olfactory pathway in the cockroach. *Annals of the New York Academy of Sciences 510*, 39–43. https://doi.org/10.1111/j.1749-6632.1987.tb43464.x

Christensen, T. A., & Hildebrand, J. G. (1987). Male-specific, sex pheromone-selective projection neurons in the antennal lobes of the moth *Manduca sexta*. *Journal of Comparative Physiology A 160*, 553–569. https://doi.org/10.1007/BF00611929

Dijkstra, K.-D. B., Monaghan, M. T., & Pauls, S. U. (2014). Freshwater biodiversity and aquatic insect diversification. *Annual Review of Entomology 59*, 143–163. https://doi.org/10.1146/annurev-ento-011613-161958

el Jundi, B., Pfeiffer, K., Heinze, S., & Homberg, U. (2014). Integration of polarization and chromatic cues in the insect sky compass. *Journal of Comparative Physiology A 200*, 575–589. https://doi.org/10.1007/s00359-014-0890-6

el Jundi, B., Warrant, E. J., Byrne, M. J., Khaldy, L., Baird, E., Smolka, J., & Dacke, M. (2015). Neural coding underlying the cue preference for celestial orientation. *Proceedings of the National Academy of Sciences 112*, 11395–11400. https://doi.org/10.1073/pnas.1501272112

el Jundi, B., Warrant, E. J., Pfeiffer, K., & Dacke, M. (2018). Neuroarchitecture of the dung beetle central complex. *Journal of Comparative Neurology 526*, 2612–2630. https://doi.org/10.1002/cne.24520

el Jundi, B., Baird, E., Byrne, M. J., & Dacke, M. (2019). The brain behind straight-line orientation in dung beetles. *Journal of Experimental Biology 222*, jeb192450. https://doi.org/10.1242/jeb.192450

Fabricius, J. C. (1781). Ioh. Christ. Fabricii histor. nat. oecon. et cameral. prof. Kiloniens ... Species insectorum : exhibentes eorum differentias specificas, synonyma auctorum, loca natalia, metamorphosin : adiectis observationibus, descriptionibus. *Hamburgi et Kilonii, Impensis Carol. Ernest. Bohnii, MDCCLXXXI [1781]*.

Farris, S. M. (2008). Tritocerebral tract input to the insect mushroom bodies. *Arthropod Structure & Development 37*, 492–503. https://doi.org/10.1016/j.asd.2008.05.005

Fuscà, D., & Kloppenburg, P. (2021). Odor processing in the cockroach antennal lobe—the network components. *Cell and Tissue Research 383*, 59–73. https://doi.org/10.1007/s00441-020-03387-3

Gillet, V., Kluge, J., & Patel, R. N. (2023). A historical perspective on the insect central complex: Anatomy, development, and function. *Molecular Psychology: Brain, Behavior, and Society 2*, 19. https://doi.org/10.12688/molpsychol.17564.1

Grandcolas, P., & Grandcolas, P. (1997). The origin of biodiversity in insects: phylogenetic tests of evolutionary scenarios. *Muséum national d'Histoire naturelle*, 1–345.

Grimaldi, D. A., & Engel, M. S. (2005). Evolution of the insects. Cambridge. *Cambridge University Press*.

Hanesch, U., Fischbach, K.-F., & Heisenberg, M. (1989). Neuronal architecture of the central complex in *Drosophila melanogaster*. *Cell and Tissue Research 257*, 343–366. https://doi.org/10.1007/BF00261838

Hardcastle, B. J., Omoto, J. J., Kandimalla, P., Nguyen, B. C. M., Keleş, M. F., Boyd, N. K., Hartenstein, V., & Frye, M. A. (2021). A visual pathway for skylight polarization processing in *Drosophila*. *Elife 10*, e63225. https://doi.org/10.7554/eLife.63225

Heimonen, K., Salmela, I., Kontiokari, P., & Weckström, M. (2006). Large functional variability in cockroach photoreceptors: Optimization to low light levels. *Journal of Neuroscience 26*, 13454–13462. https://doi.org/10.1523/JNEUROSCI.3767-06.2006

Heinze, S. (2023). The Insect Central Complex. In *Oxford Research Encyclopedia of Neuroscience*. https://doi.org/10.1093/acrefore/9780190264086.013.286

Heinze, S., Florman, J., Asokaraj, S., El Jundi, B., & Reppert, S. M. (2013). Anatomical basis of sun compass navigation II: the neuronal composition of the central complex of the monarch butterfly. *Journal of Comparative Neurology 521*, 267–298. https://doi.org/10.1002/cne.23214

Heinze, S., & Homberg, U. (2007). Maplike representation of celestial *E*-vector orientations in the brain of an insect. *Science 315*, 995–997. https://doi.org/10.1126/science.1135531

Heinze, S., & Homberg, U. (2008). Neuroarchitecture of the central complex of the desert locust: intrinsic and columnar neurons. *Journal of Comparative Neurology 511*, 454–478. https://doi.org/10.1002/cne.21842

Hensgen, R., England, L., Homberg, U., & Pfeiffer, K. (2021a). Neuroarchitecture of the central complex in the brain of the honeybee: Neuronal cell types. *Journal of Comparative Neurology 529*, 159–186. https://doi.org/10.1002/cne.24941

Hensgen, R., Göthe, J., Jahn, S., Hümmert, S., Schneider, K. L., Takahashi, N., Pegel, U., Gotthardt, S., & Homberg, U. (2021b). Organization and neural connections of the lateral complex in the brain of the desert locust. *Journal of Comparative Neurology 529*, 3533–3560. https://doi.org/10.1002/cne.25209

Hensgen, R., Dippel, S., Hümmert, S., Jahn, S., Seyfarth, J., & Homberg, U. (2022). Myoinhibitory peptides in the central complex of the locust *Schistocerca gregaria* and colocalization with locustatachykinin-related peptides. *Journal of Comparative Neurology 530*, 2782–2801. https://doi.org/10.1002/cne.25374

Heisenberg, M. (1998). What do the mushroom bodies do for the insect brain? An introduction. *Learning & Memory 5*, 1–10. https://doi.org/10.1101/lm.5.1.1

Homberg, U. (2004). In search of the sky compass in the insect brain. *Naturwissenschaften 91*, 199–208. https://doi.org/10.1007/s00114-004-0525-9

Homberg, U., Christensen, T. A., & Hildebrand, J. G. (1989). Structure and function of the deutocerebrum in insects. *Annual Review of Entomology 34*, 477–501. https://doi.org/10.1146/annurev.en.34.010189.002401

Homberg, U., Hensgen, R., Jahn, S., Pegel, U., Takahashi, N., Zittrell, F., & Pfeiffer, K. (2022). The sky compass network in the brain of the desert locust. *Journal of Comparative Physiology A*, 1–22. https://doi.org/10.1007/s00359-022-01601-x

Homberg, U., Humberg, T. H., Seyfarth, J., Bode, K., & Pérez, M. Q. (2018). GABA immunostaining in the central complex of dicondylian insects. *Journal of Comparative Neurology 526*, 2301–2318. https://doi.org/10.1002/cne.24497

Homberg, U., Reischig, T., & Stengl, M. (2003). Neural organization of the circadian system of the cockroach *Leucophaea maderae*. *Chronobiology International 20*, 577–591. https://doi.org/10.1081/CBI-120022412

Homberg, U., Hensgen, R., Jahn, S., Pegel, U., Takahashi, N., Zittrell, F., & Pfeiffer, K. (2022). The sky compass network in the brain of the desert locust. *Journal of Comparative Physiology A*, 1–22. https://doi.org/10.1007/s00359-022-01601-x

Honkanen, A., Adden, A., da Silva Freitas, J., & Heinze, S. (2019). The insect central complex and the neural basis of navigational strategies. *Journal of Experimental Biology 222*, jeb188854. https://doi.org/10.1242/jeb.188854

Hösl, M. (1990). Pheromone-sensitive neurons in the deutocerebrum of *Periplaneta americana*: receptive fields on the antenna. *Journal of Comparative Physiology A 167*, 321–327. https://doi.org/10.1007/BF00192567

Hulse, B. K., Haberkern, H., Franconville, R., Turner-Evans, D., Takemura, S. Y., Wolff, T., Noorman, M., Dreher, M., Dan, C., Parekh, R., Hermundstad, A. M., Rubin, G. M., & Jayaraman, V. (2021). A connectome of the *Drosophila* central complex reveals network motifs suitable for flexible navigation and context-dependent action selection. *Elife 10*. https://doi.org/10.7554%2FeLife.66039

Ignell, R., Dekker, T., Ghaninia, M., & Hansson, B. S. (2005). Neuronal architecture of the mosquito deutocerebrum. *Journal of Comparative Neurology 493*, 207–240. https://doi.org/10.1002/cne.20800

Immonen, E. V., Dacke, M., Heinze, S., & el Jundi, B. (2017). Anatomical organization of the brain of a diurnal and a nocturnal dung beetle. *Journal of Comparative Neurology 525*, 1879–1908. https://doi.org/10.1002/cne.24169

Ito, K., Shinomiya, K., Ito, M., Armstrong, J. D., Boyan, G., Hartenstein, V., Harzsch, S., Heisenberg, M., Homberg, U., Jenett, A., Keshishian, H., Restifo, L. L., Rössler, W., Simpson, J. H., Strausfeld, N. J., Strauss, R., & Vosshall, L. B. (2014). A systematic nomenclature for the insect brain. *Neuron 81*, 755–765. http://dx.doi.org/10.1016/j.neuron.2013.12.017

Jahn, S., Althaus, V., Heckmann, J., Janning, M., Seip, A.-K., Takahashi, N., Grigoriev, C., Kolano, J., & Homberg, U. (2023). Neuroarchitecture of the central complex in the Madeira cockroach *Rhyparobia maderae*: Pontine and columnar neuronal cell types. *Journal of Comparative Neurology 531*, 1689–1714. https://doi.org/10.1002/cne.25535

Kral, K., & Prete, F. R. (1999). In the mind of a hunter: The visual world of the praying mantis. In F. R. Prete (Ed.). Complex worlds from simpler nervous systems (pp. 75–115). Cambridge: MIT Press.

Kristensen, N. P. (1999). Phylogeny of endopterygote insects, the most successful lineage of living organisms. *European Journal of Entomology 96*, 237–253.

Lu, J., Behbahani, A. H., Hamburg, L., Westeinde, E. A., Dawson, P. M., Lyu, C., Maimon, G., Dickinson, M. H., Druckmann, S., & Wilson, R. I. (2022). Transforming representations of movement from body-to world-centric space. *Nature 601*, 98–104. https://doi.org/10.1038/s41586-021-04191-x

Loesel, R., & Homberg, U. (2001). Anatomy and physiology of neurons with processes in the accessory medulla of the cockroach *Leucophaea maderae*. *Journal of Comparative Neurology 439*, 193–207. https://doi.org/10.1002/cne.1342

Loesel, R., Wolf, H., Kenning, M., Harzsch, S., & Sombke, A. (2013). Architectural principles and evolution of the arthropod central nervous system. *Arthropod Biology and Evolution: Molecules, Development, Morphology* 299–342. https://doi.org/10.1007/978-3-642-36160-9_13

Lyu, C., Abbott, L. F., & Maimon, G. (2022). Building an allocentric travelling direction signal via vector computation. *Nature 601*, 92–97. https://doi.org/10.1038/s41586-021-04067-0

Malun, D., Waldow, U., Kraus, D., & Boeckh, J. (1993). Connections between the deutocerebrum and the protocerebrum, and neuroanatomy of several classes of deutocerebral projection neurons in the brain of male *Periplaneta americana*. *Journal of Comparative Neurology 329*, 143–162. https://doi.org/10.1002/cne.903290202

Misof, B., Liu, S., Meusemann, K., Peters, R. S., Donath, A., Mayer, C., Frandsen, P. B., Ware, J., Flouri, T., Beutel, R. G., Niehuis, O., Petersen, M., Izquierdo-Carrasco, F., Wappler, T., Rust, J., Aberer, A. J., Aspöck, U., Aspöck, H., Bartel, D., Blanke, A., Berger, S., Böhm, A., Buckley, T. R., Calcott, B., Chen, J., Friedrich, F., Fukui, M., Fujita, M., Greve, C., Grobe, P., Gu, S., Huang, Y., Jermiin, L. S., Kawahara, A. Y., Krogmann, L., Kubiak, M., Lanfear, R., Letsch, H., Li, Y., Li, Z., Li, J., Lu, H., Machida, R., Mashimo, Y., Kapli, P., McKenna, D. D., Meng, G., Nakagaki, Y., Navarrete-Heredia, J. L., Ott, M., Ou, Y., Pass, G., Podsiadlowski, L., Pohl, H., von Reumont, B. M., Schütte, K., Sekiya, K., Shimizu, S., Slipinski, A., Stamatakis, A., Song, W., Su, X., Szucsich, N. U., Tan, M., Tan, X., Tang, M., Tang, J., Timelthaler, G., Tomizuka, S., Trautwein, M., Tong, X., Uchifune, T., Walzl, M. G., Wiegmann, B. M., Wilbrandt, J., Wipfler, B., Wong, T. K. F., Wu, Q., Wu, G., Xie, Y., Yang, S., Yang, Q., Yeates, D. K., Yoshizawa, K., Zhang, Q., Zhang, R., Zhang, W., Zhang, Y., Zhao, J., Zhou, C., Zhou, L., Ziesmann, T., Zou, S., Li, Y., Xu, X., Zhang, Y., Yang, H., Wang, J., Wang, J., Kjer, K. M., & Zhou, X. (2014). Phylogenomics resolves the timing and pattern of insect evolution. *Science 346*, 763–767. https://doi.org/10.1126/science.1257570

Mizunami, M., Weibrecht, J. M., & Strausfeld, N. J. (1998). Mushroom bodies of the cockroach: their participation in place memory. *Journal of Comparative Neurology 402*, 520–537. https://doi.org/10.1002/(SICI)1096-9861(19981228)402:4%3C520::AID-CNE6%3E3.0.CO;2-K

Modi, M. N., Shuai, Y., & Turner, G. C. (2020). The *Drosophila* mushroom body: from architecture to algorithm in a learning circuit. *Annual Review of Neuroscience 43*, 465–484. https://doi.org/10.1146/annurev-neuro-080317-0621333

Müller, M., Homberg, U., & Kühn, A. (1997). Neuroarchitecture of the lower division of the central body in the brain of the locust (*Schistocerca gregaria*). *Cell and Tissue Research 288*, 159–176. https://doi.org/10.1007/s004410050803

Namiki, S., Dickinson, M. H., Wong, A. M., Korff, W., & Card, G. M. (2018). The functional organization of descending sensory-motor pathways in *Drosophila*. *Elife 7*, e34272. https://doi.org/10.7554/eLife.34272

Nguyen, T. A. T., Beetz, M. J., Merlin, C., Pfeiffer, K., & El Jundi, B. (2022). Weighting of celestial and terrestrial cues in the monarch butterfly central complex. *Frontiers in Neural Circuits 16*, 862279. https://doi.org/10.3389/fncir.2022.862279

Nityananda, V., Bissianna, G., Tarawneh, G., & Read, J. (2016a). Small or far away? Size and distance perception in the praying mantis. *Philosophical Transaction of the Royal Society B: Biological Sciences 371*, 20150262. https://doi.org/10.1098/rstb.2015.0262

Nityananda, V., Joubier, C., Tan, J., Tarawneh, G., & Read, J. C. A. (2019a). Motion-in-depth perception and prey capture in the praying mantis *Sphodromantis lineola*. *Journal of Experimental Biology 222*, jeb.198614. https://doi.org/10.1242/jeb.198614

Nityananda, V., O'Keeffe, J., Umeton, D., Simmons, A., & Read, J. C. A. (2019b). Second-order cues to figure motion enable object detection during prey capture by praying mantises. *Proceedings of the National Academy of Sciences 116*, 27018–27027. https://doi.org/10.1073/pnas.1912310116

Nityananda, V., Tarawneh, G., Rosner, R., Nicolas, J., Crichton, S., & Read, J. (2016b). Insect stereopsis demonstrated using a 3D insect cinema. *Scientific Reports 6*, 18718. https://doi.org/10.1038/srep18718

Ofstad, T. A., Zuker, C. S., & Reiser, M. B. (2011). Visual place learning in *Drosophila melanogaster*. *Nature 474*, 204–207. https://doi.org/10.1038/nature10131

Okada, J., & Toh, Y. (2000). The role of antennal hair plates in object-guided tactile orientation of the cockroach (*Periplaneta americana*). *Journal of Comparative Physiology A 186*, 849–857. https://doi.org/10.1007/s003590000137c

Okubo, T. S., Patella, P., D'Alessandro, I., & Wilson, R. I. (2020). A neural network for wind-guided compass navigation. *Neuron 107*, 924–940. https://doi.org/10.1016/j.neuron.2020.06.022

Omoto, J. J., Keleş, M. F., Nguyen, B. C. M., Bolanos, C., Lovick, J. K., Frye, M. A., & Hartenstein, V. (2017). Visual input to the *Drosophila* central complex by developmentally and functionally distinct neuronal populations. *Current Biology 27*, 1098–1110. http://dx.doi.org/10.1016/j.cub.2017.02.063

Page, T. L. (1982). Transplantation of the cockroach circadian pacemaker. *Science 216*, 73–75. https://doi.org/10.1126/science.216.4541.73

Page, T. L. (2009). Circadian regulation of olfaction and olfactory learning in the cockroach *Leucophaea maderae*. *Sleep and Biological Rhythms 7*, 152–161. https://doi.org/10.1111/j.1479-8425.2009.00409.x

Pegel, U., Pfeiffer, K., Zittrell, F., Scholtyssek, C., & Homberg, U. (2019). Two compasses in the central complex of the locust brain. *Journal of Neuroscience 39*, 3070–3080. https://doi.org/10.1523/JNEUROSCI.0940-18.2019

Pfeiffer, K. (2022). The neuronal building blocks of the navigational toolkit in the central complex of insects. *Current Opinion in Insect Science*, 100972. https://doi.org/10.1016/j.cois.2022.100972

Pfeiffer, K., & Homberg, U. (2014). Organization and functional roles of the central complex in the insect brain. *Annual Review of Entomology 59*, 165–184. https://doi.org/10.1146/annurev-ento-011613-162031

Prete, F. R. ed. (1999). *The praying mantids*. Johns Hopkins University Press.

Rajashekhar, K. P., & Singh, R. N. (1994). Neuroarchitecture of the tritocerebrum of *Drosophila melanogaster*. *Journal of Comparative Neurology 349*, 633–645. https://doi.org/10.1002/cne.903490410

Reischig, T., & Stengl, M. (2003). Ectopic transplantation of the accessory medulla restores circadian locomotor rhythms in arrhythmic cockroaches (*Leucophaea maderae*). *Journal of Experimental Biology 206*, 1877–1886. https://doi.org/10.1242/jeb.00373

Ritzmann, R. E., Harley, C. M., Daltorio, K. A., Tietz, B. R., Pollack, A. J., Bender, J. A., Guo, P., Horomanski, A. L., Kathman, N. D., Nieuwoudt, C., Brown, A. E., & Quinn, R. D. (2012). Deciding which way to go: How do insects alter movements to negotiate barriers? *Frontiers in Neuroscience 6*, 97. https://doi.org/10.3389/fnins.2012.00097

Rosner, R., von Hadeln, J., Salden, T., & Homberg, U. (2017). Anatomy of the lobula complex in the brain of the praying mantis compared to the lobula complexes of the locust and cockroach. *Journal of Comparative Neurology 525*, 2343–2357. https://doi.org/10.1002/cne.24208

Rosner, R., von Hadeln, J., Tarawneh, G., & Read, J. C. A. (2019). A neuronal correlate of insect stereopsis. *Nature Communications 10*, 2845. https://doi.org/10.1038/s41467-019-10721-z

Rosner, R., Tarawneh, G., Lukyanova, V., & Read, J. C. A. (2020). Binocular responsiveness of projection neurons of the praying mantis optic lobe in the frontal visual field. *Journal of Comparative Physiology A 206*, 165–181. https://doi.org/10.1007/s00359-020-01405-x

Rossel, S. (1979). Regional differences in photoreceptor performance in the eye of the praying mantis. *Journal of Comparative Physiology 131*, 95–112. https://doi.org/10.1007/BF00619070

Rossel, S. (1983). Binocular stereopsis in an insect. *Nature 302*, 821–822. https://doi.org/10.1038/302821a0

Sayre, M. E., Templin, R., Chavez, J., Kempenaers, J., & Heinze, S. (2021). A projectome of the bumblebee central complex. *Elife 10*, e68911. https://doi.org/10.7554/eLife.68911

Schafer, R. (1971). Antennal sense organs of the cockroach, *Leucophaea maderae*. *Journal of Morphology 134*, 91–103. https://doi.org/10.1002/jmor.1051340106

Schmidt-Rhaesa, A., Harzsch, S., & Purschke, G. (2016). Structure and evolution of invertebrate nervous systems. First edition. *Oxford University Press*.

Schulze, J., Neupert, S., Schmidt, L., Predel, R., Lamkemeyer, T., Homberg, U., & Stengl, M. (2012). Myoinhibitory peptides in the brain of the cockroach *Leucophaea maderae* and colocalization with pigment-dispersing factor in circadian pacemaker cells. *Journal of Comparative Neurology 520*, 1078–1097. https://doi.org/10.1002/cne.22785

Scudder, G. G. E. (2017). The importance of insects. In: Insect Biodiversity. Science and Society. Foottit, R. G., Adler, P. H., eds. *John Wiley & Sons*, 9–43.

Seelig, J. D., & Jayaraman, V. (2015). Neural dynamics for landmark orientation and angular path integration. *Nature 521*, 186–191. https://doi.org/10.1038/nature14446

Smarandache-Wellmann, C. R. (2016). Arthropod neurons and nervous system. *Current Biology 26*, R960–R965. https://doi.org/10.1016/j.cub.2016.07.063

Smith, D. S., & Treherne, J. E. (1963). Functional aspects of the organization of the insect nervous system. In: *Advances in Insect Physiology 1*, 401–484. Academic Press. https://doi.org/10.1016/S0065-2806(08)60179-4

Sreng, L. (1984). Morphology of the sternal and tergal glands producing the sexual pheromones and the aphrodisiacs among the cockroaches of the subfamily oxyhaloinae. *Journal of Morphology 182*, 279–294. https://doi.org/10.1002/jmor.1051820304

Stengl, M., & Arendt, A. (2016). Peptidergic circadian clock circuits in the Madeira cockroach. *Current Opinion in Neurobiology 41*, 44–52. https://doi.org/10.1016/j.conb.2016.07.010

Stengl, M., & Homberg. U. (1994). Pigment-dispersing hormone-immunoreactive neurons in the cockroach *Leucophaea maderae* share properties with circadian pacemaker neurons. *Journal of Comparative Physiology A 175*, 203–213. https://doi.org/10.1007/BF00215116

Stengl, M., Werckenthin, A., & Wei, H. (2015). How does the circadian clock tick in the Madeira cockroach? *Current Opinion in Insect Science 12*, 38–45. https://doi.org/10.1016/j.cois.2015.09.007

Stone, T., Webb, B., Adden, A., Weddig, N. B., Honkanen, A., Templin, R., Wcislo, W., Scimeca. L., Warrant, E., & Heinze, S. (2017). An anatomically constrained model for path integration in the bee brain. *Current Biology 27*, 3069–3085. https://doi.org/10.1016/j.cub.2017.08.052

Stopfer, M. (2014). Central processing in the mushroom bodies. *Current Opinion in Insect Science 6*, 99–103. https://doi.org/10.1016/j.cois.2014.10.009

Stork, N. E. (2018). How many species of insects and other terrestrial arthropods are there on earth? *Annual Review of Entomology 63*, 31–45. https://doi.org/10.1146/annurev-ento-020117- 043348

Strausfeld, N. J. (2012). *Arthropod brains: evolution, functional elegance, and historical significance.* Harvard University Press.

Takahashi, N., Zittrell, F., Hensgen, R., & Homberg, U. (2022). Receptive field structures for two celestial compass cues at the input stage of the central complex in the locust brain. *Journal of Experimental Biology 225*, jeb243858. https://doi.org/10.1242/jeb.243858

Tihelka, E., Cai, C., Giacomelli, M., Lozano-Fernandez, J., Rota-Stabelli, O., Huang, D., Engel, M. S., Donoghue, P. C. J., & Pisani, D. (2021). The evolution of insect biodiversity. *Current Biology 31*, R1299–R1311. https://doi.org/10.1016/j.cub.2021.08.057

Timm, J., Scherner, M., Matschke, J., Kern, M., & Homberg, U. (2021). Tyrosine hydroxylase immunostaining in the central complex of dicondylian insects. *Journal of Comparative Neurology 529*, 3131–3154. https://doi.org/10.1002/cne.25151

Träger, U., Wagner, R., Bausenwein, B., & Homberg, U. (2008). A novel type of microglomerular synaptic complex in the polarization vision pathway of the locust brain. *Journal of Comparative Neurology 506*, 288–300. https://doi.org/10.1002/cne.21512

Truman, J. W. (2019). The evolution of insect metamorphosis. *Current Biology 29*, R1252–R1268. https://doi.org/10.1016/j.cub.2019.10.009

Turner-Evans, D. B., & Jayaraman, V. (2016). The insect central complex. *Current Biology 26*, R453–R457. https://doi.org/10.1016/j.cub.2016.04.006

Turner-Evans, D., Wegener, S., Rouault, H., Franconville, R., Wolff, T., Seelig, J. D., Druckmann, S., & Jayaraman, V. (2017). Angular velocity integration in a fly heading circuit. *Elife 6*, e23496. https://doi.org/10.7554/eLife.23496

Varga, A. G., Kathman, N. D., Martin, J. P., Guo, P., & Ritzmann, R. E. (2017). Spatial navigation and the central complex: sensory acquisition, orientation, and motor control. *Frontiers in Behavioral Neuroscience 11*, 4. https://doi.org/10.3389/fnbeh.2017.00004

Vitzthum, H., Müller, M., & Homberg, U. (2002). Neurons of the central complex of the locust *Schistocerca gregaria* are sensitive to polarized light. *Journal of Neuroscience 22*, 1114–1125. https://doi.org/10.1523/JNEUROSCI.22-03-01114.2002

von Hadeln, J., Hensgen, R., Bockhorst, T., Rosner, R., Heidasch, R., Pegel, U., Quintero Pérez, M., & Homberg, U. (2020). Neuroarchitecture of the central complex of the desert locust: Tangential neurons. *Journal of Comparative Neurology 528*, 906–934. https://doi.org/10.1002/cne.24796

Wei, H., el Jundi, B., Homberg, U., & Stengl, M. (2010). Implementation of pigment-dispersing factor-immunoreactive neurons in a standardized atlas of the brain of the cockroach *Leucophaea maderae*. *Journal of Comparative Neurology 518*, 4113–4133. https://doi.org/10.1002/cne.22471

Williams, J. L. D. (1975). Anatomical studies of the insect central nervous system: A ground-plan of the midbrain and an introduction to the central complex in the locust, *Schistocerca gregaria* (Orthoptera). *Journal of Zoology 176*, 67–86. https://doi.org/10.1111/j.1469-7998.1975.tb03188.x

Wolff, T., Iyer, N. A., & Rubin, G. M. (2015). Neuroarchitecture and neuroanatomy of the *Drosophila* central complex: A GAL4-based dissection of protocerebral bridge neurons and circuits. *Journal of Comparative Neurology 523*, 997–1037. https://doi.org/10.1002/cne.23705

Wolff, T., & Rubin, G. M. (2018). Neuroarchitecture of the *Drosophila* central complex: A catalog of nodulus and asymmetrical body neurons and a revision of the protocerebral bridge catalog. *Journal of Comparative Neurology 526*, 2585–2611. https://doi.org/10.1002/cne.24512

Wolken, J. J., & Gupta, P. D. (1961). Photoreceptro structures. The retinal cells of the cockroach eye: IV. *Periplaneta americana* and *Blaberus giganteus*. *Journal of Biophysical and Biochemical Cytology 9*, 720–724. https://doi.org/10.1083%2Fjcb.9.3.720

Zhang, W., Ricketts, T. H., Kremen, C., Carney, K., & Swinton, S. M. (2007). Ecosystem services and dis-services to agriculture. *Ecological Economics 64*, 253–260. https://doi.org/10.1016/j.ecolecon.2007.02.024

Zittrell, F., Pfeiffer, K., & Homberg, U. (2020). Matched-filter coding of sky polarization results in an internal sun compass in the brain of the desert locust. *Proceedings of the National Academy of Sciences 117*, 25810–25817. https://doi.org/10.1073/pnas.2005192117

Zittrell, F., Pabst, K., Carlomagno, E., Rosner, R., Pegel, U., Endres, D. M., & Homberg, U. (2023). Integration of optic flow into the sky compass network in the brain of the desert locust. *Frontiers in Neural Circuits 17*, 1111310. https://doi.org/10.3389/fncir.2023.1111310

Puplikationen

Kapitel 1   Anatomie des Gehirns dictyopterer Insekten

Projekt I

Veröffentlicht unter dem Titel **,3D-atlas of the brain of the cockroach *Rhyparobia maderae'** in *Journal of Comparative Neurology* (2022). https://doi.org/10.1002/cne.25396

Seite 36-67

Projekt II

Manuskript eingereicht und in Revisionunter dem Titel **,Anatomical organization of the cerebrum of the praying mantis *Hierodula membranacea'*** in *Journal of Comparative Neurology* (Stand: Januar 2024).

Seite 68-124

Kapitel 2   Neuroarchitektur des Zentralkomplexes von *Rhyparobia maderae*

Projekt III

Veröffentlicht unter dem Titel **,Neuroarchitecture of the central complex in the Madeira cockroach *Rhyparobia maderae*: pontine and columnar cell types'** in *Journal of Comparative Neurology* (2023). https://doi.org/10.1002/cne.25535

Seite 128-154

Kapitel 1   Anatomie des Gehirns dictyopterer Insekten

Synopsis (Projekt I und II)

Insektengehirne weisen trotz ihrer geringen Größe eine erstaunliche Leistungsfähigkeit auf. Ihre neuroanatomische Komplexität stellt ein faszinierendes Forschungsgebiet dar, insbesondere angesichts der enormen Vielfalt von Insektenarten und ihrer vielseitigen ökologischen Anpassungen. Die wegweisende Arbeit von Ito et al. (2014) legte den Grundstein für eine kontinuierlich anwachsende Sammlung an drei-dimensional rekonstruierter Gehirne verschiedener Spezies. Bei *Drosophila melanogaster* wurden erstmals sämtliche Bereiche des Gehirns in ihre Neuropile unterteilt, was zur Entstehung einer umfassenden drei-dimensionalen Karte des Gehirns führte. In Kombination mit dem Konnektom des ‚Hemibrains' in *D. melanogaster* (https://www.virtualflybrain.org/) entstand somit bereits eine sehr detaillierte Darstellung des Gehirns dieser Fliege. Auf Basis dieser Daten folgten weitere Gehirnatlanten von unterschiedlichen Insektenarten. Hierzu gehörte als hemimetaboles Insekt die Wüstenheuschrecke *S. gregaria* (von Hadeln et al., 2018), sowie die Gehirne der holometabolen Ameisen *Cardiocondyla obscurior* (Bressan et al., 2015) und *Cataglyphis nodus* (Habenstein et al., 2020), des Monarchfalters *Danaus plexippus* (Heinze & Reppert, 2012), der Honigbiene *Apis mellifera* (Habenstein et al., 2023), der Mistkäfer *Scarabaeus lamarcki* und *satyrus* (Immonen et al., 2017), und der Bogongmotte *Agrotis infusa* (Adden et al., 2020). Die Einführung einer allgemeingültigen Nomenklatur der einzelnen Neuropile (Ito et al., 2014) begründete damit den Beginn einer umfangreichen kooperativen Forschungsarbeit, die darauf abzielt die neuroanatomischen Strukturen unterschiedlicher Insektenspezies zu untersuchen und sie miteinander vergleichbar zu machen. Die Webseite www.insectbraindb.org dient als Plattform, um Erkenntnisse anatomischer und physiologischer Daten zu sammeln und zur Verfügung zu stellen. Diese stetig anwachsende Datenbank fördert so ein besseres Verständnis für die Komplexität von Insektengehirnen zu entwickeln.

Obwohl einige Bereiche des Insektengehirns, wie die Pilzkörper und der Zentralkomplex, recht prominent sind, waren bislang große Teile des Cerebrums noch nicht in definierte strukturelle Bereiche unterteilt worden. In der vorliegenden Arbeit wurde die bisher vorhandene drei-dimensionale Darstellung der Pilzkörper, des Zentralkomplexes und der optischen Loben in der Schabe *Rhyparobia maderae* (Wei et al., 2010; Rosner et al., 2017) und der Gottesanbeterin *Hierodula membranacea* (Rosner et al., 2017) durch Rekonstruktionen der übrigen Gehirnareale komplementiert. Beide Insektengehirne wurden in ihre spezifischen Hirnbereiche detailliert eingeteilt und als drei-dimensionale Atlanten in allen Einzelheiten, Lagebeschreibungen und Landmarken aufgeführt. Im Gegensatz zu *D. melanogaster*, bei dem unter anderem genetische Marker, Calcium-imaging und genetische Modifizierungen des Gehirns recht leicht durchgeführt werden können, war der Einsatz dieser Techniken in den untersuchten Insektenarten nur bedingt oder gar nicht möglich.

Dennoch konnten die Neuropile anhand von Trakten, Kommissuren, Antikörperfärbungen und Einzelzellinjektionen identifiziert werden. Zusätzlich zu den in Ito et al. (2014) beschriebenen Neuropilen konnten in *R. maderae* neue Gehirnbereiche beschrieben werden. Insgesamt wurden 49 Neuropile (teilweise mit weiteren Untereinheiten) in der Schabe rekonstruiert (Projekt I), wobei die meisten von ihnen äquivalent zu Neuropilen aus der Taufliege sind. Besonders interessant ist die erstmalige Beschreibung des Rubus außerhalb von *D. melanogaster*. Darüber hinaus wurden neu beschriebene Bereiche eingeführt, darunter der 'prong', eine Region mit hoher Synapsindichte in der bestimmte kolumnäre Neurone des CX (CPU1 und CPU2 Neurone) verzweigen, sowie die 'inferior bridge cap', die ebenfalls durch eine starke Synapsinfärbung auffällt und durch Einzelzellfärbungen abgegrenzt werden konnte.

Im Rahmen der Untersuchungen am Mantisgehirn (Projekt II) konnten insgesamt 42 Neuropile (ohne optischen Lobus) identifiziert werden, einige davon mit weiteren Untereinheiten. Alle diese konnten entweder auch in *D. melanogaster* oder in den anderen untersuchten Polyneoptera definiert werden. Die Erarbeitung zweier Gehirnatlanten innerhalb der Polyneoptera, deren Lebensweisen kaum unterschiedlicher sein könnten, stellt einen bedeutenden Schritt in der Sammlung anatomischer Daten dar. Dies wird es hoffentlich zukünftigen Forschungen immer mehr erleichtern, verschiedene strukturelle Bereiche im Gehirn ihren funktionellen Aufgaben zuzuordnen oder Rückschlüsse auf die Lebensweisen der Spezies ziehen zu können. Ein anschauliches Beispiel für die Bedeutung dieser Arbeit sind Unterschiede in der Größe und Komplexität der Pilzkörper und optischen Loben in der Schabe *R. maderae* im Vergleich zu denen der Heuschrecke *S. gregaria* oder der Gottesanbeterin *H. membranacea*. Während die beiden Pilzkörper in der Heuschrecke und Mantis etwas schmaler („langezogen') ausgeprägt sind, sind die der Schabe außerordentlich groß und stark ausgeprägt. Dagegen sind die optischen Loben der Gottesanbeterin und auch der Heuschrecke wesentlich komplexer aufgebaut als die der Schabe (Rosner et al., 2017). Beide Unterschiede stehen vermutlich mit den unterschiedlichen Lebensweisen der Schabe, Heuschrecke und Gottesanbeterin in Verbindung. Die weniger stark ausgeprägten Pilzkörper und stärker ausgeprägten optischen Loben deuten auf die ausgeprägte visuelle Orientierung der Mantis und auch der Heuschrecke hin. Im Gegensatz dazu basiert die Lebensweise der nachtaktiven Schabe auf die Nutzung ihrer langen, komplexen Antennen. Die Verarbeitung von Antenneninformationen umfasst insbesondere die Antennalloben (die bei der Schabe groß und komplex sind), den glomerulären Lobus (stark ausgeprägt in der Schabe) und die bereits erwähnten Pilzkörper. Ein bekanntes Beispiel von besonders ausgeprägten Pilzkörpern ist die Honigbiene *Apis mellifera* (Brandt et al., 2005; Habenstein et al., 2023) Diese wir auch als beliebter Modellorganismus genutzt für die Untersuchungen von olfaktorischem Lernen, in dem *A. mellifera* herausragende Fähigkeiten gezeigt hat (Paoli & Galizia, 2021).

Solche Vergleiche, auch aus evolutionsbiologischer Perspektive, gewinnen durch die Erstellung von Gehirnatlanten von unterschiedlichen Insektenspezies zunehmend an Bedeutung.

Des Weiteren besteht ein Ziel dieser Arbeiten darin, die Verzweigungsbereiche neuronaler Verbindungen genauer zu beschreiben und analysieren zu können. Diese Verzweigungen sollen nicht nur anatomisch, sondern bestenfalls auch physiologisch den entsprechenden Gehirnbereichen zugeordnet werden können. In beiden Manuskripten wurde der Atlas auch erstmals angewendet. Erstmalig wurden in Wei et al. (2010) PDH-immunoreaktive Neurone in einen standartisierten Atlas der Pilzkörper, Zentralkomplexes, optischen Loben und Antennalloben eingerechnet. Diese Arbeit wurde hier weitergeführt und die genauen Verzweigungsgebiete explizit bestimmt, die für die chronobiologischen Forschung besondere Bedeutung haben.

In der Mantis wurden erste Schritte von uns unternommen, den Atlas zur funktionellen Einordnung von Neuronen zu nutzen. Ich war in der Lage, Neurone dreidimensional zu rekonstruieren und in den Atlas zu registrieren, insbesondere solche, die in das stereoskopische Sehen des Tieres involviert sind (aus Rosner et al., 2019 & 2020). Durch die Registierung der Neurone wurden die von ihnen innervierten Gehirnbereiche genauer identifiziert und konnten so in den speziesübergreifenden Kontext gesetzt werden. Diese Herangehensweise eröffnet die Möglichkeit, zukünftig neuronale Netzwerke zu rekonstruieren und potenzielle synaptische Verbindungen zu ermitteln.

Referenzen

Adden, A., Wibrand, S., Pfeiffer, K., Warrant, E., & Heinze, S. (2020). The brain of a nocturnal migratory insect, the Australian Bogong moth. *Journal of Comparative Neurology 528*, 1942–1963. https://doi.org/10.1002/cne.24866

Brandt, R., Rohlfing, T., Rybak, J., Krofczik, S., Maye, A., Westerhoff, M., Hege, R., & Menzel, R. (2005). Three-dimensional average-shape atlas of the honeybee brain and its applications. *Journal of Comparative Neurology 492*, 1–19. https://doi.org/10.1002/cne.20644

Bressan, J. M., Benz, M., Oettler, J., Heinze, J., Hartenstein, V., & Sprecher, S. G. (2015). A map of brain neuropils and fiber systems in the ant *Cardiocondyla obscurior*. *Frontiers in Neuroanatomy 8*, 166. https://doi.org/10.3389/fnana.2014.00166

Habenstein, J., Amini, E., Grübel, K., el Jundi, B., & Rössler, W. (2020). The brain of *Cataglyphis* ants: Neuronal organization and visual projections. *Journal of Comparative Neurology 528*, 3479–3506. https://publons.com/publon/10.1002/cne.24934

Habenstein, J., Grübel, K., Pfeiffer, K., & Rössler, W. (2023). 3D atlas of cerebral neuropils with previously unknown demarcations in the honey bee brain. *Journal of Comparative Neurology*. https://doi.org/10.1002/cne.25486

Heinze, S., & Reppert, S. M. (2012). Anatomical basis of sun compass navigation I: the general layout of the monarch butterfly brain. *Journal of Comparative Neurology 520*, 1599–1628. https://doi.org/10.1002/cne.23054

Immonen, E. V., Dacke, M., Heinze, S., & el Jundi, B. (2017). Anatomical organization of the brain of a diurnal and a nocturnal dung beetle. *Journal of Comparative Neurology 525*, 1879–1908. https://doi.org/10.1002/cne.24169

Ito, K., Shinomiya, K., Ito, M., Armstrong, J. D., Boyan, G., Hartenstein, V., Harzsch, S., Heisenberg, M., Homberg, U., Jenett, A., Keshishian, H., Restifo, L. L., Rössler, W., Simpson, J. H., Strausfeld, N. J., Strauss, R., & Vosshall, L. B. (2014). A systematic nomenclature for the insect brain. *Neuron 81*, 755–765. http://dx.doi.org/10.1016/j.neuron.2013.12.017

Paoli, M., & Galizia, G. C. (2021). Olfactory coding in honeybees. *Cell and Tissue Research 383*, 35–58. https://doi.org/10.1007/s00441-020-03385-5

Rosner, R., von Hadeln, J., Salden, T., & Homberg, U. (2017). Anatomy of the lobula complex in the brain of the praying mantis compared to the lobula complexes of the locust and cockroach. *Journal of Comparative Neurology 525*, 2343–2357. https://doi.org/10.1002/cne.24208

Rosner, R., von Hadeln, J., Tarawneh, G., & Read, J. C. (2019). A neuronal correlate of insect stereopsis. *Nature Communications 10*, 2845. https://doi.org/10.1038/s41467-019-10721-z

Rosner, R., Tarawneh, G., Lukyanova, V., & Read, J. C. (2020). Binocular responsiveness of projection neurons of the praying mantis optic lobe in the frontal visual field. *Journal of Comparative Physiology A 206*, 165–181. https://doi.org/10.1007/s00359-020-01405-x

von Hadeln, J., Althaus, V., Häger, L., & Homberg, U. (2018). Anatomical organization of the cerebrum of the desert locust *Schistocerca gregaria*. *Cell and Tissue Research 374*, 39–62. https://doi.org/10.1007/s00441-018-2844-8

von Hadeln, J., Hensgen, R., Bockhorst, T., Rosner, R., Heidasch, R., Pegel, U., Quintero Pérez, M., & Homberg, U. (2020). Neuroarchitecture of the central complex of the desert locust: Tangential neurons. *Journal of Comparative Neurology 528*, 906–934. https://doi.org/10.1002/cne.24796

Wei, H., el Jundi, B., Homberg, U., & Stengl, M. (2010). Implementation of pigment-dispersing factor-immunoreactive neurons in a standardized atlas of the brain of the cockroach *Leucophaea maderae. Journal of Comparative Neurology 518*, 4113–4133. https://doi.org/10.1002/cne.22471

Projekt I

3D-atlas of the brain of the cockroach *Rhyparobia maderae*

RESEARCH ARTICLE

3D-atlas of the brain of the cockroach *Rhyparobia maderae*

Vanessa Althaus[1] | Stefanie Jahn[1] | Azar Massah[2] | Monika Stengl[2] |
Uwe Homberg[1,3]

[1]Department of Biology, Animal Physiology, Philipps-University of Marburg, Marburg, Germany

[2]Faculty of Mathematics and Natural Sciences, Institute of Biology, Animal Physiology, University of Kassel, Kassel, Germany

[3]Center for Mind Brain and Behavior (CMBB), University of Marburg and Justus Liebig University of Giessen, Marburg, Germany

Correspondence
Uwe Homberg, Department of Biology, Animal Physiology, Philipps-University of Marburg, Marburg D-35032, Germany.
Email: homberg@staff.uni-marburg.de

Abstract

The Madeira cockroach *Rhyparobia maderae* is a nocturnal insect and a prominent model organism for the study of circadian rhythms. Its master circadian clock, controlling circadian locomotor activity and sleep–wake cycles, is located in the accessory medulla of the optic lobe. For a better understanding of brain regions controlled by the circadian clock and brain organization of this insect in general, we created a three-dimensional (3D) reconstruction of all neuropils of the cerebral ganglia based on anti-synapsin and anti-γ-aminobutyric acid immunolabeling of whole mount brains. Forty-nine major neuropils were identified and three-dimensionally reconstructed. Single-cell dye fills complement the data and provide evidence for distinct subdivisions of certain brain areas. Most neuropils defined in the fruit fly *Drosophila melanogaster* could be distinguished in the cockroach as well. However, some neuropils identified in the fruit fly do not exist as distinct entities in the cockroach while others are lacking in the fruit fly. In addition to neuropils, major fiber systems, tracts, and commissures were reconstructed and served as important landmarks separating brain areas. Being a nocturnal insect, *R. maderae* is an important new species to the growing collection of 3D insect brain atlases and only the second hemimetabolous insect, for which a detailed 3D brain atlas is available. This atlas will be highly valuable for an evolutionary comparison of insect brain organization and will greatly facilitate addressing brain areas that are supervised by the circadian clock.

KEYWORDS
3D reconstruction, brain atlas, insect brain, *Leucophaea maderae*, neuroanatomy, *Rhyparobia maderae*

Abbreviations: ABR, anterior bridge; AFP, anterior fiber plexus; AL, antennal lobe; ALA, accessory lamina; ALI, anterior lip; ALO, anterior lobula; ALT, antennal lobe tract; AME, accessory medulla; AMMC, antennal mechanosensory and motor center; AOT, anterior optic tract; AOTU, anterior optic tubercle; ASOC, anterior superior optic commissure; ATL, antler; AVLP, anterior ventrolateral protocerebrum; BU, bulb; CA, calyx; CB, central body; CBL, lower division of the CB; CBU, upper division of the CB; CL, clamp; CO, cones; CRE, crepine; CX, central complex; dALA, dorsal ALA; DAMMC, dorsal AMMC; DLO, dorsal lobula; EPA, epaulette; GA, gall; GABA, γ-aminobutyric acid; GC, great commissure; GLO, glomerular lobe; GOR, gorget; hVLPF, horizontal ventrolateral protocerebrum fascicle; IB, inferior bridge; IBC, IB cap; ICA, inner CA; ICL, inferior CL; IFS, inferior fiber system; INP, inferior neuropils; IT, isthmus tract; LA, lamina; LAL, lateral accessory lobe; LALC, LAL commissure; lALT, lateral ALT; LAMMC, lateral AMMC; LCA, lateral CA; LEF, lateral equatorial fascicle; LH, lateral horn; LLAL, lower LAL; LO, lobula; LOVT, LO valley tract; LOX, LO complex; LU, lower unit of the AOTU; LX, lateral complex; MAL, medial accessory lobe; mALT, medial ALT; MAMMC, medial AMMC; MB, mushroom body; MBDL, median bundle; MC, median crescent; MCA, medial CA; ME, medulla; MEF, medial equatorial fascicle; ML, medial lobe; mlALT, mediolateral ALT; N, neck; NO, noduli; NOL, lower unit of the NO; NOU, upper unit of the NO; OCA, outer CA; OCN, ocellar nerve; OL, optic lobe; OLO, outer LO; OR, ocellar root; PB, protocerebral bridge; PC, protocerebrum; PDH, pigment-dispersing hormone; PED, pedunculus; PEDD, PED divide; PENP, periesophageal neuropils; PLF, posterior lateral fascicle; PLP, posterior lateral PC; POC, posterior optic commissure; POTU, posterior optic tubercle; pPLPC, posterior PLP commissure; PRO, prong; PS, posterior slope; PVLP, posterior ventrolateral PC; PYF, pyriform fascicle; RUB, rubus; SCL, superior CL; SFS, superior fiber system; SIP, superior intermediate PC; SLP, superior lateral PC; SMP, superior medial PC; SNP, superior neuropils; SPU, spur; TC, tritocerebrum; TH, teeth; TUBUT, tubercle-bulb tract; ULAL, upper LAL; UU, upper unit of the AOTU; vALA, ventral ALA; VES, vest; VFA, ventral area of flagellar afferents; VL, vertical lobe; VLNP, ventrolateral neuropils; VLP, ventrolateral PC; VMNP, ventromedial neuropils; VX, ventral complex; WED, wedge.

37

1 | INTRODUCTION

The cerebral ganglia of insects consist of the trito-, deuto-, and protocerebrum. Except for some well-characterized neuropils such as mushroom bodies (MBs) or optic lobes (OLs), many brain areas are still poorly defined. To provide a basis for a uniform nomenclature and to facilitate interspecies comparisons, a detailed map of brain areas has been established for the fruit fly *Drosophila melanogaster* (Ito et al., 2014). Synapsin immunolabeling and additional morphological data often not available for other insect species support segmentation of the fly's brain into distinct neuropils, fiber tracts, and commissures. This atlas has greatly facilitated interpretation of gene expression studies (Brovero et al., 2021), as well as brain wide networks underlying sensory processing (Pacheco et al., 2021; Patella & Wilson, 2018; Tsubouchi et al., 2017), sensory motor control (Cheong et al., 2020), sexual brain differences (Nojima et al., 2021), and sleep control (Tomita et al., 2017). Using the same principles of segmentation and nomenclature as in *D. melanogaster*, detailed 3D atlases are meanwhile available for the desert locust *Schistocerca gregaria* (von Hadeln et al., 2018), the dung beetles *Scarabaeus lamarcki* and *Scarabaeus satyrus* (Immonen et al., 2017), the ants *Cardiocondyla obscurior* (Bressan et al., 2014) and *Cataglyphis nodus* (Habenstein et al., 2020), the monarch butterfly *Danaus plexippus* (Heinze & Reppert, 2012), and the Bogong moth *Agrotis infusa* (Adden et al., 2020). These atlases are highly valuable for interspecies comparisons and were often motivated by analysis of brain functions that encompass multiple brain areas, such as spatial orientation (Heinze & Reppert, 2012; Immonen et al., 2017; von Hadeln et al., 2018) or multisensory memory formation (Bressan et al., 2014; Habenstein et al., 2020).

Here, we provide a digital 3D atlas of the brain of a cockroach. As nocturnal animals, cockroaches largely depend on their antennal sense organs for spatial orientation (Baba et al., 2010; Okada & Toh, 2000). Chemosensory processing has been intensely investigated in the American cockroach *Periplaneta americana*, both at the level of the antennal lobe (AL) and antennal mechanosensory and motor center (AMMC; Boeckh & Ernst, 1987; Boeckh & Tolbert, 1993; Fuscà & Kloppenburg, 2021; Watanabe et al., 2010), but also at the level of secondary processing centers, the lateral horn (LH) and MB in the protocerebrum (Strausfeld & Li, 1999; Takahashi et al., 2017, 2019). An enlarged macroglomerulus in the AL of male *P. americana*, not present in females, receives input from receptor cells specialized to process the primary component of the female sex pheromone. Neurons of the MBs not only receive olfactory but also visual input, indicating multimodal information processing (Li & Strausfeld, 1997, 1999; Nishino et al., 2012).

Functional studies on the central complex (CX) in the cockroach *Blaberus discoidalis* contributed substantially to understanding the role of this brain area in spatial orientation. The CX comprises a group of midline brain neuropils integrating multisensory inputs for the control of orientation in space (Fisher, 2022; Heinze & Reppert, 2012; Homberg et al., 2011; Honkanen et al., 2019; Ritzmann et al., 2012). Extracellular recordings and electrical stimulation in fixed and walking cockroaches showed that the CX is not only involved in coding of heading direction but also controls walking direction, walking speed, and turning (Martin et al., 2015; Varga et al., 2017).

The Madeira cockroach *R. maderae* is an established model organism in circadian rhythm research (Homberg et al., 2003b; Page, 1982; Stengl & Arendt, 2016; Stengl et al., 2015). Lesion and transplantation experiments identified the accessory medulla (AME) as the circadian clock that controls sleep–wake cycles entrained to the light–dark cycle (Reischig & Stengl, 2003a; Stengl & Homberg, 1994). Prominent neurons of the AME with wide ramifications throughout the brain contain the neuropeptide pigment-dispersing factor (PDF). These neurons are responsible for circadian rhythms in rest and activity and are, likewise, involved in light entrainment and gating of photic inputs to the circadian clock (Arnold et al., 2020; Loesel & Homberg, 2001; Stengl & Arendt, 2016). While a morphological analysis of the PDF neurons and their implementation into a general standard cockroach brain has been achieved (Wei et al., 2010), a detailed map of cockroach brain neuropils is still missing. The present work provides a detailed 3D analysis and rendition of brain organization of the cockroach *R. maderae* to serve as the basis for implementation of morphologically and physiologically identified neurons and to promote studies on brain organization and control of behavior in a highly adaptive ancient insect species.

2 | MATERIAL AND METHODS

2.1 | Animals

Madeira cockroaches (*Rhyparobia maderae*, formerly termed *Leucophaea maderae*) were raised in crowded colonies at the Institute of Biology, University of Kassel. Animals were kept at a temperature of 25–26°C and 50% relative humidity and were reared under a 12:12 h light/dark cycle. Only adult males were used for the whole mount preparations. Cockroaches used in all other experiments were raised at the Department of Biology, University of Marburg under similar conditions. Individuals of both sexes were used for these supplementary experiments.

2.2 | Preparation and immunohistochemistry of whole mounts

Cockroaches were anesthetized by placing them for around 30 min at 4°C in the refrigerator. Brains were dissected from the head and fixed for 2 h at room temperature in 4% formaldehyde (FA) in 0.1 mol L^{-1} sodium phosphate buffer (PBS; containing 78.8 mmol L^{-1} Na$_2$HPO$_4$ × 2H$_2$O and 19 mmol L^{-1} NaH$_2$PO$_4$ × H$_2$O at pH 7.4; Rothi-Histofix; Roth, Karlsruhe, Germany). To prevent dehydration of the brain, further preparation was carried out in insect saline (128 mmol L^{-1} NaCl, 2.7 mmol L^{-1} KCl, 2 mmol L^{-1} CaCl$_2$, 1.2 mmol L^{-1} NaHCO$_3$, dissolved in 2× distilled H$_2$O, pH 7.25). The brains were transferred into Tris-buffered saline (TBS; containing 0.1 mol L^{-1} Tris-HCl and 0.3 mol L^{-1} NaCl, pH 7.4) and rinsed 6 × 20 min in TBS. To facilitate antibody penetration, the brains were

TABLE 1 Primary antibodies used

Antigen	Immunogen	Source	Host species	Concentration	Reference
γ-Aminobutyric acid (GABA)	GABA conjugated to bovine serum albumin	Sigma–Aldrich	Rabbit	1:750	Giese et al. (2018) RRID: AB_477652
Synapsin	Fusion proteins of glutathione-S-transferase and *D. melanogaster* SYN1	E. Buchner and C. Wegener	Mouse	1:50	Wei et al. (2010) RRID: AB_2315425
Serotonin	Serotonin coupled to bovine serum albumin	ImmunoStar	Goat	1:10,000	RRID: AB_572262
Serotonin	Conjugates of serotonin creatinine sulfate and bovine serum albumin	Sigma–Aldrich	Rabbit	1:40,000	Giese et al. (2018) RRID: AB_477522
Orcokinin	Asn^{13}-orcokinin	H. Dircksen	Rabbit	1:6000	Bungart et al. (1994) RRID: AB_2315017
Pigment-dispersing-hormone (PDH)	Conjugates of *Leptuca pugilator* ß-PDH and bovine thyroglobulin	H. Dircksen	Rabbit	1:20,000	RRID: AB_2315088
LomTK-II	Locustatachykinin II coupled to bovine thyroglobulin	H.-J. Agricola	Rabbit	1:20,000	Vitzthum and Homberg (1998) RRID: AB_2341129

incubated in 1 mg collagenase/dispase (Roche, Mannheim, Germany) diluted in 1 mL TBS for 40 min at 37°C. After the treatment with collagenase, the brains were washed in TBS containing 0.3% Triton X-100 (TrX) 6 × 20 min. For preincubation, the brains were transferred overnight at 4°C in 2% normal goat serum (NGS; Dianova, Hamburg, Germany) in TBS (0.3% TrX). To visualize neuropil boundaries, the brains were labeled for 8 days at 4°C with antibodies against synapsin and GABA (Table 1). This was achieved by incubation in 2% NGS, 0.02% sodium azide, anti-GABA (rabbit polyclonal, Sigma–Aldrich, 1:750) and anti-SYNORF1 (synapsin, mouse monoclonal, Developmental Studies Hybridoma Bank, 1:50) in TBS (0.3% TrX). After two rinses with TBS (0.1% TrX), four washing steps followed for at least 20 min. Then, the brains were incubated in the secondary antibody solution, containing goat-anti-rabbit conjugated with Alexa 674 (GaR-Alexa674; Dianova, 1:500), goat-anti-mouse conjugated with cyanine-3 (GaM-Cy3; Dianova, 1:300), 1% NGS and 0.02% sodium azide in TBS (0.3% TrX) for 6 days at 4°C. After 4 × 20 min final washing steps in TBS (0.1% TrX), the brains were dehydrated using an ascending ethanol series (50, 70, 90, 95, and 100% ethanol solution) each step for 15 min. Following, the brains were transferred into a 1:1 solution of ethanol/methyl salicylate for 15 min and further placed in 100% methyl salicylate for 1 h. Finally, the brains were embedded in Permount mounting medium (Permount™; Fisher Scientific, Schwerte, Germany) under coverslips.

2.3 | Immunolabeling on 130-μm sections

For detailed analysis of selected brain areas, 130-μm sections of the cockroach brain were double labeled with antibodies against pigment-dispersing hormone (PDH) and synapsin, or triple-labeled with anti-

bodies against serotonin, orcokinin, and synapsin (Table 1). Brains were dissected and fixed as described above, except for overnight fixation in 8% FA for PDH immunolabeling. After fixation, brains were washed 4 × 10 min with PBS and once for 5 min with saline-substituted Tris buffer (SST; containing 0.1 mol L^{-1} Tris–HCl/0.3 mol L^{-1} NaCl, pH 7.4) containing 0.1% TrX only for triple labeling for serotonin, orcokinin and synapsin. Following, the brains were embedded in albumin/gelatin (12% ovalbumin, 4.8% gelatin in demineralized water) and again fixed at 4°C in 6% FA in PBS overnight. The next day, brains were sectioned with a vibrating-blade microtome (VT 1200 S; Leica Biosystems, Wetzlar, Germany) in frontal plane adjusted to 130 μm. After cutting, the sections were washed 2 × 10 min with 0.1 mol L^{-1} PBS and 4 × 10 min with PBT (PBS + 0.3% TrX). Preincubation was accomplished for 3 h at room temperature or overnight at 4°C in 5% normal donkey serum (NDS) for the serotonin/orcokinin/synapsin staining and in 5% NGS for PDH/synapsin immunolabeling in 0.1 mol L^{-1} PBT. The brains were transferred into the primary antibodies. For triple labeling, we used anti-synapsin (mouse monoclonal, SYNORF1, 1:50, kindly provided by Dr. E. Buchner and C. Wegener, Würzburg, Germany), anti-serotonin (goat polyclonal, ImmunoStar, 1:10,000) and anti-orcokinin (1:6000; Bungart et al., 1994) in PBT with 2% NDS. For the PDH/synapsin double immunolabeling, anti-synapsin and anti-Leptuca-PDH (rabbit polyclonal, 1:20,000; kindly provided by Dr. H. Dircksen, Stockholm, Sweden) in PBT with 2% NGS were used. Sections were incubated for 3 days at 4°C and, after rinsing with PBT for 6 × 15 min, the brains were incubated in the secondary antibodies for 5 days at 4°C. For serotonin/orcokinin/synapsin immunolabeling, Cy2-conjugated donkey-anti-mouse (DaM-Cy2; Dianova; 1:300), Cy3-conjugated donkey-anti-rabbit (DaR-Cy3; Dianova; 1:300), and Cy5-conjugated donkey-anti-goat (DaG-Cy5; Dianova; 1:300) in 1% NDS in PBT were used. For PDH/synapsin double staining Cy2-conjugated

goat-anti-rabbit (GaR-Cy2; Dianova, 1:300) and Cy5-conjugated goat-anti-mouse (GaM-Cy5; Dianova, 1:300) were used with 1% NGS in PBT. Sections were subsequently rinsed in PBT for 4×15 min followed by final washing steps 2×15 min in 0.1 mol L^{-1} PBS. Dehydration and embedding followed the procedure used for whole mounts, except that the time of each step was reduced to 5 min for each ethanol step and 1:1 ethanol/methyl salicylate, and 15 min in 100% methyl salicylate.

2.4 | Immunolabeling on 30-μm sections

Further support for the establishment of neuropil boundaries was achieved by immunocytochemically labeled brain sections following the indirect peroxidase–antiperoxidase (PAP) technique (Sternberger, 1979). Brains were dissected as described above and fixed for 3 h in 4% paraformaldehyde (PFA) at room temperature. After rinsing 4×10 min in 0.1 mol L^{-1} PBS and once for 5 min in 0.1 mol L^{-1} PBT (0.3% TrX) they were embedded in albumin/gelatin. For further fixation, the albumin/gelatin blocks were submerged in 6% FA overnight at 4°C. The next day, the embedded brains were sectioned with a vibrating-blade microtome at 30 μm in frontal plane. After cutting, the sections were washed 3×10 min in SST (0.1% TrX) and preincubated for 1 h at room temperature in SST (0.5% TrX) containing 8% NGS to reduce nonspecific staining. Following, incubation in the primary antibody was carried out for 18–20 h (anti-serotonin, 1:40,000; Sigma or anti-LomTK-II, 1:20,000, kindly provided by Dr. Hans-Jürgen Agricola, University of Jena; Table 1) with 2% NGS in SST (0.5% TrX). Sections were washed again 4×10 min in SST (0.1% TrX) and were incubated for 1 h at room temperature in the secondary antibody goat-anti-rabbit IgG (1:40 in SST, 0.5% TrX and 2% NGS, RRID: AB_261363). After washing 5×10 min in SST (0.5% TrX), brains were incubated in PAP complex (1:300, rabbit PAP, RRID: AB_2315056) for 1 h with 2% NGS in SST (0.1% TrX). To remove excess PAP, brains were washed again 5×10 min with SST. 3,3′-Diaminobenzidine tetrahydrochloride (0.03 mg/ml) was given to the sections with H_2O_2 (1:2000) in 0.1 mol L^{-1} sodium phosphate buffer (PB; containing 28.04 g $Na_2HPO_4 \times 2H_2O$, 5.244 g $NaH_2PO_4 \times H_2O$ in 2 L H_2O). Under visual control, the reaction was stopped by rinsing the sections in PB. The sections were mounted onto chrome alum-gelatin-coated slides, dried and embedded in Entellan (Merck, Darmstadt, Germany) under cover slips.

2.5 | Antibody characterization

The antiserum against GABA (Sigma–Aldrich cat# A2052, RRID: AB_477652; Table 1) was raised in rabbit against GABA conjugated to bovine serum albumin. On brain sections of *R. maderae* the pattern of immunolabeling was identical to that obtained with an antiserum against the GABA-synthesizing enzyme glutamic acid decarboxylase (Massah et al., 2022). Liquid-phase preadsorption of the diluted antiserum with 10 μmol L^{-1} GABA-BSA conjugate abolished all immunostaining on brain sections of *R. maderae* (Giese et al., 2018).

Two antisera against serotonin were used. The antiserum raised in goat (ImmunoStar, anti 5-HT, cat# 20079, RRID AB_572262; Table 1) was directed against serotonin coupled to bovine serum albumin with PFA. Preadsorption of the diluted antiserum with 100 μg/mL serotonin/BSA conjugate completely abolished labeling (ImmunoStar product information sheet). The second antiserum was obtained from Sigma (cat# S5545, RRID: AB_477522; Table 1). The antiserum was raised in rabbit against conjugates of serotonin creatinine sulfate and bovine serum albumin. Preadsorption of the diluted antiserum with 100 μmol L^{-1} serotonin abolished immunostaining on gelatin-embedded sections of *R. maderae* brains (Giese et al., 2018). The staining obtained with both antisera resulted in identical staining patterns in the brain of *R. maderae*.

The antiserum against locustatachykinin II (LomTK-II; Cat# ABD-045, RRID: AB_2341129; Table 1) was raised in rabbit against synthetic locustatachykinin II coupled via glutaraldehyde to bovine thyroglobulin (Veenstra et al., 1995) and was kindly provided by Dr. Hans-Jürgen Agricola (University of Jena). The staining pattern obtained with this antiserum on *R. maderae* brain sections is identical to that obtained by an antiserum against the related peptide LomTK-I (Muren et al., 1995). The specificity of the antiserum has been characterized in the locust *S. gregaria* (Vitzthum & Homberg, 1998), the cockroach *P. americana* (Fusca et al., 2015), the blowfly *Calliphora vomitoria* (Nässel et al., 1995), the beetle *Tenebrio molitor* (Wegerhoff, 1997), and the mosquito *Aedes aegypti* (Veenstra et al., 1995). Preadsorption of the diluted antiserum with 10–25 μmol L^{-1} LomTK-II abolished immunostaining on brain sections from locust, blowfly, and beetle, and with 100 μmol L^{-1} LomTK-I on cockroach brain sections.

The polyclonal antiserum against orcokinin (RRID: AB_2315017; Table 1) was raised in rabbit against Asn^{13}-orcokinin from the crayfish *Orconectes limosus* (Bungart et al., 1994). The specificity of the antiserum has been demonstrated in *O. limosus* by Bungart et al. (1994) using enzyme-linked immmunosorbent assays of HPLC fractions. Preadsorption of the diluted antiserum with 1 nmol L^{-1} Asn^{13}-orcokinin abolished labeling in *R. maderae* brain sections (Hofer et al., 2005).

The antiserum against PDH (#3B3, RRID: AB_2315088; Table 1) was raised against conjugates of *Leptuca pugilator/Cancer magister* ß-PDH and bovine thyroglobulin (Dircksen et al., 1987). Immunodot-blot analysis of HPLC-separated crustacean sinus-gland extracts showed PDH immunoreactivity only in biologically active fractions (Dircksen et al., 1987). In *R. maderae*, preadsorption of the diluted antiserum with 10 μmol L^{-1} ß-PDH completely abolished immunostaining (Stengl & Homberg, 1994).

The monoclonal antibody against synapsin (#3C11, RRID: AB_2315425; Table 1) was obtained from Drs. E. Buchner and C. Wegener (University of Würzburg) or the Developmental Studies Hybridoma Bank, University of Iowa, Iowa City, USA. It was raised in mice against fusion proteins consisting of glutathione-S-transferase and parts of the *D. melanogaster* synaptic vesicle protein SYN1 (Klagges et al., 1996). Its specificity has been demonstrated in *D. melanogaster* by Klagges et al. (1996). The antibody labels synaptic neuropils as shown

in different insect species, including *R. maderae* (Rosner et al., 2017; Wei et al., 2010).

2.6 | Neurobiotin injections of single neurons

Single-cell tracer injections provided evidence for neuropil subcompartments in certain brain areas. Cockroaches were cold-anesthetized at 4°C overnight. To reduce movement of the animals, they were fixed with their head up at a metal holder with dental wax. The head was fixed in a planar position, so the head capsule could be opened anteriorly. After removing the cuticula, fat and trachea above the brain were removed. To stabilize the brain during tracer injections, a twisted wire was formed as a spoon and positioned posterior to the brain. Throughout the whole time the brain was kept moist with insect saline (containing 4.088 g NaCl, 0.186 g KCl, 0.102 g MgCl$_2$ × 6H$_2$O, 0.168 g NaHCO$_3$, 0.4125 g NaH$_2$PO$_4$, 0.801 g glucose in 0.5 L distilled H$_2$O, pH 7.25). For injection, we used sharp glass capillaries from borosilicate glass (Hilgenberg, Malsfeld, Germany), heated and drawn using a Flaming/Brown horizontal puller (P-97; Sutter Instrument, Novato, CA). Tips of the electrodes were filled with 4% Neurobiotin (Vector Laboratories, Burlingame, CA) in 1 mol L^{-1} KCl, and the shanks were loaded with 1 mol L^{-1} KCl. The glass electrode controlled by a micromanipulator (Leica Microsystems) was positioned above the desired brain area and advanced in a stepwise manner. When action potentials indicated intracellular recording, Neurobiotin was injected by positive current of 1–3 nA for up to 10 min. After injection of Neurobiotin, brains were dissected out of the head capsule and fixed in Neurobiotin fixative solution (4% PFA, 0.25% glutaraldehyde, 0.2% saturated picric acid in 0.1 mol L^{-1} PBS, pH 7.4) overnight at 4°C. After fixation, brains were transferred in PB for storage up to 2 weeks. For visualization of the injected neurons, brains were rinsed 4 × 15 min in 0.1 mol L^{-1} PBS and incubated for 3 days in streptavidin–cyanine-3 (Strep–Cy3; Dianova, 1:1000 in 0.1 mol L^{-1} PBT, cat# SP-1120, RRID: AB_2337244). The brains were then washed 2 × 30 min in 0.1 mol L^{-1} PBT (0.3% TrX) and 3 × 20 min in 0.1 mol L^{-1} PBS. Following, brains were dehydrated in an ascending ethanol series (30, 50, 70, 90, 95, and 100% ethanol) 15 min each and cleared in methyl salicylate:ethanol (1:1 for 15 min) and in 100% methyl salicylate for 30 min. The brains were finally mounted in Permount between two cover slips. Seven reinforcement rings were placed as spacers between the cover slips.

2.7 | In vivo backfills of the antenna

Cold anesthetized cockroaches of both sexes were used and the preparation was performed on ice to reduce animal movement. The animals were fixed with tape to a metal plate, and the head was passed through a hole in the middle and also fixed with tape. The antenna was cut at the joint between the scape and pedicel or at the basal segments of the flagellum. The stump was inserted into a self-made bowl, filled with 4% Neurobiotin and afterwards capped with petroleum jelly. Animals were kept overnight at 4°C in the refrigerator. The next day, the brains were

dissected out of the head capsule and fixed for 3 h in 4% PFA. After fixation, the brains were washed 3 × 15 min in PBT (0.3% TrX) and incubated in Strep–Cy3 (1:1000 in PBT) for 3 d at 4°C, followed by washing steps, 4 × 15 min with PBT and 2 × 15 min in PBS. Brains were dehydrated in an ascending ethanol series and finally mounted in Permount as described above.

2.8 | Image acquisition

Whole mount preparations and immunolabeled sections were scanned by a confocal laser scanning microscope (Leica, TCS SP5, Leica Microsystems) with a 20× oil immersion objective (HC PL APO 20×/0.75 Imm Corr CS2). Images were acquired at a resolution of 1024 × 1024 pixels in the *xy*-plane (pixel size 0.75 μm × 0.75 μm) and a step size of 1 μm in *z*-direction. Scanning frequency was 400 Hz. Cy3 fluorescence was excited by a diode-pumped solid-state laser (561 nm, DPSS 10 mW), Alexa674/Cy5 fluorescence with a helium neon laser (633 nm, HeNe 10 mW), and Cy2 with an argon laser (488 nm). The image stacks were merged with the software AMIRA 6.5 (ThermoFisher Scientific, Waltham, MA, USA). Images from sections that were labeled following the PAP technique were photographed using a digital camera (ProgRes C12plus, Jenoptik) connected to a transmission light microscope (Axioskop; Zeiss, Oberkochen, Germany). Captured images were adjusted in brightness and contrast using Affinity Photo (Serif, Nottingham, UK) and to create final figures.

2.9 | Anatomical reconstruction

Three-dimensional reconstructions were performed with AMIRA 6.5. Boundaries were set manually by using synapsin- and GABA immunofluorescence labeling. Different levels of each neuropil were marked in all planes, *x*-, *y*-, and *z*-direction creating a three-dimensional grid. This grid was the basic structure to generate a surface view. For each neuropil, polygonal surfaces were created by the *Wrap*-function and *Generate Surface*-module and then visualized with the *SurfaceView*-module. To smooth the surface of reconstructed neuropils and reduce data size, reconstructions were *simplified*. In addition to neuropils, some tracts, fiber bundles, and commissures that were used as borders were reconstructed and visualized in a similar way.

3 | RESULTS

For 3D reconstruction of neuropils and fiber tracts in the cerebral ganglia of the Madeira cockroach *R. maderae* we used a whole mount preparation double labeled for synapsin and GABA (see Movies S1–S4). We identified 49 major neuropils, some of them with additional subunits (Figure 1), and 22 major tracts, fiber systems, and commissures (Figure 2). The CX, MB, OL, and AL were reconstructed in previous studies (Rosner et al., 2017; Wei et al., 2010). For the sake of completeness, they were reconstructed here again and are partly shown
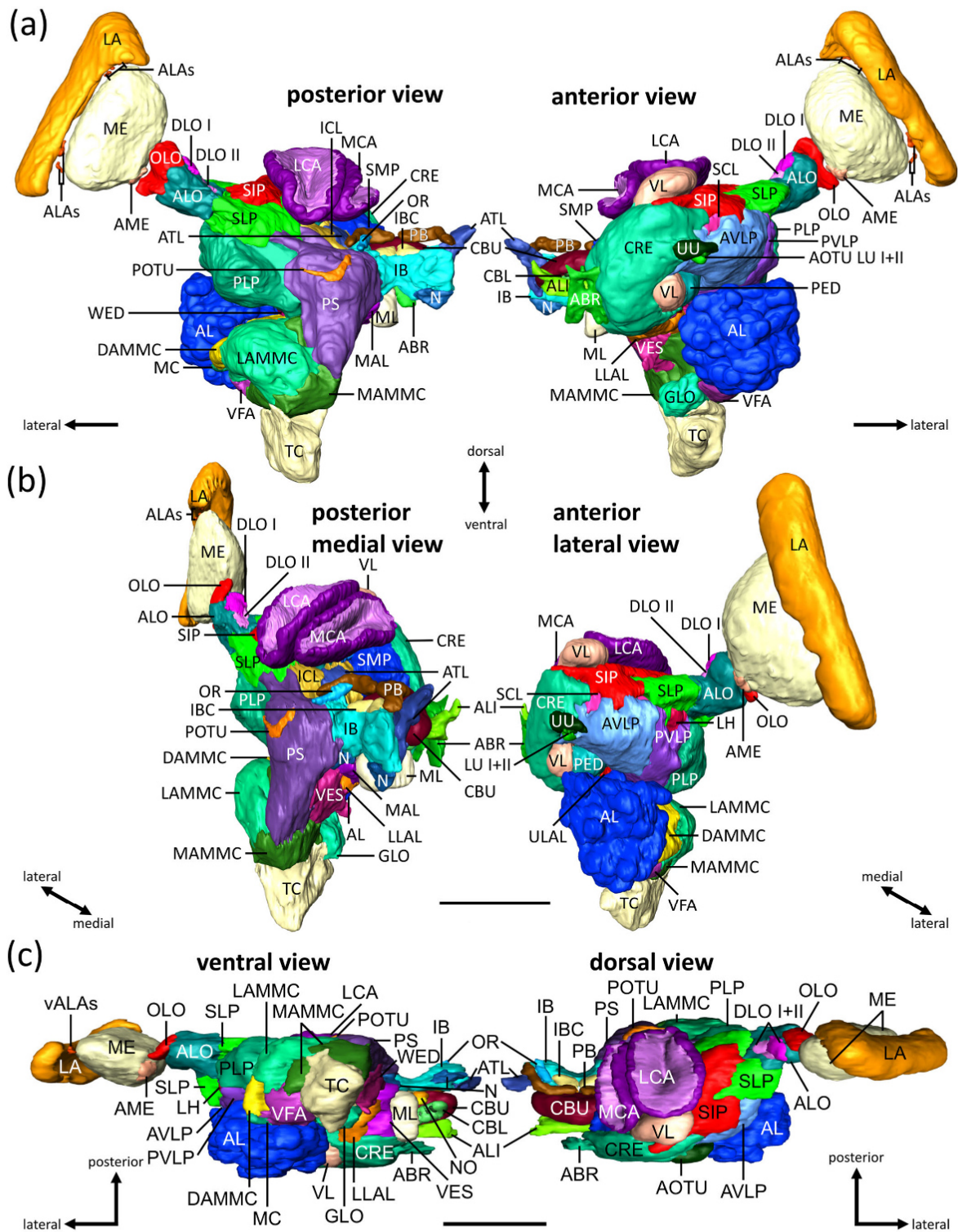
FIGURE 1 Overview of all reconstructed neuropils of the cockroach brain. (a) Posterior (left) and anterior (right) view of three-dimensionally reconstructed neuropils in the hemibrain of a male cockroach. (b) Oblique posterior medial (left) and anterior lateral (right) views of the brain. (c)

(Continues)

FIGURE 1 (Continued)

Ventral (left) and dorsal (right) views of the brain. ABR, anterior bridge; AL, antennal lobe; ALA, accessory LA; ALI, anterior lip; ALO, anterior LO; AME, accessory ME; AMMC, antennal mechanosensory and motor center; AOTU, anterior optic tubercle; ATL, antler; AVLP, anterior VLP; CA, calyx; CB, central body; CBL, lower division of the CB; CBU, upper division of the CB; CL, clamp; CRE, crepine; DAMMC, dorsal AMMC; DLO I +II, dorsal LO I and II; GLO, glomerular lobe; IB, inferior bridge; IBC, inferior bridge cap; ICL, inferior CL; LA, lamina; LAL, lateral accessory lobe; LAMMC, lateral AMMC; LCA, lateral CA; LH, lateral horn; LLAL, lower LAL; LO, lobula; LU I+II, lower unit I+II of the AOTU; MAL, medial accessory lobe; MAMMC, medial AMMC; MC, median crescent; MCA, medial CA; ME, medulla; ML, medial lobe; N, neck; OLO, outer LO; OR, ocellar root; PB, protocerebral bridge; PED, pedunculus; PLP, posterior lateral protocerebrum; POTU, posterior optic tubercle; PS, posterior slope; PVLP, posterior VLP; SCL, superior CL; SIP, superior inferior protocerebrum; SLP, superior lateral protocerebrum; SMP, superior medial protocerebrum; TC, tritocerebrum; ULAL, upper LAL; UU, upper unit of the AOTU; VES, vest; VFA, ventral area of flagellar afferents; VL, vertical lobe; VLP, ventrolateral protocerebrum; WED, wedge. Scale bars = 400 μm

in more detail (Figure 1). Neuropil boundaries and nomenclature are based on the criteria established by Ito et al. (2014) for the brain of the fruit fly *D. melanogaster*. We, therefore, focused to identify corresponding essential landmarks in the cockroach brain in order to compare the cockroach brain with that of the fruit fly in spite of evolutionary anatomical differences. Immunostainings with antisera against PDH, serotonin, LomTK-II and orcokinin were used as additional markers for confirmation of neuropil boundaries and identification of potential subunits. Single-cell dye fills were used to differentiate small neuropils characterized by the arborization domains of specific neurons.
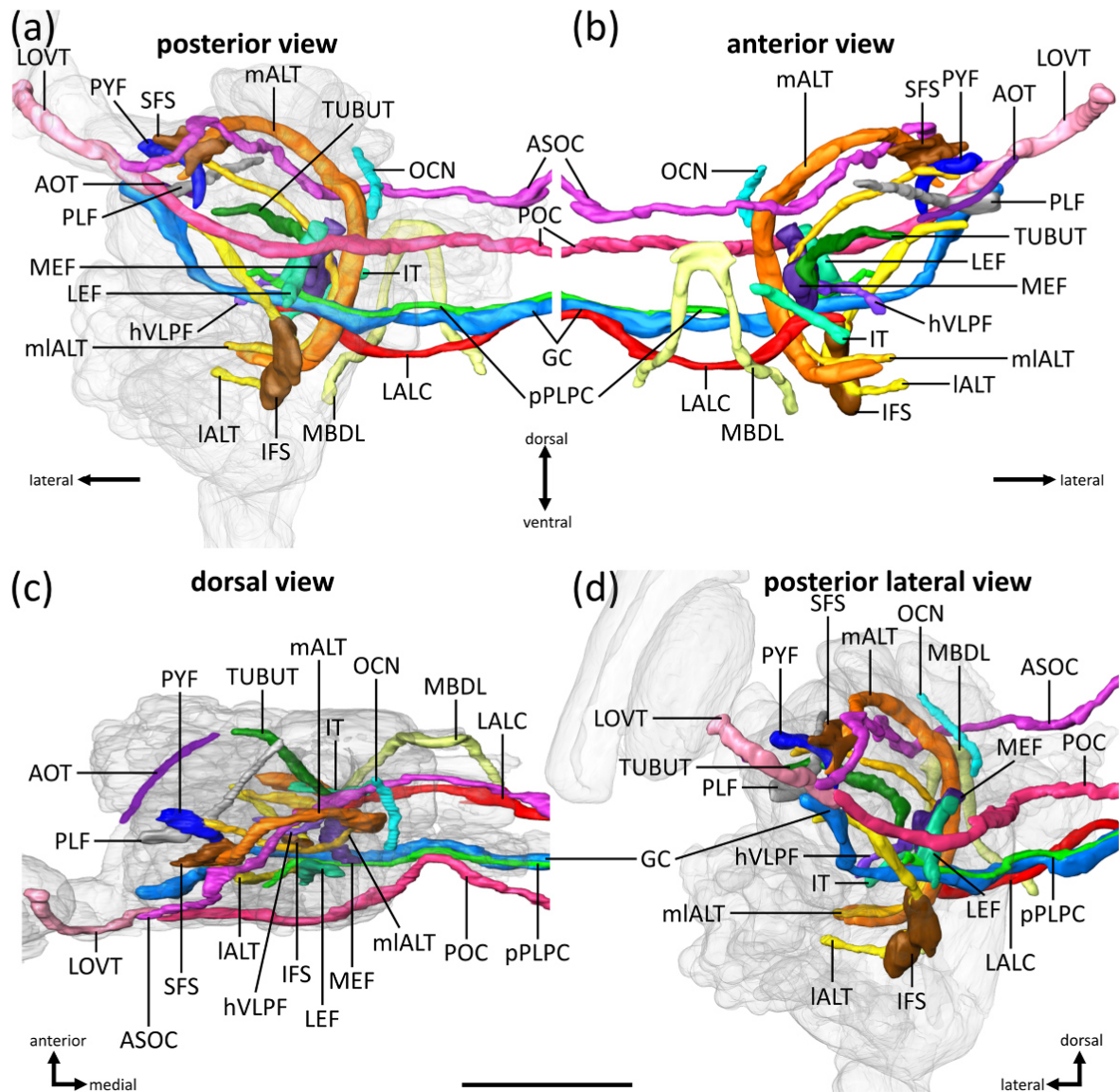
3.1 | Tracts, commissures, and fiber systems

Based on GABA immunolabeling and lack of synapsin, we reconstructed a selection of fiber systems (Figure 2). Bundles of nerve fibers that connect neuropils within one brain hemisphere are called fascicles, tracts, or bundles, while fiber systems connecting neuropils in both hemispheres, crossing the brain's midline, are termed commissures. They served as landmarks to demarcate neuropils distinguished correspondingly in other insects. Two fascicles in the lateral brain are the posterior lateral fascicle (PLF) and the pyriform fascicle (PYF; Figure 2). The PLF (Figures 3d–h and 4a–g) emerges dorsal to the posterior ventrolateral protocerebrum (PVLP) and forms the border between the PVLP and the LH. It takes a posterior course ventrally along the LH, ends in the superior intermediate protocerebrum (SIP) and defines boundaries of the superior neuropils (SNP). The PLF contains GABA-immunoreactive fibers with somata in the anterior soma rind below the lobula complex (LOX) (in the G7 cluster; Massah et al., 2022). These fibers run through the superior clamp (SCL) toward the crepine (CRE) and have no connection to the other reconstructed tracts. The PYF (Figures 4c–g) establishes the border between the superior lateral protocerebrum (SLP) and SIP. It runs ventro-anterior to the dorsal surface of the LH while ending in the superior fiber system (SFS; Figure 4g,h). Two of the most prominent fascicles in the cockroach brain are the medial (MEF) and lateral equatorial fascicle (LEF). The LEF (Figures 5b–e) is located in the posterior brain, between the inferior clamp (ICL) and posterior slope (PS), running ventrally in direction of the great commissure (GC; Figure 5c). The MEF (Figures 4e–h and 5a and 5b) lies medio-anterior to the LEF and is just as noticeable as the LEF. It emerges dorsally at the level of the most posterior part of the

protocerebral bridge (PB) and extends between the ICL and inferior bridge (IB; Figure 5a). The horizontal ventrolateral protocerebrum fascicle (hVLPF) is significantly more slender. It enters the brain dorsal to the AL and ends in the region between the lateral accessory lobe (LAL), ICL and epaulette (EPA), separating medial parts of the ventrolateral protocerebrum (VLP) from surrounding neuropils (Figures 4e–g).

Brain commissures often connect bilaterally symmetric neuropils of both hemispheres. Three out of seven OL commissures described by Reischig and Stengl (2002) are included here. One of the most prominent commissures of the cockroach brain is the GC (Figure 2). It corresponds to the inferior optic commissure (tract 5) of Reischig and Stengl (2002) and connects both OLs with each other (Figures 5a–e). The posterior lateral protocerebrum (PLP) commissure (pPLPC) crosses the brain midline at the same level. It extends to both PLPs (Figures 5a–d). The LAL commissure (LALC) connects both LALs with each other and forms the landmark separating the upper and lower LAL (Figures 4c and 4d). The posterior optic commissure (POC; Figure 5) corresponding to the POC (tract 7) of Reischig and Stengl (2002), connects both medullae of the OL, and crosses the brain midline at the posterior dorsal surface while running between the PS and posterior optic tubercle (POTU; Figure 5f). The anterior superior optic commissure (ASOC; "anterior superior optic tract" in Habenstein et al., 2020) corresponds to the anterior optic commissure (tract 4) of Reischig and Stengl (2002) and crosses the brain midline in the anterior brain (Figure 2). It connects the SLP and the superior medial protocerebrum (SMP) in both hemispheres with the AME of both OLs. Both the POC (Figure 5) and the ASOC (Figures 3f–h and 4) originate from the lobula valley tract (LOVT; Figures 5e–g). They contain PDH-immunoreactive fibers from pacemaker neurons of the AME (Reischig & Stengl, 2002). The LOVT (Figures 2 and 5d–g) is a major fiber bundle running from the proximal medulla to the proximal end of the LOX. It bifurcates at the transition of the LOX and SLP and distributes its axons mainly to the POC and ASOC (Figure 2).

Regions where fiber bundles converge from various directions are called fiber systems (Ito et al., 2014). We distinguished two prominent fiber systems in the cockroach brain. The inferior fiber system (IFS) is a major fiber system in the inferior posterior brain, between the wedge (WED) and the vest (VES; Figures 4h and 5a–d). Another notable fiber system is the SFS (Figures 4g–h, and 5a) that lies superior medial to the LH, between the LH and the SLP/SIP. The medial AL tract (mALT) and PYF run through it (Figures 4g and 4h), setting distinct boundaries within the SNP.

FIGURE 2 3D reconstruction of fiber bundles, commissures, tracts, and fiber systems defining neuropil boundaries. Tracts are displayed in a transparent 3D brain hemisphere, as shown in Figure 1 in posterior (a), anterior (b), dorsal (c), and oblique posterior lateral (d) views. ALT, antennal lobe tract; AOT, anterior optic tract; ASOC, anterior superior optic commissure; GC, great commissure; hVLPF, horizontal VLP fascicle; IFS, inferior fiber system; IT, isthmus tract; LALC, lateral accessory lobe commissure; lALT, lateral ALT; LEF, lateral equatorial fascicle; LOVT, lobula valley tract; mALT, medial ALT; MBDL, median bundle; MEF, medial equatorial fascicle; mlALT, mediolateral ALT; OCN, ocellar nerve; PLF, posterior lateral fascicle; POC, posterior optic commissure; pPLPC, posterior PLP commissure; PYF, pyriform fascicle; SFS, superior fiber system; TUBUT, tubercle-bulb tract. Scale bar = 400 μm

A number of tracts penetrate the cockroach brain. The following selected tracts were used as landmarks for the 3D reconstruction. The anterior optic tract (AOT; Figures 3c–h and 4a–c) extends from the lobula (LO) to the anterior optic tubercle (AOTU) along the anterior lateral brain surface (tract 1, Reischig & Stengl, 2002). It is an impor-

tant landmark in determining the position of the AOTU (Figure 3c). A second tract that emerges at the level of the AOTU is the tubercle-bulb tract (TUBUT; Figures 3b–h and 4a–c). It originates between the upper and lower units of the AOTU (Figure 3b), runs through the anterior VLP (AVLP) and passes posteriorly by the vertical lobe (VL). It
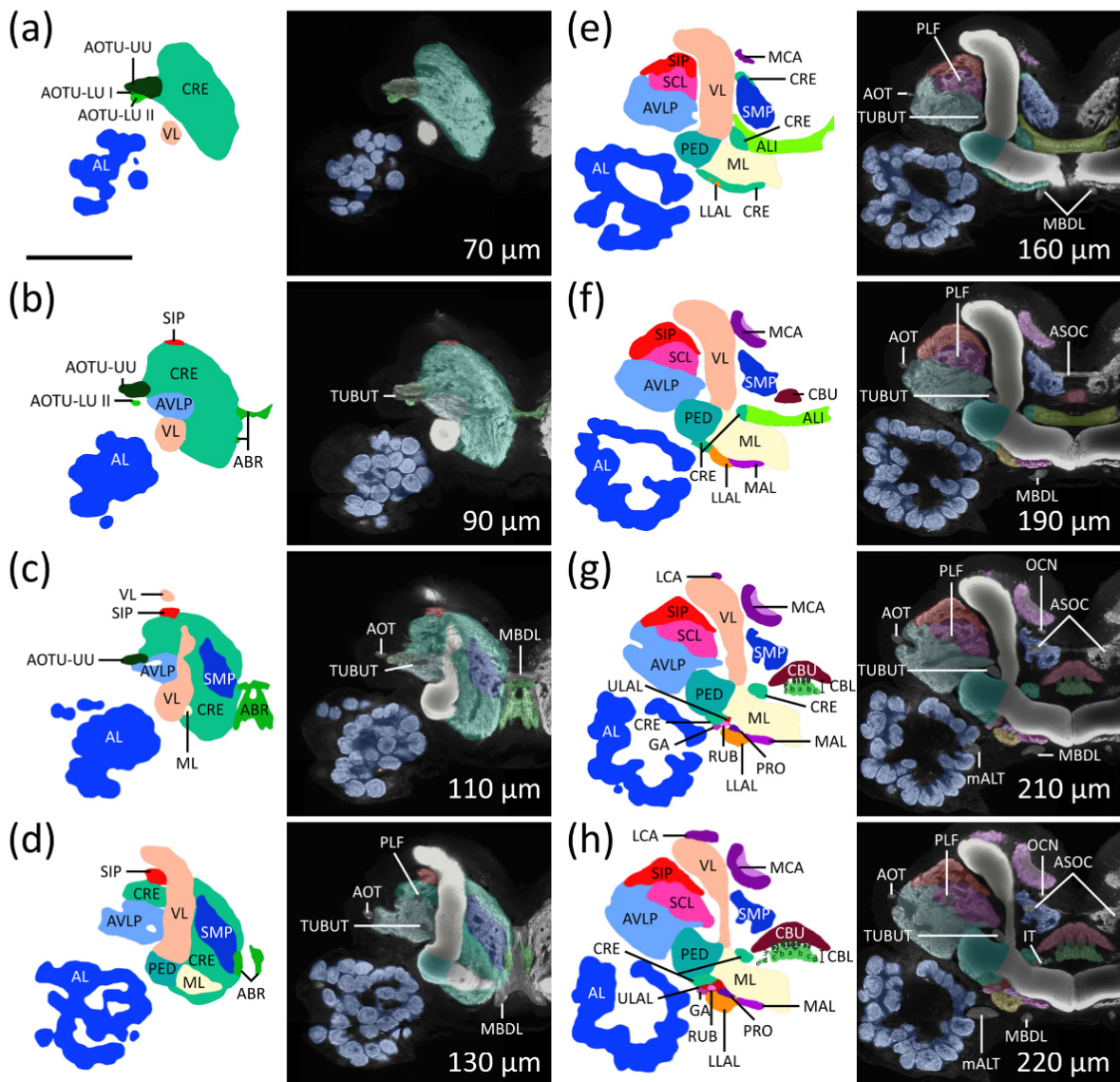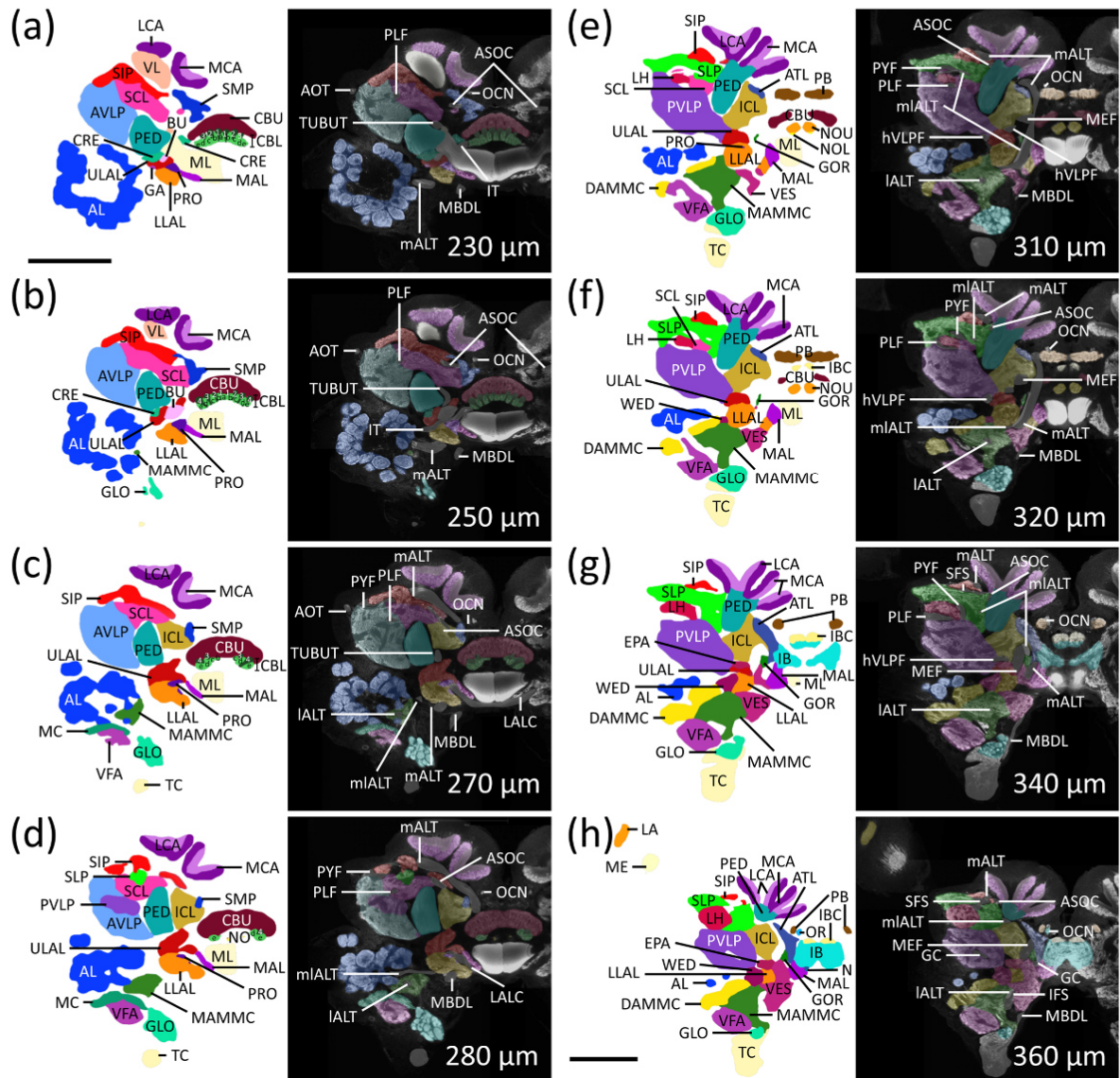
FIGURE 3 Series of frontal optical sections through the cockroach brain from the anterior brain surface (a) to a depth of 220 μm (h). Left panels: surface cuts of the 3D reconstruction with labeled neuropils. Right panels: corresponding confocal sections showing synapsin staining overlayed with a transparent surface cut of the 3D reconstruction. Tracts, fiber systems, and commissures are labeled. ABR, anterior bridge; AL, antennal lobe; ALI, anterior lip; ALT, antennal lobe tract; AOT, anterior optic tract; AOTU, anterior optic tubercle; AVLP, anterior VLP; CA, calyx; CB, central body; CBL, lower division of the CB; CBU, upper division of the CB; CRE, crepine; GA, gall; LAL, lateral accessory lobe; LCA, lateral CA; LLAL, lower LAL; LU, lower unit of the AOTU; MAL, medial accessory lobe; mALT, medial ALT; MBDL, median bundle; MCA, medial CA; ML, medial lobe; OCN, ocellar nerve; PED, pedunculus; PRO, prong; RUB, rubus; SCL, superior clamp; SIP, superior inferior protocerebrum; SMP, superior medial protocerebrum; TUBUT, tubercle-bulb tract; UU, upper unit of the AOTU; ULAL, upper LAL; VL, vertical lobe; VLP, ventrolateral protocerebrum. Scale bar = 400 μm

then turns ventrally and enters the bulb (BU) from dorsal direction (Figures 4a and 4b). We detected this tract with the help of two single-labeled neurons that arborize in the lower AOTU and connect it with the BU. A prominent structure within the lateral complex (LX) is the

isthmus tract (IT) that forms part of the border between the upper (ULAL) and lower LAL (LLAL), similar to the LALC. Numerous central-complex neurons run through the IT, including GABA-immunoreactive tangential neurons of the lower division of the central body (CBL;

FIGURE 4 Series of frontal optical sections ranging from a depth of 230 μm from the frontal brain surface (a) to a depth of 360 μm (h). Left panels: surface cuts of the 3D reconstruction with labeled neuropils. Right panels: corresponding confocal sections showing synapsin staining overlayed with a transparent surface cut of the 3D reconstruction. Tracts, fiber systems, and commissures are labeled. AL, antennal lobe; ALT, antennal lobe tract; AMMC, antennal mechanosensory and motor center; ATL, antler; AVLP, anterior VLP; AOT, anterior optic tract; BU, bulb; CA, calyx; CB, central body; CBL, lower division of the CB; CBU, upper division of the CB; GA, gall; GC, great commissure; GLO, glomerular lobe; GOR, gorget; CRE, crepine; DAMMC, dorsal AMMC; EPA, epaulette; IB, inferior bridge; IBC, IB cap; ICL, inferior clamp; IT, isthmus tract; LA, lamina; LAL, lateral accessory lobe; LALC, LAL commissure; LCA, lateral CA; LH, lateral horn; LLAL, lower LAL; MAL, medial accessory lobe; mALT, medial ALT; MAMMC, medial AMMC; MBDL, median bundle; MC, median crescent; MCA, medial CA; ME, medulla; MEF, medial equatorial fascicle; ML, medial lobe; mlALT, mediolateral ALT; NO, noduli; NOL, lower unit of the NO; NOU, upper unit of the NO; OCN, ocellar nerve; OR, ocellar root; PB, protocerebral bridge; PED, pedunculus; PLF, posterior lateral fascicle; PRO, prong; PVLP, posterior VLP; PYF, pyriform fascicle; SCL, superior clamp; SFS, superior fiber system; SIP, superior inferior protocerebrum; SLP, superior lateral protocerebrum; SMP, superior medial protocerebrum; TC, tritocerebrum; TUBUT, tubercle-bulb tract; ULAL, upper LAL; VES, vest; VFA, ventral area of flagellar afferents; VL, vertical lobe; VLP, ventrolateral protocerebrum; WED, wedge. Scale bar = 400 μm
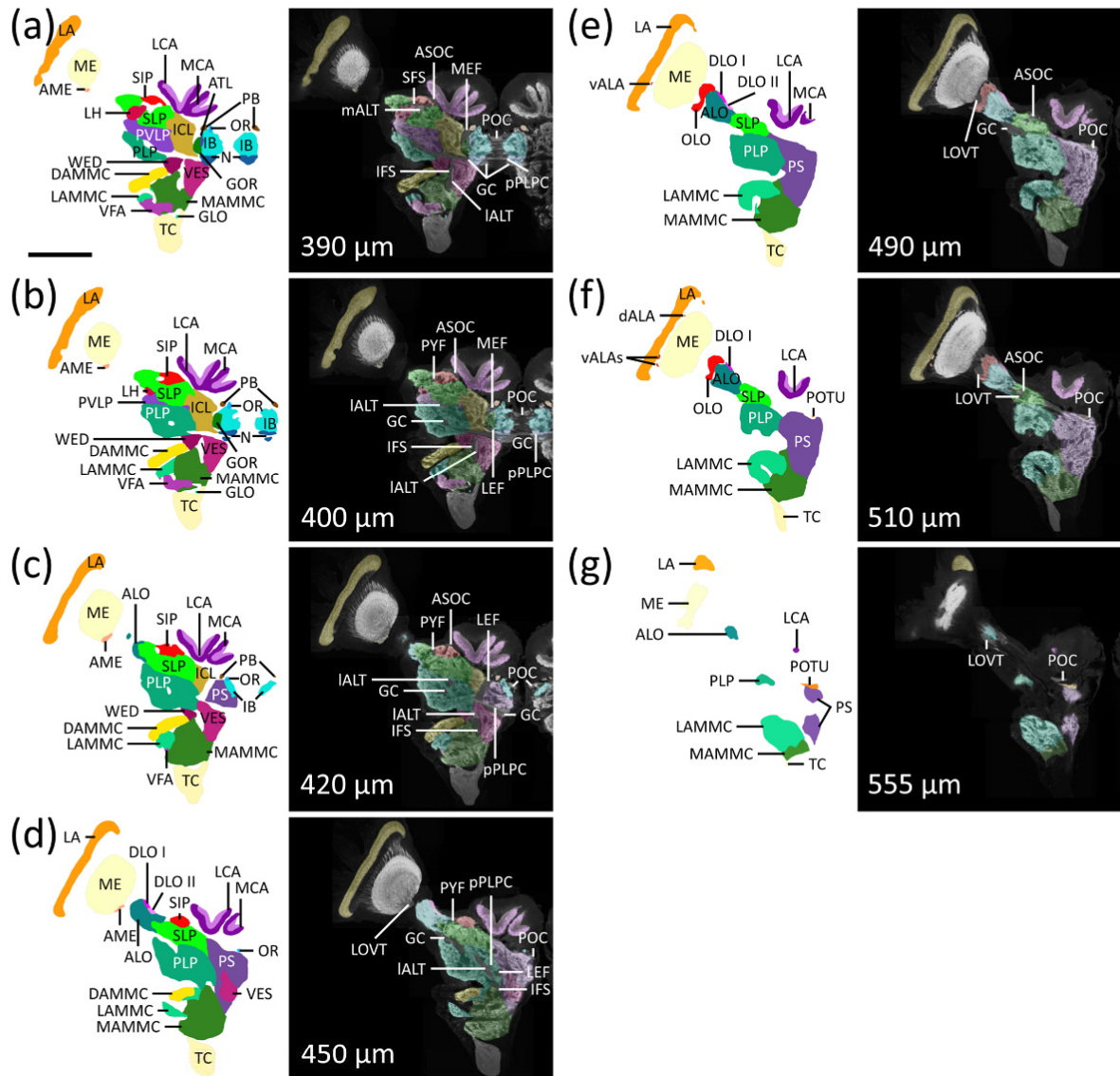
FIGURE 5 Series of frontal optical sections ranging from a depth of 390 μm from the anterior brain surface (a) to the posterior brain surface (g). Left panels: surface cuts of the 3D reconstruction with labeled neuropils. Right panels: corresponding confocal sections showing synapsin staining overlayed with a transparent surface cut of the 3D reconstruction. Tracts, fiber systems, and commissures are labeled. ALA, accessory LA; ALO, anterior LO; ALT, antennal lobe tract; AME, accessory ME; AMMC, antennal mechanosensory and motor center; ATL, antler; CA, calyx; LA, lamina; dALA, dorsal ALA; DAMMC, dorsal AMMC; DLO, dorsal LO; GC, great commissure; GLO, glomerular lobe; GOR, gorget; IB, inferior bridge; ICL, inferior clamp; IFS, inferior fiber system; LAMMC, lateral AMMC; LCA, lateral CA; LEF, lateral equatorial fascicle; LH, lateral horn; LO, lobula; mALT, medial ALT; MAMMC, medial AMMC; MCA, medial CA; ME, medulla; MEF, medial equatorial fascicle; N, neck; OR, ocellar root; PB, protocerebral bridge; PLP, posterior lateral protocerebrum; POC, posterior optic commissure; PS, posterior slope; PVLP, posterior VLP; PYF, pyriform fascicle; SFS, superior fiber system; SIP, superior inferior protocerebrum; SLP, superior lateral protocerebrum; TC, tritocerebrum; vALA, ventral ALA; VES, vest; VFA, ventral area of flagellar afferents; VLP, ventrolateral protocerebrum; WED, wedge. Scale bar = 400 μm

Homberg et al., 2018). Therefore, the IT (Figures 3h and 4a and 4b) is the major connection between the central body (CB) and LX. Additionally, we identified three ALTs, the mALT, lateral ALT (lALT), and mediolateral ALT (mlALT). The mALT is one of the most prominent tracts in nearly all known insect brains. It emerges dorsally from the AL, bypasses the CB posterior-laterally and turns anterior-laterally at the level of the PB (Figures 3g–h, and 4). From there, it continues ventrally along the calyces (CAs), bypasses the pedunculus (PED) anteriorly and terminates in the LH (Figures 4 and 5a). Arising from the AL, the lALT extends dorso-laterally through the VLP directly to the LH (Figures 4c–h and 5a–d). This tract was difficult to distinguish by synapsin labeling, because many of its fibers innervate the surrounding neuropils (Malun et al., 1993). Thirdly, the mlALT lies directly lateral to the mALT. It contains many GABA-immunolabeled fibers, and was, thus, easy to reconstruct. It runs up to the IB, then ventrally along the antler (ATL) and dorsal to the ICL, bypasses the PED anteriorly, and targets the LH (Figures 4c–h). Ocellar nerves (OCNs) comprise neurites from the ocelli that enter the PS through the ocellar roots (OR). Cockroaches have two OCNs, corresponding with the number of ocelli (Figures 3g–h, and 4). Finally, we identified the median bundle (MBDL). It extends dorso-ventrally along the anterior face of the brain midline, is located posterior to the anterior bridge (ABR), and splits ventrally into a fiber bundle in each hemisphere that runs ventrally along the lateral side of the esophagus (Figures 3c–h and 4). Neurosecretory cells of the pars intercerebralis (Gundel & Penzlin, 1980; Pipa, 1978) as well as intersegmental neurons (to and from the tritocerebrum) have axonal fibers within the MBDL.

3.2 | Optic lobe

The OL (Figures 5 and 6a–c) consists of the lamina (LA), accessory laminae (ALAs), medulla (ME), AME, and the LOX. All of these neuropils process visual signals from the compound eye. The three-layered LA and 10-layered ME are connected by fibers in the first optic chiasma and have been investigated in detail before (Arnold et al., 2020; Giese et al., 2018; Massah et al., 2022). Five ALAs are associated with the LA. They are small oval and synapsin-rich areas at the proximal posterior edge of the LA, three at the dorsal posterior edge (dALAs) and two at the ventral edge (vALAs), clearly separated by the first optic chiasma between the LA and ME (Figures 5e–f, 6a, and 6c) and innervated by PDH-immunoreactive processes (Massah et al., 2022). The AME (Figures 5a–d and 6a–c), the master circadian pacemaker of the cockroach, is a small neuropil anteriormedial to the ME (Homberg et al., 2003b; Petri et al., 1995; Reischig & Stengl, 2003a,b). Six PDH-immunoreactive fibers connect the AME via the LOVT to targets in the ipsilateral (n = 2) and contralateral (n = 4) central brain (Petri et al., 1995). The medially adjacent LOX is subdivided into the anterior LO (ALO), outer LO (OLO), and dorsal LO (DLO) I + II. Rosner et al. (2017) defined the LOX subunits and we based our 3D reconstruction on their data. The DLO consists of two small elongated neuropils at the dorsal, lateral surface of the LOX and is distinguishable by dense GABA immunostaining (Figure 6b). It is subdivided into two layers by a clear

cut in synapsin staining as described by Rosner et al. (2017). The OLO extends over the most distal parts of the LOX, wedged between the ALO and ME/AME (Figures 6a and 6c). The ALO is the largest part of the LOX. Its neuropil is confluent with the medially adjacent SLP (Figures 1, 5d–f, 6b, and 6c).

3.3 | Mushroom body

The bilaterally symmetrical MBs take up considerable space in the cockroach brain. They receive input from projection neurons of the AL and play an important role in chemosensory signal processing, learning and memory formation. In R. maderae the MB consists of the PED, the VL, the medial lobe (ML), and two calyces (CA). The PED, VL, ML, and CAs are clearly delineated by surrounding glial processes and fiber tracts (Figures 6d–f). The PED and lobes served as references for several neuropil boundaries, especially for the separation of the inferior neuropils (INP) of the protocerebrum. The two CAs, the medial (MCA) and lateral CA (LCA), extend over almost the entire dorsal surface of the protocerebrum (Figures 1 and 6e). Each CA is further divided into an outer sheet (OCA) innervated by large GABA- and SIFamide-labeled fibers (Arendt et al., 2016; Massah et al., 2022) and an inner sheet (ICA) that contains neurites of Kenyon cells (Strausfeld & Li, 1999). The ICA is free of GABA- and synapsin immunostaining (Figures 3–5) and can be described as a bifurcated extension of the PED (Figure 6d, yellow asterisks). The Kenyon-cell axon bundles from the OCA and ICA fuse at the neck of the PED neck, before constituting the PED (Figures 4e–h and 6d). The neck could not be distinguished by synapsin- and GABA immunolabeling from the rest of the PED. The PED extends ventrally and bifurcates into the VL and ML at the pedunculus divide (PEDD; Massah et al., 2022) which was not reconstructed as a separate neuropil (Figure 6f). In D. melanogaster, S. gregaria, and A. infusa the region contains a lateral extension, the spur (SPU) that could not be found in the cockroach brain. From the PEDD, the large ML extends medially, ventral to the CX and adjoins the contralateral ML at the midline (Figures 4e–h and 6f). The VL extends from the PEDD nearly parallel to but anterior from the PED in dorsal direction, up to the anterior surface of the brain (Figures 3, 4a–b, and 6d–f).

3.4 | CX and anterior lip

The neuropils of the CX span across the brain midline and consist, as in other insect species, of the CB, divided into a lower (CBL) and upper (CBU) division, the PB, and the bilaterally symmetrical globular-shaped noduli (NO; Figures 7a and 7a'). The PB is the most dorsal and posterior neuropil of the CX and lies dorsoposterior to the CB. It is an elongated neuropil shaped like a handlebar with its lateral tips bent posteriorly (Figures 1c and 7a). A thick fiber bundle that runs through the PB connects its two hemispheres (Figures 4e and 4f). A posterior chiasma of fibers connects the PB to the CB. The CBU lies ventrally from the PB and has a kidney-shaped form typical for a hemimetabolic insect (Figures 7a and 7a'). Immunolabeling with antisera against tyro-
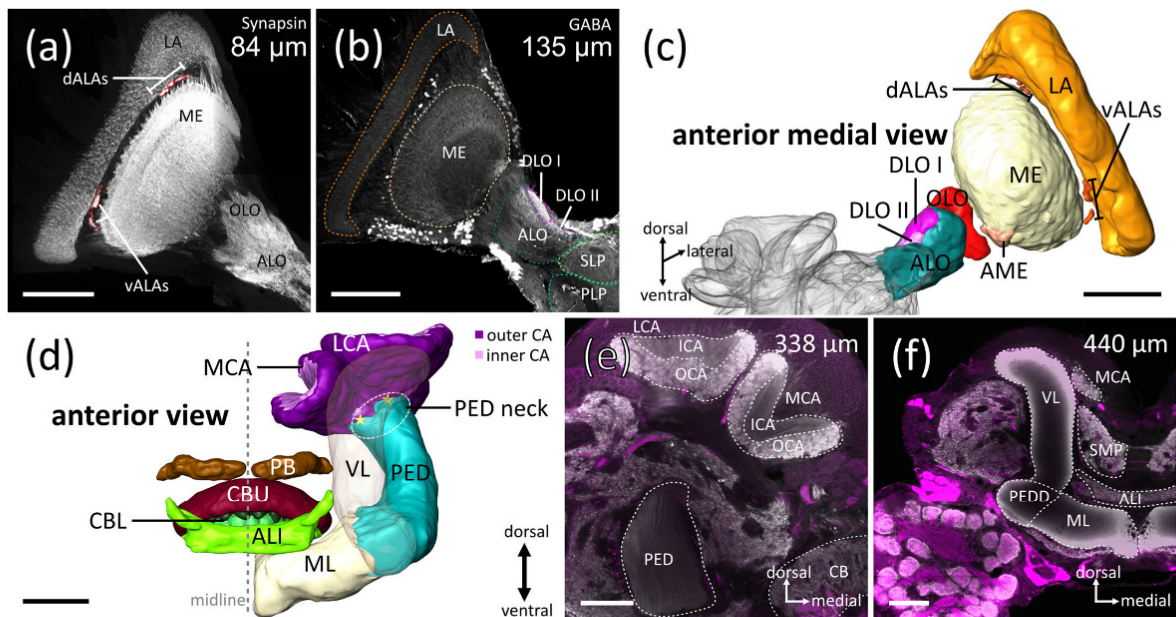
FIGURE 6 Organization of the optic lobe (a–c) and mushroom body (d–f). (a) Projection view of a stack of 40 synapsin labeled sections. At the dorsal proximal edge of the lamina (LA), three accumulations of synapsin-rich areas, the dorsal accessory LAs (dALAs), are visible. Slightly more anterior, two ventral ALAs (vALAs) lie at the proximal edge of the LA, between the LA and medulla (ME), outlined with a red dotted line. (b) Single optical section showing GABA staining. The reconstructed neuropils are surrounded by dotted lines. The dorsal lobes I and II of the lobula (DLO I and II) are distinguished by strong immunoreactivity from the less intensely stained anterior lobula (ALO). (c) Anterior medial view of the 3D reconstruction of the cockroach hemibrain, illustrating the neuropils of the optic lobe in 3D reconstruction. AME, accessory medulla; LO, lobula; OLO, outer LO; PLP, posterior lateral protocerebrum; SLP, superior lateral protocerebrum. (d–f) Organization of the mushroom body (MB). (d) Anterior view of the 3D-reconstructed neuropils of the MB and, for spatial orientation, the central body (CB) and anterior lip (ALI). The vertical lobe (VL) is half-transparent for better visibility of the underlying neuropils. Dotted ellipse marks the PED neck, and the two yellow asterisks mark the two extensions of the PED toward the calyces (CAs). (e and f) Single optical sections of synapsin- (gray) and GABA immunolabeling (magenta). The inner CA (ICA) of the lateral (LCA) and medial CA (MCA) shows poor synapsin- and GABA labeling. Dotted outlines mark the MB and surrounding neuropils. CBL, lower division of the CB; CBU, upper division of the CB; ML, medial lobe; NO, nodulus; OCA, outer CA; PB, protocerebral bridge; PED, pedunculus; PEDD, pedunculus divide; SMP, superior medial protocerebrum. Scale bars = 200 μm (a–d) and 100 μm (e and f)

sine hydroxylase (Timm et al., 2021), SIFamide (Arendt et al., 2016), GABA (Homberg et al., 2018), orcokinin (Hofer et al., 2005), and myoinhibitory peptide (Schulze et al., 2012) revealed at least three horizontal layers and nine vertical segments in the CBU, while these subcompartments could not be clearly distinguished with anti-synapsin. The CBL adjoins ventrally and shows a highly peculiar internal organization. It is divided into eight cone-like compartments (cones, CO; 1–4 in each hemisphere) and nine tooth-like structures (TH; e-d-c-b-a-b-c-d-e) framing the eight cones (Figure 7a'). Both, cones and teeth are innervated by tangential neurons that connect the CBL with the BU through the IT (Homberg et al., 2018) and are strongly GABA-immunoreactive (Figure 7d). A pair of NO (Figures 4d–f) lies posterior-ventrally from the CB and consists of larger upper units (NOU) and smaller lower units (NOL; Figure 7a'). Based on orcokinin- and synapsin immunolabeling, three layers can be distinguished in the NOU (Figure 7e).

The anterior lip (ALI) (Figures 3e–f and 7a–d") is a CX-associated neuropil that has not been recognized as a distinct neuropil in *D. melanogaster* (Ito et al., 2014). In the cockroach it is a prominent, elon-

gated neuropil fused across the brain midline. It lies directly anterior to the CB and is framed ventro-medially by the MLs and VLs and dorsally by the SMP. Small regions lateral to the ALI, characterized by GABA-immunoreactive processes, were assigned to the CRE, while the ALI itself is largely free of GABA immunostaining (Figure 7d").

3.5 | Lateral complex

Neuropils of the CX are strongly connected with the LX. The LX differs in many insect species in form, arrangement, and number of subcompartments. Based on GABA- and synapsin immunolabeling and single-cell dye injections, the LX in the cockroach is subdivided into two major areas: the BU and the LAL. The LAL is further subdivided into the gall (GA), the upper LAL (ULAL) and lower LAL (LLAL) with a newly defined neuropil, the prong (PRO) as part of the LLAL (Figure 7a,a'). Ramification areas of columnar neurons of the CBL characterize the GA (CL neurons; Figures 7b and 7b'). In *R. maderae*,
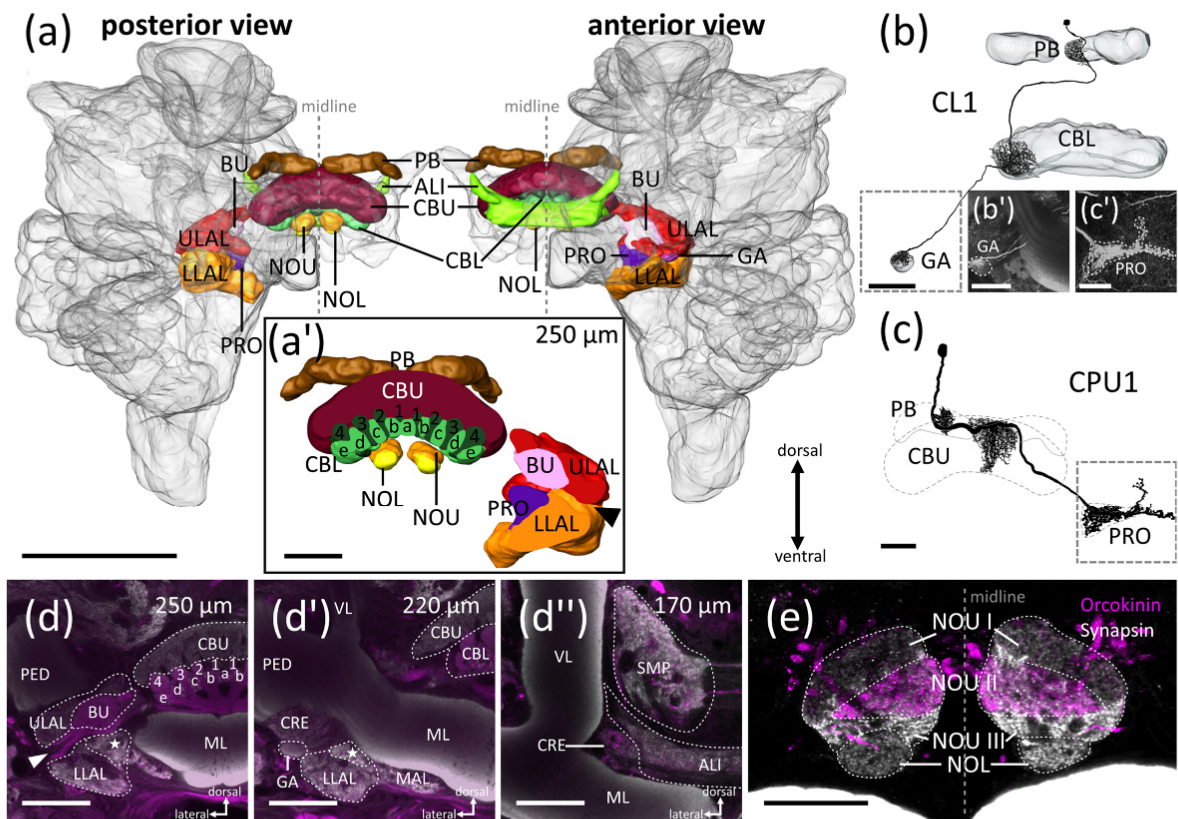
FIGURE 7 Organization of the central complex (CX) and lateral complex (LX). (a) Posterior (left) and anterior (right) view of the 3D rendition of the cockroach brain. Neuropils of the CX and LX are shown in a transparent 3D brain. (a′) Anterior view of a surface cut of the reconstructed CX and LX at a level of 250 μm. The lower division of the central body (CBL) consists of 9 teeth (labeled e-a-e) and in between 8 cones (4-1-1-4). The noduli (NO) are subdivided into upper (NOU) and lower units (NOL). The upper LAL (ULAL) is separated from the lower LAL (LLAL) by the isthmus tract (IT; black arrowhead). (b) 3D reconstruction of a columnar neuron of the CBL (CL1 neuron) in transparent reconstructed neuropils. The arborization area outside of the CX defines the gall (GA). (b′) Image stack of the ramification area of the Neurobiotin-labeled CL1 neuron in the GA. (c) 2D drawing of a columnar neuron of the protocerebral bridge (PB) and the upper division of the central body (CBU; CPU1 neuron). Its arborization area outside the CX defines the borders of the prong (PRO). (c′) Image stack of the stained CPU1 arborizations within the PRO. (d–d″) Single optical sections illustrating the organization of the CB and LX through synapsin (gray) and GABA (magenta) staining. Stars mark the position of the PRO distinguished by strong synapsin immunolabeling. (d″) GABA-immunolabeled region of the crepine (CRE) sets the boundary between the CRE and the anterior lip (ALI). (e) Single optical section of both NO, in synapsin- (gray) and orcokinin (magenta) double staining. The NOU consist of three layers, layer I with weak synapsin staining, layer II with strong orcokinin labeling, and layer III with strong synapsin staining. BU, bulb; LAL, lateral accessory lobe; MAL, medial accessory lobe; ML, medial lobe; PED, pedunculus; SMP, superior medial protocerebrum; VL, vertical lobe. Scale bars = 400 μm (a), 100 μm (a′, d–d″), and 50 μm (b–c′, e)

the GA is easily recognized by synapsin staining and appears as a smooth, small globular neuropil that lies directly anterior to the IT and between an extension of the CRE and the ULAL (Figures 3g–h, 4a, and 7a, 7b, 7b′, 7d′). The PRO is embedded in the LLAL; it has a triangular form (Figure 7a′) with two small peaks that extend posteriorly (Figures 4c–4e). It is characterized by the arborization domains of columnar neurons of the PB and CBU within the LAL (CPU neurons; Figures 7c and 7c′). It lies ventral to the IT and shows strong synapsin staining (Figures 3g–h and 4a–e). The surrounding LLAL lies ventral to the ULAL and is anteriorly covered by the ML and CRE. GABA labeling

in the CRE resulting from neurons that target the outer CA served as a criterion for defining the border between the CRE and the LLAL. Posterior boundaries of the LLAL were more difficult to determine and were set at the level of the mALT projecting toward the superior brain (Figure 4g). In addition, the posterior part of the LAL is penetrated by many fiber tracts and has, thus, a porous character that distinguishes it from the adjacent VES and WED (Figures 4e–g). Medial limits are given by the mALT, in addition to the medial accessory lobe (MAL) and VES, while anteriorly the MBDL and the cell body rind build the borders to the LAL (Figures 3f–h and 4). Both units of the LAL are

separated from each other by the LALC (Figures 4c and 4d) and IT (Figures 3a–b and 7a', 7d). The anterior boundary of the ULAL was set by the ML, except for a small ventral peak that continues further anteriorly and ends with the CRE and the ML (Figures 3g and 3h). The mALT and EPA delineate the posterior border of the ULAL (Figures 4g and 4h). The PED and VLP adjoin laterally (Figure 4). Medially, the CX, mALT (Figures 4a–f), and the GABA-immunoreactive BU and IT build the border (Figure 7d). Dorsally, the ICL, PED, and TUBUT lie next to the ULAL, whereas the border between the highly contiguous ICL and ULAL was defined by the TUBUT as it enters the BU (Figure 4b). The BU is defined as the arborization area of GABA-immunolabeled tangential neurons of the CBL. These neurons have cell bodies clustered near the AL (Homberg et al., 2018; Massah et al., 2022) and send axons through the IT to the CX. In contrast to other insects no further subdivisions were recognized in the BU of the cockroach (Homberg et al., 2018; Figures 7a, 7a', and 7d).

3.6 | Superior neuropils

Superior neuropils include the superior lateral (SLP), superior intermediate (SIP) and superior medial (SMP) protocerebrum, the anterior bridge (ABR), and the LH that span across the dorsal part of the brain, below the CAs (Figures 1 and 8a, 8b). The LH is a spheroidal structure in the lateral cerebrum and was identified by synapsin staining and massive converging fiber tracts (Figures 4e–h, 5a, 5b, and 8c). These include mostly projections from the AL that innervate the LH as a second-order processing center of olfactory cues. The mALT enters the LH dorsally (Figures 4f–h), the mlALT, likewise, enters the LH dorsally and separates it from the SLP (Figure 4e) and the lALT that runs through the IFS and targets the ventral side of the LH (Figure 5b). In addition, the SFS as well as the PYF are located dorsally from the LH and build borders between SLP and LH to the SIP (Figures 4g, 4h, 5a, and 8b, 8c). The PLF flanks the LH ventrally and sets the border between the LH and the PVLP (Figures 4e–g). The crossing point of the PYF and mlALT (depth 320 μm, Figure 8c) marks the level of the anterior boundary of the LH as described in *D. melanogaster* (Ito et al., 2014). Its borders were additionally recognizable by the lack of serotonin immunostaining within the LH (Figure 8e). The LH is dorso-posteriorly embedded in the SLP, the most lateral neuropil of the central brain positioned between the LOX and the medially adjacent SIP (Figure 1). The fusion of the PYF and the SFS not only forms the border between SLP and SIP, but also marks the anterior boundary of the SLP (Figure 8c). The lateral extent of the GC was used as the boundary between SLP and PLP (Figure 5d) and, more anteriorly, the PLF (Figure 9a) that runs between the SLP and PVLP (Figures 4f and 4g). Medial boundaries in posterior parts are the PED, ICL, and the PS (Figures 4e–h and 5). In addition, denser synapsin staining of the SIP as well as strong serotonin staining of the SLP helped in determining the boundary between SLP and SIP (Figures 8c and 8e). The dorsal edge of the SLP, departing from the ASOC, is innervated by PDH-immunoreactive arborizations, defined as fiber plexus p3, whereas the fiber plexus p1 still lies within the LOX of the cockroach (Wei et al., 2010; Figure 8d'). Small branches of the PDH-

labeled neurons (part of the anterior fiber plexus, AFP) also extend into regions of the SIP (Figure 8d).

The SIP adjoins the SLP medially, covers almost the complete superior surface of the brain (Figures 1 and 8a–c), and wraps posteriorly around the VL (Figures 4a–d). Anteriorly, the SCL and the AVLP flank the ventral part of the SIP (Figures 3e–h and 4a–d). In the anterior-most region, the CRE lies next to the SIP (Figures 3b–d) but is distinguished from it by strong synapsin staining and massive innervation by fiber tracts of the SCL (Figures 10g and 10g'). Aside from that, the SFS was used as a landmark between the SIP and the ventrally lying SLP (Figure 4h). Medially, the SIP connects with the SMP (Figures 4a, 4b and 8a, 8b). The SMP extends from the posterior face of the CRE to the anterior surface of the ICL and is relatively easy to identify by large fibers that run through this neuropil (Figures 3c–h, 4a–d). At the level where the mALT extends in vertical direction, the SMP ends (Figure 4e). Medial limits are defined by fiber bundles around the CBU and MBDL; laterally the SIP, VL, and SCL adjoin (Figures 4c–h and 5a–c). The SMP is innervated by PDH-immunolabeled fibers of the ASOC (plexus a2; Figure 8d). In *D. melanogaster* the SMP is divided into an anterior and posterior region, because the fan-shaped body protrudes into the SMP, but we observed no further partition in the cockroach. The SMPs of both hemispheres are not fused at the midline unlike in some other insects, but are connected with the ABR (Figures 3c,d and 8a). The ABR is the most medial neuropil of the SNPs and spans across the anterior brain midline (Figures 1, 3b-d, and 8a,b). Posteriorly, it borders on the MBDL, whose fibers spread bilaterally ventrally and set the lateral borders of the ABR, too (Figure 8b).

3.7 | Ventrolateral neuropils

The ventrolateral neuropils (VLNP) (Figure 9a) lie below the SNP and consist of the anterior optic tubercle (AOTU), VLP, PLP, and the WED. The AOTU is the most anterior neuropil of the VLNP and is subdivided into a large subunit (upper unit, UU) and a smaller subunit (lower unit, LU). The latter is further divided into two subunits (Figures 1a, 3a-c, and 9a,b). The AOTU was easily recognized by synapsin staining, and its subunits were distinguished with the help of two injected neurons that connect the lower subunits of the AOTU with the BU through the TUBUT (Figure 9b,b'). The TUBUT served as a landmark, separating the UU from the two LUs (Figure 3b and 9a). The AOTU receives massive bundles of fibers via the AOT that connects the LO and ME to the AOTU.

The VLP borders posteriorly on the AOTU and is divided into two regions, the AVLP and PVLP. The AVLP is anteriorly flanked by the AOTU, CRE, and the anterior cell body rind (Figure 3a-c). The CRE is distinguished from the AVLP by denser GABA staining originating from neurons innervating the CA (Figure 10g'). Posterior borders are more ambiguous and directly flanked by the PVLP. One criterion was the PED that runs dorsally when the AVLP ends and a change in synapsin staining which becomes more porous and denser (Figure 4d) like in the locust (von Hadeln et al., 2018). The AFP formed by PDH-immunoreactive arborizations (Wei et al., 2010) is confined to the
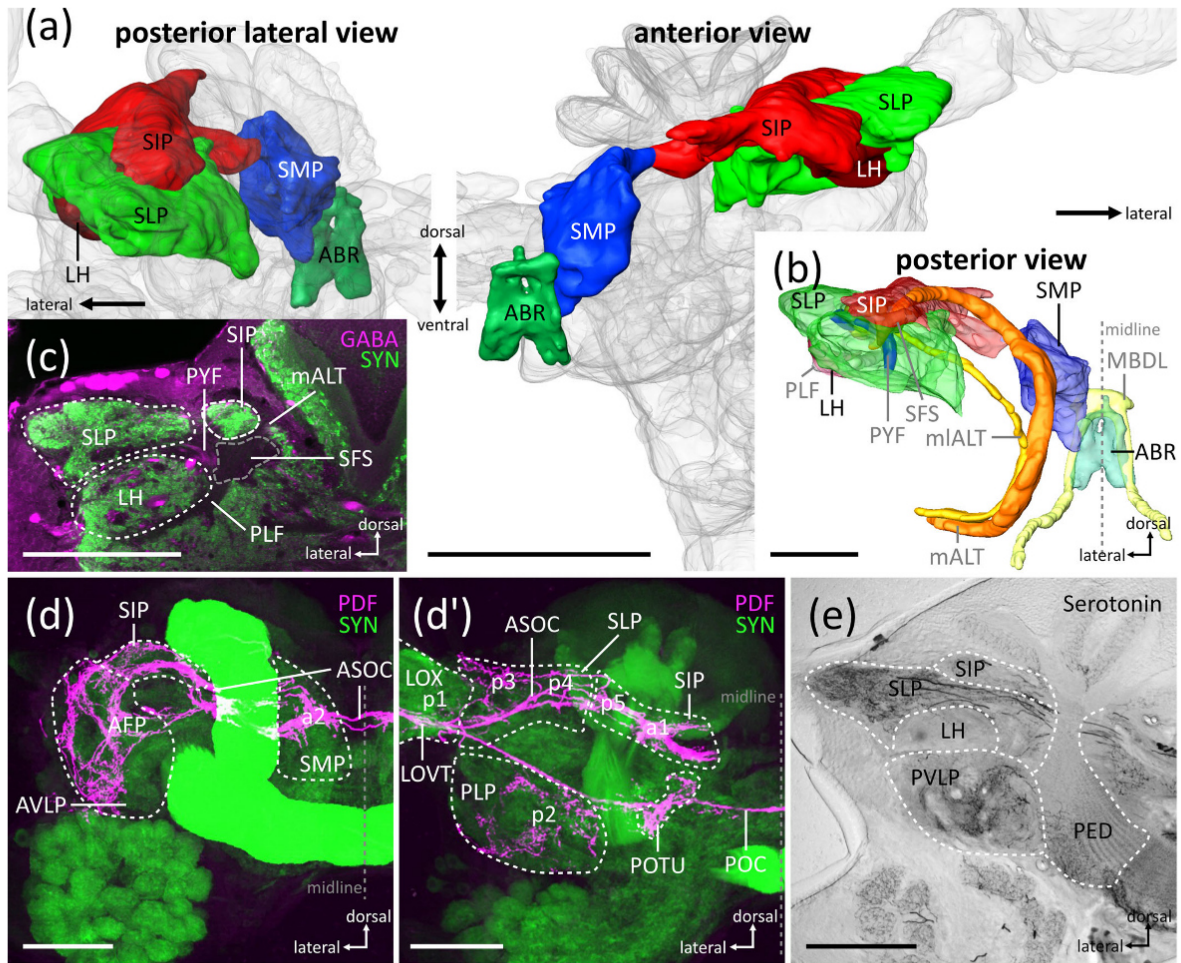
FIGURE 8 Reconstruction and boundaries of the superior neuropils (SNP). (a) 3D reconstruction of the SNP within a transparent 3D brain hemisphere. Left panel, oblique posterior lateral view, right panel, anterior view. (b) Posterior view of the reconstructed SNP (semi-transparent) with reconstructed tracts that were used as boundaries. (c) Optical section at 380 μm showing synapsin- (green) and GABA- (magenta) staining. Dotted lines mark the borders of the superior lateral protocerebrum (SLP), superior inferior protocerebrum (SIP), and the lateral horn (LH). The medial antennal lobe tract (mALT) projects posterior-medially from the SIP toward the LH. The superior fiber system (SFS, gray dotted line) separates the SIP, LH, and the inferior neuropils (INP). The posterior lateral fascicle (PLF) marks the ventral and anterior border of the LH, whereas the posterior pyriform fascicle (PYF) marks the border between SIP and LH. (d) Projection view of optical sections ranging from the anterior brain surface to a depth of 190 μm and (d') from 200 μm to the posterior brain surface of a synapsin- (green) and PDH- (magenta) stained brain. PDH-immunoreactive fibers from the accessory medulla project through the lobula valley tract (LOVT) and give rise to dense fiber networks in distinct brain regions termed plexus 1 (p1, in LOX), plexus 3 (p3, in SLP), plexus 4 (p4, in SLP), plexus 5 (p5, in SIP), area 1 (a1, in SIP), and area 2 (a2, in SMP) along the anterior superior optic commissure (ASOC). Plexus 2 (p2) lies in the posterior lateral protocerebrum (PLP) and the anterior fiber plexus (AFP), in the anterior ventrolateral protocerebrum (AVLP). PDF-fibers in the posterior optic tract innervate the posterior optic tubercle (POTU) and cross the brain midline via the posterior optic commissure (POC), (e) 40-μm section immunostained for serotonin. Dotted lines mark the borders of the SLP, SIP, LH, pedunculus (PED), and the posterior ventrolateral protocerebrum (PVLP). Scale bars = 400 μm (a), and 200 μm (b–e)

AVLP and, thus, served as a useful landmark as well (Figure 8d). The medial boundaries of the AVLP are the VL and PED (Figures 3a-h and 4a-d). Dorsally, the AVLP is flanked by the CRE, SIP and SCL, whereas the TUBUT separates the AVLP from the CRE (Figure 3c). The posterior borders of the AVLP to the SIP and SCL were not obvious in synapsin staining, but the whole VLP stands out from the rest of the brain by strong serotonin immunolabeling (Figure 8e). The PVLP

extends up to the anterior dorsal surface of the GC that was set as the separation between the PVLP and PLP (Figures 5a and 9a) as described in *S. gregaria* (von Hadeln et al., 2018). Medially lying neuropils are highly variable, including the ICL, EPA, WED and ULAL (Figures 4d-h and 5a). The hVLPF separates the PVLP from the EPA (Figure 4f,g), whereas the WED is well distinguishable from surrounding neuropils by synapsin staining and a perforated structure (Figures 4g,h and 5a,b).
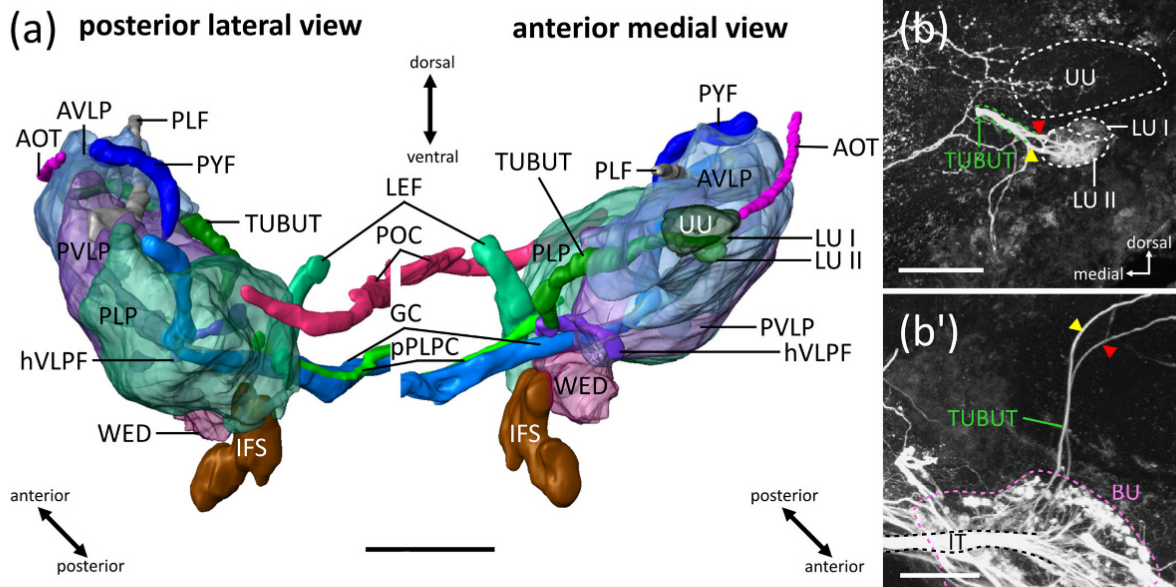
FIGURE 9 3D reconstruction and boundaries of the ventrolateral neuropils (VLNP). (a) 3D reconstruction of the VLNP (semi-transparent) and tracts and commissures defining boundaries. (b) Projection view of 30 optical sections showing two Neurobiotin-injected neurons of the tubercle-bulb tract (TUBUT, red and yellow arrowhead) innervating the lower units (LU I, LU II) of the anterior optic tubercle (AOTU). (b′) Projection view of 80 optical sections of multiple injected neurons with Neurobiotin, showing the two neurites of (b) entering the bulb (BU). No further connections are seen in the BU, because of additional massive staining of tangential neurons of the CBL that run through the isthmus tract (IT) to the BU. Scale bars = 200 μm (a), and 100 μm (b, b′)

The boundary of the PVLP (Figures 4d-h, 5a,b and 9a) to the ULAL is marked by a tract, the hVLPF (Figures 4e-g and 9a). Dorsally, the ICL, SLP, and LH flank the PVLP (Figures 4e-h and 5a). The LH and PVLP are separated by the PLF (Figure 4g), whereas the boundary between SLP and PVLP is more ambiguous and was set by the level of the PLF and the PYF (Figure 4e-g), in addition to differences in serotonin immunolabeling (Figure 8e).

Posterior to the GC, the PLP extends up to the posterior surface of the brain (Figure 5). Anteriorly, it is completely covered by the PVLP. The medial boundaries are marked by the glomerular structure of the WED, the VES, and the IFS (Figure 5). It contains PDH-immunoreactive fibers (plexus p2) that innervate the outer part of the PLP (Figure 8d′). The last neuropil of the VLNPs, the WED, was relatively easy to identify by porous appearance of synapsin staining (Figures 4g,h and 5a-c), because it is penetrated by fibers that connect it with parts of the AMMC. Medially, the IFS flanks the WED (Figure 5a-c), whereas the ventral borders were not as easy to set. Here the dorsal AMMC (DAMMC) and medial AMMC (MAMMC) adjoin and were determined with the help of synapsin staining (Figures 4g,h and 5a,b).

3.8 | Inferior neuropils

The CRE, rubus (RUB), superior (SCL) and inferior (ICL) clamp, IB and IB cap (IBC), ATL, MAL, neck (N), and the OR belong to the INP (Figure 10). In the fruit fly, the CRE is a thin neuropil that surrounds the shaft of the ML. In the cockroach, it covers large parts of the anterior surface of the protocerebrum. It extends from the MBDL/ABR near the brain midline to the SIP and AVLP laterally (Figures 1a, 3, and 10a). The VL, ML, and the SMP, except of two small bulges that wrap around the base of the ML, define its posterior border (Figure 3). The dorsal bulge of the CRE runs laterally along the ALI, between the ALI and ML up to the region where the ULAL emerges (Figures 3e-h and 4a). This region of the CRE could be distinguished from the ALI through GABA immunostaining in the CRE, which is lacking in the ALI (Figure 7d″). The ventral bulge extends ventrally around the ML and ends with the ventral lateral part of the ULAL (Figure 4a,b). This region is characterized by ramification areas of columnar neurons of the CBU (CU neurons; Schulze et al., 2012; Figures 7d′ and 10c). Because in *D. melanogaster* all ramification areas of CU neuron equivalents (FC and FR cells) outside the CX were
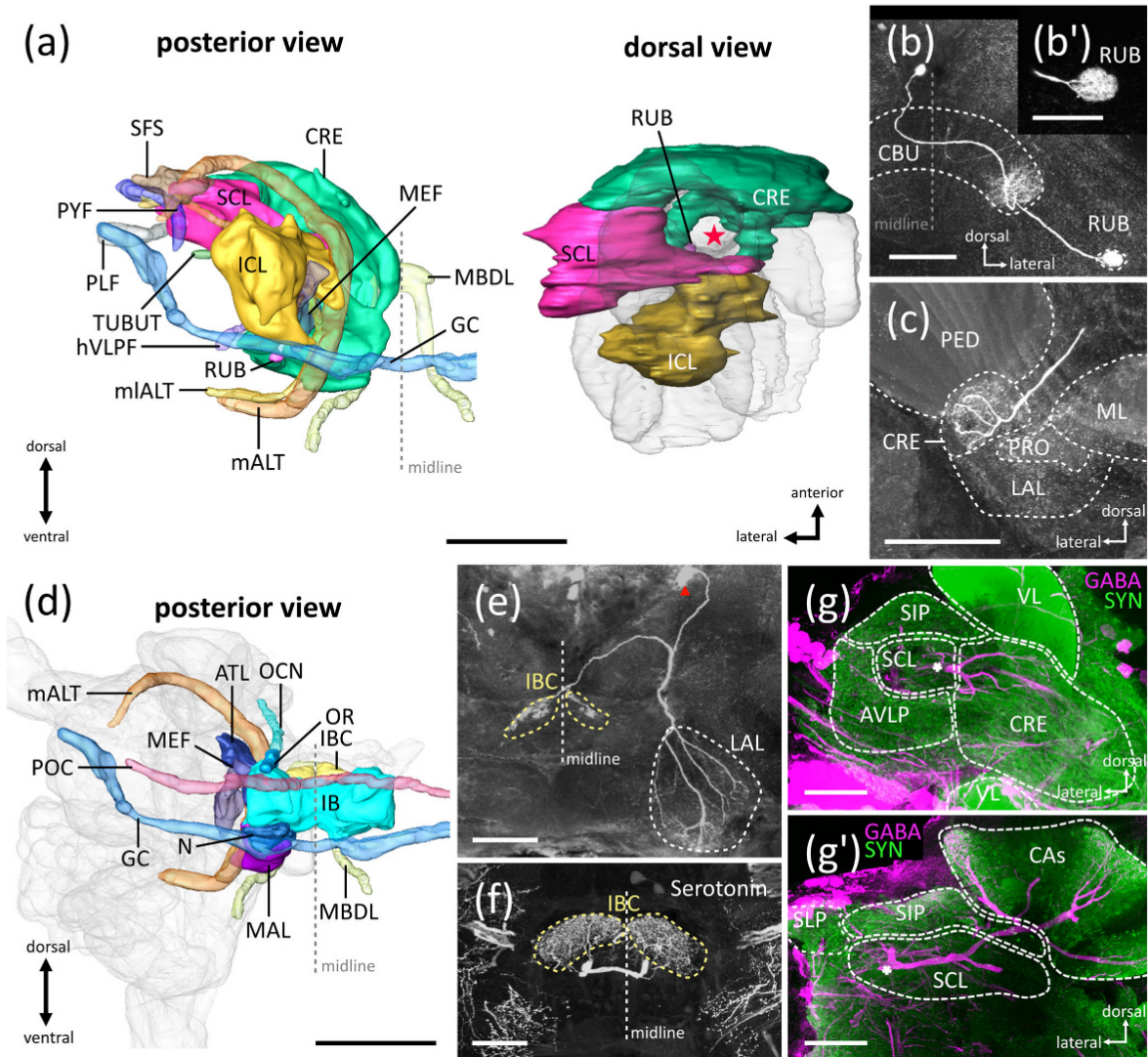
FIGURE 10 Anatomical overview of the inferior neuropils. (a) Posterior (left) and dorsal (right) view of the 3D reconstructed crepine (CRE), inferior (ICL) and superior clamp (SCL), and the rubus (RUB). The left panel includes selected tracts that were used as landmarks. The neuropils in the right panel are shown with the transparent mushroom body of one brain hemisphere. Red asterisk marks the PED. (b) Ramifications of a columnar neuron of the CBU (CU neuron) with arborizations in the RUB shown in detail in (b'). (c) Single Neurobiotin-injected CU neuron with terminals in the posterior peak of the CRE. (d) Posterior view of the inferior bridge (IB), the IB cap (IBC), the medial accessory lobe (MAL), the antler (ATL), and the ocellar root (OR). The neuropils are embedded in the transparent 3D brain hemisphere. Selected tracts that were used as landmarks are included. (e) Anterior projection view of 200 optical sections of a Neurobiotin-injected neuron with arborizations confined to the IBCs and wide arborizations in the lateral accessory lobe (LAL). Red arrowhead marks the soma. (f) Projection view of serotonin-immunostained arborizations within the IBCs. (g, g') Frontal projection views of two consecutive stacks of 150 optical sections showing GABA-immunoreactive giant neurons innervating the calyces (magenta) together with synapsin labeling (green). (g) Anterior ramifications of the GABA immunoreactive neurons in the CRE that enter from the SCL (white asterisk). Asterisk point to continuing neurites in (g'). (g') Arborizations in the calyces (CA) and the neurites running through the SCL. AVLP, anterior ventrolateral protocerebrum; SIP, superior inferior protocerebrum; SLP, superior lateral protocerebrum; TUBUT, tubercle-bulb tract; VL, vertical lobe. Scale bars = 200 μm (a, d), 50 μm (b'), and 100 μm (b, c, e–g')

assigned to the CRE, we included these regions as part of the CRE as well. A small spherical area at the posterior end of the ventral bulge of the CRE, the RUB, showed distinct synapsin labeling (Figure 3g,h). It was first recognized in the fruit fly as the termination site of fibers from the CX and was termed rubus (RUB; Scheffer et al., 2020). It lies medially adjacent to the GA and contains ramifications of a subtype of CU neurons that are confined to this area (Figure 10b,b′).

The clamp (CL), subdivided into the SCL and ICL (Figure 10a), lies in the medial protocerebrum and extends from the AVLP/SIP to the CB. The SCL is covered anteriorly by the AVLP and the CRE (Figure 3d-h). GABA-labeled neurons targeting the CAs run through the SCL and project into the CRE (Figure 10g,g′). Posteriorly, the SLP adjoins and the PYF serves as a clear border (Figure 3f). Laterally, it is restricted by the SIP, AVLP (Figures 3e-h and 4a-d), and LH (Figure 4e,f). The border between the SCL and SIP is defined by the PYF (Figure 4c,d), whereas the border between the SCL and AVLP is more ambiguous. It was determined by the appearance of synapsin immunolabeling, because the SCL is characterized by large penetrating fiber bundles that are missing in the AVLP (Figure 3g). Furthermore, the AVLP is densely innervated by PDH-immunoreactive fibers (Figure 8d). Medial boundaries of the SCL are the PED and VL (Figures 3 and 4a-d) while the SMP and ICL adjoin, flanked by the PED and VL. PDH-immunoreactive fibers in the ASOC run dorsal to the SCL/ICL and were used to define the border between the INP and SNP (Figures 4b-d, 8d,d′, and 10a). The ICL and SCL were difficult to differentiate. Their common boundary was set by the level of the ascending PED (Figure 4d) as described in *S. gregaria* (von Hadeln et al., 2018). The ICL adjoins the SCL medially and is flanked by a collection of other neuropils. Posteriorly, it is covered by the PS at the level of the LEF that runs dorsally between the PS and ICL (Figure 5c,d). Anteriorly, the SCL and SMP lie next to it (Figure 4b-d). Strong synapsin labeling and PDH-immunolabeled arborizations (a2, Figure 8d) within the SMP characterize the transition to the SMP. Several neuropils adjoin laterally: the PED, PVLP, SLP and PLP. Medially, the PS, gorget (GOR), ATL, SMP, and the CB appear. All of these neuropils were easy to differentiate from the ICL by the mALT, mlALT, and the MEF. The ULAL, EPA and GC flank the ventral side of the ICL (Figures 4c-h, 5a-c, and 10a). Whereas the GC marks the posterior boundary of the ICL (Figure 5a,b), the boundary between the ULAL and ICL was set by the TUBUT, which runs here in the direction to the BU (Figure 4c). The hVLPF frames the ICL ventrally (Figure 4e-g).

The IB is the most posterior midline neuropil (Figure 1). It ends anteriorly with the beginning of the mALT, covered by the fiber bundle system around the CB and NO (Figures 4g,h, 5a-c, and 10d). Dorsally, the IBCs (as part of the IB), the ORs and the POC adjoin (Figure 10d). The POC runs from both OL dorsally and posteriorly across the brain midline and along the dorsal surface of the IB. We defined the IBCs as distinct bilateral subunits of the IB, distinguished from the IB by strong synapsin- (Figure 4g), and serotonin immunoreactivity (Figure 10f). In addition, Neurobiotin injections revealed neurons with arborizations restricted to the IBCs connected to the LAL (Figure 10e). Both IBCs adjoin at the midline but are apparently not fused. Laterally the IB is flanked by the MEF, GOR, and more anteriorly, the ATL (Figures 4g,h, 5a-c, and 10d).
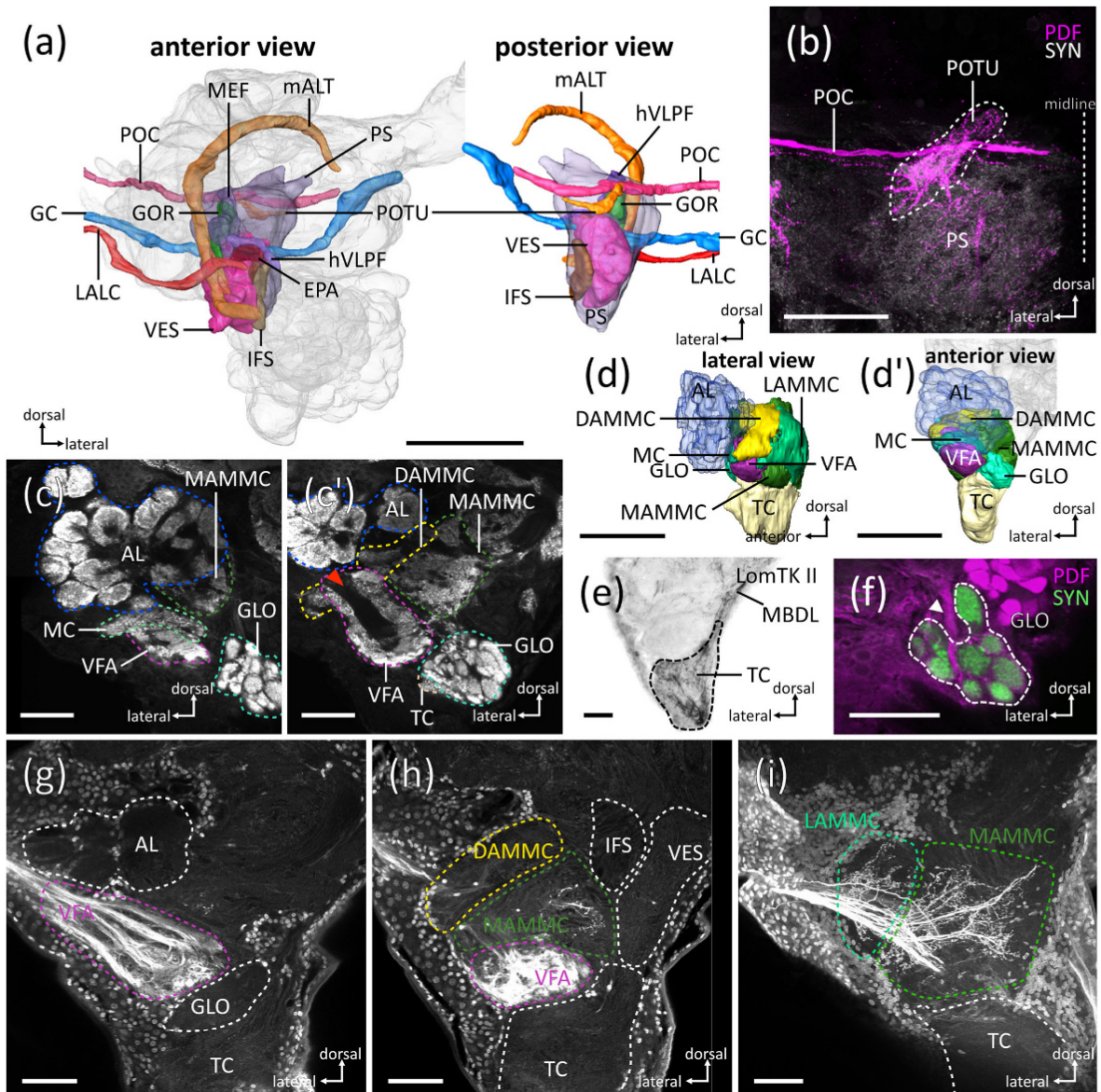
The anterior end of the ATL corresponds with the lateral bending of the mALT along its anterior-dorsal surface (Figure 4e-h). The ventral base of the ATL lies between the GOR, MAL, and VES (Figure 4g,h). The ATL was easily recognized by its ATL-like shape (Figure 10d), consistent with the homologous structures in the desert locust and fruit fly. It extends through the space between the IB and the PED, along the posterior surface of the mALT (Figure 4e-g). The neighboring ORs (Figures 4h and 5a-d) were determined by tracing the OCN toward the IB. The OR is an elongated neuropil at the dorsal surface of the brain (Figure 1c). Anteriorly it turns into the OCN that connects the OR with the ocellus. Posteriorly, the OR ends when the POC runs across the brain midline (Figure 10d). The N is a ventrally lying neuropil of the INPs of triangular pyramidal shape (Figure 5a,b). In contrast to surrounding neuropils, it is rich in synapsin labeling, and partly separated by the GC from the VES (Figures 5b and 10d). It was first described in the locust by von Hadeln et al. (2018).

At least, the MAL was identified by its glomerular-like structure and low level of synapsin staining, limited by the IB and ML at its dorsal surface (Figures 3f-h and 4). In the cockroach, it is not fused across the midline unlike in the dung beetles or locust (Immonen et al., 2017; von Hadeln et al., 2018). Anteriorly, the MAL extends as a small stripe ventrally from the ML and dorsally from the LALC and adjoins the CRE. Posteriorly, the MAL ends at the level of the GC and adjoins the N. Lateral boundaries to the GOR, mALT, ULAL, and LLAL are more ambiguous. They were set by the characteristic structure of synapsin staining of the MAL (Figures 3f-h, 4, and 10d).

3.9 | Ventromedial neuropils

The ventromedial neuropils (VMNP) comprise the ventral complex (VX) consisting of the VES, EPA and GOR, and the PS and POTU (Figures 1 and 11a). The VES is a large neuropil lateral to the esophagus (Figure 1b) and covered anteriorly by the MAL. The PS covers the VES posteriorly. As both neuropils are rather contiguous, a boundary was determined by the disappearance of the IFS. Laterally, the PLP, WED, AMMC, and LLAL flank the VES. The mALT defines the boundary with the LAL (Figure 4e-h), and the boundaries with the other neuropils were set with the help of the IFS (Figures 4h and 5a-d). Dorsally, the MAL, GOR, LLAL, EPA, N, ICL, and GC adjoin (Figures 4e-h and 5a-c). Whereas the borders between MAL, GOR, N and GC/PLPC were easily determined by differences in synapsin staining, other boundaries were more ambiguous. Nevertheless, criteria for orientation and definition of the VES were the LALC for its anterior border (Figure 4c,d), the IFS defining its medial border (Figures 4h and 5a-c), and the structure of synapsin staining at all levels. The ventral side of the VES is completely covered by the MAMMC (Figures 4e-h, 5a-d, and 11a).

The EPA (Figures 4g,h and 11a) is a small neuropil in the central brain which is flanked anteriorly by the ULAL and posteriorly limited by the GC. The level of the mALT and IFS sets the anterior surface of the EPA (Figure 4g), whereas the hVLPF builds the anterior border to the ICL/PVLP (Figure 4g). Lateral boundaries to the PVLP correspond to the plane where the superior tip of the IFS extends (Figure 11a).

ALTHAUS ET AL.

JCN
RESEARCH IN
SYSTEMS NEUROSCIENCE
THE JOURNAL OF COMPARATIVE NEUROLOGY

WILEY

3145

FIGURE 11 Anatomical overview of the ventromedial neuropils (VMNP) and the periesophageal neuropils (PENP). (a) Anterior (left) and posterior (right) view of the 3D-reconstructed VMNP. The neuropils in both panels are combined with selected tracts that served as landmarks. In the left panel the neuropils/tracts are embedded in the transparent 3D brain hemisphere. (b) Projection view of several optical sections showing synapsin- (grey) and PDH- (magenta) immunostaining. The dotted line marks the position of the posterior optic tubercle (POTU), innervated through the posterior optic commissure (POC) and posteriorly attached to the posterior slope (PS). (c, c') Frontal optical sections showing synapsin staining. Dotted lines outline the PENP. Two distinct planes were selected to visualize the borders. Red arrowhead marks entry site of the antennal nerve into the VFA. (d, d') Lateral (d) and anterior (d') view of the 3D-reconstructed PENP. The neuropils in the right panel are embedded in the transparent 3D brain hemisphere. (e) 40-μm Section immunostained for locustatachykinin II (LomTK-II). LomTK-II immunoreactive neurons projecting via the MBDL from the protocerebrum innervate the whole tritocerebrum (TC, dashed line). (f) Frontal optical section showing synapsin (green) and GABA (magenta) staining. The glomeruli of the glomerular lobe (GLO) show GABA immunostaining. (g–i) Optical sections of PENP backfilled with Neurobiotin from the scapus-pedicel joint. Numerous nuclei of glial cells and neurons show strong unspecific fluorescence. (g) Many flagellar afferents innervate the ventral area of flagellar afferents (VFA). (h) The dorsal (DAMMC) antennal mechanosensory and motor center (AMMC) lacks projections of afferents. (i) Dye filling of the scapus-pedicel joint revealed innervation of the medial AMMC (MAMMC) and the lateral AMMC (LAMMC) by antennal afferents (i). AL, antennal lobe; EPA, epaulette; GC, great commissure; GOR, gorget; hVLPF, horizontal ventrolateral protocerebrum fascicle; IFS, inferior fiber system; LALC, lateral accessory lobe commissure; mALT, medial antennal lobe tract; MC, median crescent; MEF, medial equatorial fascicle; TC, tritocerebrum; VES, vest. Scale bar = 400 μm (a, d, d'), and 100 μm (b, c, c', e–i)

The GOR shows weak synapsin staining, a glomerular appearance and extends medially to the EPA separated from it by the MEF (Figure 4g,h). It lies directly lateral to the mALT and mIALT, and extends from the dorsal peak of the VES to the region lateral of the IB (Figures 4g,h and 5a,b). Posteriorly, the GOR is covered by the IB and PS. The GC lies ventral and posterior to the GOR (Figures 4h and 5a), whereas the medial boundary is the prominent mALT and more posterior the IB and parts of the ATL (Figures 4e-h and 5a,b).

In the fruit fly, the PS covers the region between the IB and the gnathal ganglia and is divided into a superior and inferior PS, separated at the level of the WED commissure and the POC. In the cockroach the PS spans posteriorly over the entire medial protocerebrum (Figure 1a) and extends anteriorly to the GC and the IB (Figures 5c-g and 11a), where the LEF and GC converge (Figure 5c). Laterally, the SLP, ICL and PLP border on the PS (Figure 5c-g) but, unlike in *D. melanogaster*, the PS could not be further subdivided into a superior and inferior part. A major difference is the course of the POC, which runs dorsally along the brain surface in the cockroach and does not penetrate the PS as it does in the fruit fly (Ito et al., 2014). The POC innervates the POTU and continues between the POTU and the PS (Figure 11b). The POTU is a small, elongated neuropil that is embedded posteriorly in the PS and is distinguishable by PDH- and strong synapsin staining (Figures 5f,g and 11b).

3.10 | Periesophageal neuropils

The identities and boundaries of periesophageal neuropils (PENP) in the cockroach are largely based on prior data on the locust, because as a hemimetabolous insect, it shows more similarities in the morphology and alignment of the PENP than the fruit fly where deuto- and tritocerebrum are highly fused around and below the level of the esophagus. The PENP (Figure 11c-i) comprise the AL, glomerular lobe (GLO; lobus glomerulatus), median crescent (MC), tritocerebrum (TC), ventral area of flagellar afferents (VFA), and the AMMC, consisting of the dorsal (DAMMC), lateral (LAMMC), and medial AMMC (MAMMC). The AL is one of the most prominent and largest neuropils (Figure 1a) in the brain with many glomeruli that receive axonal projections from antennal olfactory receptor neurons. We counted about 180 glomeruli in this individual. The neighboring MC is characterized in the locust by NADPH-diaphorase staining (von Hadeln et al., 2018). The distribution of NADPH-diaphorase has not been studied in the cockroach, but we found a neuropil in the cockroach brain highly similar to the locust MC in shape and position. In direct neighborhood to the AL, it could be differentiated by smooth synapsin staining (Figure 4c). Posteriorly, the VFA and DAMMC extend with clear boundaries visible in synapsin immunolabeling (Figures 4d-h, 5a-d, and 11c,c′). The VFA also sets the ventral border of the MC. The MAMMC lies medial to the MC and could be distinguished from it by weaker synapsin staining and differences in its appearance (Figures 4c,d and 11c). The VFA receives afferents from the antennal flagellum (Figure 11d; Staudacher et al., 2005) and was strongly stained in antennal backfills from the flagellum (Figure 11g,h). It is a smooth synapsin-rich area posterior-ventrally

from the AL. Sensory projections from the antenna gather between the VFA and MAMMC, enter the AMMC at this level (320 μm; Figure 4f) and build a clear boundary between the VFA and adjacent AMMC. Posteriorly, the DAMMC, LAMMC, and MAMMC cover the VFA. Ventrally, it is encased by the TC and the GLO (Figure 4c-h and 11c′).

The AMMC is a compact neuropil and was separated into three subunits based on spatial position in the brain and differences in synapsin staining. It is well delineated from the dorsally adjacent VES/WED/PS and from the ventrally lying TC and GLO (Figures 4c-h and 5a-g) by prominent fiber tracts. The DAMMC is the most dorsal part of the AMMC and distinguished from the rest of the AMMC, because it did not receive input from the antenna (Figure 11h) like in the locust (von Hadeln et al., 2018). Like the LAMMC that lies on the lateral posterior parts of the AMMC, the DAMMC was also distinguished by strong synapsin immunolabeling (Figure 5). The LAMMC is ventrally bound by the MAMMC and anteriorly by the DAMMC, VFA, and GLO. In addition, it was identified by backfills from the antenna, because the LAMMC receives input from laterally branching fibers from the antenna (Figure 11i). The MAMMC takes up the largest volume of the AMMC and lies largely medially in the AMMC; it is ventrally bound by the TC and embedded in the LAMMC, DAMMC, GLO, and VFA (Figures 4, 5, and 11c-d′). The separation of the MAMMC from the other AMMC subunits was determined by the antennal innervations of the AMMC subunits, as seen in the backfills from the scapus (Figure 11h,i).

The GLO lies medial to the AL and was easy to identify by its glomerular structure and strong synapsin labeling (Figure 11f). It is often attributed to tritocerebral origin, lies ventrally from the MAMMC and is posteriorly covered by the TC and VFA, while anteriorly the cell body rind adjoins (Figures 3, 4, and 11c-d′). The GLO shows prominent GABA immunostaining, which facilitated its identification (Figure 11f). The TC is the most ventral neuropil of the cerebral ganglia (Figure 1) and was identified by synapsin-, GABA-, and locustatachykinin immunolabeling (LomTK-II; Figure 11e). Tritocerebral neurons with ascending projections in the MBDL connect the TC with the superior protocerebrum (Nässel, 2002; Nässel & Homberg, 2006; Nässel et al., 1992). In *R. maderae* LomTK-II immunoreactive neurons projecting via the MBDL from the protocerebrum innervate the whole TC (Figure 11e). It thereby defines its volume and outlines its dorsal border in accordance with synapsin staining (Figure 5).

4 | DISCUSSION

We used 3D reconstructions based on synapsin/GABA-immunolabeled wholemount preparations to provide a comprehensive map of brain areas of the cockroach *R. maderae*. Neuropil boundaries and their internal organization were further analyzed with the aid of serotonin-, PDH-, orcokinin-, and LomTK-II immunolabeling as well as single-cell dye fills. We identified and reconstructed a total of 60 neuropils (Figure 1) and 22 tracts, fiber systems, and commissures, thereby providing major connectivity schemes between these brain neuropils. Cockroaches are prominent model systems in studies on olfactory

mechanisms (Fuscà & Kloppenburg, 2021; Sakura & Mizunami, 2001; Watanabe et al., 2017), neuropeptide function (Stengl & Arendt, 2016; Zeng et al., 2021), learning and memory (Heisenberg, 1998; Hosono et al., 2016; Mizunami et al., 1998), and the neural control of walking (Martin et al., 2015; Ritzmann et al., 2012). The nocturnal cockroach *R. maderae*, studied here, is an established model in chronobiology (Page, 1982; Reischig & Stengl, 2003a; Stengl & Arendt, 2016; Stengl & Homberg, 1994). The present study will, therefore, provide an important basis for further functional analysis of the circadian clock, as well as for processing of sensory information and behavioral control in cockroaches and insects in general.

The atlas of the *R. maderae* brain resembles in large parts that of the locust *S. gregaria*, the only other available brain atlas of a hemimetabolous insect (von Hadeln et al., 2018). It shows less similarity with the brains of holometabolous insects such as the monarch butterfly *D. plexippus* (Heinze & Reppert, 2012), the fruit fly *D. melanogaster* (Ito et al., 2014), the ants *C. obscurior* (Bressan et al., 2014) and *C. nodus* (Habenstein et al., 2020), and the dung beetles *S. lamarcki/satyrus* (Immonen et al., 2017). A particularly prominent structure in the cockroach and the locust brain is the ALI that appears to be completely absent in the holometabolous insects. Amongst inferior and ventromedial neuropils, the N, MAL, and POTU are present in the cockroach, locust, and lepidopteran insects (Bogong moth, monarch butterfly), but have not been identified in the fruit fly, the ants, and dung beetles. Differences between the locust and the cockroach are particularly obvious in the OL and MB. The OL of the nocturnal cockroach is relatively small compared with that of the locust (Rosner et al., 2017), whereas their MB are relatively larger (Kurylas et al., 2008; Wei et al., 2010). Other chemosensory neuropils, such as the AL and GLO are remarkably large and complex in the cockroach, as compared to all other insect brains reconstructed. Another unusual structure of *R. maderae* is the CBL, which is distinctly subdivided into 9 teeth intersected by 8 cones, while in other insects, an organization into distinct horizontal, respectively concentric layers is more prominent (Omoto et al., 2017; von Hadeln et al., 2020).

4.1 | Optic lobe

The OL of *R. maderae* shows the typical arrangement of neuropils found in other hemimetabolous insects, but especially the ME and LO are less complex than in other polyneopteran species (Rosner et al., 2017). Acetylcholinesterase histochemistry distinguished 3 layers in the LA and 10 layers in the ME (Arnold et al., 2020). The AME of the cockroach has been identified as the site of the internal circadian clock controlling sleep–wake rhythms (Reischig & Stengl, 2003a) and has, accordingly, received particular attention (Arnold et al., 2020; Reischig & Stengl, 2003b; Stengl & Arendt, 2016; Stengl et al., 2015). It is connected to all other OL neuropils, especially the LA, ALAs, and ME, by widely ramifying neurons and, likewise, to many areas in the central brain and contralateral OL by neurons immunolabeled for PDH and other neuropeptides (Homberg et al., 1991; Stengl & Arendt, 2016; Wei et al., 2010). Some of these connections serve as photic entrainment

inputs to the AME (Arnold et al., 2020; Giese et al., 2018), others, like certain PDH-immunolabeled neurons, serve as outputs from the clock to the central brain or act in coupling the bilaterally organized clocks (Homberg et al., 1991; Petri & Stengl, 1997; Stengl & Arendt, 2016). The ALAs were first identified in intracellular recordings from light-sensitive AME neurons (Loesel & Homberg, 2001). They are strongly connected to the circadian clock, and appear to be part of its light-entrainment pathway (Arnold et al., 2020). While the target neurons of the cockroach circadian clock in the central brain have not been identified, the 3D reconstruction of the cockroach brain provided here will greatly facilitate further characterization of the circadian system.

The LOX of *R. maderae* shows a relatively basic organization. Its subdivisions are partly fused and, thus, more difficult to discern than in the locust or mantis, except for the large OLO that covers the LOX at its distal part (Rosner et al., 2017). Subcompartments like the stalk lobe (SLO) in the mantis or the inner lobe (ILO) in the locust (Rosner et al., 2017) could not be identified. This variance of the LOX neuropils is likely related to distinct visual requirements for different behavioral adaptations of the three species.

In contrast to the desert locust (Homberg & Paech, 2002), a dorsal rim area, specialized for detecting the polarization pattern of the sky, has not been characterized in the compound eye of the Madeira cockroach. Likewise, no specialized dorsal rim areas in the LA or ME were found. Dorsal rim areas in the LA and ME receiving polarized light input are prominent in the locust (Homberg & Paech, 2002), but in *D. melanogaster*, are only visible in transgenic flies and using specific labeling techniques (Sancer et al., 2019). It is, therefore, still possible that dorsal rim areas processing polarized light signals exist in the cockroach, especially because neurons sensitive to polarization angle have been identified in the OL (Loesel & Homberg, 2001). Other neuropils typical for polarization-vision pathways in insects such as the AOTU and POTU, as well as the TUBUT that transfers sky compass signals to the BU (el Jundi & Homberg, 2010; Hardcastle et al., 2021; Homberg et al., 2011) are present in the cockroach.

4.2 | Mushroom body

MBs are second-order olfactory neuropils, serve as association centers for multisensory integration, and play an important role in learning and memory (Heisenberg, 1998; Mizunami et al., 1998; Nishino et al., 2012; Owald & Waddell, 2015). Size, subdivisions and volume of MB neuropils differ greatly between insect species, but the basic composition into PED, VL, ML, and CA is largely conserved (Strausfeld et al., 2009). Kenyon cells are the principal neurons of the MB. Their numerous small somata lie in the soma rind within and above the CAs. Dendrites innervate the CA, and axonal fibers forming the PED usually bifurcate at the PEDD sending one axon collateral into the ML and the other one, into the VL. The MB of the Madeira cockroach has not been investigated in any detail but its morphology is similar to the well-studied MB of the American cockroach *P. americana* (Li & Strausfeld, 1999; Mizunami et al., 1998; Strausfeld & Li, 1999; Takahashi et al., 2017). A notable difference, however, is the absence in *R. maderae* of an accessory CA

and another small accessory neuropil medial to the VL, the lobelet (Farris & Strausfeld, 2003). The accessory CA receives specific, likely gustatory, input from the GLO (Farris, 2008). These neurons apparently synapse on a specific type of class-III Kenyon cells that innervate both accessory neuropils (Farris & Strausfeld, 2003). The accessory CA and lobelet appear to be only present in basal cockroaches like *P. americana* (Blattidae) but not in crown species like *R. maderae* (Blaberidae) (Farris & Strausfeld, 2003). Whether input from the GLO is missing in *R. maderae* or is fused into the primary CA, remains to be studied. Neural circuits and functions of the MB of the American cockroach have been investigated in great detail. Single-cell recordings revealed integration of visual and olfactory input (Li & Strausfeld, 1997, 1999; Nishino et al., 2012) and showed movement related activity changes in output elements (Okada et al., 1999). Feedback circuits from the lobes back to the CA involving giant GABA-immunoreactive inputs to the CA that are also present in *R. maderae* (Massah et al., 2022; Figure 10g,g') are likely involved in memory formation (Takahashi et al., 2017, 2019). Lesions of the PED or lobes led to impairment of spatial memory (Mizunami et al., 1998).

4.3 | CX and ALI

The CX, a group of interconnected neuropils spanning the brain midline, is highly conserved throughout the insects' genealogical tree. As shown in several species ranging from desert locusts to fruit flies, it plays a key role in head direction coding, partly through a sky compass mechanism, and goal directed spatial orientation (Fisher, 2022; Honkanen et al., 2019; Pfeiffer & Homberg, 2014; Varga et al., 2017). Its neuroarchitecture is characterized by linear series of vertical columns and horizontal layers. In most species three major classes of neurons have been distinguished: (i) tangential neurons providing input to the NO, the PB, or particular layers of the CB, (ii) pontine neurons interconnecting pairs of heterolateral columns within the CBU, and (iii) columnar neurons forming matrices of intercolumnar connections between the different substructures and axonal projections to the LX and the CRE (el Jundi et al., 2018; Heinze & Homberg, 2008; Heinze et al., 2013; Hensgen et al., 2021a; Hulse et al., 2021; von Hadeln et al., 2020). The cellular composition of the CX of *R. maderae* has not been studied so far, but the two individually labeled columnar neurons shown here (Figure 7b,c), suggest that it is highly similar to that of other insects. Extracellular recordings and current injections showed that the CX of the cockroach *B. discoidalis* receives visual and mechanosensory input, codes for head direction, and is critically involved in controlling walking direction and turns (Martin et al., 2015; Ritzmann et al., 2008; Ritzmann et al., 2012; Varga et al., 2017). Those studies, however, did not reveal the cellular substrate of these functions.

While the anatomical appearance of the PB, CBU, and NO in *R. maderae* is similar to those reported for other insects, the CBL, also termed ellipsoid body, has an unusual organization of nine teeth intersected by eight cones, which is visible in both synapsin- and GABA labeling. In other species such as the desert locust or the fruit fly, a

layered organization is more prominent (Müller et al., 1997; Omoto et al., 2017; von Hadeln et al., 2020), but at the cellular resolution, an organization into slices exists in all species studied. Interestingly, the number of CBL slices may be eight respectively 16 (fruit fly: Wolff et al., 2015; locust: Heinze & Homberg, 2008; monarch butterfly: Heinze et al., 2013), nine (dung beetle: el Jundi et al., 2018; Bogong moth: Adden et al., 2020; bumble bee: Sayre et al., 2021), or even 10 as in the mantis (Rosner et al., 2017), but here, the outermost slices are reduced in thickness to about half the size of the others. In the fruit fly *D. melanogaster*, the activity peak across the population of columnar neurons innervating the slices represents heading direction (Seelig & Jayaraman, 2015), and modeling studies suggest that this is a general principle of head direction coding in the CX (Honkanen et al., 2019; Pisokas et al., 2020). Further studies might reveal whether differences in the number of slices reflect true differences in the network of the CBL or merely species-specific differences in the emphasis of columnar versus intercolumnar space in the CBL.

In the cockroach as well as in the desert locust (von Hadeln et al., 2018), the ALI is a neuropil anterior to the CBU, that apparently does not exist in holometabolous insects (e.g., Immonen et al., 2017; Ito et al., 2014). In the locust, the ALI is highly connected with the CBU (Heinze & Homberg, 2008; Vitzthum et al., 1996). In the cockroach the ALI is particularly large, partly organized as a chain of glomerular condensations (*P. americana*; Eckert et al., 1999) and densely innervated by dopamine-immunoreactive fibers (Hamanaka et al., 2016; Timm et al., 2021).

4.4 | Lateral complex

Neuropils of the LX are strongly connected with the CX. Distinct cell types innervating the CX have arborization domains in different areas within the LX. The BU is a prominent relay in the sky compass pathway. Projection neurons from the lower unit of the AOTU form synapses in microglomerular complexes of the BU with GABAergic tangential inputs to the CBL (locust: Träger et al., 2008; honeybee: Held et al., 2016; fruit fly: Hardcastle et al., 2021). In the cockroach the BU is, likewise, targeted by projection neurons from the AOTU (Figure 9b,b') and is densely innervated by GABA-labeled neurons innervating the CBL (Homberg et al., 2018; Figure 7d) suggesting a similar role. Its microglomerular appearance is less prominent than in the locust, honeybee or fruit fly, and in contrast to those species, no subdivision of the BU was obvious. The GA has been identified as a distinct target area of columnar CL1 neurons connecting slices of the CBL and PB in the fruit fly (Wolff et al., 2015), dung beetles (Immonen et al., 2017), the honeybee (Hensgen et al., 2021a), and the monarch butterfly (Heinze & Reppert, 2012). In the cockroach it is, unlike in the locust (Hensgen et al., 2021b), visible as a distinct area in synapsin staining and was confirmed to be the GA by tracer injection into a single CL1 neuron (Figure 7b). An additional subunit of the LLAL, the PRO, is described here for the first time in an insect. In addition to synapsin-rich immunolabeling, arborizations of CPU1 columnar neurons of the PB and CBU are confined to this area. Homologous neurons

exist in all other insects studied so far (e.g. Heinze & Homberg, 2008; Hensgen et al., 2021a), but their axonal terminals are usually more diffusely distributed throughout the LAL. As targets of various CX outputs, the LALs, as shown in flies, locusts, and silk moths provide input to descending pathways and play an important role in navigational motor control (Hensgen et al., 2021b; Namiki et al., 2018; Rayshubskiy et al., 2020).

4.5 | Superior neuropils

The SNP stretch along the dorsal surface of the protocerebrum, ventral to the CAs. The SNP are major target sites of circadian clock neurons, both in the cockroach (Wei et al., 2010; Figure 8) and in flies (Reinhard et al., 2022). Prominent postsynaptic partners are, among others, neurosecretory cells of the pars lateralis and pars intercerebralis involved in hormonal control of metabolism and development (Reinhard et al., 2022). In the larger fly *Protophormia terraenovae* connections between PDF-neurons and neurosecretory cells in the SNP mediate photoperiodic responses (Hamanaka et al., 2005). Major landmarks for subdivisions of the SNP were a number of fiber systems, including the SFS, which is very prominent in the cockroach, the PLF and PYF, but also the three ALTs which allowed us to mark the boundaries of the LH in the cockroach. The LH is more ventrally embedded in the SLP than in the Bogong moth, fruit fly, or desert ant where it is the most lateral neuropil of the central brain (Adden et al., 2020; Habenstein et al., 2020; Ito et al., 2014). The SNP of the cockroach take up a large part of the brain, explainable perhaps by the importance of the antennal sensory system. While PDH-immunoreactive fibers do not innervate the LH, they target the SLP, SIP and most prominently, the SMP (Figure 8d) as their fibers project medially via the ASOC. In honeybees, the SIP, also termed ring neuropil is, in addition to the LH, strongly innervated by multiglomerular neurons of the mIALT (Abel et al., 2001) whereas in the cockroach *P. americana* these neurons target the LH, SLP, and a neuropil posterior from the ML likely corresponding to the SIP (Malun et al., 1993; Strausfeld & Li, 1999). While in the fruit fly, desert ant, and dung beetles the SIP completely surrounds the VL, it does not form a complete ring around the VL in the cockroach but leaves out an anterior-medial part, similar to the situation in the desert locust (von Hadeln et al., 2018). In *D. melanogaster* and also in dung beetles, the SMP of both brain hemispheres are fused. In the cockroach, they are not, but, as in the locust, an anterior midline neuropil, the ABR, builds the connection between the two SMPs. We decided to distinguish it from the SMP as a separate neuropil, because of obvious separation from the SMP by the MBDL.

4.6 | Ventrolateral neuropils

The VLNP are anterior-ventrally attached to the SNP. Especially the AOTU has received attention, because it is part of a neural pathway from the compound eye to the CX involved in the processing of celestial compass cues such as sun position and sky polarization pattern

(Hardcastle et al., 2021; Heinze & Reppert, 2011; Pfeiffer & Homberg, 2007). In *R. maderae*, the AOTU is, like in all other insects studied, subdivided into a larger UU and a smaller LU (Figure 9). The LU, part of the sky compass pathway, may be undivided, as in the locust (Homberg et al., 2003a), or subdivided into a species-specific number of subcompartments as in the cockroach (this study), the honey bee (Mota et al., 2011; Zeller et al., 2015), dung beetle (Immonen et al., 2017), monarch butterfly (Heinze & Reppert, 2012), Bogong moth (Adden et al., 2020), and fruit fly (Hardcastle et al., 2021). Its innervation in the cockroach by neurons that connect the LU of the AOTU with the BU of the ipsilateral hemisphere suggests that a neural pathway to the CX signaling sky compass cues in other species, is also present in *R. maderae*.

The VLP and PLP occupy a large volume in the cockroach brain. The PVLP is separated from the PLP by the GC, as in other insects. The boundary between PVLP and AVLP was more difficult to distinguish and could not be determined as in the fruit fly, where the AVLP was defined as the part of the VLP that is devoid of glomerular structures (Ito et al., 2014). The AVLP is strongly innervated by PDH-immunoreactive fibers (AFP in Figure 8d) and, in *P. americana*, appears to receive input from MB output neurons (Li & Strausfeld, 1997, 1999). The WED has no connection to the OLs, but receives second-order mechanosensory fibers from the AMMC, as shown in *D. melanogaster* (Kamikouchi et al., 2009). These neurons transmit via synapses in the WED information on wind direction to specific tangential inputs to the CBL (Okubo et al., 2020) that are also present in the desert locust (Homberg et al., 2021).

4.7 | Inferior neuropils

A large volume of the brain is occupied by the CRE. In *D. melanogaster*, the CRE is a thin region that surrounds the ML of the MB and borders frontally onto the SMP, above the AL and medially to the VL/SIP. In the cockroach and locust, the CRE does not completely envelop the VL, but forms two extensions that frame the VL and extend to the LAL. Many GABA-immunoreactive neurons of the CRE run around the MB and form extensive connections with Kenyon-cell fibers (Strausfeld & Li, 1999). Ito et al. (2014) and Yamazaki et al. (1998) first described an embedded neuropil in the CRE, the RUB. The RUB was defined as a subunit of the CRE, lying just posteriorly attached to the ML in *D. melanogaster*. It is specifically innervated by FR columnar neurons of the CX (Hulse et al., 2021) that terminate here. We found a corresponding neuropil in the cockroach, adjoining the CRE posteriorly and in direct connection to the LAL right beneath the GA. It is, likewise, innervated by a specific type of columnar neuron of the CBU. The RUB has not been identified in the locust, dung beetles, or ants.

The CL occupies another large volume of the INP. It surrounds the PED, like in the locust, whereas the CL of the fruit fly and dung beetle only half encloses the PED. The CL of *R. maderae* is separated into two subunits, the ICL and SCL, as in the fruit fly and the locust. In *D. melanogaster*, neurons of the CL penetrate the PED (Ito et al., 2014), whereas the nearby SIP and CRE receive input from many MB extrinsic neurons that connect these neuropils with the VL and ML. The superior

ellipsoid commissure and the superior arch commissure penetrate the CL in *D. melanogaster* and were used as landmarks separating the ICL and SCL. We could not identify these commissures in the cockroach and so we used the PED as the landmark between SCL and ICL, like in the locust. Medial to the ICL, the IB and the ATL adjoin. The IB is one of the neuropils fused across the midline. It has also been identified in the dung beetles, fruit fly, and locust. The IB is largely enclosed by fiber tracts, like the mALT, MEF, and processes around the CX and, in contrast to dung beetles and the fruit fly, shows strong synapsin immunoreactivity in comparison to the GOR (Immonen et al., 2017; Ito et al., 2014). In *R. maderae*, we distinguished a dorsal part of the IB, the IB cap (IBC), because of its cap-like form. It is a bilateral neuropil, specifically innervated by several bilateral neurons in the brain (Figure 10e,e') and characterized by strong serotonin- and synapsin immunostaining. Whether the IBC also exists in other insect species remains to be determined.

The MAL has, so far, only been described in the locust brain, but we could also identify a corresponding region in *R. maderae*. In contrast to *S. gregaria*, however, the MAL of *R. maderae* is not fused across the midline, but occupies the same small region below the MLs and above the esophagus. As first described in *S. gregaria*, we also identified the N, a paired neuropil ventrally to the GC. It is distinguishable by its very bright synapsin immunofluorescence and its triangular shape. The clear borders are similar to its counterpart in the locust. The OR is, like in the locust, a small INP serving as input site for the OCN. The cockroach has two ocelli, one on each side and corresponding to the number of ocelli, two bilaterally arranged ORs. Unlike in the locust and cockroach, ORs have not been described as distinct neuropils in holometabolous insects.

4.8 | Ventromedial neuropils

The VX in *R. maderae*, as described in the fruit fly (Ito et al., 2014), is subdivided into three regions: the VES, EPA, and GOR. The description and partition of the VX in *D. melanogaster* (Ito et al., 2014) correlate with the orientation of the three neuropils in the cockroach brain, except for the position of the GOR. The VES is the largest region lying medially at either side of the esophagus. Major boundaries used in the cockroach, locust, and fruit fly are the esophagus, GC, IFS, and its orientation relative to the CX. In the ant *C. nodus,* the VX could not be subdivided further, because of lack of landmarks (Habenstein et al., 2020), and the IFS was used as the most important boundary at the anterior and posterior end of the undivided VX, together with the lALT at the lateral side, similar to the data in dung beetles (Immonen et al., 2017). In the monarch butterfly, the region of the VMNP was differently segmented: into the PS, posterior medial protocerebrum and ventromedial anterior neuropil (VMAN). The VES presumably occupies part of the VMAN, as well as the GOR and EPA (Heinze & Reppert, 2012), and in the ant *C. obscurior*, parts of the ventromedial protocerebrum (Bressan et al., 2014). The EPA, a small region dorsal to the VES, is positioned in the fruit fly below the ICL, posterior to the LAL and in front of the GC. Medially, the mALT and mlALT are prominent landmarks as well as the

hVLPF between the EPA and LAL/CL (Ito et al., 2014). These criteria could be transferred to the cockroach brain. Only the IFS was not used as a boundary unlike in *D. melanogaster*, because the IFS in the cockroach is located more posterior. The identification of the EPA in the dung beetles and locust support the reconstruction in the cockroach brain (Immonen et al., 2017; von Hadeln et al., 2018). Owing to the fact that the VX could not be further subdivided, the EPA was not mentioned in the brain atlases of the ants *C. nodus*, *C. obscurior* (Bressan et al., 2014; Habenstein et al., 2020) and the monarch butterfly (Heinze & Reppert, 2012). The third neuropil of the VX, the GOR, was more difficult to distinguish. Its position and shape closely follow its characterization in the fruit fly but not that of the locust, where the GOR is dorsally embedded in the ICL and ventrally attached to the EPA (von Hadeln et al., 2018). In contrast the GOR in the fruit fly and cockroach protrudes medial to the ICL, between the mALT and the MEF/LEF (Ito et al., 2014). In the dung beetles, the GOR lies just below the NO, and landmarks like the mALT, MEF, and GC were also used. Different from the situation in *R. maderae*, the GOR of the dung beetles is flanked by the VES (Immonen et al., 2017), whereas in the cockroach the GOR is elongated from the dorsal tip of the VES to the IB. In contrast to the other insect brains studied, the GOR in *R. maderae* shows relatively weak synapsin labeling.

The PS in the cockroach occupies the most posterior part of the brain, highly similar to the PS of the locust. In both species, the PS is not subdivided further into an inferior and superior part, unlike in the fruit fly. In *D. melanogaster*, the PS partition was set by the POC crossing the PS (Ito et al., 2014). In *S. gregaria* and *R. maderae*, however, the POC runs along the dorsal border of the PS, and could, thus not serve as a demarcation between two PS subdivisions (von Hadeln et al., 2018). The PS in the ant *C. nodus* (Habenstein et al., 2020), monarch butterfly (Heinze & Reppert, 2012), and dung beetles (Immonen et al., 2017) is, likewise, not subdivided. The POTU is attached dorso-posteriorly to the PS. It is involved in visual processing and connected with tangential neurons of the PB (Beetz et al., 2015). In *R. maderae* it was identified through PDH immunolabeling (Figure 11b). The POTU is connected with the AME, PLP, and the contralateral POTU and plays an important role in the transfer of circadian signals (Reischig & Stengl, 2002; Stengl & Homberg, 1994; Wei et al., 2010). The POTU has not been recognized in ants (Bressan et al., 2014; Habenstein et al., 2020), dung beetles (Immonen et al., 2017), and the fruit fly (Ito et al., 2014).

4.9 | Periesophageal neuropils

The massive AL occupies a large volume in the cockroach brain (Figures 1 and 11c-d). In the reconstructed male brain, we counted around 180 glomeruli of similar size, but did not identify individual glomeruli. The large AL can probably be attributed to the way of life of the cockroach, which largely relies on its antennae for sensory input. Three AL tracts, the mALT, mlALT, and lALT, carry olfactory information from the AL to higher brain centers. The number and organization of AL glomeruli are highly variable across different insect species (Schachtner et al., 2005). In many moths and cockroaches, glomeruli

that are targeted by sex pheromone receptors are extremely large and form a distinct cluster usually located close to the entry point of the antennal nerve into the AL (Anton & Homberg, 1999; Schachtner et al., 2005). In the American cockroach *P. americana*, a macroglomerulus is present in the AL of males, but not in females (Ernst et al., 1977; Malun, 1991). Female American cockroaches attract their males with sex pheromones, detected by pheromone receptors on the male antenna that project to the macroglomerulus (Burrows et al., 1982; Hawkins, 1978; Kuwahara & Mori, 1990; Nishino et al., 2018; Seelinger, 1985). In the Madeira cockroach, in contrast, mating behavior is initiated by the male producing sex pheromones released by the sternal glands (Farine et al., 2007; Sreng, 1984). Correspondingly, we found no evidence for enlarged macroglomeruli in the AL of male specimens. Likewise, enlarged glomeruli were not evident in females as well.

The MC has only been described in the locust (von Hadeln et al., 2018). It was distinguished by NADPH-diaphorase staining and a crescent-shape directly positioned between the AL and the VFA. Although the distribution of NADPH-diaphorase in *R. maderae* has not been studied, we classified a corresponding region in the cockroach as the MC, because of its striking similarity in form and position with the MC of the locust (von Hadeln et al., 2018).

All other PENPs show considerable deviations and unclear homology with their likely counterparts, the cantle, flange, prow, and saddle, in holometabolous insects (Habenstein et al., 2020; Ito et al., 2014) and, therefore largely followed the segmentation in the locust. The volume of the AMMC in the cockroach is relatively large and was separated into four regions: the DAMMC, LAMMC, MAMMC, and the VFA. The VFA is laterally attached to the GLO and innervated by flagellar afferents. In the cockroach it is synapsin-rich and penetrated by large mechanosensory fibers from the antennal nerve (Figure 11c,g). Its general structure is similar to the VFA of the locust (von Hadeln et al., 2018) and cricket (Staudacher & Schildberger, 1999; Staudacher et al., 2005). The separation of these areas was based on subunit location within the AMMC and different brightness levels of synapsin immunolabeling and the antennal backfills with innervation of the MAMMC and LAMMC (Figure 11i). Homologies of these subunits with parts of the saddle, which houses the AMMC and its five subdivisions in the fruit fly (Ito et al., 2014; Kamikouchi et al., 2006) remain to be demonstrated. The DAMMC is, as shown in the locust *S. gregaria* (von Hadeln et al., 2018), apparently not targeted directly by antennal afferents (Figure 11h).

The GLO is absent, or may be fused with the AL, in most holometabolous species (Farris, 2008), with the notable exception of the beetle *Tribolium castaneum* (Dippel et al., 2016). In the cockroach it has a prominent glomerular structure (Figure 11c,c'). It receives input from chemosensory afferents of the maxillary palps (Ernst et al., 1977) and is connected with the AL by GABA-immunoreactive fibers (Massah et al., 2022). A first functional study by Sun et al. (2022) showed that olfactory sensory neurons from the maxillary palps of *Locusta migratoria* targeting the GLO are involved in odor-induced vomiting.

Neurons of the TC provide contact with the stomatogastric nervous system supplying parts of the gut, retrocerebral complex, superior protocerebrum, and the ventral nerve cord (Aubele & Klemm, 1977; Eckert et al., 1999; Maestro et al., 1998). Subdivisions of the TC could

not be distinguished, but may be revealed by more detailed investigations into the innervation patterns of different neuronal cell types, as in the locust (Aubele & Klemm, 1977). In the fruit fly different neuropils are presumably of tritocerebral origin, including the prow, saddle, and perhaps also some parts of the AMMC (Ito et al., 2014). Owing to the fusion of the gnathal and cerebral ganglia and thus elimination of circumesophageal connectives in holometabolous insects, some of these areas, in particular the prow and parts of the saddle, have moved to a level below the esophageal foramen. Further clarification of homology may thus be facilitated after including detailed analysis of subesophageal neuropils also in hemimetabolus species such as the cockroach.

5 | SUMMARY

We provide a 3D atlas of the cerebral ganglia in the nocturnal cockroach *R. maderae*, with detailed reconstructions of single neuropils. The atlas forms an important basis for further morphological and physiological studies. It will be highly valuable for further analysis of brain areas that are controlled by the circadian clock and might reveal novel insights into the neural basis underlying spatial orientation of this insect. The anatomical organization of the cockroach brain corresponds closest to that of the locust *S. gregaria* (von Hadeln et al., 2018), the only other hemimetabolous insect for which a 3D neuropil atlas of the brain has been established. Considerable similarities in brain organization, however, also exist with holometabolous insects, even if some areas are lacking in the cockroach while others were newly introduced, such as the PRO, cones, and teeth of the CBL, as well as the IBC. How these differences in brain organization relate to functional differences in neural circuits underlying species-specific behavioral repertoires requires further analysis. The availability of different brain atlases provides increasing opportunities for evolutionary comparison between the species.

AUTHOR CONTRIBUTIONS

Study concept and design: U. H., M. S., and V. A.; *acquisition of data*: V. A., S. J., and A. M.; *data analysis and interpretation*: V. A., S. J., U. H., and M. S.; *drafting the manuscript*: V. A.; *review and editing*: U. H., V. A., and M. S.

CONFLICT OF INTEREST
The authors declare no conflict of interest.

DATA AVAILABILITY STATEMENT

All data that support the findings of this study are available from the corresponding author. Four movies through stacked frontal brain sections can be found on the journal website as Supporting Information. Movie 1 shows colored label fields of the reconstructed neuropils of the cockroach brain (*Rhyparobia maderae*) with synapsin immunolabeling in gray, movie 2 shows labeling for synapsin only, movie 3 shows double labeling for synapsin (gray) and GABA (magenta), and movie 4 shows immunolabeling for GABA (magenta) only.

ORCID

Vanessa Althaus https://orcid.org/0000-0001-8018-0555
Stefanie Jahn https://orcid.org/0000-0002-1151-2875
Azar Massah https://orcid.org/0000-0001-6597-5456
Monika Stengl https://orcid.org/0000-0002-7896-872X
Uwe Homberg https://orcid.org/0000-0002-8229-7236

PEER REVIEW

The peer review history for this article is available at https://publons.com/publon/10.1002/cne.25396

REFERENCES

Abel, R., Rybak, J., & Menzel, R. (2001). Structure and response patterns of olfactory interneurons in the honeybee, *Apis mellifera*. *Journal of Comparative Neurology*, *437*, 363–383. https://doi.org/10.1002/cne.1289

Adden, A., Wibrand, S., Pfeiffer, K., Warrant, E., & Heinze, S. (2020). The brain of a nocturnal migratory insect, the Australian Bogong moth. *Journal of Comparative Neurology*, *528*, 1942–1963. https://doi.org/10.1002/cne.24866

Anton, S., & Homberg, U. (1999). Antennal lobe structure. In (Hansson, B. S. Ed.), *Insect olfaction* (pp. 98–124). Berlin Heidelberg: Springer. https://doi.org/10.1007/978-3-662-07911-9_5

Arendt, A., Neupert, S., Schendzielorz, J., Predel, R., & Stengl, M. (2016). The neuropeptide SIFamide in the brain of three cockroach species. *Journal of Comparative Neurology*, *524*, 1337–1360. https://doi.org/10.1002/cne.23910

Arnold, T., Korek, S., Massah, A., Eschstruth, D., & Stengl, M. (2020). Candidates for photic entrainment pathways to the circadian clock via optic lobe neuropils in the Madeira cockroach. *Journal of Comparative Neurology*, *528*, 1754–1774. https://doi.org/10.1002/cne.24844

Aubele, E., & Klemm, N. (1977). Origin, destination and mapping of tritocerebral neurons of locust. *Cell and Tissue Research*, *178*, 199–219. https://doi.org/10.1007/BF00219048

Baba, Y., Tsukada, A., & Comer, C. M. (2010). Collision avoidance by running insects: Antennal guidance in cockroaches. *Journal of Experimental Biology*, *213*, 2294–2302. https://doi.org/10.1242/jeb.036996

Beetz, M. J., el Jundi, B., Heinze, S., & Homberg, U. (2015). Topographic organization and possible function of the posterior optic tubercles in the brain of the desert locust *Schistocerca gregaria*. *Journal of Comparative Neurology*, *523*, 1589–1607. https://doi.org/10.1002/cne.23736

Boeckh, J., & Ernst, K.-D. (1987). Contribution of single unit analysis in insects to an understanding of olfactory function. *Journal of Comparative Physiology A*, *161*, 549–565. https://doi.org/10.1007/BF00603661

Boeckh, J., & Tolbert, L. P. (1993). Synaptic organization and development of the antennal lobe in insects. *Microscopy Research and Technique*, *24*, 260–280. https://doi.org/10.1002/jemt.1070240305

Bressan, J. M. A., Benz, M., Oettler, J., Heinze, J., Hartenstein, V., & Sprecher, S. G. (2014). A map of brain neuropils and fiber systems in the ant *Cardiocondyla obscurior*. *Frontiers in Neuroanatomy*, *8*, 166. https://doi.org/10.3389/fnana.2014.00166

Brovero, S. G., Fortier, J. C., Hu, H., Lovejoy, P. C., Newell, N. R., Palmateer, C. M., Tzeng, R.-Y., Lee, P.-T., Zinn, K., & Arbeitman, M. N. (2021). Investigation of *Drosophila* fruitless neurons that express Dpr/DIP cell adhesion molecules. *eLife*, *10*, e63101. https://doi.org/10.7554/eLife.63101

Bungart, D., Dircksen, H., & Keller, R. (1994). Quantitative determination and distribution of the myotropic neuropeptide orcokinin in the nervous system of astacidean crustaceans. *Peptides*, *15*, 393–400. https://doi.org/10.1016/0196-9781(94)90194-5

Burrows, M., Boeckh, J., & Esslen, J. (1982). Physiological and morphological properties of interneurones in the deutocerebrum of male cockroaches which respond to female pheromone. *Journal of Comparative Physiology*, *145*, 447–457. https://doi.org/10.1007/BF00612810

Cheong, H. S., Siwanowicz, I., & Card, G. M. (2020). Multi-regional circuits underlying visually guided decision-making in *Drosophila*. *Current Opinion in Neurobiology*, *65*, 77–87. https://doi.org/10.1016/j.conb.2020.10.010

Dippel, S., Kollmann, M., Oberhofer, G., Montino, A., Knoll, C., Krala, M., Rexer, K.-H., Frank, S., Kumpf, R., Schachtner, J., & Wimmer, E. A. (2016). Morphological and transcriptomic analysis of a beetle chemosensory system reveals a gnathal olfactory center. *BMC Biology*, *14*, 90. https://doi.org/10.1186/s12915-016-0304-z

Dircksen, H., Zahnow, C. A., Gaus, G., Keller, R., Rao, K. R., & Riehm, J. P. (1987). The ultrastructure of nerve endings containing pigment-dispersing hormone (PDH) in crustacean sinus glands: Identification by an antiserum against a synthetic PDH. *Cell and Tissue Research*, *250*, 377–387. https://doi.org/10.1007/BF00219082

Eckert, M., Predel, R., & Gundel, M. (1999). Periviscerokinin-like immunoreactivity in the nervous system of the American cockroach. *Cell and Tissue Research*, *295*, 159–170. https://doi.org/10.1007/s004410051222

el Jundi, B., & Homberg, U. (2010). Evidence for the possible existence of a second polarization-vision pathway in the locust brain. *Journal of Insect Physiology*, *56*, 971–979. https://doi.org/10.1016/j.jinsphys.2010.05.011

el Jundi, B., Warrant, E. J., Pfeiffer, K., & Dacke, M. (2018). Neuroarchitecture of the dung beetle central complex. *Journal of Comparative Neurology*, *526*, 2612–2630. https://doi.org/10.1002/cne.24520

Ernst, K. D., Boeckh, J., & Boeckh, V. (1977). A neuroanatomical study on the organization of the central antennal pathways in insects. *Cell and Tissue Research*, *176*, 285–306. https://doi.org/10.1007/BF00221789

Farine, J. P., Sirugue, D., Abed-Vieillard, D., Everaerts, C., Le Quéré, J. L., Bonnard, O., & Brossut, R. (2007). The male abdominal glands of *Leucophaea maderae*: Chemical identification of the volatile secretion and sex pheromone function. *Journal of Chemical Ecology*, *33*, 405–415. https://doi.org/10.1007/s10886-006-9224-7

Farris, S. M. (2008). Tritocerebral tract input to the insect mushroom bodies. *Arthropod Structure & Development*, *37*, 492–503. https://doi.org/10.1016/j.asd.2008.05.005

Farris, S. M., & Strausfeld, N. J. (2003). A unique mushroom body substructure common to basal cockroaches and to termites. *Journal of Comparative Neurology*, *456*, 305–320. https://doi.org/10.1002/cne.10517

Fisher, Y. E. (2022). Flexible navigational computations in the *Drosophila* central complex. *Current Opinion in Neurobiology*, *73*, 102514. https://doi.org/10.1016/j.conb.2021.12.001

Fusca, D., Schachtner, J., & Kloppenburg, P. (2015). Colocalization of allatotropin and tachykinin-related peptides with classical transmitters in physiologically distinct subtypes of olfactory local interneurons in the cockroach (*Periplaneta americana*). *Journal of Comparative Neurology*, *523*, 1569–1586. https://doi.org/10.1002/cne.23757

Fuscà, D., & Kloppenburg, P. (2021). Odor processing in the cockroach antennal lobe - the network components. *Cell and Tissue Research*, *383*, 59–73. https://doi.org/10.1007/s00441-020-03387-3

Giese, M., Gestrich, J., Massah, A., Peterle, J., Wei, H., & Stengl, M. (2018). GABA- and serotonin-expressing neurons take part in inhibitory as well as excitatory input pathways to the circadian clock of the Madeira cockroach *Rhyparobia maderae*. *European Journal of Neuroscience*, *47*, 1067–1080. https://doi.org/10.1111/ejn.13863

Gundel, M., & Penzlin, H. (1980). Identification of neuronal pathways between the stomatogastric nervous system and the retrocerebral complex of the cockroach *Periplaneta americana* (L.). *Cell and Tissue Research*, 208, 283–297. https://doi.org/10.1007/BF00234877

Habenstein, J., Amini, E., Grübel, K., el Jundi, B., & Rössler, W. (2020). The brain of *Cataglyphis* ants: Neuronal organization and visual projections. *Journal of Comparative Neurology*, 528, 3479–3506. https://doi.org/10.1002/cne.24934

Hamanaka, Y., Minoura, R., Nishino, H., Miura, T., & Mizunami, M. (2016). Dopamine- and tyrosine hydroxylase-immunoreactive neurons in the brain of the American cockroach, *Periplaneta americana*. *PLoS One*, 11, e0160531. https://doi.org/10.1371/journal.pone.0160531

Hamanaka, Y., Yasuyama, K., Numata, H., & Shiga, S. (2005). Synaptic connections between pigment-dispersing factor-immunoreactive neurons and neurons in the pars lateralis of the blow fly *Protophormia terraenovae*. *Journal of Comparative Neurology*, 491, 390–399. https://doi.org/10.1007/s00441-007-0433-3

Hardcastle, B. J., Omoto, J. J., Kandimalla, P., Nguyen, B.-C. M., Keleş, M. F., Boyd, N. K., Hartenstein, V., & Frye, M. A. (2021). A visual pathway for skylight polarization processing in *Drosophila*. *eLife*, 10, e63225. https://doi.org/10.7554/eLife.63225

Hawkins, W. A. (1978). Effects of sex pheromone on locomotion in the male American cockroach, *Periplaneta americana*. *Journal of Chemical Ecology*, 4, 149–160. https://doi.org/10.1007/BF00988051

Heinze, S., Florman, J., Asokaraj, S., el Jundi, B., & Reppert, S. M. (2013). Anatomical basis of sun compass navigation II: The neuronal composition of the central complex of the monarch butterfly. *Journal of Comparative Neurology*, 521, 267–298. https://doi.org/10.1002/cne.23214

Heinze, S., & Homberg, U. (2008). Neuroarchitecture of the central complex of the desert locust: Intrinsic and columnar neurons. *Journal of Comparative Neurology*, 511, 454–478. https://doi.org/10.1002/cne.21842

Heinze, S., & Reppert, S. M. (2011). Sun compass integration of skylight cues in migratory monarch butterflies. *Neuron*, 69, 345–358. https://doi.org/10.1016/j.neuron.2010.12.025

Heinze, S., & Reppert, S. M. (2012). Anatomical basis of sun compass navigation I: The general layout of the monarch butterfly brain. *Journal of Comparative Neurology*, 520, 1599–1628. https://doi.org/10.1002/cne.23054

Heisenberg, M. (1998). What do the mushroom bodies do for the insect brain? An introduction. *Learning & Memory*, 5, 1–10. https://doi.org/10.1101/lm.5.1.1

Held, M., Berz, A., Hensgen, R., Muenz, T. S., Scholl, C., Rössler, W., Homberg, U., & Pfeiffer, K. (2016). Microglomerular synaptic complexes in the sky-compass network of the honeybee connect parallel pathways from the anterior optic tubercle to the central complex. *Frontiers in Behavioral Neuroscience*, 10, 186. https://doi.org/10.3389/fnbeh.2016.00186

Hensgen, R., England, L., Homberg, U., & Pfeiffer, K. (2021a). Neuroarchitecture of the central complex in the brain of the honeybee: Neuronal cell types. *Journal of Comparative Neurology*, 529, 159–186. https://doi.org/10.1002/cne.24941

Hensgen, R., Göthe, J., Jahn, S., Hümmert, S., Schneider, K. L., Takahashi, N., Pegel, U., Gotthardt, S., & Homberg, U. (2021b). Organization and neural connections of the lateral complex in the brain of the desert locust. *Journal of Comparative Neurology*, 529, 3533–3560. https://doi.org/10.1002/cne.25209

Hofer, S., Dircksen, H., Tollbäck, P., & Homberg, U. (2005). Novel insect orcokinins: Characterization and neuronal distribution in the brains of selected dicondylian insects. *Journal of Comparative Neurology*, 490, 57–71. https://doi.org/10.1002/cne.20650

Homberg, U., & Paech, A. (2002). Ultrastructure and orientation of ommatidia in the dorsal rim area of the locust compound eye. *Arthropod Structure & Development*, 30, 271–280. https://doi.org/10.1016/S1467-8039(02)00010-5

Homberg, U., Heinze, S., Pfeiffer, K., Kinoshita, M., & el Jundi, B. (2011). Central neural coding of sky polarization in insects. *Philosophical Transactions of the Royal Society of London. Series B, Biological Sciences*, 366, 680–687. https://doi.org/10.1098/rstb.2010.0199

Homberg, U., Hensgen, R., Rieber, E., Seyfarth, J., Kern, M., Dippel, S., Dircksen, H., Spänig, L., & Kina, Y. P. (2021). Orcokinin in the central complex of the locust *Schistocerca gregaria*: Identification of immunostained neurons and colocalization with other neuroactive substances. *Journal of Comparative Neurology*, 529, 1876–1894. https://doi.org/10.1002/cne.25062

Homberg, U., Hofer, S., Pfeiffer, K., & Gebhardt, S. (2003a). Organization and neural connections of the anterior optic tubercle in the brain of the locust, *Schistocerca gregaria*. *Journal of Comparative Neurology*, 462, 415–430. https://doi.org/10.1002/cne.10771

Homberg, U., Humberg, T.-H., Seyfarth, J., Bode, K., & Quintero Pérez, M. (2018). GABA immunostaining in the central complex of dicondylian insects. *Journal of Comparative Neurology*, 526, 2301–2318. https://doi.org/10.1002/cne.24497

Homberg, U., Reischig, T., & Stengl, M. (2003b). Neural organization of the circadian system of the cockroach *Leucophaea maderae*. *Chronobiology International*, 20, 577–591. https://doi.org/10.1081/CBI-120022412

Homberg, U., Würden, S., Dircksen, H., & Rao, K. R. (1991). Comparative anatomy of pigment-dispersing hormone-immunoreactive neurons in the brain of orthopteroid insects. *Cell and Tissue Research*, 266, 343–357. https://doi.org/10.1007/BF00318190

Honkanen, A., Adden, A., da Silva Freitas, J., & Heinze, S. (2019). The insect central complex and the neural basis of navigational strategies. *Journal of Experimental Biology*, 222, (Pt Suppl 1), https://doi.org/10.1242/jeb.188854

Hosono, S., Matsumoto, Y., & Mizunami, M. (2016). Interaction of inhibitory and facilitatory effects of conditioning trials on long-term memory formation. *Learning & Memory*, 23, 669–678. https://doi.org/10.1101/lm.043513.116

Hulse, B. K., Haberkern, H., Franconville, R., Turner-Evans, D. B., Takemura, S.-Y., Wolff, T., Noorman, M., Dreher, M., Dan, C., Parekh, R., Hermundstad, A. M., Rubin, G. M., & Jayaraman, V. (2021). A connectome of the *Drosophila* central complex reveals network motifs suitable for flexible navigation and context-dependent action selection. *eLife*, 10, e66039. https://doi.org/10.7554/eLife.66039

Immonen, E.-V., Dacke, M., Heinze, S., & el Jundi, B. (2017). Anatomical organization of the brain of a diurnal and a nocturnal dung beetle. *Journal of Comparative Neurology*, 525, 1879–1908. https://doi.org/10.1002/cne.24169

Ito, K., Shinomiya, K., Ito, M., Armstrong, J. D., Boyan, G., Hartenstein, V., Harzsch, S., Heisenberg, M., Homberg, U., Jenett, A., Keshishian, H., Restifo, L. L., Rössler, W., Simpson, J. H., Strausfeld, N. J., Strauss, R., & Vosshall, L. B. (2014). A systematic nomenclature for the insect brain. *Neuron*, 81, 755–765. https://doi.org/10.1016/j.neuron.2013.12.017

Kamikouchi, A., Inagaki, H. K., Effertz, T., Hendrich, O., Fiala, A., Göpfert, M. C., & Ito, K. (2009). The neural basis of *Drosophila* gravity-sensing and hearing. *Nature*, 458, 165–171. https://doi.org/10.1038/nature07810

Kamikouchi, A., Shimada, T., & Ito, K. (2006). Comprehensive classification of the auditory sensory projections in the brain of the fruit fly *Drosophila melanogaster*. *Journal of Comparative Neurology*, 499, 317–356. https://doi.org/10.1002/cne.21075

Klagges, B. R. E., Heimbeck, G., Godenschwege, T. A., Hofbauer, A., Pflugfelder, G. O., Reifegerste, R., Reisch, D., Schaupp, M., Buchner, S., & Buchner, E. (1996). Invertebrate synapsins: A single gene codes for several isoforms in *Drosophila*. *Journal of Neuroscience*, 16, 3154–3165. https://doi.org/10.1523/JNEUROSCI.16-10-03154.1996

Kurylas, A. E., Rohlfing, T., Krofczik, S., Jenett, A., & Homberg, U. (2008). Standardized atlas of the brain of the desert locust, *Schistocerca gregaria*. *Cell and Tissue Research*, 333, 125–145. https://doi.org/10.1007/s00441-008-0620-x

Kuwahara, S., & Mori, K. (1990). Synthesis of (-)-Periplanone-B, a sex pheromone component of the American cockroach (*Periplaneta*

americana). *Tetrahedron, 46,* 8075–8082. https://doi.org/10.1016/S0040-4020(01)81464-2

Li, Y., & Strausfeld, N. J. (1997). Morphology and sensory modality of mushroom body extrinsic neurons in the brain of the cockroach, *Periplaneta americana. Journal of Comparative Neurology, 387,* 631–650. https://doi.org/10.1002/(SICI)1096-9861(19971103)387:4%3C631::AID-CNE9%3E3.0.CO;2-3

Li, Y., & Strausfeld, N. J. (1999). Multimodal efferent and recurrent neurons in the medial lobes of cockroach mushroom bodies. *Journal of Comparative Neurology, 409,* 647–663. https://doi.org/10.1002/(SICI)1096-9861(19990712)409:4647::AID-CNE93.0.CO;2-3

Loesel, R., & Homberg, U. (2001). Anatomy and physiology of neurons with processes in the accessory medulla of the cockroach *Leucophaea maderae. Journal of Comparative Neurology, 439,* 193–207. https://doi.org/10.1002/cne.1342

Maestro, J. L., Bellés, X., Piulachs, M.-D., Thorpe, A., & Duve, H. (1998). Localization of allatostatin-immunoreactive material in the central nervous system, stomatogastric nervous system, and gut of the cockroach *Blattella germanica. Archives of Insect Biochemistry and Physiology, 37,* 269–282. https://doi.org/10.1002/(SICI)1520-6327(1998)37:4269::AID-ARCH23.0.CO;2-M

Malun, D. (1991). Inventory and distribution of synapses of identified uniglomerular projection neurons in the antennal lobe of *Periplaneta americana. Journal of Comparative Neurology, 305,* 348–360. https://doi.org/10.1002/cne.903050215

Malun, D., Waldow, U., Kraus, D., & Boeckh, J. (1993). Connections between the deutocerebrum and the protocerebrum, and neuroanatomy of several classes of deutocerebral projection neurons in the brain of male *Periplaneta americana. Journal of Comparative Neurology, 329,* 143–162. https://doi.org/10.1002/cne.903290202

Martin, J. P., Guo, P., Mu, L., Harley, C. M., & Ritzmann, R. E. (2015). Central-complex control of movement in the freely walking cockroach. *Current Biology, 25,* 2795–2803. https://doi.org/10.1016/j.cub.2015.09.044

Massah, A., Neupert, S., Brodesser, S., Homberg, U., & Stengl, M. (2022). Distribution and daily oscillation of GABA in the circadian system of the cockroach *Rhyparobia maderae. Journal of Comparative Neurology, 530,* 770–791. https://doi.org/10.1002/cne.25244

Mizunami, M., Weibrecht, J. M., & Strausfeld, N. J. (1998). Mushroom bodies of the cockroach: Their participation in place memory. *Journal of Comparative Neurology, 402,* 520–537. https://doi.org/10.1002/(SICI)1096-9861(19981228)402:4520::AID-CNE63.0.CO;2-K

Mota, T., Yamagata, N., Giurfa, M., Gronenberg, W., & Sandoz, J.-C. (2011). Neural organization and visual processing in the anterior optic tubercle of the honeybee brain. *Journal of Neuroscience, 31,* 11443–11456. https://doi.org/10.1523/JNEUROSCI.0995-11.2011

Müller, M., Homberg, U., & Kühn, A. (1997). Neuroarchitecture of the lower division of the central body in the brain of the locust (*Schistocerca gregaria*). *Cell and Tissue Research, 288,* 159–176. https://doi.org/10.1007/s004410050803

Muren, J. E., Lundquist, C. T., & Nässel, D. R. (1995). Abundant distribution of locustatachykinin-like peptide in the nervous system and intestine of the cockroach *Leucophaea maderae. Philosophical Transactions of the Royal Society of London, Series B Biological Sciences, 348,* 423–444. https://doi.org/10.1098/rstb.1995.0079. PMID: 7480113

Namiki, S., Wada, S., & Kanzaki, R. (2018). Descending neurons from the lateral accessory lobe and posterior slope in the brain of the silkmoth *Bombyx mori. Scientific Reports, 8,* 9663. https://doi.org/10.1038/s41598-018-27954-5

Nässel, D. R. (2002). Neuropeptides in the nervous system of *Drosophila* and other insects: Multiple roles as neuromodulators and neurohormones. *Progress in Neurobiology, 68,* 1–84. https://doi.org/10.1016/S0301-0082(02)00057-6

Nässel, D. R., & Homberg, U. (2006). Neuropeptides in interneurons of the insect brain. *Cell and Tissue Research, 326,* 1–24. https://doi.org/10.1007/s00441-006-0210-8

Nässel, D. R., Cantera, R., & Karlsson, A. (1992). Neurons in the cockroach nervous system reacting with antisera to the neuropeptide leucokinin I. *Journal of Comparative Neurology, 322,* 45–67. https://doi.org/10.1002/cne.903220105

Nässel, D. R., Kim, M. Y., & Lundquist, C. T. (1995). Several forms of callitachykinins are distributed in the central nervous system and intestine of the blowfly *Calliphora vomitoria. Journal of Experimental Biology, 198,* 2527–2536. https://doi.org/10.1242/jeb.198.12.2527

Nishino, H., Iwasaki, M., Yasuyama, K., Hongo, H., Watanabe, H., & Mizunami, M. (2012). Visual and olfactory input segregation in the mushroom body calyces in a basal neopteran, the American cockroach. *Arthropod Structure & Development, 41,* 3–16. https://doi.org/10.1016/j.asd.2011.08.005

Nishino, H., Iwasaki, M., Paoli, M., Kamimura, I., Yoritsune, A., & Mizunami, M. (2018). Spatial receptive fields for odor localization. *Current Biology, 28,* 600–608. https://doi.org/10.1016/j.cub.2017.12.055

Nojima, T., Rings, A., Allen, A. M., Otto, N., Verschut, T. A., Billeter, J. -C., Neville, M. C., & Goodwin, S. F. (2021). A sex-specific switch between visual and olfactory inputs underlies adaptive sex differences in behavior. *Current Biology, 31,* 1175–1191.e6. https://doi.org/10.1016/j.cub.2020.12.047

Okada, J., & Toh, Y. (2000). The role of antennal hair plates in object-guided tactile orientation of the cockroach (*Periplaneta americana*). *Journal of Comparative Physiology A, 186,* 849–857. https://doi.org/10.1007/s003590000137

Okada, R., Ikeda, J., & Mizunami, M. (1999). Sensory responses and movement-related activities in extrinsic neurons of the cockroach mushroom bodies. *Journal of Comparative Physiology A, 185,* 115–129. https://doi.org/10.1007/s003590050371

Okubo, T. S., Patella, P., D'Alessandro, I., & Wilson, R. I. (2020). A neural network for wind-guided compass navigation. *Neuron, 107,* 924–940.e18. https://doi.org/10.1016/j.neuron.2020.06.022

Omoto, J. J., Keleş, M. F., Nguyen, B.-C. M., Bolanos, C., Lovick, J. K., Frye, M. A., & Hartenstein, V. (2017). Visual input to the *Drosophila* central complex by developmentally and functionally distinct neuronal populations. *Current Biology, 27,* 1098–1110. https://doi.org/10.1016/j.cub.2017.02.063

Owald, D., & Waddell, S. (2015). Olfactory learning skews mushroom body output pathways to steer behavioral choice in *Drosophila. Current Opinion in Neurobiology, 35,* 178–184. https://doi.org/10.1016/j.conb.2015.10.002

Pacheco, D. A., Thiberge, S. Y., Pnevmatikakis, E., & Murthy, M. (2021). Auditory activity is diverse and widespread throughout the central brain of *Drosophila. Nature Neuroscience, 24,* 93–104. https://doi.org/10.1038/s41593-020-00743-y

Page, T. L. (1982). Transplantation of the cockroach circadian pacemaker. *Science (New York, N.Y.), 216,* 73–75. https://doi.org/10.1126/science.216.4541.73

Patella, P., & Wilson, R. I. (2018). Functional maps of mechanosensory features in the *Drosophila* brain. *Current Biology, 28,* 1189–1203.e5. https://doi.org/10.1016/j.cub.2018.02.074

Petri, B., & Stengl, M. (1997). Pigment-dispersing hormone shifts the phase of the circadian pacemaker of the cockroach *Leucophaea maderae. Journal of Neuroscience, 17,* 4087–4093. https://doi.org/10.1523/JNEUROSCI.17-11-04087.1997

Petri, B., Stengl, M., Würden, S., & Homberg, U. (1995). Immunocytochemical characterization of the accessory medulla in the cockroach *Leucophaea maderae. Cell and Tissue Research, 282,* 3–19. https://doi.org/10.1007/BF00319128

Pfeiffer, K., & Homberg, U. (2007). Coding of azimuthal directions via time-compensated combination of celestial compass cues. *Current Biology, 17,* 960–965. https://doi.org/10.1016/j.cub.2007.04.059

Pfeiffer, K., & Homberg, U. (2014). Organization and functional roles of the central complex in the insect brain. *Annual Review of Entomology, 59,* 165–184. https://doi.org/10.1146/annurev-ento-011613-162031

Pipa, R. L. (1978). Locations and central projections of neurons associated with the retrocerebral neuroendocrine complex of the cockroach *Periplaneta americana* (L.). *Cell and Tissue Research, 193*, 443–455. https://doi.org/10.1007/BF00225342

Pisokas, I., Heinze, S., & Webb, B. (2020). The head direction circuit of two insect species. *eLife, 9*, e53985. https://doi.org/10.7554/eLife.53985

Rayshubskiy, A., Holtz, S. L., D'Alessandro, I., Li, A. A., Vanderbeck, Q. X., Haber, I. S., Gibb, P. W., & Wilson, R. I. (2020). Neural circuit mechanisms for steering control in walking *Drosophila*. *bioRxiv preprint*, https://doi.org/10.1101/2020.04.04.024703

Reischig, T., & Stengl, M. (2003a). Ectopic transplantation of the accessory medulla restores circadian locomotor rhythms in arrhythmic cockroaches (*Leucophaea maderae*). *Journal of Experimental Biology, 206*, 1877–1886. https://doi.org/10.1242/jeb.00373

Reischig, T., & Stengl, M. (2003b). Ultrastructure of pigment-dispersing hormone-immunoreactive neurons in a three-dimensional model of the accessory medulla of the cockroach *Leucophaea maderae*. *Cell and Tissue Research, 314*, 421–435. https://doi.org/10.1007/s00441-003-0772-7

Reischig, T., & Stengl, M. (2002). Optic lobe commissures in a three-dimensional brain model of the cockroach *Leucophaea maderae*: A search for the circadian coupling pathways. *Journal of Comparative Neurology, 443*, 388–400. https://doi.org/10.1002/cne.10133

Reinhard, N., Schubert, F. K., Bertolini, E., Hagedorn, N., Manoli, G., Sekiguchi, M., Yoshii, T., Rieger, D., & Helfrich-Förster, C. (2022). The neuronal circuit of the dorsal circadian clock neurons in *Drosophila melanogaster*. *Frontiers in Physiology, 13*, 886432. https://doi.org/10.3389/fphys.2022.886432

Ritzmann, R. E., Harley, C. M., Daltorio, K. A., Tietz, B. R., Pollack, A. J., Bender, J. A., Guo, P., Horomanski, A. L., Kathman, N. D., Nieuwoudt, C., Brown, A. E., & Quinn, R. D. (2012). Deciding which way to go: How do insects alter movements to negotiate barriers? *Frontiers in Neuroscience, 6*, 97. https://doi.org/10.3389/fnins.2012.00097

Ritzmann, R. E., Ridgel, A. L., & Pollack, A. J. (2008). Multi-unit recording of antennal mechano-sensitive units in the central complex of the cockroach, *Blaberus discoidalis*. *Journal of Comparative Physiology A, 194*, 341–360. https://doi.org/10.1007/s00359-007-0310-2

Rosner, R., von Hadeln, J., Salden, T., & Homberg, U. (2017). Anatomy of the lobula complex in the brain of the praying mantis compared to the lobula complexes of the locust and cockroach. *Journal of Comparative Neurology, 525*, 2343–2357. https://doi.org/10.1002/cne.24208

Sakura, M., & Mizunami, M. (2001). Olfactory learning and memory in the cockroach *Periplaneta americana*. *Zoological Science, 18*, 21–28. https://doi.org/10.2108/zsj.18.21

Sancer, G., Kind, E., Plazaola-Sasieta, H., Balke, J., Pham, T., Hasan, A., Münch, L. O., Courgeon, M., Mathejczyk, T. F., & Wernet, M. F. (2019). Modality-specific circuits for skylight orientation in the fly visual system. *Current Biology, 29*, 2812–2825.e4. https://doi.org/10.1016/j.cub.2019.07.020

Sayre, M. E., Templin, R., Chavez, J., Kempenaers, J., & Heinze, S. (2021). A projectome of the bumblebee central complex. *eLife, 10*, e68911. https://doi.org/10.7554/eLife.68911

Schachtner, J., Schmidt, M., & Homberg, U. (2005). Organization and evolutionary trends of primary olfactory brain centers in Tetraconata (Crustacea+Hexapoda). *Arthropod Structure & Development, 34*, 257–299. https://doi.org/10.1016/j.asd.2005.04.003

Scheffer, L. K., Xu, C. S., Januszewski, M., Lu, Z., Takemura, S. Y., Hayworth, K. J., Huang, G. B., Shinomiya, K., Maitlin-Shepard, J., Berg, S., Clements, J., Hubbard, P. M., Katz, W. T., Umayam, L., Zhao, T., Ackerman, D., Blakely, T., Bogovic, J., Dolafi, T., … Plaza, S. M. (2020). A connectome and analysis of the adult *Drosophila* central brain. *Elife, 9*, e57443. https://doi.org/10.7554/eLife.57443

Schulze, J., Neupert, S., Schmidt, L., Predel, R., Lamkemeyer, T., Homberg, U., & Stengl, M. (2012). Myoinhibitory peptides in the brain of the cockroach *Leucophaea maderae* and colocalization with pigment-dispersing factor in circadian pacemaker cells. *Journal of Comparative Neurology, 520*, 1078–1097. https://doi.org/10.1002/cne.22785

Seelig, J. D., & Jayaraman, V. (2015). Neural dynamics for landmark orientation and angular path integration. *Nature, 521*, 186–191. https://doi.org/10.1038/nature14446

Seelinger, G. (1985). Behavioural responses to female sex pheromone components in *Periplaneta americana*. *Animal Behaviour, 33*, 591–598. https://doi.org/10.1016/S0003-3472(85)80083-X

Sreng, L. (1984). Morphology of the sternal and tergal glands producing the sexual pheromones and the aphrodisiacs among the cockroaches of the subfamily Oxyhaloinae. *Journal of Morphology, 182*, 279–294. https://doi.org/10.1002/jmor.1051820304

Staudacher, E., & Schildberger, K. (1999). A newly described neuropile in the deutocerebrum of the cricket: Antennal afferents and descending interneurons. *Zoology, 102*, 212–226.

Staudacher, E., Gebhardt, M., & Dürr, V. (2005). Antennal movements and mechanoreception: Neurobiology of active tactile sensors. *Advances in Insect Physiology, 32*, 49–205. https://doi.org/10.1016/S0065-2806(05)32002-9

Stengl, M., & Arendt, A. (2016). Peptidergic circadian clock circuits in the Madeira cockroach. *Current Opinion in Neurobiology, 41*, 44–52. https://doi.org/10.1016/j.conb.2016.07.010

Stengl, M., & Homberg, U. (1994). Pigment-dispersing hormone-immunoreactive neurons in the cockroach *Leucophaea maderae* share properties with circadian pacemaker neurons. *Journal of Comparative Physiology. A, 175*, 203–213. https://doi.org/10.1007/BF00215116

Stengl, M., Werckenthin, A., & Wei, H. Y. (2015). How does the circadian clock tick in the Madeira cockroach? *Current Opinion in Insect Science, 12*, 38–45. https://doi.org/10.1016/j.cois.2015.09.007

Sternberger, L. A. (1979). The unlabeled antibody (PAP) method, introduction. *Journal of Histochemistry & Cytochemistry, 27*(12), 1657–1657. https://doi.org/10.1177/27.12.392001

Strausfeld, N. J., & Li, Y. (1999). Organization of olfactory and multimodal afferent neurons supplying the calyx and pedunculus of the cockroach mushroom bodies. *Journal of Comparative Neurology, 409*, 603–625. https://doi.org/10.1002/(SICI)1096-9861(19990712)409:4603::AID-CNE73.0.CO;2-P

Strausfeld, N. J., Sinakevitch, I., Brown, S. M., & Farris, S. M. (2009). Ground plan of the insect mushroom body: Functional and evolutionary implications. *Journal of Comparative Neurology, 513*, 265–291. https://doi.org/10.1002/cne.21948

Sun, L., Pan, X., Li, H., Zhang, X., Zhao, X., Zhang, L., & Zhang, L. (2022). Odor-induced vomiting is combinatorially triggered by palp olfactory receptor neurons that project to the lobus glomerulatus in locust brain. *Frontiers in Physiology, 13*, 855522. https://doi.org/10.3389/fphys.2022.855522

Takahashi, N., Katoh, K., Watanabe, H., Nakayama, Y., Iwasaki, M., Mizunami, M., & Nishino, H. (2017). Complete identification of four giant interneurons supplying mushroom body calyces in the cockroach *Periplaneta americana*. *Journal of Comparative Neurology, 525*, 204–230. https://doi.org/10.1002/cne.24108

Takahashi, N., Nishino, H., Domae, M., & Mizunami, M. (2019). Separate but interactive parallel olfactory processing streams governed by different types of GABAergic feedback neurons in the mushroom body of a basal insect. *Journal of Neuroscience, 39*, 8690–8704. https://doi.org/10.1523/JNEUROSCI.0088-19.2019

Timm, J., Scherner, M., Matschke, J., Kern, M., & Homberg, U. (2021). Tyrosine hydroxylase immunostaining in the central complex of dicondylian insects. *Journal of Comparative Neurology, 529*, 3131–3154. https://doi.org/10.1002/cne.25151

Tomita, J., Ban, G., & Kume, K. (2017). Genes and neural circuits for sleep of the fruit fly. *Neuroscience Research, 118*, 82–91. https://doi.org/10.1016/j.neures.2017.04.010

Träger, U., Wagner, R., Bausenwein, B., & Homberg, U. (2008). A novel type of microglomerular synaptic complex in the polarization vision pathway of the locust brain. *Journal of Comparative Neurology, 506*, 288–300. https://doi.org/10.1002/cne.21512

Tsubouchi, A., Yano, T., Yokoyama, T. K., Murtin, C., Otsuna, H., & Ito, K. (2017). Topological and modality-specific representation of somatosensory information in the fly brain. *Science (New York, N.Y.)*, *358*, 615–623. https://doi.org/10.1126/science.aan4428

Varga, A. G., Kathman, N. D., Martin, J. P., Guo, P., & Ritzmann, R. E. (2017). Spatial navigation and the central complex: Sensory acquisition, orientation, and motor control. *Frontiers in Behavioral Neuroscience*, *11*, 4. https://doi.org/10.3389/fnbeh.2017.00004

Veenstra, J. A., Lau, G. W., Agricola, H. J., & Petzel, D. H. (1995). Immunohistological localization of regulatory peptides in the midgut of the female mosquito *Aedes aegypti*. *Histochemistry and Cell Biology*, *104*, 337–347. https://doi.org/10.1007/BF01458127

Vitzthum, H., & Homberg, U. (1998). Immunocytochemical demonstration of locustatachykinin-related peptides in the central complex of the locust brain. *Journal of Comparative Neurology*, *390*, 455–469. https://doi.org/10.1002/(SICI)1096-9861(19980126)390:4455::AID-CNE13.0.CO;2-%23

Vitzthum, H., Homberg, U., & Agricola, H. (1996). Distribution of Dipallatostatin I-like immunoreactivity in the brain of the locust *Schistocerca gregaria* with detailed analysis of immunostaining in the central complex. *Journal of Comparative Neurology*, *369*, 419–437. https://doi.org/10.1002/(SICI)1096-9861(19960603)369:3419::AID-CNE73.0.CO;2-8

von Hadeln, J., Althaus, V., Häger, L., & Homberg, U. (2018). Anatomical organization of the cerebrum of the desert locust *Schistocerca gregaria*. *Cell and Tissue Research*, *374*, 39–62. https://doi.org/10.1007/s00441-018-2844-8

von Hadeln, J., Hensgen, R., Bockhorst, T., Rosner, R., Heidasch, R., Pegel, U., Quintero Pérez, M., & Homberg, U. (2020). Neuroarchitecture of the central complex of the desert locust: Tangential neurons. *Journal of Comparative Neurology*, *528*, 906–934. https://doi.org/10.1002/cne.24796

Watanabe, H., Nishino, H., Mizunami, M., & Yokohari, F. (2017). Two parallel olfactory pathways for processing general odors in a cockroach. *Frontiers in Neural Circuits*, *11*, 32. https://doi.org/10.3389/fncir.2017.00032

Watanabe, H., Nishino, H., Nishikawa, M., Mizunami, M., & Yokohari, F. (2010). Complete mapping of glomeruli based on sensory nerve branching pattern in the primary olfactory center of the cockroach *Periplaneta americana*. *Journal of Comparative Neurology*, *518*, 3907–3930. https://doi.org/10.1002/cne.22452

Wegerhoff, R. (1997). Metamorphic development of locusta-tachykinin immunoreactive neurons of the antennal lobes of the beetle *Tenebrio molitor* and the effect of fenvalerate application. *Experimental Biology Online*, *2*, 1–13. https://doi.org/10.1007/s00898-997-0014-7

Wei, H., el Jundi, B., Homberg, U., & Stengl, M. (2010). Implementation of pigment-dispersing factor-immunoreactive neurons in a standardized atlas of the brain of the cockroach *Leucophaea maderae*. *Journal of Comparative Neurology*, *518*, 4113–4133. https://doi.org/10.1002/cne.22471

Wolff, T., Iyer, N. A., & Rubin, G. M. (2015). Neuroarchitecture and neuroanatomy of the *Drosophila* central complex: A GAL4-based dissection of protocerebral bridge neurons and circuits. *Journal of Comparative Neurology*, *523*, 997–1037. https://doi.org/10.1002/cne.23705

Yamazaki, Y., Nishikawa, M., & Mizunami, M. (1998). Three classes of GABA-like immunoreactive neurons in the mushroom body of the cockroach. *Brain Research*, *788*, 80–86. https://doi.org/10.1016/S0006-8993(97)01515-1

Zeller, M., Held, M., Bender, J., Berz, A., Heinloth, T., Hellfritz, T., & Pfeiffer, K. (2015). Transmedulla neurons in the sky compass network of the honeybee (*Apis mellifera*) are a possible site of circadian input. *PLoS One*, *10*, e0143244. https://doi.org/10.1371/journal.pone.0143244

Zeng, H., Qin, Y., Du, E., Wei, Q., Li, Y., Huang, D., Wang, G., Veenstra, J. A., Li, S., & Li, N. (2021). Genomics- and peptidomics-based discovery of conserved and novel neuropeptides in the American cockroach. *Journal of Proteome Research*, *20*, 1217–1228. https://doi.org/10.1021/acs.jproteome.0c00596

SUPPORTING INFORMATION

Additional supporting information can be found online in the Supporting Information section at the end of this article.

Projekt II

Anatomical organization of the cerebrum of the praying mantis *Hierodula membranacea*

Anatomical organization of the cerebrum of the praying mantis

Hierodula membranacea

Vanessa Althaus[1], Gesa Exner[1,2], Joss von Hadeln[3], Uwe Homberg[1,2,*], Ronny Rosner[4,*]

[1]Department of Biology, Animal Physiology, Philipps-University of Marburg, D-35032 Marburg, Germany

[2]Center for Mind Brain and Behavior (CMBB), University of Marburg and Justus Liebig University of Giessen, D-35032 Marburg, Germany

[3]Justus-Liebig-University Giessen, D-35392 Gießen

[4]Department of Biology, Institute of Developmental Biology and Neurobiology, Johannes Gutenberg University of Mainz, D-55128 Mainz

*Shared correspondence to: Ronny Rosner, Department of Biology, Institute of Developmental Biology and Neurobiology, Johannes Gutenberg University of Mainz, D-55128 Mainz, Germany, E-mail: rrosner@uni-mainz.de

and Uwe Homberg, Department of Biology, Animal Physiology, Philipps-University of Marburg, D-35032 Marburg, Germany, Tel. +49-6421-2823402, Fax +49-6421-2828941, E-mail: homberg@staff.uni-marburg.de

ORCIDs

Vanessa Althaus, https://orcid.org/0000-0001-8018-0555

Ronny Rosner, https://orcid.org/0000-0002-5829-8626

Uwe Homberg, https://orcid.org/0000-0002-8229-7236

39

40 **Data availability statement**

41 All data that support the findings of this study are available from the corresponding authors.

42

43 **Conflict of interest disclosure**

44 The authors declare no conflict of interest.

45

46 **Author contributions**

47 Study concept and design: R.R., U.H.; acquisition of data: R. R., J. v H., G. E., V. A.; data analysis and

48 interpretation: V. A., G. E., R. R., J. v H., U. H.; drafting the manuscript: V. A., G. E.; review and editing:

49 U. H., R. R., V. A.

50

51 **Abbreviations**

52 ABR, anterior bridge; ACAR, accessory calyx ring; AL, antennal lobe; ALH, AL hub; ALI, anterior lip;

53 ALO, anterior lobe of the lobula complex; ALT, antennal lobe tract; AMMC, antennal mechanosensory

54 and motor center; AOT, anterior optic tract; AOTU, anterior optic tubercle; ATL, antler; AVLP,

55 anterior ventrolateral protocerebrum; BU, bulb; CA, calyx; CB, central body; CBL, lower division of the

56 CB; CBU, upper division of the CB; CL, clamp; CRE, crepine; CX, central complex; DAMMC, dorsal

57 AMMC; DLO, dorsal lobe of the lobula complex; EPA, epaulette; GA, gall; GABA, γ-aminobutyric acid;

58 GC, great commissure; GLO, glomerular lobe; GOR, gorget; IB, inferior bridge; ICA, inner CA; ICL,

59 inferior CL; IFS, inferior fiber system; INP, inferior neuropils; IT, isthmus tract; LAL, lateral accessory

60 lobe; LALC, LAL commissure; LAMMC, lateral AMMC; LCA, lateral CA; LEF, lateral equatorial fascicle;

61 LH, lateral horn; LLAL, lower LAL; LO, lobula; LOX, LO complex; LU, lower unit of the AOTU; LX, lateral

62 complex; MAL, medial accessory lobe; mALT, medial ALT; MAMMC, medial AMMC; MB, mushroom

63 body; MBDL, median bundle; MCA, medial CA; ME, medulla; MEF, medial equatorial fascicle; ML,

64 medial lobe; NO, noduli; OCA, outer CA; OCN, ocellar nerve; OLO, outer lobe of the LOX; OR, ocellar

65 root; PB, protocerebral bridge; PED, pedunculus; PEDD, PED divide; PENP, periesophageal neuropils;

66 PLP, posterior lateral protocerebrum; POC, posterior optic commissure; POTU, posterior optic

67 tubercle; PS, posterior slope; PVLP, posterior ventrolateral protocerebrum; SCL, superior CL; SIP,

68 superior intermediate protocerebrum; SLO; stalk lobe of the LOX; SLP, superior lateral

69 protocerebrum; SMP, superior medial protocerebrum; SNP, superior neuropils; SPU, spur; TC,

70   tritocerebrum; TH, tyrosine hydroxylase; TUBUT, tubercle-bulb tract; ULAL, upper LAL; UU, upper

71   unit of the AOTU; VES, vest; VFA, ventral area of flagellar afferents; VL, vertical lobe; VLNP,

72   ventrolateral neuropils; VLP, ventrolateral protocerebrum; VMNP, ventromedial neuropils; VX,

73   ventral complex; WED, wedge; WEDC, WED commissure

74

75

76 **Abstract**

77 Many predatory animals, such as the praying mantis, use vision for prey detection and capture.

78 Mantises are known in particular for their capability to estimate distances to prey by stereoscopic

79 vision. While the initial visual processing centers have been extensively documented, we lack

80 knowledge on the architecture of central brain regions, pivotal for sensory motor transformation and

81 higher brain functions. To close this gap, we provide a three-dimensional (3D) reconstruction of the

82 central brain of the Asian mantis, *Hierodula membranacea*. The atlas facilitates in-depth analysis of

83 neuron ramification regions and aides in elucidating potential neuronal pathways. We registered seven

84 3D-reconstructed visual interneurons into the atlas. In total, 42 distinct neuropils of the cerebrum were

85 reconstructed based on synapsin immunolabeled whole mount brains. Backfills from the antenna and

86 maxillary palps, immunolabeling of γ-aminobutyric acid (GABA) and tyrosine hydroxylase (TH) further

87 substantiate the identification and boundaries of brain areas. The composition and internal

88 organization of the neuropils were compared to the anatomical organization of the brain of the fruit

89 fly *Drosophila melanogaster* and the two available brain atlases of Polyneoptera, the desert locust

90 *Schistocerca gregaria* and the Madeira cockroach *Rhyparobia maderae*. This study paves the way for

91 detailed analyses of neuronal circuitry and promotes cross-species brain comparisons. We discuss

92 differences in brain organization between holometabolous and polyneopteran insects. Identification

93 of ramification sites of the visual neurons registered into the atlas support previously made claims

94 about homologous structures in the optic lobes of flies and mantises.

95

96 **Key words:** insect brain; *Hierodula membranacea*; neuroanatomy; 3D-reconstruction; brain atlas

97

98 **Introduction**

99 Insects show astonishing visual perception abilities employed for spatial orientation (Merlin et al.,

100 2012; Warrant & Dacke, 2011; Heinze et al., 2018), object categorization (Avarguès-Weber et al.,

101 2011; Giurfa, 2021), and object tracking (O'Carrol, 1993; Nordström et al., 2009; Olberg, 2012;

102 Gonzalez-Bellido et al., 2016), which often rival those of vertebrates. Understanding the

103 neuroarchitectures that enable these abilities requires an in-depth analysis of brain areas and

104 neuronal networks. The insect brain comprises neurons with cell bodies arranged in a peripheral cell

105 body rind enclosing the neural processes and synaptic contacts in cell body free neuropils that are

106 interconnected by axonal fiber tracts (Strausfeld, 1976; Ito et al., 2014). Certain brain areas like the

107 central complex (Pfeiffer & Homberg, 2014), the antennal lobe (Schachtner et al., 2005), the optic

108 lobe (Strausfeld, 2005), and the mushroom body (Fahrbach, 2006) are well-defined brain areas in the

109 insect brain. These neuropils have been described in many insect species and are extensively studied,

110 due to their pivotal roles in sensory-motor transformation and learning and memory (Strausfeld,

111 2012; Kinoshita & Homberg, 2017). Other areas in the brain are extensively interconnected and are

112 more difficult to identify and subdivide into distinct neuropils (Ito et al., 2014). Orientation, size and

113 number of neuropils differ between insect species, but clear definitions of boundaries between brain

114 areas set by Ito et al. (2014) provide a basis for comparative subdivisions of the cerebrum across

115 insects. The brains of the fly *D. melanogaster* (Ito et al., 2014), the ants *Cardiocondyla obscurior*

116 (Bressan et al., 2015) and *Cataglyphis nodus* (Habenstein et al., 2020), the locust *S. gregaria* (von

117 Hadeln et al., 2018), the monarch butterfly *Danaus plexippus* (Heinze & Reppert, 2012), the Bogong

118 moth *Agrotis infusa* (Adden et al., 2020), the cockroach *R. maderae* (Althaus et al., 2022), the honey

119 bee *Apis mellifera* (Habenstein et al., 2023), and the dung beetles *Scarabaeus lamarcki* and

120 *Scarabaeus satyrus* (Immonen et al., 2017) have already been fully segmented into 3D digital brain

121 atlases.

122   This study provides a 3D-atlas of the brain of a third polyneopteran insect, the praying mantis

123 *H. membranacea*. Being a predatory insect, it occupies an ecological niche that is different from that

124 of the locust and cockroach. Behavioral studies in praying mantises examined prey recognition,

125 distance perception, prey capture, mating behavior, and defensive behavior (Poteser & Kral, 1995;

126 Kral & Prete, 1999; Hurd, 1999; Nityananda et al., 2016a, 2019a,b). Mantises are ambush predators

127 that rely strongly on vision for hunting and spatial orientation. They are the only insect group known

128 to use stereopsis for distance perception (Rossel, 1983; Nityananda et al., 2016b; Read, 2023). Their

129 compound eyes provide a nearly full panoramic view and exhibit binocular overlap in the frontal

130 visual field (Rossel, 1979). Recent studies have examined the anatomical basis of visual performance

131 in mantises in more detail. Their optic lobe comprises a larger volume than the central brain (Rosner

132 et al., 2017) and consists of a thin lamina covering a large medulla (ME) and a joint lobula complex

133 (LOX). The mantis LOX is highly segregated and consists of 5 neuropils. In contrast, the LOX of the

134 closely related *R. maderae* shows a simpler three-lobe organization (Rosner et al., 2017). The

135 composite structure of the LOX goes along with the processing of different aspects of the visual

136 scenery. Intracellular recordings from individual neurons suggest that the processing of widefield

137 motion is segregated from object motion (Rosner et al., 2019, 2020; Yamawaki, 2019).

138   To advance these functional insights on an anatomical level, we digitally segmented the

139 cerebrum of the giant Asian mantis *H. membranacea,* one of the most common studied species, into

140 distinct neuropils. While most neuropils have counterparts in the fruit fly, and the two other

141 polyneopteran species studied, the desert locust and Madeira cockroach, their relative volumes and

142 shapes usually differ considerably. Registration of physiologically characterized visual interneurons

143 into the 3D-brain allows us now to clearly define their central targets. This will facilitate dissecting

144   parallel visual inputs to the mantis brain with respect to prey recognition and capture as well as

145   other visually driven behaviors.

146   **Material and Methods**

147   **Animals**

148   Praying mantises (*Hierodula membranacea)* were obtained as nymphs from a commercial breeder

149   (M&M Wüst, Mühlheim, Germany). They were raised under a 12:12 h light/dark cycle and a

150   temperature of 24 °C at the Department of Biology of the University of Marburg. The animals for the

151   single cell stainings were kept as previously reported (Rosner et al., 2019 and 2020) at 25 °C and at

152   the Biosciences Institute of Newcastle University. The animals were fed with desert locusts or

153   crickets, respectively. Only female mantises were used for the 3D-atlas, the immunolabelings and for

154   the single-cell stainings that were used for the registration into the atlas.

155   **Immunolabeling of whole mounts**

156   Analysis of the different brain areas is largely based on whole mount brains labeled with antibodies

157   against synapsin and supplemented by whole mount preparations immunolabeled for tyrosine

158   hydroxylase (TH), the rate limiting enzyme in dopamine synthesis. Animals were cold-anesthetized

159   for about 20 min at 4 °C. Afterwards, the head capsule of the animals was opened, and the brains

160   were pre-fixed with 4 % formaldehyde (FA) in phosphate-buffered saline (PBS, containing 78.8 mmol

161   l^{-1} Na_2HPO_4 x 2 H_2O and 19 mmol l^{-1} NaH_2PO_4 x H_2O; pH 7.4) for 10-60 min. After prefixation, the

162   brains were dissected (in PBS) and fixed overnight in 4 % FA in PBS at 4 °C. For TH immunolabeling

163   the brains were fixed overnight in 2 % PFA in Millonig's phosphate buffer (containing 0.13 mol l^{-1}

164   NaH_2PO_4 x H_2O, 0.1 mol l^{-1} NaOH, 0.3 mmol l^{-1} $CaCl_2$, 1.2 % glucose; pH 7.3-7.4). The next day, the

165   brains were rinsed 4 x 10 min in 0.1 mol l^{-1} PBT (PBS, containing 5 % Triton X-100, TrX). To facilitate

166   penetration of the synapsin antibody, the brains were treated for 1 h with 1 mg/ml

167   collagenase/dispase in 0.05 mol l^{-1} Tris-HCl (pH 7.6). After several washing steps the brains were

168   preincubated overnight with 5 % normal goat serum (NGS; RRID: AB_2336990) in PBT (for TH

169   immunostaining with extra 2% bovine serum albumin) at 4 °C. Brains were incubated for 5 days at 4

170   °C with anti-synapsin (mouse monoclonal, SYNORF1, 1:50, kindly provided by Drs. E. Buchner and C.

171   Wegener, Würzburg, Germany, RRID: AB_2315425) or with the TH antibody (Immunostar, 1:1,000,

172   RRID: AB_572268) in a solution of 1 % NGS in 0.1 mol l^{-1} PBT. After incubation, the brains were

173   washed 3 x 10 min with PBT. For incubation with the secondary antibodies, the brains were

174   transferred to cyanine-3 conjugated goat-anti-mouse (GaM-Cy3, 1:300, Jackson ImmunoResearch,

175   RRID: AB_2338006) diluted in PBT with 1 % NGS for 3 days at 4 °C. The brains were finally rinsed 2 x

176   20 min in PBT and 3 x 20 min in PBS followed by dehydration in an ascending ethanol series (25 %,

177   50 %, 70 %, 90 %, 95 %, and 100 %; 15 min each). For clearing the tissue, brains were transferred to a

178 solution of 50 % ethanol and 50 % methyl salicylate (Merck, Darmstadt, Germany) for 20 min and

179 cleared for 20 min in 100 % methyl salicylate. The whole mounts were embedded in Permount

180 medium (Fisher Scientific, Schwerte, Germany) between two cover slips. Reinforcement rings were

181 used as spacers.

182 **In vivo backfills of the antenna and maxillary palp**

183 Animals were cold-anesthetized on ice for about 30 min. One maxillary palp or antenna was

184 transected, and the cut nerve was submerged for 1 min in demineralized H_2O. The cut antennal nerve

185 or maxillary nerve was subsequently placed in a drop of 4 % Neurobiotin in 1 mol l^{-1} potassium

186 chloride (KCl), sealed with petroleum jelly and incubated at 4 °C overnight in the refrigerator. The

187 next day, the brains were dissected from the head capsule and transferred into fixative solution (4 %

188 paraformaldehyde, 0.25 % glutaraldehyde and 0.2 % saturated picric acid; pH 7.4) in 0.1 mol l^{-1} PBS

189 for 3 h at room temperature. Afterwards, they were washed 3 x 15 min in 0.1 mol l^{-1} PBT (0.3 % TrX).

190 The brains were preincubated with 5 % NGS in PBT for 1-2 h at room temperature and subsequently

191 incubated with streptavidin-cyanine-3 (Strep-Cy3, 1:1,000, Dianova, Hamburg, Germany, RRID:

192 AB_2337244) and anti-synapsin in a solution of 2 % NGS in 0.1 mol l^{-1} PBT. After 3-4 days at 4 °C, the

193 brains were washed 4 x 10 min in PBT followed by incubation in secondary antibody, goat-anti-

194 mouse-cyanine-5 (GaM-Cy5, 1:300, Dianova, Hamburg, Germany) and Strep-Cy3 (1:1,000) in PBT with

195 2 % NGS for 2-3 days at 4 °C. Brains were, finally, washed 2 x 15 min in PBT and 2 x 15 min in PBS.

196 Afterwards, dehydration, clearing and embedding of the whole mounts were performed as described

197 above.

198 **Immunolabeling on 30-μm sections**

199 To facilitate the establishment of neuropil boundaries, brain sections were labeled with antiserum

200 against γ-aminobutyric acid (GABA) using the indirect peroxidase-antiperoxidase (PAP) technique

201 (Sternberger, 1979). Brains of cold-anesthetized animals were dissected in 0.1 mol l^{-1} PBS from the

202 head capsule. They were incubated in fixative containing 25 % glutardialdehyde, 74 % saturated

203 picric acid, and 1 % acetic acid for 4 h at room temperature. After rinsing 4 x 10 min in PBS and once

204 in 0.1 mol l^{-1} PBT (0.3 % TrX), the brains were frontally embedded in gelatin/albumin blocks and again

205 fixed at 4 °C in 8 % paraformaldehyde (PFA) overnight for sectioning. The next day, the brains were

206 sliced with a vibrating blade microtome (VT 1200 S, Leica Biosystems, Wetzlar, Germany) in frontal

207 plane to 30-μm sections, followed by preincubation for 1 h at room temperature in 8 % NGS diluted

208 in saline substituted Tris-buffer (SST; containing 1 % TrX). Sections were incubated in anti-GABA

209 antiserum raised in rabbit (1:8,000, kindly provided by Dr. T. G. Kingan, University of Arizona, Tuscon,

210 AZ; RRID: AB_2314457) in SST with 2 % NGS for 20 h at room temperature. Following, brains were

211 washed in SST (0.1 % TrX) and transferred to the secondary antibody solution, goat anti-rabbit IgG

212 (1:40, RRID: AB_261363) in SST (containing 0.5 % TrX and 1 % NGS) for 1 h at room temperature.

213 After rinsing in SST (0.1 % TrX), sections were transferred to rabbit-PAP solution (1:300, RRID:

214 AB_2315056) in SST (containing 0.5 % TrX and 1 % NGS) for 1 h. To remove excess PAP, the brains

215 were washed 5 x 10 min with SST (0.5 % TrX). 3,3'-Diaminobenzidine tetrahydrochloride (DAB, 0.03

216 mg/ml) was applied to the sections with H_2O_2 (0.02 %) in 0.1 mol l^{-1} phosphate buffer (pH 7.4). After

217 staining, the sections were washed for 3 x 10 min in phosphate buffer to stop the reaction and

218 mounted on coated microscope slides. Afterwards, the sections were dehydrated in an ascending

219 ethanol series, cleared in xylenes and mounted in Entellan (Merck, Darmstadt, Germany) under cover

220 slips.

221 **Antibody characterization**

222 The anti-GABA antiserum (# 9/24, provided by T. G. Kingan, RRID: AB_2314457) is an affinity purified

223 antiserum raised in rabbit against conjugates of GABA-glutaraldeyde-keyhole limpet hemocyanin

224 (KLH; Hoskins et al., 1986). The antiserum has been used to characterize GABA-immunoreactive

225 neurons in many insect species, including the praying mantis *H. membranacea* (Rosner et al., 2017;

226 Homberg et al., 2018). On brain sections of the sphinx moth *Manduca sexta*, immunostaining was

227 abolished by preadsorption of the diluted antiserum with 24 nmol l^{-1} GABA-KLH conjugates but

228 staining was not reduced by preadsorption with conjugates of L-glutamic acid, L-glutamine, taurine,

229 or β-alanine (Hoskins et al., 1986). Preadsorption of the diluted antiserum with 50 μmol l^{-1} GABA-

230 glutaraldehyde complex abolished all immunostaining on vibratome sections of *H. membranacea*

231 brains (Rosner et al., 2017).

232 The monoclonal antibody against synapsin (#3C11, SYNORF1, RRID: AB_2315425) was

233 obtained from Drs. E. Buchner and C. Wegener (University of Würzburg). It was raised in mice against

234 fusion proteins consisting of glutathione-S-transferase and parts of the *D. melanogaster* synaptic

235 vesicle protein SYN1 (Klagges et al., 1996). Its specificity has been demonstrated in *D. melanogaster*

236 by Klagges et al. (1996). The antibody labels synaptic neuropils as shown in different insect species,

237 including *H. membranacea* (Rosner et al., 2017).

238 The monoclonal TH antibody (Immunostar, cat# 22941, RRID: AB_572268) was raised in

239 mouse against full-length TH purified from rat PC12 cells. The antibody recognizes an epitope in the

240 catalytic core of the TH which is highly conserved during evolution (Calvo et al., 2011). Being the rate-

241 limiting enzyme in dopamine synthesis, the antibody labels putatively dopaminergic neurons in a

242 wide range of animals including various insect species (Hamanaka et al., 2016; Timm et al., 2021).

243 Staining patterns obtained with the TH antibody and a dopamine antiserum were highly similar in the

244 brain of a cockroach (Hamanaka et al., 2016) and a locust (Timm et al., 2021). In immunoblots of

245 brain homogenates from crickets, backswimmer, cockroaches, and water strider, the antibody labels

246 a single lane at 54-66 kDa (Hamanaka et al., 2016; Timm et al., 2021) which corresponds well with

247 the molecular weight of human TH (60 kDa, Immunostar).

248 **Image acquisition**

249 Fluorescently labeled whole mount preparations and sections were scanned by a confocal laser

250 scanning microscope (Leica, TCS SP5, Leica Microsystems, Wetzlar, Germany). Preparations were

251 scanned with a 20x oil immersion objective lens (HC PL APO 20x/0.75 Imm Corr CS2). Cy3

252 fluorescence was excited by a diode-pumped solid-state laser (561 nm, DPSS 10 mW) and the Cy5

253 fluorescence with a helium neon laser (633 nm, HeNe 10 mW). The synapsin-stained whole mounts

254 were scanned at a resolution of 1024 x 1024 pixels in the xy-plane (pixel size 0.75 µm x 0,75 µm),

255 with a z-step size of 1 µm, a line average of 4, and scanning velocity of 400 Hz for the synapsin

256 labeling and a line average of 2 for the backfills. The resulting data stacks were further processed in

257 Amira 6.5 and 5.6 (Thermo Fisher Scientific, Waltham, USA).

258 Images of GABA-labeled sections were obtained using a digital camera (ProgRes C12plus,

259 Jenoptik) connected to a transmission light microscope (Axioskop, Zeiss, Oberkochen, Germany).

260 Contrast and brightness of the images were adjusted in Affinity Photo (Serif, Nottingham, UK), and

261 the final figures of all created images were made in Affinity Designer (Serif, Nottingham, UK).

262 **Anatomical reconstruction of neuropils and neurons**

263 3D-reconstructions of neuropils were created with the software Amira 6.5. Sequential scans of a

264 selected synapsin labeled whole mount brain were opened and processed in the *Segmentation*

265 *editor.* Boundaries of the neuropils were set manually with correspondence to additional

266 information. Characteristic levels of each neuropil were marked in all planes of the image stack

267 resulting in a 3D grid that built the basis for a polygonal surface. To generate a 3D-model from the

268 grid, we used the *Wrap*-module. It created a polygonal surface, that was visualized using *SurfaceGen,*

269 and displayed with *SurfaceView*. To smooth and minimalize the generated data size, the

270 reconstruction was *Simplified*. We reconstructed neuropils and, in addition, some fiber tracts and

271 commissures that were used as boundaries between these neuropils.

272 We identified the arborization areas of seven visual interneurons that were recorded and

273 labeled by Neurobiotin injections in previous studies (Rosner et al., 2019 and 2020). Four of these

274 neurons were published in Rosner et al. (2020) and the other three in Rosner et al. (2019). The

275 reconstruction of the individual neurons was done in Amira 5.6 by using the *Skeletonize* plugin.

276 Neurites, somata and branches were manually traced in the confocal data stacks by fitting the

277 diameter and path of each part/segment of the neuron corresponding to the gray values in the

278 staining. The complete reconstructions of all seven neurons were registered into the 3D-atlas to

279 identify their arborization areas in the cerebrum in detail, in addition to their innervation sites in the

280 optic lobes examined previously (Rosner et al., 2019 and 2020).

281 **Registration of neurons in the mantis brain atlas**

282 Neuron registration was performed manually using Amira 6.5. For each neuron, at least three

283 associated neuropils of the cerebrum were individually 3D-reconstructed, to ensure a correct spatial

284 arrangement. The registration process began by aligning the individually reconstructed neuropils to

285 the brain atlas, making adjustments in translation, rotation, and scaling using the *Transform editor*.

286 Once both reconstructions were aligned, the parameters from the three reconstructed neuropils were

287 transferred to the associated neuron using the command console commands *>getTransform* and

288 *>setTransform*.

289

290 **Results**

291 We reconstructed 42 major neuropils, some with additional subunits, and 12 fiber tracts and

292 commissures of the cerebrum from a mature female mantis *H. membranacea* (Figure 1, see Movie

293 S1). The reconstruction is based on a synapsin immunolabeled whole mount brain and additional

294 data from GABA immunolabeled brain sections, TH immunolabeling, individually injected neurons,

295 and backfills of the antennal flagellum and maxillary palp. To facilitate identification of neuropils and

296 fiber tracts, a series of annotated frontal optical sections through the mantis brain is provided in

297 Figures 2-5. Neuropil boundaries were set based on the criteria of Ito et al. (2014). For the

298 periesophageal neuropils the 3D reconstructions of the locust (von Hadeln et al., 2018) and the

299 cockroach (Althaus et al., 2022) brains were used as references, because correspondence of these

300 brain areas in polyneopteran insects with those in the fly and other Holometabola has not yet been

301 resolved. The optic lobe is not included here, because a 3D-reconstruction of optic-lobe neuropils

302 was already provided by Rosner et al. (2017). This study will facilitate neural network analyses in the

303 mantis brain. To demonstrate these possibilities, we registered seven neurons previously

304 characterized by Rosner et al. (2019 and 2020) into the 3D-reconstructed brain.

305 **Mushroom body**

306 The mushroom bodies (MBs) are distinct bilaterally paired neuropils in the cerebrum of *H.*

307 *membranacea*. Each MB comprises a pedunculus (PED), a medial lobe (ML), a vertical lobe (VL), two

308 calyces (CAs), each consisting of an inner (ICA) and outer CA (OCA), and an accessory CA ring (ACAR).

309 The MBs extend from the level of the central body to the dorsal surface and through the whole depth

310 of the protocerebrum (Figure 6a,b).

311 In each brain hemisphere, two cup-shaped structures, a medial (MCA) and a lateral CA (LCA)

312 are present. The cups in each hemisphere are fused (Figures 4b,c, 5 and 6a-c) and are the most dorsal

313 neuropils in the mantis cerebrum. Each cup is further subdivided into an inner (ICA) and outer (OCA)

314 structure. The ICAs consist of fiber bundles of Kenyon cells (Strausfeld & Li, 1999) and can be seen as

315 extensions of the PED (Figure 6e). They are free of GABA immunolabeling (Figure 6e) and show only

316 weak synapsin staining (Figure 6c). In contrast, the OCAs are densely innervated by GABA

317 immunolabeled neurons and thereby clearly distinguishable from the rest of the MB (Figure 6e). A

318 ring-shaped neuropil, the ACAR, emerges ventrally attached to the CAs and spans around both

319 strands of the PED (Figure 4c, 5a, and 6a,b). It shows a smooth texture of synapsin immunolabeling,

320 but conspicuous accumulations of synapsin (Figure 6d), which is unique to the region of the ACAR.

321   The point of fusion of the ML, VL, and PED, called PED divide (PEDD; Figure 6b), is located at

322 the anterior-most part of the MB. The PEDD was not reconstructed as an individual neuropil, because

323 it could not be distinguished from the lobes by synapsin immunolabeling (Figure 2b,c). Furthermore,

324 no structural equivalent of a spur, a small lateral protrusion of the PEDD described in *S. gregaria* (von

325 Hadeln et al., 2018), *A. infusa* (Adden et al., 2020), and *D. melanogaster* (Ito et al., 2014, Tanaka et

326 al., 2008), but not in *R. maderae* (Althaus et al., 2022), was found. The ML extends horizontally from

327 the PEDD toward the brain midline, nearly touching its contralateral counterpart, but without

328 apparent fusion (Figures 2b,c, 3 and 4a,b). Adjacent to the ML, the medial accessory lobe (MAL) is

329 positioned ventrally, while the anterior lip (ALI) and central body (CB) are dorsally to the ML (Figures

330 3 and 4a,b). The VL extends dorsally from the PEDD, passing through the protocerebrum. Its dorsal

331 tip almost contacts the ventral border of the MCA. Both, the VL and PED are essential landmarks for

332 defining boundaries of the superior (SNP) and inferior neuropils (INP). The VL touches laterally the

333 superior clamp (SCL) and medially the ALI, a small bulge of the crepine (CRE), and the superior medial

334 protocerebrum (SMP). It shows, similar to the ML, smoothly structured synapsin labeling and was

335 easily identified by its concise borders (Figures 2b,c, 3 and 4a,b). The PED leaves the PEDD laterally

336 and is ventro-laterally limited by the extension of the anterior (AVLP) and posterior ventrolateral

337 protocerebrum (PVLP). The PED extends through the inferior protocerebrum and turns dorsally

338 between the SLP and ICL toward the CAs (Figures 2b,c, 3, 4, and 5a,b). Near its dorsal end, the PED

339 bifurcates at the region of the PED neck. The PED neck was not reconstructed as a separate neuropil,

340 because it was not recognizable by synapsin immunolabeling. However, it is located at the point of

341 fusion of the two strands of Kenyon cell axons originating from the MCA and LCA (Figure 6e).

342 **Central complex, anterior lip and lateral complex**

343 The central complex (CX) is a midline crossing group of neuropils (Figure 6h) and comprises the

344 central body (CB), the protocerebral bridge (PB), and the paired noduli (NO). The CB is composed of

345 an upper (CBU) and a lower division (CBL), both having a semitoroidal shape. The CBU is larger than

346 the CBL and encases the latter dorso-posteriorly (Figures 4 and 6i-g). In *D. melanogaster*, the

347 equivalents are referred to as the fan-shaped body (FB) and ellipsoid body (EB) respectively, denoting

348 their distinct shapes. Both subdivisions of the CB are surrounded by a large mass of fibers. They are

349 covered by the SMP and the ALI (anterior), and the inferior bridge (IB) and the antler (ATL; posterior).

350 We distinguished 10 vertical slices in the CBU based on synapsin- and GABA immunolabeling,

351 consistent with the findings of Rosner et al. (2017). Although we could not discern horizontal layers

352 of the CBU, Timm et al. (2021) identified at least three layers using TH immunolabeling. Similar to the

353 CBU, the CBL is composed of 10 bean-like vertical subunits, 5 per hemisphere. As reported by Rosner

354 et al. (2017), the outermost columns (R5, L5) in the CBL and CBU are noticeably smaller than the

355 other slices. GABA-immunolabeled fibers of tangential neurons enter the CBL through the isthmus

356 tract (IT) and give rise to strong immunostaining in the columns of the CBL (Figure 6g).

357 The paired NO (Figures 4b,c and 6h) are located ventral to the CB. They are small neuropils,

358 in most insect species separated into upper and lower units, but we were unable to identify these

359 subunits here. The third neuropil of the CX is the paired PB (Figures 5b,c and 6j). Positioned

360 dorsoposterior to the CB, the PB consists of two elongated neuropils that bend laterally in posterior

361 direction, resembling a handlebar shape as a whole. The two arms, one in each brain hemisphere,

362 are spatially separated but connected by a fiber bundle crossing the midline.

363 The ALI is a slender elongated synapsin-rich area (Figure 3) that extends horizontally across

364 the brain midline, directly anterior to the CB. The ALI appears anteriorly between the CREs, VLs and

365 MLs of both hemispheres (Figure 3). The SMP and the CRE are the dorsal and anterior limits of the

366 ALI, respectively. A small region ventrolateral to the ALI was assigned to the CRE based on GABA

367 immunolabeling. While the CRE is widely pervaded by GABA immunolabeled fibers, the ALI is nearly

368 devoid of GABA staining (Figure 6f). In holometabolous insects such as the fruit fly *D. melanogaster*,

369 the ALI has not been observed as a distinct neuropil, but in other Polyneoptera like the cockroach *R.*

370 *maderae* or locust *S. gregaria*, the ALI is closely associated with the CX (von Hadeln et al., 2020; Timm

371 et al., 2021; Jahn et al., 2023).

372 Another prominent CX-associated neuropil group is the lateral complex (LX; Figure 7). It is

373 divided into the bulb (BU) and the lateral accessory lobe (LAL), which is further subdivided into the

374 lower (LLAL) and upper (ULAL) LAL, along with the gall (GA). The LAL is positioned ventrolaterally

375 from the CX and is, among other criteria, characterized by the quite prominent LAL commissure

376 (LALC) that connects the bilateral LALs across the brain midline segregating the LLAL from the ULAL

377 (Figure 3b,c). The LAL is further traversed by the isthmus tract (IT), a major fiber bundle containing

378 GABA-labeled neurites that connect the LX and CX. The IT courses from the CX through the LAL and

379 serves as an additional boundary between the ULAL, LLAL and BU (Figure 7a,b,c'). The ULAL (Figures

380 2b,c, 3, and 4a) emerges at the anterior surface of the cerebrum between the PED, ML, and antennal

381 lobe (AL). It is, thus, posteriorly and medio-ventrally attached by the LLAL, separated by the LALC and

382 the IT. The VL adjoins at the dorsal surface of the ULAL, the ventrolateral protocerebrum (VLP)

383 laterally, the MAL and LLAL medially. The posterior boundaries are demarcated by the appearance of

384 the epaulette (EPA) and the great commissure (GC), which is noticeably large in the mantis. The

385   medial antennal lobe tract (mALT) serves as a landmark indicating the posterior boundary of the LAL

386   (Figure 4a,b), as described in the locust (von Hadeln et al., 2018) and the cockroach (Althaus et al.,

387   2022), together with the inferior fiber system (IFS). Its medial boundaries (Figures 2b,c, 3 and 4a)

388   from anterior to posterior include the cell body rind, median bundle (MBDL), mALT, vest (VES), and

389   MAL. Ventrally, the LAL is delimited by the mALT, IFS, and the neuropils of the antennal

390   mechanosensory and motor center (AMMC).

391   The uniform BU is embedded dorso-anteriorly between the ULAL and LLAL. It lies posterior to

392   the CRE, anterolateral to the IT, and ventral to the PED/ML (Figures 2c, 3a,b, 6f, and 7c'). The BU was

393   identified by its finer and denser synapsin staining compared to surrounding regions, as well as

394   intense GABA immunolabeling (Figure 6f), as it houses the dendrites of GABA-immunoreactive

395   tangential neurons of the CBL. Furthermore, we discovered the tubercle-bulb tract (TUBUT), which

396   connects the anterior optic tubercle (AOTU) with the BU (Figures 2 and 3a,b).

397   The GA, characterized as a distinct area of axonal projections of CX outputs in *D. melanogaster*

398   (Wolff et al., 2015), the dung beetles *S. lamarki* and *S. satyrus* (el Jundi et al., 2018), the cockroach *R.*

399   *maderae* (Althaus et al., 2022), and the locust *S. gregaria* (Hensgen et al., 2021a), was identified based

400   on its strong synapsin immunolabeling, smooth and demarcated structure, and similar positioning to

401   that observed in the other insects. The GA has a small elongated shape and lies on the ventral anterior

402   border between the LLAL and ULAL (Figures 2b and 7c).

403   **Superior neuropils and lateral horn**

404   The superior lateral (SLP), superior intermediate (SIP), superior medial protocerebrum (SMP),

405   anterior bridge (ABR), and the lateral horn (LH) are neuropils located in the superior protocerebrum

406   and occupy the most dorsal parts of the mantis brain (Figures 1 and 8a).

407   The SLP (Figure 2b,c, 3, 4, and 5a,b) is the most lateral neuropil of the cerebrum and is

408   through the optic stalk directly attached to the stalk lobe (SLO) of the lobula complex (LOX). It

409   occupies a large volume of the dorso-lateral brain region and encases dorsally the LH. The SLP

410   extends the superior space posterior-laterally to the SIP and laterally to the PED. Its medial

411   boundaries include the ICL and posterior slope (PS; posterior region), as well as the SIP, SCL and PED

412   (anterior region). The SLP is separated ventrally from the PVLP by the LH and GC (Figure 4c). The

413   medially lying SCL was differentiated from the SLP by numerous fibers penetrating this brain area,

414   creating a porous appearance in synapsin immunolabeling (Figure 3). Distinguishing the SIP from the

415   SLP was more challenging; their boundaries were set by the presence of stronger and smoother

416   synapsin immunolabeling in the SIP compared to the SLP (Figures 2, 3 and 4a,b). The SIP (Figures 2, 3

417   and 4a,b) emerges anteriorly between the anterior optic tract (AOT) and AVLP and expands posterior

418   to the AOTU. As an elongated neuropil, the SIP extends anteriorly to the mALT and CAs along the

419   dorsal soma rind. The boundary between the SIP and the medially lying SMP was set at the level of

420   the ascending VL (Figure 3). The distinction between the SIP, SLP and nearby CRE was made by GABA-

421   immunolabeled fibers that run through the SCL, targeting the CRE (Figure 9c-e). The ventral limitation

422   of the SIP is formed by the AVLP and SCL, identifiable by strong synapsin immunolabeling of the SIP

423   (Figure 2b,c).

424   The SMP was identified by its characteristic shape and its synapsin immunolabeling that is

425   distinctive by large penetrating fibers (Figures 2b,c, 3 and 4). Unlike in the locust (von Hadeln et al.,

426   2018) and cockroach (Althaus et al., 2022), the SMP is fused across the midline (Figure 3). It extends

427   posteriorly to the ABR, partly surrounding the strands of the MBDL (Figure 8a). The SMP is situated

428   medially to the SIP, medio-posteriorly to the CRE, and expands dorsally along the ALI. It is lateral

429   demarcated by the VLs and more posterior by the CAs of the MBs. The mALT defines the posterior

430   boundary of the SMP (Figures 4c and 5a), and dorsally the SMP is bordered by the soma rind, while

431   the fiber system around the CX and ALI covers most of its ventral face. It is attached to the SCL and

432   ICL ventrolaterally, separated at the point where the VL ascends (Figure 4). At the dorso-anterior

433   brain surface, the ABR, a thin neuropil, spans across the brain midline (Figures 2b,c and 8a,b). It has a

434   grainy and fibrous structure, which is best visible in GABA immunolabeling (Figure 8b). The MBDL

435   runs posterior from the ABR (Figure 8a). The ABR has also been identified as a distinct neuropil in the

436   cockroach and locust (von Hadeln et al., 2018; Althaus et al., 2022), but not in holometabolous

437   insects.

438   The olive-shaped LH (Figures 3b,c, 4 and 5a) protrudes laterally from the SLP toward the optic

439   lobe (OL) and shows dense GABA immunolabeling (Figure 8c). The prominent mALT passes through

440   the SLP, targeting the LH, thereby serving as a landmark for the identification of the LH (Figures 4c

441   and 8d). The entire neuropil is separated from the surrounding neuropils, such as the SLP dorsally

442   and the PVLP ventrally, by diverse fibers, clearly visible in synapsin- and GABA immunolabeling

443   (Figure 8c,d).

444   **Ventrolateral neuropils**

445   The ventrolateral neuropils (VLNP; Figure 8e,f) comprise the ventrolateral protocerebrum (VLP) with

446   an anterior (AVLP) and a posterior (PVLP) region, the posterior lateral protocerebrum (PLP), the

447   wedge (WED), and the anterior optic tubercle (AOTU) with a smaller lower unit (LU) and a larger

448   upper unit (UU).

449   Massive fiber tracts crossing the ventral protocerebrum were used as landmarks to divide the

450   VLP into an anterior and a posterior region (Figures 2 and 3). The AVLP (Figure 2) commences directly

451   beneath the cell body rind and is located in the lower lateral part of the anterior brain. It touches

452   medially the CRE and more posteriorly the PED and ULAL. Its dorsal boundaries are the SIP, SCL, SLP,

453   while the PVLP supersedes the AVLP at its posterior surface (Figures 3 and 8e,f). The AVLP has a

454   denser and smoother texture (Figure 2), whereas the PVLP, the posterior part of the VLP, has a

455 glomerular structure in synapsin staining (Figure 8h) and is heavily interspersed by fibers and large

456 tracts (Figures 3 and 8h). Both parts of the VLP are limited by the cell body rind laterally and

457 ventrally. The PVLP lies ventrally to the SCL, SLP and the LH, while the PED, ICL, ULAL, and the WED

458 adjoin medially (Figure 3). The GC marks the dorsal and posterior boundary of the PVLP to the

459 adjacent PLP (Figures 4c, 5a, and 8e,f). The PLP in the mantis brain is relatively small and extends

460 from the PVLP to the posterior brain surface (Figure 5a-c). It is medially limited by the lateral

461 equatorial fascicle (LEF, Figure 5b and 8e,f), the ICL, and is more posteriorly surrounded by the PS.

462 Dorsally, the PLP is limited by the SLP, ICL, and the lateral extension of the PS, while the WED is

463 attached ventromedial to the PLP (Figures 5a-c and 8e,f).

464   One of the most ventrally lying neuropils of the protocerebrum is the WED (Figure 8e). It

465 differs from the surrounding neuropils by its texture in synapsin immunolabeling (Figure 4) and

466 isspotted by many tracheae and tracts that penetrate it. It is framed medially by parts of the LLAL,

467 IFS, and the VES and is dorsally flanked by the EPA, GC, VES and dorso-posteriorly by the PLP and PS

468 (Figures 3b,c, 4 and 5a-c). The PVLP adjoins laterally, while ventrally the AMMC and bundles of

469 intersegmental neurons limit the WED. It is covered posteriorly by the PS.

470   The AOTU is the most anterior neuropil of the protocerebrum (Figure 8e,f). It lies dorsally on

471 the surface of the CRE (Figure 1). As in the cockroach (Althaus et al., 2022) but in contrast to the

472 AOTU of bees (Habenstein et al., 2023) and locusts (von Hadeln et al., 2018), it is relatively small. Two

473 subunits, a larger upper unit (AOTU-UU) and a smaller lower unit (AOTU-LU) are distinguishable

474 (Figure 8g). The AOT extends from the OL dorso-laterally along the SIP and enters the AOTU laterally.

475 The TUBUT served to distinguish the two subunits, because it separates the UU from the LU (Figure

476 8g) and connects the AOTU with the BU in the LX (Figures 2 and 3a,b).

477 **Inferior neuropils**

478 The inferior neuropils (INP) consist of the crepine (CRE), superior (SCL) and inferior clamp (ICL),

479 inferior bridge (IB), antler (ATL), ocellar root (OR), and the medial accessory lobe (MAL). In the

480 mantis, the CRE is a flat neuropil forming the anterior surface of the brain (Figure 9a,b). The CRE lies

481 ventral to the AOTU. The TUBUT runs through the CRE and targets the BU (Figure 2). The lateral

482 boundaries of the CRE are demarcated by several neuropils, the AVLP, SIP, SCL, VL, and the PED.

483 Medially, the SMP emerges and extends over the dorsoposterior region of the CRE (Figure 2). The

484 posterior termination of the CRE corresponds to the level of the PEDD, except for a small protrusion

485 between the ALI and ML (Figure 3). It almost surrounds the PEDD and ends dorsally at the ULAL

486 (Figure 3). This bulge of the CRE is distinguishable from the ALI by GABA immunostaining, which is

487 absent in the ALI (Figure 9c). The identification of the CRE was based on its fibrous appearance in

488 synapsin immunolabeling and the presence of GABA-immunolabeled fibers that innervate the CRE

489 after running through the SCL (Figure 9c-e, blue arrowheads), similar to findings in the cockroach

490 (Althaus et al., 2022).

491   The MAL in the mantis is a midline-spanning neuropil (Figure9a-c), like in the locust (von

492 Hadeln et al., 2018). It lies ventrally to the ML and extends from the posteriorly lying IB toward the

493 anteriorly lying CRE (Figures 3 and 4a,b). The massive LALC serves as a prominent ventral boundary of

494 the MAL (Figure 9c). The MAL is relatively easy to identify by glomerular appearance of synapsin

495 staining (Figures 3, 4a,b and 6i). In contrast to the dorsally adjacent MLs, it exhibits a distinct pattern

496 with numerous tracheae and tracts passing through it, resulting in dense perforated synapsin

497 immunolabeling. In addition, the MAL shows strong GABA immunostaining (Figure 9c).

498   Another large midline-spanning neuropil of the INP is the IB covering the CB posteriorly

499 (Figure 9a,b). Its lateral boundaries are determined by the mALT and the medial equatorial fascicle

500 (MEF). Posterior-laterally, the IB is flanked by the ORs, which are defined as the entry neuropils of

501 the ocellar nerves (OCNs), and the PS, distinguished by weaker synapsin immunolabeling (Figures 4a

502 and 5a-c). The OR extends from the OCN posteriorly and curves medially to the posterior bend of the

503 PB (Figure 5c). The anterior surface of the IB is attached to the MAL (Figure 4b,c), and the dorso-

504 anterior side is covered by the ATL that spreads over the entire surface of the IB (Figure 9a,b).

505 Further posteriorly, the fiber system space below the PB serves as the dorsal boundary of the IB

506 (Figure 5b). Ventrally, the IB is mainly framed by the GC (Figure 5a-c) and, more anteriorly, by

507 another large undefined commissure and the VES (Figure 4c).

508   As mentioned above, the ATL extends along the dorsal surface of the IB and is, thus, the third

509 midline-spanning neuropil of the INP. It is positioned ventro-posteriorly to the CB (Figure 4c). The ATL

510 extends from the midline into both hemispheres and has a club-like shape (Figure 5a). It is dorsally

511 framed by the mALT and ventrally by the ICL and MEF (Figure 5a). The posterior part of the ATL is

512 superseded by the PS and IB (Figure 5a,b).

513   The most inferior region of the hemispheres is occupied by the clamp (CL). Similar to the

514 locust and cockroach (von Hadeln et al., 2018; Althaus et al., 2022), the ascending PED serves as a

515 boundary between the two subdivisions of the CL (Figure 3), the SCL and ICL (Figure 9b). The latter is

516 positioned anterior to the PS, separated from it by the LEF (Figure 5a,b). Posterior medial boundaries

517 are defined by the MEF, while the anterior medial boundaries are formed by the IB, ATL, and the

518 fiber system around the CX. Laterally, the ascending PED limits the ICL, and its ventral borders are

519 marked by the ULAL, EPA, gorget (GOR), GC, and PVLP/PLP (Figures 4 and 5a). The area located

520 anteriorly to the PED and laterally to the VL is defined as the SCL (Figures 2, 3 and 4a,b). The SCL lies

521 anteriorly between the CRE, the SIP, and the AVLP. In the more posterior part, the SCL is encased by

522 the SIP/VL/SMP (dorsally), the CX/ICL/VL (medially), the SLP (laterally), and the PED and PVLP

523   (ventrally). GABA-immunolabeled fibers run through the SCL along the lateral face of the VL and

524   target the CRE (Figure 9c-e, blue arrowheads).

Ventromedial neuropils

525

526   The ventromedial neuropils (VMNP) are located posterior and inferior to the AL. This group of

527   neuropils in the ventromedial cerebrum includes the epaulette (EPA), gorget (GOR), vest (VES),

528   posterior slope (PS), and the posterior optic tubercle (POTU).

529   The POTU was identified by synapsin- and more clearly by TH immunolabeling at the

530   posterior surface of the mantis brain (Figure 9h). It lies posterior from the PS and is dorsally attached

531   to the posterior optic commissure (POC; Figures 5d and 9h). The EPA, GOR and VES comprise the

532   ventral complex (VX), with the VES being the largest in volume (Figure 9g). The VES (Figures 4, 5a-c

533   and 9g,i) extends along the esophageal passage posterior to the mALT. Its lateral boundaries are

534   defined by the IFS, LLAL, EPA, and WED. Ventrally, the boundary is formed by the AMMC, while the

535   dorso-anterior boundary is marked by the MAL and EPA. Its dorso-posterior limitation is set by the

536   GC (Figure 5a,b). The posterior surface of the VES is covered by the PS, and the WEDC serves as a

537   significant landmark for distinguishing PS and VES (Figure 5c).

538   The other VX-associated neuropils, the EPA and GOR are significantly smaller in size. The GOR

539   (Figures 4b and 9f,g,i) is attached dorsally to the VES and has been described in *D. melanogaster* as

540   an extension of the VES (Ito et al., 2014). In the mantis brain, it protrudes lateral to the mALT,

541   corresponding to the GOR in the cockroach (Althaus et al., 2022). It is characterized by its

542   conspicuous porous synapsin immunolabeling and the presence of surrounding tracts (Figures 4b and

543   9i). The GOR ascends toward the ICL and is laterally limited by the EPA. The EPA (Figures 4b and

544   9f,g,i) lies dorso-lateral from the VES. It lies anterior to the GC and posterior to the ULAL. The EPA

545   serves as a 'connection' between the VES and ICL, similar to its description in the fruit fly (Ito et al.,

546   2014).

547   In addition to the VX, the PS (Figures 5b-f and 9f,g) is also part of the VMNP. It occupies a

548   large volume and covers most parts of the posterior surface of the brain. The PS is located posterior

549   to the GC and may be further divided into a superior and inferior PS as described in the fruit fly,

550   where both are divided by the POC (Ito et al., 2014). However, in the mantis, no subdivisions of the

551   PS were recognized, so that it is considered as a single unit.

Antennal lobe, periesophageal neuropils

552

553   The antennal lobe (AL) occupies a position ventral from the LX and the VMNP and covers the

554   periesophageal neuropils (PENP) anteriorly (Figures 2 and 3). It consists of numerous olfactory

555   glomeruli that exhibit dense synapsin labeling. The glomeruli are largely arranged along the

556   periphery of the AL, while the center of the AL, the antennal lobe hub (ALH), consisting of fibers of

557   projection and local neurons, shows considerably lower levels of synapsin staining (Figure 2a).

558 Surrounded by extensive glial sheaths, the AL is clearly distinguishable from adjacent brain areas. The
559 PENP are located posterior to the AL and comprise the strongly interconnected AMMC subunits and
560 the glomerular lobe (GLO) and the more ventrally lying tritocerebrum (TC) that is positioned most
561 ventrally within the cerebral ganglia (Figure 10a).

562　　The AMMC is the most voluminous area of deutocerebral origin and is subdivided into four
563 units: the dorsal AMMC (DAMMC), the lateral AMMC (LAMMC), the medial AMMC (MAMMC), and
564 the ventral area of flagellar afferents (VFA). Originating in the AL, the mALT sets the anterior border
565 of the DAMMC that follows the AL posteriorly (Figures 3a,b and 10a). The VFA lies at its ventral
566 border, while the DAMMC adjoins the ULAL ventrally. The LAMMC (Figures 3, 4, 5a, and 10a,c',c'')
567 lies posterior-laterally from the DAMMC and is characterized by its hill-like bulge that protrudes
568 laterally toward the cell cortex. It is ventrally bound by the VFA, GLO, and TC and bordered dorsally
569 by the WED and LLAL. The LAMMC is surrounded by massive intersegmental fibers in medio-
570 posterior direction, and the majority of its medial parts are covered by the MAMMC. The third area
571 of the AMMC, the MAMMC, borders on a medial soma cluster along the esophageal foramen, lies
572 ventro-posterior to the DAMMC and touches the WED, LLAL and the VES medio-dorsally (Figures 3, 4,
573 5a, and 10a,c',c''). It is ventrally limited by the GLO and the TC, and its most posterior region is
574 surrounded by fibers of the circumesophageal connective. The last unit of the AMMC, the VFA
575 (Figures 2c, 3a,b, and 10c) adjoins the AL at its posterior face and is enclosed by the compartments of
576 the AMMC. It is located dorsally to the GLO. Its identification is based on backfills from the antennal
577 flagellum (Figure 10c). It receives innervation from flagellar afferents, clearly differentiating it from
578 surrounding areas. Mechanosensory afferents labeled by antennal backfills split into several tracts
579 and fascicles, corresponding to tracts T5 – T7 in the cricket (Staudacher and Schildberger, 2000).
580 Tract 5/6 terminates in the AMMC, previously called dorsal lobe, and splits into two strands, T6I and
581 T6II. T6I spreads into the MAMMC with two strings running into parts of the LAMMC (Figure 10c',
582 white arrowheads) and ventral parts of the DAMMC (Figure 10c''). In contrast, T6II runs more
583 ventrally with projections in the MAMMC (Figure 10c',c'') and further projects ventral into the
584 pharyngeal connectives. Tract T7 projects into the VFA (Figure 10c).

585　　The TC, the most ventral neuropil of the mantis brain (Figures 3, 4 and 10a,b), was clearly
586 discernible by synapsin immunostaining. A granular region appears ventrally to the AL, embedded in
587 the dorsal region of the TC and extends further posteriorly. This texture is characteristic for the GLO.
588 Identification of the GLO by synapsin immunolabeling in the mantis brain was challenging (Figures
589 3b,c and 4a,b). It is less distinctive than in the cockroach, where it is a prominent glomerular neuropil
590 (Althaus et al., 2022). Therefore, we confirmed its presence by backfills from the ipsilateral maxillary
591 palp. The GLO was strongly stained by backfilled maxillary afferents (Figure 10b), enabling clear
592 differentiation for the 3D-reconstruction.

593 **Tracts and commissures**

594 We identified and reconstructed 12 fiber tracts, fiber systems, and commissures (Figure 1) that serve

595 as landmarks in the mantis brain. They were determined based on the absence of synapsin labeling in

596 the whole mount preparation.

597   Among the most prominent tracts is the mALT (Figures 3 and 4), which originates from the AL

598 and runs dorsally between the AMMC and LLAL. It then continues medially between the LLAL and

599 VES/MAL. Along the lateral CX, the mALT extends dorsally and protrudes laterally along the dorsal

600 surface of the ATL. It bypasses the PED anteriorly, runs through the SLP and targets the LH from

601 dorsal direction. Another easily identifiable tract is the IT (Figure 3a,b), characterized by strong GABA

602 immunostaining (Figure 6g). The IT contains numerous neurons connecting the LX to the CX. These

603 include many GABA-labeled tangential neurons arborizing in the CBL, BU with somata in a cluster

604 near the AL (Homberg et al., 2018). The IT serves to differentiate the ULAL and LLAL, similar to the

605 LALC. Two tracts associated with the AOTU are the AOT and the TUBUT (Figures 2 and 3a,b). The AOT

606 connects the optic lobe with the AOTU. It runs along the anterior face of the SLP and SIP. Its

607 identification, along with the TUBUT, was essential for recognizing the AOTU. The TUBUT originates

608 between the lower and upper units of the AOTU (Figure 8g) and establishes connections with the BU.

609 It runs from the AOTU through the CRE, along the medial border of the SCL, to the BU and delineates

610 the boundary between the SCL and ULAL/BU (Figure 3a,b). The OCNs (Figures 4c and 5a-c) were easy

611 to identify, as they comprise the neurites of ocellar interneurons. These neurons enter the brain from

612 dorsal direction, bypass the PB posteriorly, and target the OR.

613   Two prominent fascicles that were identified in the mantis brain are the LEF and MEF, both

614 located in the posterior protocerebrum. The LEF (Figure 5a,b) emerges from the GC between the ICL

615 and VES and runs dorsally through the ICL, extending further posteriorly through the dorsal area of

616 the PS. The MEF (Figure 5a-c) is positioned more medially than the LEF. It extends from the posterior

617 tip of the PB ventrally towards the GC, forming the lateral boundary of the IB. Another dominant

618 tract is the MBDL (Figures 2c, 3 and 4a,b). It contains fibers of neurosecretory cells of the pars

619 intercerebralis, among others, and extends along the anterior midline of the brain. Ventral to the

620 MAL, it splits into two fiber bundles that continue their ventral course along the lateral sides of the

621 esophagus before many of its fibers enter the corpora cardiaca nerve. The MBDL marks the posterior

622 borders of the ABR and SMP.

623   In the fruit fly, two major fiber systems, the IFS and superior fiber system (SFS), were used for

624 identifying neuropil boundaries. In the mantis brain, we could only identify the IFS, as the SFS is not

625 as prominent as in the fruit fly or the Madeira cockroach. The IFS is a fiber system in the ventral brain

626 region, lying between the VES and WED limiting the LAL posteriorly (Figure 4a,b).

627   We identified four commissures that cross the midline of the mantis brain. These

628   commissures primarily connect bilateral neuropils of both brain hemispheres. Notably, the GC and

629   LALC stand out due to their large size. The LALC (Figures 3b,c and 4a,b) connects the right and left

630   LAL, and served as the boundary between the ULAL and LLAL, along with the IT. Moreover, the LALC

631   forms the ventral border of the MAL as it crosses the brain midline. The GC (Figures 4c and 5a-c)

632   connects both OLs with each other. It was used for the separation of the LH and PVLP, as well as PVLP

633   and PLP. It also defined the border between the ICL and the VES. While crossing the brain midline,

634   the GC also sets the ventral border of the IB. The posterior optic commissure (POC) runs along the

635   dorsoposterior brain surface, between the PS and the POTU (Figure 5d). It connects both optic lobes

636   with each other and contains TH-immunoreactive neurons that innervate the POTU (Figure 9h).

637   Lastly, we identified the WEDC (Figure 5b,c), which connects the two WEDs with each other. The

638   WEDC helped in determining the boundaries of the WED and partly served as the border between

639   the VES and PS.

640   **Anatomical organization of optic lobe neurons**

641   To demonstrate the usefulness of the atlas for the analysis of the location of neuronal arborizations

642   in the mantis brain, we registered seven intracellularly recorded neurons of the optic lobes into the

643   3D-atlas. The cells had been published in Rosner et al. (2019, 2020) and comprise four projection

644   neurons (TOpro1, TOpro2, TApro$_{prox}$1, TAOpro), two centrifugal neurons (TAcen and TMEcen), and a

645   commissural neuron (COcom) interconnecting both optic lobes. We list the ramification sites of these

646   neurons in Table 1. Additionally, we scrutinized the branching areas of the remaining types of neuron

647   published by Rosner at al. (2019 and 2020) and took into account the insights from this study about

648   neuropil locations within the central brain. We provide the updated information about the

649   ramification sites of these cells in Table 1 as well.

650   The TOpro1 and 2 neurons are tangential projection neurons with input in the outer lobes

651   (OLO) 1 and 2 of the LOX (Rosner et al., 2020). The soma of TOpro1 is located in the OL, specifically in

652   the dorsoanterior region near the stalk lobe (SLO). The cell body fiber runs ventrally through the

653   'tunnel' of the SLO and connects to the main neurite (Rosner et al., 2020). This main neurite enters

654   the brain through the GC and has widely spread beaded arborization in several neuropils in the

655   ipsilateral brain, including the PLP, PS, WED, EPA, and the dorsal region of the VES (Figure 11a-b'').

656   The innervation of the transition area from the PVLP to the PLP (Figure 11b'; small area above the

657   GC) is particularly noteworthy, as this area is also innervated by the TOpro2 and COcom neuron. The

658   axon of the TOpro2 runs along the ventral part of the GC and gives rise to beaded projections in the

659   PVLP and PLP of the ipsilateral hemisphere of the brain (Figure 11c-d), as well as in the transition

660   area from the PLP to the PVLP (Figure 11c).

661   The TApro$_{prox}$1 neuron ramifies in proximal parts of the ventral lobe of the anterior lobe of

662   the lobula complex (ALO-V; Rosner et al., 2020) and has axonal terminals in the ipsilateral

663   protocerebrum. The soma of the TApro$_{prox}$1 is located in the soma rind near the PVLP (Rosner et al.

664   2020; Figure 12b''). From the OL, the main neurite runs anteriorly through to the AOT. It enters the

665   AVLP and gives off small, beaded processes in the anterior shell of the AVLP (Figure 12a,b'). The

666   neurite continues posteriorly, makes a ventral turn, and sends side branches into anterior parts of

667   the LLAL and small beaded branches into the anterior ULAL. Wide arborizations are finally

668   concentrated in the VES and WED (Figure 12a-b'). The TAOpro neuron is a tangential projection

669   neuron with dendrites in OLO1/2 and in the distal layer of the ALO and axonal terminals in the

670   ipsilateral protocerebrum. Its soma is located posterior to the SLO (Rosner et al., 2019; Figure 12c,d').

671   The main neurite runs from the OL through the GC into the central brain. The neuron shows sparse

672   ramifications in the PLP and PVLP, as well as in the transition area of the PLP and PVLP dorsal to the

673   GC (Figure 12d), like the TOpro1 and 2 neurons. The TAOpro neuron continues from the GC into the

674   IFS along the lateral side of the VES, with two fine branches that innervate the VES (Figure 12c,d).

675   The COcom neuron is a commissural neuron connecting the OLO1/2 of both optic lobes. Its

676   main neurite runs along the GC and has mirrored ramifications in both hemispheres of the central

677   brain, but differs in the optic lobes. The neuron has smooth ramification in the OL ipsilateral to the

678   soma (input) and beaded endings in the contralateral OL (output). The arborizations, from lateral to

679   medial, invade the transition area from the PLP to the PVLP (adjacent dorsally to the GC), the PLP,

680   the WED, and the VES with bleb-like endings (Figure 13a-b'). The TAcen neuron is a tangential

681   centrifugal neuron with broad ramifications in the distal parts of the ALO (Rosner et al., 2019; Figure

682   14 a,b). The soma of this neuron is located near the ventromedial edge of the AVLP. The cell body

683   fiber enters the protocerebrum posteriorly, runs along the dorsoanterior surface of the PLP, and then

684   continues in anteromedial direction. Sparse fine side branches are given off into the DAMMC and

685   MAMMC, while the main second neurite runs through the WED and sends a side branch posteriorly

686   into the PLP and PS (Figure 14a,b) before it continues dorsolateral to the PLP in the optic stalk. The

687   TMEcen neuron is a tangential centrifugal neuron with wide ramifications across the contralateral

688   medulla (ME; Rosner et al., 2019; Figure 14d). Its soma is located in the posterior soma rind of the

689   central brain. The neuron ramifies bilaterally in the central brain (Figure 14d'). Ipsilateral

690   ramifications are in the posterior lateral VES, from which the main neurite crosses the midline

691   posteriorly. It further exhibits contralateral processes in the PS, VES, WED, PLP, and a small branch

692   projecting into the GOR (Figure 13c,d').

693

694 **Discussion**

695 We have analyzed and reconstructed a total of 42 neuropils and 12 tracts and commissures of the

696 cerebrum of the mantis *H. membranacea*, in addition to the seven reconstructed neuropils of the

697 mantis OL presented by Rosner et al. (2017). This opens up new possibilities for detailed anatomical

698 analysis. Therefore, we integrated seven 3D-reconstructed neurons published in Rosner et al. (2019

699 and 2020) into the 3D-atlas, allowing for detailed identification of their arborization areas in the

700 central brain. This provides a basis for mapping neuronal connections in future anatomical and

701 physiological studies. We found prominent, strongly innervated neuropils, including the PLP, PVLP, as

702 well as the WED and VES targeted by the optic lobe neurons. The GC is strikingly prominent in the

703 mantis brain, potentially serving binocular computations. Brain areas, such as the ALI, ABR and MAL,

704 present in the mantis brain, seem to be unique in polyneopteran insects (cockroach *R. maderae* and

705 locust *S. gregaria*). However, a correspondence of the neck, identified in the locust and cockroach,

706 was not found in the mantis brain. The MB of the mantis appears relatively slim compared to the MB

707 of the cockroach and locust. Other chemosensory neuropils such as the GLO and AL are, likewise, less

708 prominent, while visual neuropils of the OL are large and partitioned in a highly complex manner in

709 the mantis brain. This is likely due to the mantis' strong reliance on visual input.

710 **Mushroom body**

711 The CAs vary in number and complexity across different insect species, and in aquatic species, may

712 be completely absent (Strausfeld et al., 2009). Our findings in the mantis support the previously

713 described fused double cup organization of the CA (Rosner et al., 2017) and unveil the presence of an

714 ICA and OCA within each CA. In addition, an ACAR encircling the PED neck of the MB is present. As

715 demonstrated in various insects, like the honey bee *A. mellifera*, the cockroach *P. americana*, and the

716 fly *D. melanogaster*, the MBs are strongly involved in learning, memory, and integration of

717 multisensory, in particular olfactory, inputs (Heisenberg, 1998; Mizunami et al. 1998; Nishino et al.,

718 2012; Modi et al., 2020; Li et al., 2020; Menzel, 2022). The MBs in the mantis have relatively slender

719 dimensions, in contrast to their counterparts in the cockroach (Althaus et al., 2022, Wei et al., 2010),

720 locust (Kurylas et al., 2008, von Hadeln et al., 2018), or the honey bee (Strausfeld, 2002). This

721 difference may be related to the ecology of mantises, which rely mainly on visual input, rather than

722 olfaction.

723 **Central complex, anterior lip and lateral complex**

724 The CX is a structure highly conserved across insect species. In the mantis, both divisions of the CB

725 are divided into ten vertical slices (5 per hemisphere). Their shape can be described as wedge-like,

726 similar to the teeth in the CBL of the cockroach *R. maderae* (Althaus et al., 2022; Jahn et al., 2023).

727 The outer slice of the CBL was previously described as half-sized (Rosner et al., 2017), which is

728   consistent with our observations. The CX is strongly involved in controlling spatial behavior and

729   processing of navigational information. It receives input from various sensory sources, including

730   various visual and antennal mechanosensory cues (Pfeiffer and Homberg, 2014; Honkanen et al.,

731   2019; Pfeiffer, 2022). Extracellular recordings in the freely moving Chinese mantis *Tenodera sinensis*

732   suggest that CX neurons are involved in prey detection and tracking (Wosnitza et al., 2022). The ALI,

733   covering the CB frontally, has been identified as a CX-associated neuropil in the cockroach (Althaus et

734   al., 2022, Jahn et al., 2023) locust (Vitzthum et al., 1996; Heinze & Homberg, 2008), and honey bee

735   (Hensgen et al., 2021b). In the polyneopteran species the ALI is large, it is considerably smaller in

736   bees and not present as a distinct neuropil in fruit flies (Ito et al., 2014).

737   The neuropils of the LX are closely linked with the CX and serve as an input and output site

738   for various information to and from the CX (Hensgen et al., 2021a; Hulse et al., 2021; Pfeiffer &

739   Homberg, 2014). In the mantis, the LX is largely unexplored, but we discovered input from optic lobe

740   neurons (TApro$_{prox}$1, TADpro; Table 1). In the fruit fly *D. melanogaster*, descending neurons convey

741   information from the LAL downstream to regions involved in motor control (Namiki et al., 2018a)

742   that may be similar in the mantis. The microglomerular organization of the BU of in the mantis is less

743   prominent than in the honey bee (Habenstein et al., 2023) or fruit fly (Ito et al., 2014), and it appears

744   to be undivided, as in the cockroach (Homberg et al., 2018; Althaus et al., 2022). In contrast, the BU

745   in the desert locust constitutes two spatially separated subunits, a medial and a lateral part (Träger

746   et al., 2008; Hensgen et al., 2021a). The BU houses arborizations of GABA-immunoreactive tangential

747   neurons of the CBL and is known to be part of the sky-compass pathway (*S. gregaria*: Homberg et al.,

748   2023; *D. plexippus*: Heinze & Reppert; 2011; Beetz & el Jundi, 2023; *A. mellifera*: Held et al., 2016; *D.*

749   *melanogaster*: Hardcastle et al., 2021)

750   The nearby GA is defined by the arborization area of CL columnar neurons of the CBL

751   (Hensgen et al., 2021a,b; Jahn et al., 2023). Although little is known about the neuronal organization

752   of the mantis CX, we identified a distinct area between the ULAL and LLAL as the GA based on its

753   identical position in the locust, cockroach, fruit fly, and honey bee (Ito et al., 2014; Hensgen et al.,

754   2021b; Jahn et al., 2023). Future investigations using single-cell tracer injections will be necessary to

755   confirm the identity of this region as the GA.

756   **Superior neuropils and lateral horn**

757   The LH, along with the MB, is a higher order neuropil involved in processing olfactory information

758   from the AL. The LH can be easily identified by GABA- and synapsin immunolabeling, as well as by

759   tracing the prominent mALT that projects into it. In the mantis, the LH lies at the same position as in

760   the Madeira cockroach (Althaus et al., 2022) and desert locust (von Hadeln et al., 2018) and is

761   dorsally encased by the SLP. However, unlike in the fruit fly (Ito et al., 2014), dung beetles (Immonen

762 et al., 2017), or the desert ants (Habenstein et al., 2020), the LH in the mantis is not laterally attached

763 to the SLP.

764   The superior lateral (SLP), superior intermediate (SIP), and superior medial protocerebrum

765 (SMP), forming the dorsal face of the brain, are distinguished in all available insect brain atlases.

766 These neuropils contain prominent arborization areas of neurosecretory cells of the pars

767 intercerebralis and lateralis (Reinhard et al., 2022). In mantises, the SMP is relatively large and fused

768 across the midline, similar to the SMP in dung beetles (Immonen et al., 2017), where it is directly

769 attached to the midline crossing ATL. This is in contrast to other polyneopteran insects where the

770 SMPs of both hemispheres are not fused and appear smaller (von Hadeln et al., 2018; Althaus et al.,

771 2022). An additional distinct neuropil, the ABR, was identified within the superior neuropils, which is

772 apparently exclusive to polyneopteran insects. The ABR spans the midline and covers the antero-

773 dorsal part of the SMP. It could be clearly distinguished by its fibrous structure observed in synapsin

774 immunolabeling. In other insects, it may have been considered as part of the SMP (Ito et al., 2014;

775 Habenstein et al., 2020 and 2023). The SIP, like the SMP and SLP, extends from the anterior to the

776 posterior surface of the brain. Its position and shape strongly correspond to those in other

777 polyneopteran insects, but it occupies more space than in the fruit fly (Ito et al., 2014). In the mantis,

778 the SIP does not completely surround the VL, but rather covers its dorsal surface and surrounds it

779 anteriorly. Tracing experiments conducted in fruit flies have revealed that olfactory information from

780 the LH may enter the SLP and SCL, possibly forming connections to the SIP and SMP (Yu et al., 2013).

781 In honey bees, the SIP (also known as the ring neuropil) is targeted by output neurons from the MB

782 (Abel et al., 2001; Rybak & Menzel, 1993).

783 **Ventrolateral neuropils**

784 The VLP in the mantis mirrors the shape and position observed in the cockroach and locust (Althaus

785 et al., 2022; von Hadeln et al., 2018) and is divided into an anterior and posterior region in all three

786 species. The PVLP has been described as a region with glomerular structure in flies and bumblebees

787 (Ito et al., 2014; Paulk et al., 2009), and we have, likewise, identified a glomerular organization in the

788 mantis brain (Figure 8h). In *D. melanogaster* the WED and PVLP serve as secondary auditory

789 neuropils connected by interneurons to auditory afferents from Johnston's organ that terminate in

790 the AMMC (Matsuo et al., 2016; Patella & Wilson, 2018). Direct input from Johnston's organ to the

791 VLP was also found in ants (Grob et al., 2021). In desert locusts, the PLP and PVLP receive massive

792 input from ascending neurons providing auditory and cercal wind-sensory input (Staudacher et al.,

793 2023). The glomerular organization of the PVLP and PLP in *D. melanogaster* is largely based on a

794 visual feature map provided by parallel projections of lobula columnar neurons signaling various

795 aspects of moving objects (Aptekar et al., 2015; Wu et al., 2016; Klapoetke et al., 2022). As shown in

796 the fruit fly and silk moth, some of these sensory inputs likely converge onto specific descending

797   neurons (Namiki et al., 2018a and b). In the mantis, the VLP and WED, likewise, receive prominent

798   input from visual interneurons (Table 1). Consequently, the VLNP in the mantis might function as a

799   premotor center, processing visual data and facilitating swift, accurate responses to visual stimuli.

800   The anterior ventrolateral area of the mantis brain houses the AOTU, which consists of a

801   larger UU and a smaller LU separated by the TUBUT. The separation of the AOTU into UU and LU

802   appears to be consistent across various insect species, while the number of subunits of the LU

803   appears to be more variable (Mota et al., 2011; Immonen et al., 2017; Heinze and Reppert, 2012;

804   Adden et al., 2020; Hardcastle et al., 2021; Homberg et al., 2003). The LU of the AOTU is involved in

805   the processing of celestial cues, including the sun's position and the polarization pattern of the sky

806   (Hardcastle et al., 2021; Homberg et al., 2023), while the UU receives LOX input from neurons

807   involved in object detection (Collett, 1972; Aptekar et al., 2015; Ribeiro et al., 2018). This information

808   is transmitted through the TUBUT, via the BU, and a parallel fiber bundle via the LAL to the CX, where

809   further processing related to goal-directed navigation takes place (Homberg et al., 2003; Heinze,

810   2017; Hardcastle et al., 2021; Homberg et al., 2023). While central neural substrates such as the

811   AOTU, TUBUT and its connection to the CX are present in the mantis, their involvement in sky

812   compass orientation or other functions still needs to be established.

813   **Inferior neuropils**

814   The large group of INP includes the CRE. In the fruit fly, the CRE surrounds the shaft of the ML, which

815   has not been observed in the mantis, locust (von Hadeln et al., 2018), and cockroach (Althaus et al.,

816   2022). GABA-immunolabeled fibers from the CRE target the CA (Yamazaki et al., 1998; Strausfeld &

817   Li, 1999), and have also served in the cockroach brain for identification of the CRE (Althaus et al.,

818   2022). In the fruit fly (Ito et al., 2014) and cockroach (Althaus et al., 2022), a small spherical neuropil

819   is part of the CRE, called the rubus (RUB). While we were unable to distinguish the RUB by synapsin

820   labeling in the mantis, it may be identified by tracer injections into columnar neurons of the CBU,

821   whose arborizations outside the CX are confined to the RUB (Ito et al., 2014; Hulse et al., 2021; Jahn

822   et al., 2023). The remaining parts of the CRE are connected to the LAL as examined in the locust

823   (Hensgen et al., 2021a) and the fruit fly (Hulse et al., 2021). In the fruit fly, the CRE is also innervated

824   by output neurons of the MB (Li et al., 2020), although little is known about the physiology of these

825   neurons.

826   The SCL and ICL in the mantis stretch from the CB to the lateral SLP. In the fruit fly, the clamp

827   is divided into SLC and ILC by the superior arch- and ellipsoid commissures (Ito et al., 2014). Because

828   we did not observe corresponding landmarks in the mantis, we referred to the 3D atlases of the

829   locust (von Hadeln et al., 2018) and the cockroach brain (Althaus et al., 2022), where the clamp was

830   subdivided with the help of the arising PED. Medially adjacent to the ICL, the IB crosses the posterior

831   brain midline. The IB has been identified in the brains of the locust, cockroach, dung beetle, ant,

832   honey bee and fly, but not in *T. castaneum* (Farnworth et al., 2022), *C. obscurior* (Bressan et al.,

833   2015), *A. infusa* (Adden et al., 2020), and *D. plexippus* (Heinze & Reppert, 2012). The IB in the mantis

834   was, as in the locust and cockroach, discernible due to strong synapsin staining and the lateral

835   adjoining fascicles (MEF and LEF).

836   The ATL in the mantis differs in its shape from that of other insect species. It is fused at the

837   midline and elongated along the dorsal surface of the IB. This suggests that, similar to the findings in

838   *D. melanogaster* (Ito et al., 2014), the ATL may be part of the IB. This is consistent with our results, as

839   the ATL was difficult to differentiate from the IB and shows elongation along its dorsal surface. In

840   contrast, the OR was much easier to identify by tracing the course of the OCN. In *H. membranacea*,

841   the number of ocelli corresponds to the number of the ORs in the brain, with one ocellus per

842   hemisphere. The ORs serve as the input station of visual input from the ocelli. Their position is similar

843   to those in the locust (von Hadeln et al., 2018) and cockroach (Althaus et al., 2022). The mantis brain

844   features a quite prominent MAL, which has not been described in holometabolous insects but is

845   easily distinguishable in polyneopteran insects. In the mantis, the MAL is fused across the midline, as

846   in the locust (von Hadeln et al., 2018), but different from the more closely related Madeira cockroach

847   where it does not span the midline (Althaus et al., 2022).

848   **Ventromedial neuropils**

849   The functional role of the ventromedial neuropils is not well understood. The POTU is involved in the

850   processing of celestial cues and is connected to the PB via tangential neurons. In the cockroach *R.*

851   *maderae*, the POTU is also associated with the circadian system and is strongly labeled by antisera

852   against pigment-dispersing factor (Stengl & Homberg, 1994). In the mantis, we specified the POTU by

853   tyrosine hydroxylase labeling, along with the identification of the POC that projects to the POTU and

854   connects both OLs. In *D. melanogaster*, the PS is subdivided into a superior and an inferior region

855   separated by the POC (Ito et al., 2014). In the mantis a subdivision was, like in the cockroach, dung

856   beetles, and locust (von Hadeln et al., 2018; Immonen et al., 2017; Althaus et al., 2022) not obvious.

857   The PS is a major target of motion-sensitive projection neurons from the ME and LOX signaling ego

858   motion (Strausfeld, 1976; Strausfeld & Bassemir, 1985a and b; Paulk et al., 2008 and 2009; Suver et

859   al., 2016; Namiki, 2018a; Ryu et al., 2022), and is innervated by numerous descending and ascending

860   neurons (Strausfeld, 1976; Staudacher, 1998; Okada et al., 2003; Staudacher et al., 2023; Ryu et al.

861   2022). In addition, the PS receives input from numerous brain areas including the LAL, as reported in

862   the silk moth *Bombyx mori*, where these neurons seem to be involved in motor control for

863   pheromone processing (Namiki et al., 2018b). Neurons connecting the LAL and PS in the desert locust

864   may play a role in spatial orientation (Heinze & Homberg, 2009). As shown in Table 1 seven out of 15

865   characterized visual interneurons of the OL of the mantis arborize in the PS. Five out of these are

866   projection neurons from the LOX that may target descending neurons in the PS for initiating

867   orientation responses. The presence of branches within the LAL in one of these neurons (Table 1,

868   TADpro), shows parallel processing of visual input in the PS and LAL.

869   The VX comprises the EPA, GOR and VES, with the VES being the largest region. This

870   organization aligns with findings from *D. melanogaster* (Ito et al., 2014), *S. gregaria* (von Hadeln et

871   al., 2018), and *R. maderae* (Althaus et al., 2022). In the monarch butterfly, the VX is reconstructed as

872   a single structure within the ventromedial anterior neuropil (Heinze & Reppert, 2012), while in ants,

873   it is considered part of the ventromedial protocerebrum (Bressan et al., 2015). Major landmarks for

874   identifying the VES in the mantis are the IFS and GC, as also reported in other established brain

875   atlases. The EPA and GOR are dorsally attached to the VES and have similar positions in the fruit fly

876   (Ito et al., 2014). In the mantis, the GOR was difficult to distinguish and could only be identified by its

877   shape and position, similar to data in the fruit fly (Ito et al., 2014) and in the cockroach (Althaus et al.,

878   2022).

879   **Periesophageal neuropils, tritocerebrum and the antennal lobe**

880   Many insects rely on olfactory stimuli for various behaviors, such as foraging or searching for sexual

881   partners. Despite the relatively small size of their antennae, studies have shown that praying

882   mantises are responsive to olfactory cues (Allen et al., 2012; Carle et al., 2014). Male mantises can

883   recognize a female's willingness to mate based on sex pheromones released by the females (Lelito

884   and Brown, 2008). The primary olfactory center of insects is the glomerular AL (Hansson and Anton,

885   2000). In *H. membranacea*, the AL has relatively large glomeruli, similar to those in the cockroach *R.*

886   *maderae*, although in a smaller number, probably due to the mantis' strong reliance on visual input.

887   In the Chinese mantis *Tenodera aridifolia* 54 glomeruli were identified in the AL (Carle et al., 2017),

888   while the number of glomeruli in *H. membranacea* was not analyzed in our study. The glomeruli are

889   connected through different AL tracts to higher brain areas for further processing of olfactory cues.

890   We identified one of these tracts, the mALT, which contains a large number of projection neurons

891   targeting the CA of the mushroom body and LH.

892   The VFA is closely linked to the antennae and can be reliably identified by backfills of the

893   antennal flagellum, as it receives massive innervation by flagellar afferents (Staudacher &

894   Schildberger, 2000; Staudacher et al., 2005). In contrast, differentiating the mantis VFA solely by

895   synapsin staining was difficult, unlike in the cockroach or locust, where the VFA is a synapsin-rich

896   area between the AL and GLO (von Hadeln et al., 2018; Althaus et al., 2022). The mantis VFA is

897   relatively small compared to the VFA of the cricket or cockroach, which may relate to differences in

898   lifestyle and the less prominent organization of the mantis antennae. The VFA has not been

899   recognized in holometabolous insects studied thus far. It is part of the AMMC, which also includes

900   the DAMMC, LAMMC and MAMMC. In fruit flies, these regions likely correspond to the saddle, which

901   contains the fly AMMC. The organization of the mantis AMMC into a dorsal, medial, and lateral

902   region follows the corresponding organization in the locust (von Hadeln et al., 2018). The

903   subdivisions were established by considering their spatial arrangement in the brain and were aided

904   by antennal backfills.

905   The GLO, a termination site for maxillary palp afferents in polyneopteran insects (Ignell et al.,

906   2000), was also identified in a holometabolous insect, the beetle *Tribolium castaneum* (Dippel et al.,

907   2016). It was proposed that the GLO is involved in odor processing by olfactory neurons of the

908   mouthparts, without involvement of the ALs (Dippel et al., 2016). In the migratory locust *Locusta*

909   *migratoria*, the GLO is involved in odor-induced vomiting (Sun et al., 2022). In the cockroach *R.*

910   *maderae*, the GLO is a highly glomerular neuropil and is easily identified using synapsin

911   immunolabeling (Althaus et al., 2022). However, in the mantis, the GLO is less prominent and was

912   only established by backfills of the maxillary palps. The GLO is assumed to be of tritocerebral origin,

913   because the TC is, among other neuronal connections, innervated by nerves from the mouthparts

914   and the stomatogastric system (Aubele & Klemm, 1977; Rajashekhar & Singh, 1994; Farris, 2008). The

915   mantis TC, located as the most ventral area of the central brain, appears to be undivided as in other

916   polyneopteran insects (von Hadeln et al., 2018; Althaus et al., 2022). Owing to fusion of the gnathal

917   and cerebral ganglia in holometabolous insects, its correspondence with neuropils like the prow and

918   saddle in the fruit fly (Ito et al., 2014) is difficult and has not been investigated.

919   **Insights from ramification sites of optic lobe neurons**

920   We registered 7 neurons published previously (Rosner et al., 2019, 2020) into the mantis brain atlas

921   (Figures 11-14) and, in addition, provide detailed information about ramification sites of additional

922   neurons not registered here (Table 1). Rosner et al. (2017, 2019, 2020) suggested corresponding

923   substructures in the LOX in mantises and flies. The data presented here support these claims. The fly

924   LOX comprises two nested neuropils, the lobula plate and the lobula. Widefield motion is processed

925   in a directionally selective manner in the lobula plate while in the lobula several types of projection

926   neurons respond to motion of small, dark targets (Klapoetke et al., 2022; Ryu et al., 2022). In the

927   mantis widefield motion is processed in a directionally selective manner by neurons ramifying in

928   distal layers of the ALO (TADpro, TApro$_{dist}$1, TAcen in Rosner et al., 2019, 2020; TAproM1 and

929   TAproM2 in Yamawaki, 2019) and, additionally, by neurons with input exclusively in the DLO of the

930   LOX (Yamawaki, 2019). Thus, these neurons share physiological properties with lobula plate

931   tangential cells in flies. Lobula plate tangential cells have central brain ramifications in the PS and PLP

932   but not in the VLP (Ito et al., 2014; Namiki et al., 2018b; Ryu et al., 2022). As shown here this also

933   holds for the investigated widefield sensitive cells in the mantis (TADpro, TApro$_{dist}$1, TAcen).

934   All other LOX neurons presented in Table 1 ramify in the VLP (AVLP or PVLP). In the fly VLP

935   ramifications are indicative of lobula neurons (Ito et al., 2014; Otsuna & Ito, 2006). Mantis neurons

936   that have LOX ramifications exclusively in the OLO or the SLO respond strongly to motion of small

937   dark, prey-like objects (TOproM/TOpro1, TOproL, COcom, Scom, Yamawaki, 2019; Rosner et al.,

938   2020). The physiological features of the OLO and SLO in conjunction with the VLP ramifications of

939   neurons originating in OLO and SLO (TOpro1, TOpro2, COcom, TOpro3, Spro in Table 1) support

940   previous claims that the OLO, perhaps together with the SLO, corresponds to the fly lobula.

941   Two tangential projection neurons (TApro$_{prox}$1, TADpro) provide input to the LAL. TApro$_{prox}$1

942   responds to dark flashing bars (Rosner et al., 2020) while the TADpro/TAproM2 neuron responds

943   best to bright flashing bars and moving gratings, i.e. widefield motion (Rosner et al., 2020; Yamawaki,

944   2019). The LALs are sensory motor relay neuropils that are highly linked with the CX. In bees the CX is

945   suspected to harbor neurons that determine traveled distances by integrating optic flow (Stone et

946   al., 2017). Widefield motion-sensitive neurons in the CX suggested to play a role in distance

947   perception receive input in the LALs (Stone et al., 2017). Thus, homologs of the mantis TADpro

948   neuron in bees could link the optic lobe with the CX and provide signals for travel distance estimation

949   in path integration.

950   The praying mantis is a formidable predator of the insect world with a highly specialized

951   visual system attuned to detecting and hunting prey. The identification and 3D mapping of neuropils

952   and fiber tracts in the mantis brain is an important step toward linking behavioral data to activities in

953   particular brain areas. The mantis brain atlas has been enriched by registering specific neurons

954   previously studied, offering a more detailed understanding of the brain's structure and function. The

955   data underscore potential homologies between the mantis and other insects, particularly in the LOX

956   region. Distinct pathways in the LOX allow the mantis to detect both small moving objects and

957   widefield motion, a feature also observed in flies. The integration of these neurons into the atlas not

958   only provides insights into the unique visual system of the mantis, but also emphasizes the atlas as a

959   tool for analyzing neural networks involved in visual perception and behavior

960

961   **References**
962   Abel, R., Rybak, J., & Menzel, R. (2001). Structure and response patterns of olfactory interneurons in
963   the honeybee, *Apis mellifera. Journal of Comparative Neurology, 437,* 363–383.
964   https://doi.org/10.1002/cne.1289
965   Adden, A., Wibrand, S., Pfeiffer, K., Warrant, E., & Heinze, S. (2020). The brain of a nocturnal
966   migratory insect, the Australian Bogong moth. *Journal of Comparative Neurology, 528,* 1942–
967   1963. https://doi.org/10.1002/cne.24866
968   Allen, L. E., Barry, K. L., & Holwell, G. I. (2012). Mate location and antennal morphology in the praying
969   mantid *Hierodula majuscula. Australian Journal of Entomology, 51,* 133–140.
970   https://doi.org/10.1111/j.1440-6055.2011.00843.x
971   Althaus, V., Jahn, S., Massah, A., Stengl, M., & Homberg, U. (2022). 3D-atlas of the brain of the
972   cockroach *Rhyparobia maderae. Journal of Comparative Neurology, 530,* 3126–3156.
973   https://doi.org/10.1002/cne.25396

974   Aptekar, J. W., Keleş, M. F., Lu, P. M., Zolotova, N. M., & Frye, M. A. (2015). Neurons forming optic
975   glomeruli compute figure–ground discriminations in *Drosophila*. *Journal of Neuroscience, 35*,
976   7587–7599. https://doi.org/10.1523/JNEUROSCI.0652-15.2015
977   Aubele, E., & Klemm, N. (1977). Origin, destination and mapping of tritocerebral neurons of locust.
978   *Cell and Tissue Research, 178*, 199–219. https://doi.org/10.1007/BF00219048
979   Avarguès-Weber, A., Deisig, N., & Giurfa, M. (2011). Visual cognition in social insects. *Annual Review*
980   *of Entomology, 56*, 423–443. https://doi.org/10.1146/annurev-ento-120709-144855
981   Beetz, M. J., & el Jundi, B. (2023). The neurobiology of the Monarch butterfly compass. *Current*
982   *Opinion in Insect Science*, 101109. https://doi.org/10.1016/j.cois.2023.101109
983   Bressan, J. M. A., Benz, M., Oettler, J., Heinze, J., Hartenstein, V., & Sprecher, S. G. (2015). A map of
984   brain neuropils and fiber systems in the ant *Cardiocondyla obscurior*. *Frontiers in Neuroanatomy,*
985   *8*, 166. https://doi.org/10.3389/fnana.2014.00166
986   Calvo, A. C., Pey, A. L., Miranda-Vizuete, A., Døskeland, A. P., & Martinez, A. (2011). Divergence in
987   enzyme regulation between *Caenorhabditis elegans* and human tyrosine hydroxylase, the key
988   enzyme in the synthesis of dopamine. *Biochemical Journal, 434,* 133–141.
989   https://doi.org/10.1042/BJ20101561
990   Carle, T., Toh, Y., Yamawaki, Y., Watanabe, H., & Yokohari, F. (2014). The antennal sensilla of the
991   praying mantis *Tenodera aridifolia*: A new flagellar partition based on the antennal macro-,
992   micro- and ultrastructures. *Arthropod Structure & Development, 43*, 103–116.
993   https://doi.org/10.1016/j.asd.2013.10.005
994   Carle, T., Watanabe, H., Yamawaki, Y., & Yokohari, F. (2017). Organization of the antennal lobes in
995   the praying mantis (*Tenodera aridifolia*). *Journal of Comparative Neurology, 525*, 1685–1706.
996   https://doi.org/10.1002/cne.24159
997   Collett, T. (1972). Visual neurones in the anterior optic tract of the privet hawk moth. *Journal of*
998   *Comparative Physiology*, *78*, 396–433. https://doi.org/10.1007/BF01417943
999   Dippel, S., Kollmann, M., Oberhofer, G., Montino, A., Knoll, C., Krala, M., Rexer, K.-H., Frank, S.,
1000   Kumpf, R., Schachtner, J., & Wimmer, E. A. (2016). Morphological and transcriptomic analysis of a
1001   beetle chemosensory system reveals a gnathal olfactory center. *BMC Biology, 14*, 1–31.
1002   https://doi.org/10.1186/s12915-016-0304-z
1003   el Jundi, B., Warrant, E. J., Pfeiffer, K., & Dacke, M. (2018). Neuroarchitecture of the dung beetle
1004   central complex. *Journal of Comparative Neurology*, *526*, 2612–2630.
1005   https://doi.org/10.1002/cne.24520
1006   Fahrbach, S. E. (2006). Structure of the mushroom bodies of the insect brain. *Annual Review of*
1007   *Entomology, 51*, 209–232. https://doi.org/10.1146/annurev.ento.51.110104.150954
1008   Farnworth, M. S., Bucher, G., & Hartenstein, V. (2022). An atlas of the developing *Tribolium*
1009   *castaneum* brain reveals conservation in anatomy and divergence in timing to *Drosophila*
1010   *melanogaster*. *Journal of Comparative Neurology, 530,* 2335–2371.
1011   https://doi.org/10.1002/cne.25335
1012   Farris, S. M. (2008). Tritocerebral tract input to the insect mushroom bodies. *Arthropod Structure &*
1013   *Development, 37*, 492–503. https://doi.org/10.1016/j.asd.2008.05.005
1014   Giurfa, M. (2021). Learning of sameness/difference relationships by honey bees: performance,
1015   strategies and ecological context. *Current Opinion in Behavioral Sciences, 37*, 1–6.
1016   https://doi.org/10.1016/j.cobeha.2020.05.008
1017   Gonzalez-Bellido, P. T., Fabian, S. T., & Nordström, K. (2016). Target detection in insects: optical,
1018   neural and behavioral optimizations. *Current Opinion in Neurobiology*, *41*, 122–128.
1019   https://doi.org/10.1016/j.conb.2016.09.001
1020   Grob, R., Tritscher, C., Grübel, K., Stigloher, C., Groh, C., Fleischmann, P. N., & Rössler, W. (2021).
1021   Johnston's organ and its central projections in *Cataglyphis* desert ants. *Journal of Comparative*
1022   *Neurology*, *529*, 2138–2155. https://doi.org/10.1002/cne.25077
1023   Habenstein, J., Amini, E., Grübel, K., el Jundi, B., & Rössler, W. (2020). The brain of *Cataglyphis* ants:
1024   Neuronal organization and visual projections. *Journal of Comparative Neurology, 528*, 3479–
1025   3506. https://doi.org/10.1002/cne.24934

Habenstein, J., Grübel, K., Pfeiffer, K., & Rössler, W. (2023). 3D atlas of cerebral neuropils with previously unknown demarcations in the honey bee brain. *Journal of Comparative Neurology, 531,* 1163–1183. https://doi.org/10.1002/cne.25486

Hamanaka, Y., Minoura, R., Nishino, H., Miura, T., & Mizunami, M. (2016). Dopamine- and tyrosine hydroxylase-immunoreactive neurons in the brain of the American cockroach, *Periplaneta americana. PLoS One, 11,* e0160531. https://doi.org/10.1371/journal.pone.0160531

Hansson, B. S., & Anton, S. (2000). Function and morphology of the antennal lobe: new developments. *Annual Review of Entomology, 45,* 203–231. https://doi.org/10.1146/annurev.ento.45.1.203

Hardcastle, B. J., Omoto, J. J., Kandimalla, P., Nguyen, B.-C. M., Keleş, M. F., Boyd, N. K., Hartenstein, V., & Frye, M. A. (2021). A visual pathway for skylight polarization processing in *Drosophila. eLife 10*, e63225. https://doi.org/10.7554/eLife.63225

Heinze, S. (2017). Unraveling the neural basis of insect navigation. *Current Opinion in Insect Science*, 24, 58–67. https://doi.org/10.1016/j.cois.2017.09.001

Heinze, S., & Homberg, U. (2008). Neuroarchitecture of the central complex of the desert locust: Intrinsic and columnar neurons. *Journal of Comparative Neurology, 511*, 454–478. https://doi.org/10.1002/cne.21842

Heinze, S., & Homberg, U. (2009). Linking the input to the output: new sets of neurons complement the polarization vision network in the locust central complex. *Journal of Neuroscience, 29*, 4911–4921. https://doi.org/10.1523/JNEUROSCI.0332-09.2009

Heinze, S., Narendra, A., & Cheung, A. (2018). Principles of insect path integration. *Current Biology, 28*, R1043–R1058. https://doi.org/10.1016/j.cub.2018.04.058

Heinze, S., & Reppert, S. M. (2011). Sun compass integration of skylight cues in migratory monarch butterflies. *Neuron 69*, 345–358. http://dx.doi.org/10.1016/j.neuron.2010.12.025

Heinze, S., & Reppert, S. M. (2012). Anatomical basis of sun compass navigation I: the general layout of the monarch butterfly brain. *Journal of Comparative Neurology, 520*, 1599–1628. https://doi.org/10.1002/cne.23054

Heisenberg, M. (1998). What do the mushroom bodies do for the insect brain? An introduction. *Learning & Memory, 5*, 1–10. https://doi.org/10.1101/lm.5.1.1

Held, M., Berz, A., Hensgen, R., Muenz, T. S., Scholl, C., Rössler, W., Homberg, U., & Pfeiffer, K. (2016). Microglomerular synaptic complexes in the sky-compass network of the honeybee connect parallel pathways from the anterior optic tubercle to the central complex. *Frontiers in Behavioral Neuroscience*, 10, 186. https://doi.org/10.3389/fnbeh.2016.00186

Hensgen, R., Göthe, J., Jahn, S., Hümmert, S., Schneider, K. L., Takahashi, N., Pegel, U., Gotthardt, S., & Homberg, U. (2021a). Organization and neural connections of the lateral complex in the brain of the desert locust. *Journal of Comparative Neurology, 529*, 3533–3560. https://doi.org/10.1002/cne.25209

Hensgen, R., England, L., Homberg, U., & Pfeiffer, K. (2021b). Neuroarchitecture of the central complex in the brain of the honeybee. Neuronal cell types. *Journal of Comparative Neurology, 529* (1), 159–186. https://doi.org/10.1002/cne.24941

Homberg, U., Hensgen, R., Jahn, S., Pegel, U., Takahashi, N., Zittrell, F., & Pfeiffer, K. (2023). The sky compass network in the brain of the desert locust. *Journal of Comparative Physiology A 209*, 641–662. https://doi.org/10.1007/s00359-022-01601-x

Homberg, U., Hofer, S., Pfeiffer, K., & Gebhardt, S. (2003). Organization and neural connections of the anterior optic tubercle in the brain of the desert locust. *Journal of Comparative Neurology, 462*, 415–430. https://doi.org/10.1002/cne.10771

Homberg, U., Humberg, T.-H., Seyfarth, J., Bode, K., & Quintero Pérez, M. (2018). GABA immunostaining in the central complex of dicondylian insects. *Journal of Comparative Neurology, 526*, 2301–2318. https://doi.org/10.1002/cne.24497

Homberg, U., Kirchner, M., Kowalewski, K., Pitz, V., Kinoshita, M., Kern, M., & Seyfarth, J. (2023). Comparative morphology of serotonin-immunoreactive neurons innervating the central complex

1077   in the brain of dicondylian insects. *Journal of Comparative Neurology*.
1078   https://doi.org/10.1002/cne.25529
1079   Honkanen, A., Adden, A., da Silvas Freitas, J., & Heinze, S. (2019). The insect central complex and the
1080   neural basis of navigational strategies. *Journal of Experimental Biology, 222* (Pt Suppl 1),
1081   jeb188854. https://doi.org/10.1242/jeb.188854
1082   Hoskins, S. G., Homberg, U., Kingan, T. G., Christensen, T. A., & Hildebrand, J. G. (1986).
1083   Immunocytochemistry of GABA in the antennal lobes of the sphinx moth *Manduca sexta*. *Cell and
1084   Tissue Research, 244*, 243–252. https://doi.org/10.1007/BF00219199
1085   Hulse, B. K., Haberkern, H., Franconville, R., Turner-Evans, D. B., Takemura, S. Y., Wolff, T., Noorman,
1086   M., Dreher, M., Dan, C., Parekh, R., Hermundstad, A. M., Rubin, G. M., & Jayaraman, V. (2021). A
1087   connectome of the *Drosophila* central complex reveals network motifs suitable for flexible
1088   navigation and context-dependent action selection. *Elife*, *10*, e66039.
1089   https://doi.org/10.7554/eLife.66039
1090   Hurd, L. E. (1999) Ecology of praying mantises. In: Prete, F. R., Wells, H., Wells, P. H., & Hurd, L. E.
1091   (Eds), *The Praying Mantids* (pp. 43–60). John Hopkins University Press, Baltimore.
1092   Ignell, R., Anton, S., & Hansson, B. S. (2000). The maxillary palp sensory pathway of
1093   Orthoptera. *Arthropod Structure & Development*, *29*, 295–305. https://doi.org/10.1016/S1467-
1094   8039(01)00016-0
1095   Immonen, E. V., Dacke, M., Heinze, S., & el Jundi, B. (2017). Anatomical organization of the brain of a
1096   diurnal and a nocturnal dung beetle. *Journal of Comparative Neurology, 525*, 1879–1908.
1097   https://doi.org/10.1002/cne.24169
1098   Ito, K., Shinomiya, K., Ito, M., Armstrong, J. D., Boyan, G., Hartenstein, V., Harzsch, S., Heisenberg, M.,
1099   Homberg, U., Jenett, A., Keshishian, H., Restifo, L. L., Rössler, W., Simpson, J. H., Strausfeld, N. J.,
1100   Strauss, R., & Vosshall, L. B. (2014). A systematic nomenclature for the insect brain. *Neuron, 81*,
1101   755–765. https://doi.org/10.1016/j.neuron.2013.12.017
1102   Jahn, S., Althaus, V., Heckmann, J., Janning, M., Seip, A.-K., Takahashi, N., Grigoriev, C., Kolano, J., &
1103   Homberg, U. (2023). Neuroarchitecture of the central complex in the Madeira cockroach
1104   *Rhyparobia maderae*: Pontine and columnar neuronal cell types. Journal of Comparative
1105   Neurology, *531*, 1689–1714. https://doi.org/10.1002/cne.25535
1106   Kinoshita, M., & Homberg, U. (2017). Insect brains: minute structures controlling complex behaviors.
1107   In: Shigeno, S., Murakami, Y., Nomura, T. (Eds.), *Brain Evolution by Design. Diversity and
1108   Commonality in Animals* (pp. 123–151). Springer, Tokyo. https://doi.org/10.1007/978-4-431-
1109   56469-0_6
1110   Klagges, B. R. E., Heimbeck, G., Godenschwege, T. A., Hofbauer, A., Pflugfelder, G. O., Reifegerste, R.,
1111   Reisch, D., Schaupp, M., Buchner, S., & Buchner, E. (1996). Invertebrate synapsins: a single gene
1112   codes for several isoforms in *Drosophila*. *Journal of Neuroscience, 16*, 3154–3165.
1113   https://doi.org/10.1523/JNEUROSCI.16-10-03154.1996
1114   Klapoetke, N. C., Nern, A., Rogers, E. M., Rubin, G. M., Reiser, M. B., & Card, G. M. (2022). A
1115   functionally ordered visual feature map in the *Drosophila* brain. *Neuron*, *110*, 1700–1711.
1116   https://doi.org/10.1016/j.neuron.2022.02.013
1117   Kral, K., & Prete, F. R. (1999). In the mind of a hunter: The visual world of the praying mantis. In:
1118   Prete, F. R. (Ed.). *Complex worlds from simpler nervous systems* (pp. 75–116). MIT Press,
1119   Cambridge, MA.
1120   Kurylas, A. E., Rohlfing, T., Krofczik, S., Jenett, A., & Homberg, U. (2008). Standardized atlas of the
1121   brain of the desert locust, *Schistocerca gregaria*. *Cell and Tissue Research*, *333*, 125–145.
1122   https://doi.org/10.1007/s00441-008-0620-x
1123   Lelito, J. P., & Brown, W. D. (2008). Mate attraction by females in a sexually cannibalistic praying
1124   mantis. *Behavioral Ecology and Sociobiology, 63*, 313–320. https://doi.org/10.1007/s00265-008-
1125   0663-8
1126   Li, F., Lindsey, J. W., Marin, E. C., Otto, N., Dreher, M., Dempsey, G., Stark, I., Bates, A. S., Pleijzier, M.
1127   W., Schlegel, P., Nern, A., Takemura, S., Eckstein, N., Yang, T., Francis, A., Braun, A., Parekh, R.,
1128   Costa, M., Scheffer, L. K., Aso, Y., Jefferis, G. S., Abbott, L. F., Litwin-Kumar, A., Waddell, S., &

1129   Rubin, G. M. (2020). The connectome of the adult *Drosophila* mushroom body provides insights
1130   into function. *Elife*, *9*, e62576. https://doi.org/10.7554/eLife.62576
1131   Matsuo, E., Seki, H., Asai, T., Morimoto, T., Miyakawa, H., Ito, K., & Kamikouchi, A. (2016).
1132   Organization of projection neurons and local neurons of the primary auditory center in the fruit
1133   fly *Drosophila melanogaster*. *Journal of Comparative Neurology*, *524*, 1099–1164.
1134   https://doi.org/10.1002/cne.23955
1135   Menzel, R. (2022). In search for the retrievable memory trace in an insect brain. *Frontiers in Systems
1136   Neuroscience*, *16*, 876376. https://doi.org/10.3389/fnsys.2022.876376
1137   Merlin, C., Heinze, S., & Reppert, S. M. (2012). Unraveling navigational strategies in migratory insects.
1138   *Current Opinion in Neurobiology*, *22*, 353–361. https://doi.org/10.1016/j.conb.2011.11.009
1139   Modi, M. N., Shuai, Y., & Turner, G. C. (2020). The *Drosophila* mushroom body: from architecture to
1140   algorithm in a learning circuit. *Annual Review of Neuroscience*, *43*, 465–484.
1141   https://doi.org/10.1146/annurev-neuro-080317-0621333
1142   Mota, T., Yamagata, N., Giurfa, M., Gronenberg, W., & Sandoz, J. C. (2011). Neural organization and
1143   visual processing in the anterior optic tubercle of the honey bee brain. *Journal of Neuroscience,
1144   31*, 11443–11456. https://doi.org/10.1523/JNEUROSCI.0995-11.2011
1145   Mizunami, M., Weibrecht, J. M., & Strausfeld, N. J. (1998). Mushroom bodies of the cockroach: their
1146   participation in place memory. *Journal of Comparative Neurology*, *402*, 520–537.
1147   https://doi.org/10.1002/(SICI)1096-9861(19981228)402:4%3C520::AID-CNE6%3E3.0.CO;2-K
1148   Namiki, S., Dickinson, M. H., Wong, A. M., Korff, W., & Card, G. M. (2018a). The functional
1149   organization of descending sensory-motor pathways in *Drosophila*. *Elife*, *7*, e34272.
1150   https://doi.org/10.7554/eLife.34272
1151   Namiki, S., Wada, S., & Kanzaki, R. (2018b). Descending neurons from the lateral accessory lobe and
1152   posterior slope in the brain of the silkmoth *Bombyx mori*. *Scientific Report, 8*, 1–19.
1153   https://doi.org/10.1038/s41598-018-27954-5
1154   Nishino, H., Iwasaki, M., Yasuyama, K., Hongo, H., Watanabe, H., & Mizunami, M. (2012). Visual and
1155   olfactory input segregation in the mushroom body calyces in a basal neopteran, the American
1156   cockroach. *Arthropod Structure & Development*, *41*, 3–16.
1157   https://doi.org/10.1016/j.asd.2011.08.005
1158   Nityananda, V., Bissianna, G., Tarawneh, G., & Read, J. (2016a). Small or far away? Size and distance
1159   perception in the praying mantis. *Philosophical Transactions of the Royal Society of London. B,
1160   Biological Sciences*, *371*, 20150262. https://doi.org/10.1098/rstb.2015.0262
1161   Nityananda, V., Joubier, C., Tan, J., Tarawneh, G., & Read, J. C. (2019a). Motion-in-depth perception
1162   and prey capture in the praying mantis *Sphodromantis lineola*. *Journal of Experimental Biology,
1163   222*, jeb198614. https://doi.org/10.1242/jeb.198614
1164   Nityananda, V., O'Keeffe, J., Umeton, D., Simmons, A., & Read, J. C. (2019b). Second-order cues to
1165   figure motion enable object detection during prey capture by praying mantises. *Proceedings of
1166   the National Academy of Sciences, 116*, 27018–27027. https://doi.org/10.1073/pnas.19123101
1167   Nityananda, V., Tarawneh, G., Rosner, R., Nicolas, J., Crichton, S., & Read, J. (2016b). Insect stereopsis
1168   demonstrated using a 3D insect cinema. *Scientific Report, 6*, 18718.
1169   https://doi.org/10.1038/srep18718
1170   Nordström, K., & O'Carroll, D. C. (2009). Feature detection and the hypercomplex property in
1171   insects. *Trends in Neurosciences*, *32*, 383–391. https://doi.org/10.1016/j.tins.2009.03.004
1172   O'Carroll, D. (1993). Feature-detecting neurons in dragonflies. *Nature*, *362*, 541–543.
1173   https://doi.org/10.1038/362541a0
1174   Okada, R., Sakura, M., & Mizunami, M. (2003). Distribution of dendrites of descending neurons and
1175   its implications for the basic organization of the cockroach brain. *Journal of Comparative
1176   Neurology*, *458*, 158–174. https://doi.org/10.1002/cne.10580
1177   Olberg, R. M. (2012). Visual control of prey-capture flight in dragonflies. *Current Opinion in
1178   Neurobiology*, *22*, 267–271. https://doi.org/10.1016/j.conb.2011.11.015
1179   Otsuna, H., & Ito, K. (2006). Systematic analysis of the visual projection neurons of *Drosophila
1180   melanogaster*. I. Lobula-specific pathways. *Journal of Comparative Neurology*, *497*, 928–958.
1181   https://doi.org/10.1002/cne.21015

Patella, P., & Wilson, R. I. (2018). Functional maps of mechanosensory features in the *Drosophila* brain. *Current Biology, 28*, 1189–1203. https://doi.org/10.1016/j.cub.2018.02.074

Paulk, A. C., Phillips-Portillo, J., Dacks, A. M., Fellous, J. M., & Gronenberg, W. (2008). The processing of color, motion, and stimulus timing are anatomically segregated in the bumblebee brain. *Journal of Neuroscience, 28*, 6319–6332. https://doi.org/10.1523/JNEUROSCI.1196-08.2008

Paulk, A. C., Dacks, A. M., Phillips-Portillo, J., Fellous, J. M., & Gronenberg, W. (2009). Visual processing in the central bee brain. *Journal of Neuroscience, 29*, 9987–9999. https://doi.org/10.1523/JNEUROSCI.1325-09.2009

Pfeiffer, K. (2022). The neuronal building blocks of the navigational toolkit in the central complex of insects. *Current Opinion in Insect Science*, 100972. https://doi.org/10.1016/j.cois.2022.100972

Pfeiffer, K., & Homberg, U. (2014). Organization and functional roles of the central complex in the insect brain. *Annual Review of Entomology, 59*, 165–184. https://doi.org/10.1146/annurev-ento-011613-162031

Poteser, M., & Kral, K. (1995). Visual distance discrimination between stationary targets in praying mantis: an index of the use of motion parallax. *Journal of Experimental Biology, 198*, 2127–2137. https://doi.org/10.1242/jeb.198.10.2127

Rajashekhar, K. P., & Singh, R. N. (1994). Neuroarchitecture of the tritocerebrum of *Drosophila melanogaster*. *Journal of Comparative Neurology, 349*, 633–645. https://doi.org/10.1002/cne.903490410

Read, J. C. (2023). Stereopsis without correspondence. *Philosophical Transactions of the Royal Society B, 378*, 20210449. https://doi.org/10.1098/rstb.2021.0449

Reinhard, N., Schubert, F. K., Bertolini, E., Hagedorn, N., Manoli, G., Sekiguchi, M., Yoshii, T., Rieger, D., & Helfrich-Förster, C. (2022). The neuronal circuit of the dorsal circadian clock neurons in *Drosophila melanogaster*. *Frontiers in Physiology, 13*, 886432. https://doi.org/10.3389/fphys.2022.886432

Ribeiro, I. M., Drews, M., Bahl, A., Machacek, C., Borst, A., & Dickson, B. J. (2018). Visual projection neurons mediating directed courtship in *Drosophila*. *Cell, 174*(, 607–621. https://doi.org/10.1016/j.cell.2018.06.020

Rosner, R., Tarawneh, G., Lukyanova, V., & Read, J. C. (2020). Binocular responsiveness of projection neurons of the praying mantis optic lobe in the frontal visual field. *Journal of Comparative Physiology A, 206*, 165–181. https://doi.org/10.1007/s00359-020-01405-x

Rosner, R., von Hadeln, J., Salden, T., & Homberg, U. (2017). Anatomy of the lobula complex in the brain of the praying mantis compared to the lobula complexes of the locust and cockroach. *Journal of Comparative Neurology, 525*, 2343–2357. https://doi.org/10.1002/cne.24208

Rosner, R., von Hadeln, J., Tarawneh, G., & Read, J. C. (2019). A neuronal correlate of insect stereopsis. *Nature Communications, 10*, 1–9. https://doi.org/10.1038/s41467-019-10721-z

Rossel, S. (1979). Regional differences in photoreceptor performance in the eye of the praying mantis. *Journal of Comparative Physiology, 131*, 95–112. https://doi.org/10.1007/BF00619070

Rossel, S. (1983) Binocular stereopsis in an insect. *Nature, 302*, 821–822. https://doi.org/10.1038/302821a0

Ryu, L., Kim, S. Y., & Kim, A. J. (2022). From photons to behaviors: neural implementations of visual behaviors in *Drosophila*. *Frontiers in Neuroscience, 16*, 883640. https://doi.org/10.3389/fnins.2022.883640

Rybak, J., & Menzel, R. (1993). Anatomy of the mushroom bodies in the honey bee brain: the neuronal connections of the alpha-lobe. *Journal of Comparative Neurology, 334*, 444–465. https://doi.org/10.1002/cne.903340309

Schachtner, J., Schmidt, M., & Homberg, U. (2005). Organization and evolutionary trends of primary olfactory brain centers in Tetraconata (Crustacea+Hexapoda). *Arthropod Structure & Development, 34*, 257–299. https://doi.org/10.1016/j.asd.2005.04.003

Staudacher, E. (1998). Distribution and morphology of descending brain neurons in the cricket *Gryllus bimaculatus*. *Cell and Tissue Research, 294*, 187–202. https://doi.org/10.1007/s004410051169

1234 Staudacher, E. M., Cigan, M. L., Wenz, F., Pollun, A., Beck, S., Beck, M., Reh, F., Haas, J., & Homberg,
1235   U. (2023). Organization of descending neurons in the brain of the desert locust. *Journal of*
1236   *Comparative Neurology*. https://doi.org/10.1002/cne.25513
1237 Staudacher, E. M., Gebhardt, M., & Dürr, V. (2005). Antennal movements and mechanoreception:
1238   neurobiology of active tactile sensors. *Advances in Insect Physiology*, *32*, 49–205.
1239   https://doi.org/10.1016/S0065-2806(05)32002-9
1240 Staudacher, E., & Schildberger, K. (2000). A newly described neuropile in the deutocerebrum of the
1241   cricket: antennal afferents and descending interneurons. *Zoology 102*, 212–226.
1242 Stengl, M., & Homberg, U. (1994). Pigment-dispersing hormone-immunoreactive neurons in the
1243   cockroach *Leucophaea maderae* share properties with circadian pacemaker neurons. *Journal of*
1244   *Comparative Physiology A*, *175*, 203–213. https://doi.org/10.1007/BF00215116
1245 Sternberger, L. A. (1979). Immunocytochemistry. John Wiley and Sons, New York.
1246 Stone, T., Webb, B., Adden, A., Weddig, N. B., Honkanen, A., Templin, R., Wcislo W., Scimeca L.,
1247   Warrant E., & Heinze, S. (2017). An anatomically constrained model for path integration in the
1248   bee brain. *Current Biology*, *27*, 3069–3085. http://dx.doi.org/10.1016/j.cub.2017.08.052
1249 Strausfeld, N. J. (1976). Atlas of an insect brain. Springer, Berlin Heidelberg New York
1250 Strausfeld, N. J. (2002). Organization of the honey bee mushroom body: representation of the calyx
1251   within the vertical and gamma lobes. *Journal of Comparative Neurology*, *450*, 4–33.
1252   https://doi.org/10.1002/cne.10285
1253 Strausfeld, N. J. (2005) The evolution of crustacean and insect optic lobes and the origins of
1254   chiasmata. *Arthropod Structure & Development*, *34*, 235–256.
1255   https://doi.org/10.1016/j.asd.2005.04.001
1256 Strausfeld, N. J. (2012). *Arthropod brains: evolution, functional elegance, and historical significance.*
1257   Belknap Press.
1258 Strausfeld, N. J., & Bassemir, U. K. (1985a). Lobula plate and ocellar interneurons converge onto a
1259   cluster of descending neurons leading to neck and leg motor neuropil in *Calliphora*
1260   *erythrocephala. Cell and Tissue Research*, *240*, 617–640. https://doi.org/10.1007/BF00216351
1261 Strausfeld, N. J., & Bassemir, U. K. (1985b). The organization of giant horizontal-motion-sensitive
1262   neurons and their synaptic relationships in the lateral deutocerebrum of *Calliphora*
1263   *erythrocephala* and *Musca domestica. Cell and Tissue Research*, *242*, 531–550.
1264   https://doi.org/10.1007/BF00225419
1265 Strausfeld, N. J., & Li, Y. (1999). Organization of olfactory and multimodal afferent neurons supplying
1266   the calyx and pedunculus of the cockroach mushroom bodies. *Journal of Comparative Neurology*,
1267   *409*, 603–625. https://doi.org/10.1002/(SICI)1096-9861(19990712)409:4<603::AID-
1268   CNE7>3.0.CO;2-P
1269 Strausfeld, N. J., Sinakevitch, I., Brown, S. M., & Farris, S. M. (2009). Ground plan of the insect
1270   mushroom body: functional and evolutionary implications. *Journal of Comparative Neurology*,
1271   *513*, 265–291. https://doi.org/10.1002/cne.21948
1272 Sun, L., Pan, X., Li, H., Zhang, X., Zhao, X., Zhang, L., & Zhang, L. (2022). Odor-induced vomiting is
1273   combinatorially triggered by palp olfactory receptor neurons that project to the lobus
1274   glomerulatus in locust brain. *Frontiers in Physiology*, *13*, 855522.
1275   https://doi.org/10.3389/fphys.2022.855522
1276 Suver, M. P., Huda, A., Iwasaki, N., Safarik, S., & Dickinson, M. H. (2016). An array of descending
1277   visual interneurons encoding self-motion in *Drosophila. Journal of Neuroscience*, *36*, 11768–
1278   11780. https://doi.org/10.1523/JNEUROSCI.2277-16.2016
1279 Tanaka, N. K., Tanimoto, H., & Ito, K. (2008). Neuronal assemblies of the *Drosophila* mushroom body.
1280   *Journal of Comparative Neurology*, *508*, 711–755. https://doi.org/10.1002/cne.21692
1281 Timm, J., Scherner, M., Matschke, J., Kern, M., & Homberg, U. (2021). Tyrosine hydroxylase
1282   immunostaining in the central complex of dicondylian insects. *Journal of Comparative Neurology*,
1283   *529*, 3131–3154. https://doi.org/10.1002/cne.25151
1284 Träger, U., Wagner, R., Bausenwein, B., & Homberg, U. (2008). A novel type of microglomerular
1285   synaptic complex in the polarization vision pathway of the locust brain. *Journal of Comparative*
1286   *Neurology 506*, 288–300. https://doi.org/10.1002/cne.21512

1287 Vitzthum, H., Homberg, U., & Agricola, H. (1996). Distribution of Dip-allatostatin I-like
1288   immunoreactivity in the brain of the locust *Schistocerca gregaria* with detailed analysis of
1289   immunostaining in the central complex. *Journal of Comparative Neurology, 369,* 419–437.
1290   https://doi.org/10.1002/(SICI)1096-9861(19960603)369:3<419::AID-CNE7>3.0.CO;2-8
1291 von Hadeln, J., Althaus, V., Häger, L., & Homberg, U. (2018). Anatomical organization of the cerebrum
1292   of the desert locust *Schistocerca gregaria*. *Cell and Tissue Research, 374*, 39–62.
1293   https://doi.org/10.1007/s00441-018-2844-8
1294 Warrant, E., & Dacke, M. (2011). Vision and visual navigation in nocturnal insects. *Annual Review of*
1295   *Entomology, 56*, 239–254. https://doi.org/10.1146/annurev-ento-120709-144852
1296 Wei, H., el Jundi, B., Homberg, U., & Stengl, M. (2010). Implementation of pigment-dispersing factor-
1297   immunoreactive neurons in a standardized atlas of the brain of the cockroach *Leucophaea*
1298   *maderae*. *Journal of Comparative Neurology*, *518*, 4113–4133.
1299   https://doi.org/10.1002/cne.22471
1300 Wolff, T., Iyer, N. A., & Rubin, G.M. (2015). Neuroarchitecture and neuroanatomy of the *Drosophila*
1301   central complex: A GAL4-based dissection of protocerebral bridge neurons and circuits. *Journal of*
1302   *Comparative Neurology, 523*, 997–1037. https://doi.org/10.1002/cne.23705
1303 Wosnitza, A., Martin, J. P., Pollack, A. J., Svenson, G. J., & Ritzmann, R. E. (2022). The role of central
1304   complex neurons in prey detection and tracking in the freely moving praying mantis (*Tenodera*
1305   *sinensis). Frontiers in Neural Circuits, 16,* 893004. https://doi.org/10.3389/fncir.2022.893004
1306 Wu, M., Nern, A., Williamson, W. R., Morimoto, M. M., Reiser, M. B., Card, G. M., & Rubin, G. M.
1307   (2016). Visual projection neurons in the *Drosophila* lobula link feature detection to distinct
1308   behavioral programs. *Elife*, *5*, e21022. https://doi.org/10.7554/eLife.21022.002
1309 Yamawaki, Y. (2019). Unraveling the functional organization of lobula complex in the mantis brain by
1310   identification of visual interneurons. *Journal of Comparative Neurology, 527*, 1161–1178.
1311   https://doi.org/10.1002/cne.24603
1312 Yamazaki, Y., Nishikawa, M., & Mizunami, M. (1998). Three classes of GABA-like immunoreactive
1313   neurons in the mushroom body of the cockroach. *Brain Research, 788*, 80–86.
1314   https://doi.org/10.1016/S0006-8993(97)01515-1
1315 Yu, H. H., Awasaki, T., Schroeder, M. D., Long, F., Yang, J. S., He, Y., Ding, P., Kao, J.-C., Wu, G. Y.-Y.,
1316   Peng, H., Myers, G., & Lee, T. (2013). Clonal development and organization of the adult
1317   *Drosophila* central brain. *Current Biology, 23*, 633–643.
1318   https://doi.org/10.1016/j.cub.2013.02.057
1319

1320 **Figure Legends**

1321 **Figure 1** Three-dimensional reconstruction of the cerebrum of the mantis. (a) Anterior (left) and

1322 posterior (right), (b) lateral, (c) dorsal (left) and ventral (right) views of the reconstructed neuropils

1323 (labeled in black) and tracts, fiber systems, and commissures (labeled in grey) of the mantis brain. a,

1324 anterior; ABR, anterior bridge; ACAR, accessory calyx ring; AL, antennal lobe; ALI, anterior lip; AMMC,

1325 antennal mechanosensory and motor center; AOT, anterior optic tract; AOTU, anterior optic

1326 tubercle; ATL, antler; AVLP, anterior ventrolateral protocerebrum; CA, calyx; CBU, upper division of

1327 the central body; CRE, crepine; d, dorsal; DAMMC, dorsal AMMC; GA, gall; GC, great commissure;

1328 GLO, glomerular lobe; IB, inferior bridge; IT, isthmus tract; l, lateral; LAL, lateral accessory lobe; LALC,

1329 LAL commissure; LAMMC, lateral AMMC; LCA, lateral CA; LEF, lateral equatorial fascicle; LH, lateral

1330 horn; LLAL, lower LAL; LU, lower unit of the AOTU; MAL, medial accessory lobe; mALT, medial

1331 antennal lobe tract; MAMMC, medial AMMC; MBDL, median bundle; MCA, medial CA; MEF, medial

1332 equatorial fascicle; ML, medial lobe; NO, noduli; OCN, ocellar nerve; OR, ocellar root; p, posterior; PB,

1333 protocerebral bridge; PED, pedunculus; PLP, posterior lateral protocerebrum; POC, posterior optic

1334 commissure; POTU, posterior optic tubercle; PS, posterior slope; PVLP, posterior ventrolateral

1335 protocerebrum; SIP, superior intermediate protocerebrum; SLP, superior lateral protocerebrum;

1336 SMP, superior medial protocerebrum; TC, tritocerebrum; ULAL, upper LAL; UU, upper unit of the

1337 AOTU; v, ventral; VES, vest; VFA, ventral area of flagellar afferents; VL, vertical lobe; WED, wedge;

1338 WEDC, WED commissure. Scale bars = 200 μm

1339 **Figure 2** Series of frontal optical sections through the mantis brain from a depth of 86 μm relative to

1340 the anterior brain surface (a) to a depth of 158 μm (c). Right panels show synapsin immunolabeling in

1341 confocal sections, left panels show the same sections overlayed with a transparent surface cut of the

1342 three-dimensional reconstructions. Tracts, fiber systems and commissures are labeled in yellow,

1343 neuropils in white. ABR, anterior bridge; AL, antennal lobe; ALH, AL hub; AOT anterior optic tract;

1344 AOTU, anterior optic tubercle; AVLP, anterior ventrolateral protocerebrum; BU, bulb; CRE, crepine;

1345 GA, gall; IT, isthmus tract; LAL, lateral accessory lobe; LLAL, lower LAL; LU, lower unit of the AOTU;

1346 MAL, medial accessory lobe; MBDL, median bundle; ML, medial lobe; PED, pedunculus; SCL, superior

1347 clamp; SIP, superior intermediate protocerebrum; SLP, superior lateral protocerebrum; SMP,

1348 superior medial protocerebrum; Syn, synapsin; TUBUT, tubercle-bulb tract; ULAL, upper LAL; UU,

1349 upper unit of the AOTU; VFA, ventral area of flagellar afferents; VL, vertical lobe. Scale bar = 200 μm

1350 **Figure 3** Series of frontal optical sections through the mantis brain from a depth of 196 μm (a) to a

1351 depth of 231 μm (c). Right panels show confocal sections of synapsin immunolabeling, left panels

1352 show the same sections overlayed with a transparent surface cut of the three-dimensional

1353 reconstructions. Tracts, fiber systems and commissures are labeled in yellow, neuropils in white. ALI,

1354   anterior lip; AMMC, antennal mechanosensory and motor center; AOT, anterior optic tract; AVLP,

1355   anterior ventrolateral protocerebrum; BU, bulb; CRE, crepine; DAMMC, dorsal AMMC; GLO,

1356   glomerular lobe; IT, isthmus tract; LAL, lateral accessory lobe; LALC, LAL commissure; LAMMC, lateral

1357   AMMC; LH, lateral horn; LLAL, lower LAL; LU, lower unit of the AOTU; MAL, medial accessory lobe;

1358   mALT, medial antennal lobe tract; MAMMC, medial AMMC; MBDL, median bundle; ML, medial lobe;

1359   PED, pedunculus; PVLP, posterior ventrolateral protocerebrum; SCL, superior clamp; SIP, superior

1360   intermediate protocerebrum; SLP, superior lateral protocerebrum; SMP, superior medial

1361   protocerebrum; Syn, synapsin; TC, tritocerebrum; TUBUT, tubercle-bulb tract; ULAL, upper LAL; VES,

1362   vest; VFA, ventral area of flagellar afferents; VL, vertical lobe; WED, wedge. Scale bar = 200

1363   **Figure 4** Series of frontal optical sections through the mantis brain from a depth of 261 µm (a) to a

1364   depth of 339 µm (c). Right panels show confocal sections of synapsin immunolabeling, left panels

1365   show the same sections overlayed with a transparent surface cut of the three-dimensional

1366   reconstructions. Tracts, fiber systems and commissures are labeled in yellow, neuropils in white.

1367   ACAR, accessory CA ring; AMMC, antennal mechanosensory and motor center; ATL, antler; CA, calyx;

1368   CB, central body; CBL, lower division of the CB; CBU, upper division of the CB; EPA, epaulette; GC,

1369   great commissure; GLO, glomerular lobe; GOR, gorget; IB, inferior bridge; ICA, inner CA; ICL, inferior

1370   clamp; IFS, inferior fiber system; LAL, lateral accessory lobe; LALC, LAL commissure; LAMMC, lateral

1371   AMMC; LH, lateral horn; LLAL, lower LAL; MAL, medial accessory lobe; mALT, medial antennal lobe

1372   tract; MAMMC, medial AMMC; MBDL, median bundle; ML, medial lobe; NO, noduli; OCA, outer CA;

1373   OCN, ocellar nerve; PED, pedunculus; PLP, posterior lateral protocerebrum; PVLP, posterior

1374   ventrolateral protocerebrum; SCL, superior clamp; SIP, superior intermediate protocerebrum; SLP,

1375   superior lateral protocerebrum; SMP, superior medial protocerebrum; Syn, synapsin; TC,

1376   tritocerebrum; ULAL, upper LAL; VES, vest; VL, vertical lobe; WED, wedge. Scale bar = 200

1377   **Figure 5** Series of frontal optical sections through the mantis brain from a depth of 364 µm (a) to a

1378   depth of 453 µm (d). Right panels show confocal sections of synapsin immunolabeling, left panels

1379   show the same sections overlayed with a transparent surface cut of the three-dimensional

1380   reconstructions. Tracts, fiber systems and commissures are labeled in yellow, neuropils in white.

1381   ACAR, accessory CA ring; AMMC, antennal mechanosensory and motor center; ATL, antler; CA, calyx;

1382   GC, great commissure; IB, inferior bridge; ICA, inner CA; ICL, inferior clamp; LAMMC, lateral AMMC;

1383   LEF, lateral equatorial fascicle; LH, lateral horn; mALT, medial antennal lobe tract; MAMMC, medial

1384   AMMC; MEF, medial equatorial fascicle; OCA, outer CA; OCN, ocellar nerve; OR, ocellar root; PB,

1385   protocerebral bridge; PED, pedunculus; PLP, posterior lateral protocerebrum; POC, posterior optic

1386   commissure; POTU, posterior optic tubercle; PS, posterior slope; PVLP, posterior ventrolateral

1387   protocerebrum; SLP, superior lateral protocerebrum; Syn, synapsin; TC, tritocerebrum; VES, vest;

1388   WED, wedge; WEDC, WED commissure. Scale bars = 200

1389 **Figure 6** Organization of the mushroom body (MB) (a-e), central complex (CX) (g-j), and anterior lip

1390 (ALI) (f,h) in frontal views. a,b Three-dimensional reconstruction of the mushroom body in a semi-

1391 transparent brain hemisphere in anterior (a) and posterior (b) view. Dotted lines show the region of

1392 the pedunculus divide (PEDD). (c,d) Frontal optical sections showing synapsin immunolabeling in the

1393 calyx (CA) (c) and the accessory CA ring (ACAR). Yellow arrowhead in (d) points to accumulation of

1394 synapsin staining in the ACAR (dotted outline). (e-g) 30-µm sections immunolabeled for GABA.

1395 Dotted lines mark the borders of the CA (e), the ALI, CX and the bulb (BU). (h) Three-dimensional

1396 reconstruction of the CX in posterior (top), anterior (middle) and anterior surface cut (bottom) views.

1397 (i,j) Frontal optical sections showing synapsin immunolabeling in the neuropils of the CX. CB, central

1398 body; CBL, lower division of the CB; CBU, upper division of the CB; CRE, crepine; d, dorsal; GABA, γ-

1399 aminobutyric acid; ICA, inner CA; IB, inferior bridge; IT, isthmus tract; l, lateral; LCA, lateral CA; MAL,

1400 medial accessory lobe; MCA, medial CA; ML, medial lobe; NO, noduli; OCA, outer CA; PB,

1401 protocerebral bridge; PED, pedunculus; VL, vertical lobe. Scale bars = 100 µm

1402 **Figure 7** Organization of the lateral complex (LX). (a) Three-dimensional reconstruction of the LX with

1403 prominent tracts in a semi-transparent brain hemisphere, frontal view. The CX is included for better

1404 orientation. (b) Lateral view of neuropils of the LX (labeled in black) and prominent tracts (labeled in

1405 grey). (c,c') Frontal optical sections showing synapsin immunolabeling in the LX. Dotted lines mark

1406 the neuropils of the LX and the blue arrowhead the isthmus tract (IT). a, anterior; AL, antennal lobe;

1407 BU, bulb; CB, central body; CBL, lower division of the CB; CBU, upper division of the CB; d, dorsal; GA,

1408 gall; l, lateral; LAL, lateral accessory lobe; LALC, LAL commissure; LLAL, lower LAL; m, medial; ML,

1409 medial lobe; NO, noduli; PED, pedunculus; PB, protocerebral bridge; Syn, synapsin; ULAL, upper LAL;

1410 VL, vertical lobe. Scale bars = 100 µm

1411 **Figure 8** Organization of the superior (SNP) (a-d) and ventrolateral neuropils (VLNP) (e-h). (a) Anterior

1412 view of the SNP with prominent tracts in a half-transparent brain hemisphere. (b,c) 30-µm sections

1413 immunolabeled for GABA. Dotted lines mark the SNP and adjoining neuropils. (d) Frontal optical

1414 section of the synapsin immunolabeled brain with outlines of the reconstructed label fields. (e,f)

1415 Anterior (e, left), posterior (e, right) and dorsal (f) views of the neuropils of the VLNP in a half-

1416 transparent brain hemisphere. (g) Frontal optical sections of the synapsin immunolabeled brain with

1417 outlines of the reconstructed label fields. (h) Frontal projection view of 10 slices showing synapsin

1418 immunolabeled glomerular structures in the posterior ventrolateral protocerebrum (PVLP). ABR,

1419 anterior bridge; AOT, anterior optic tract; AOTU, anterior optic tubercle; AVLP, anterior ventrolateral

1420 protocerebrum; CA, calyx; d, dorsal; GABA, γ-aminobutyric acid; GC, great commissure; IFS, inferior

1421 fiber system; l, lateral; LH, lateral horn; LU, lower unit of the AOTU; m, medial; mALT, medial

1422 antennal lobe tract; MBDL, median bundle; LEF, lateral equatorial fascicle; p, posterior; PLP, posterior

1423 lateral protocerebrum; PVLP, posterior ventrolateral protocerebrum; SIP, superior intermediate

1424   protocerebrum; SLP, superior lateral protocerebrum; SMP, superior medial protocerebrum; TUBUT,

1425   tubercle-bulb tract; UU, upper unit of the AOTU; WED, wedge; WEDC, WED commissure. Scale bars =

1426   200 μm (a,d-g) and 100 μm (b,c,h)

1427   **Figure 9** Organization of the inferior neuropils (INP) (a-e) and ventromedial neuropils (VMNP) (f-i). (a)

1428   Anterior (left) and posterior (right) view and (b) ventral view of the INPs with prominent tracts

1429   (labeled in grey) in a half-transparent brain hemisphere. Red dashed circles mark the penetration of

1430   the pedunculus/pedunculus divide (PED/PEDD) in (a) and the vertical lobe (VL) in (b). (c-e) 30-μm

1431   sections immunolabeled for GABA. Dotted lines mark the neuropils of the INP and associated

1432   neuropils. (f) Dorsal view of the VMNP with prominent tracts (labeled in grey). (g) Posterior view of

1433   the reconstructed VMNP with prominent tracts (labeled in grey) in a half-transparent brain

1434   hemisphere. The posterior slope (PS) is presented semi-transparently for a better visualization of the

1435   underlying neuropils. (h) Posterior projection view of 20 optical sections showing tyrosine

1436   hydroxylase (magenta) immunostaining of the posterior optic commissure (POC) and posterior optic

1437   tubercle (POTU). (i) Frontal optical section showing the reconstructed label fields of VMNP in

1438   synapsin staining. a, anterior; AL, antennal lobe; ALI, anterior lip; AOTU, anterior optic tubercle; ATL,

1439   antler; AVLP, anterior ventrolateral protocerebrum; BU, bulb; CB, central body; CRE, crepine; d,

1440   dorsal; EPA, epaulette; GABA, γ-aminobutyric acid; GC, great commissure; GOR, gorget; IB, inferior

1441   bridge; ICL, inferior clamp; IFS, inferior fiber system; l, lateral; LALC, lateral accessory lobe

1442   commissure; LEF, lateral equatorial fascicle; m, medial; MAL, medial accessory lobe; mALT, medial

1443   antennal lobe tract; MBDL, median bundle; MEF, medial equatorial fascicle; ML, medial lobe; OCN,

1444   ocellar nerve; OR, ocellar root; POC, posterior optic commissure; POTU, posterior optic tubercle; SCL,

1445   superior clamp; VES, vest. Scale bars = 200 μm (a-d,f,g,i) and 100 μm (e,h)

1446   **Figure 10** Organization of the antennal lobe (AL), the periesophageal neuropils (PENP), and the

1447   tritocerebrum (TC). (a) Anterior (left) and posterior (right) views of the reconstructed neuropils in a

1448   semi-transparent brain hemisphere. The AL and the inferior fiber system (IFS) are, likewise, displayed

1449   half-transparently for better visualization of the adjoining neuropils. (b) Projection view of a stack of

1450   190 labeled sections showing a backfill of the maxillary nerve from the maxillary palp (magenta).

1451   (c,c') Single frontal optical sections showing the PENs following a backfill of the antennal nerve from

1452   the flagellum of the antenna. Asterisks marks the adjoining glomeruli of the antennal lobe. (c'')

1453   Projection view of a stack of 70 optical sections showing the projections of antennal afferents

1454   revealed by a backfill of the antennal nerve from the scapus-pedicel joint (magenta). AMMC,

1455   antennal and mechanosensory and motor center; DAMMC, dorsal AMMC; GLO, glomerular lobe;

1456   LAMMC, lateral AMMC; MAMMC, medial AMMC; T5-7, tract 5-7; TC, tritocerebrum; VFA, ventral

1457   area of flagellar afferents. Scale bar = 200 μm (a) and 100 μm (b-c'')

1458   **Figure 11** Three-dimensional reconstructions of the TOpro1 and TOpro2 neurons (Rosner et al., 2020)

1459   registered into the 3D-atlas of the mantis brain. (a) TOpro1 neuron registered in a half-transparent

1460   3D-atlas, showing innervated, colored neuropils in posterior (right), dorsal (middle), and ventral

1461   views (left bottom). Red arrowheads point to arborizations in the posterior slope (PS). Inset (top left)

1462   shows the reconstructed neuron from Rosner et al. (2020) with innervated neuropils of the optic

1463   lobe. (b-b'') Anterior projection view of 100 slices (b), 115 slices (b'), and 25 slices (b'') of the

1464   Neurobiotin-injected TOpro1 neuron. Yellow asterisk marks the connection to the posterior

1465   ramifications of the neuron (b''). It arborizes widely in the outer lobe of the lobula complex (OLO)

1466   and enters the cerebrum via the great commissure (GC). The neuron has wide arborizations in the

1467   ipsilateral brain hemisphere. (c, c') Projection view of 120 slices of the Neurobiotin-injected TOpro2

1468   neuron in the ipsilateral cerebrum (c) and of 120 slices of the optic lobe (c'). The neuron has wide

1469   arborizations in the OLO, anterior lobe of the lobula complex (ALO) and the stalk lobe of the lobula

1470   complex (SLO), anterior view. (d) TOpro2 neuron registered into the 3D-brain atlas with innervated

1471   neuropils highlighted in color in posterior (top) and dorsal views (bottom). Inset shows image of the

1472   reconstructed neuron from Rosner et al. (2020) with the innervated areas in the optic lobe (right

1473   middle). a, anterior; AVLP, anterior ventrolateral protocerebrum; CX, central complex; d, dorsal; EPA,

1474   epaulette; l, lateral; LA, lamina; m, medial; ME, medulla; OL, optic lobe; PLP posterior lateral

1475   protocerebrum; PVLP, posterior ventrolateral protocerebrum; VES, vest; WED, wedge. Scale bar =

1476   200 µm (a,b), 100 µm (b'-c'), and 400 µm (d)

1477   **Figure 12** Three-dimensional reconstruction of the TApro$_{prox}$1 (Rosner et al. 2020) and TAOpro

1478   neuron (Rosner et al. 2019). (a) Three-dimensional reconstruction of the TApro$_{prox}$1 neuron

1479   registered into the half-transparent 3D-atlas with colored innervated neuropils in posterior (right)

1480   and anterior lateral views (left). Inset shows neuron from Rosner et al. (2020) in anterior view with

1481   innervated areas of the optic lobe (middle). (b-b'') Anterior projection views from posterior (130

1482   slices in b) to anterior (50 slices in b' and 60 slices in b''). (c) Three-dimensional reconstruction of the

1483   TAOpro neuron registered in the half transparent 3D-atlas with innervated neuropils and the great

1484   commissure (GC) in colors, posterior (top) and dorsal (bottom) views. Inset shows neuron from

1485   Rosner et al. (2019) in anterior view with innervated areas of the optic lobe (OL). (d-d') Anterior

1486   projection view of the Neurobiotin-injected TAOpro neuron from 80 slices of the central brain (d) and

1487   60 slices of the OL (d'). a, anterior; ALO, anterior lobe of the lobula complex; ALO-V, ventral ALO;

1488   AVLP, anterior ventrolateral protocerebrum; CX, central complex; d, dorsal; IFS, inferior fiber system;

1489   l, lateral; LLAL, lower lateral accessory lobe; m, medial; OLO, outer lobe of the lobula complex; PLP,

1490   posterior lateral protocerebrum; PVLP, posterior ventrolateral protocerebrum; SLO, stalk lobe of the

1491   lobula complex; ULAL, upper lateral accessory lobe; VES, vest; WED, wedge. Scale bar = 200 µm (a),

1492   100 µm (b,b',b'', d), 200 µm (d'), and 300 µm (c)

1493   **Figure 13** (a)Three-dimensional reconstruction of the COcom neuron (Rosner et al., 2019) registered

1494   in the half transparent 3D-atlas with innervated neuropils and the great commissure (GC) in colors,

1495   posterior view. Inset shows neuron from Rosner et al. (2019) in anterior view with innervated areas

1496   of the optic lobes (OLs). (b-b') Anterior projection view of the Neurobiotin-injected COcom neuron

1497   from 70 slices of the whole neuron (b) and 20 slices of the arborization in the transition area from

1498   the posterior lateral protocerebrum (PLP) to the posterior ventrolateral protocerebrum (PVLP) (b').

1499   CX, central complex; d, dorsal; m, medial; OLO, outer lobe of the lobula complex; VES, vest; WED,

1500   wedge. Scale bar = 500 μm (a), 600 μm (b), 200 μm (b')

1501   **Figure 14** Three-dimensional reconstructions of the TAcen and the TMEcen neurons (Rosner et al.,

1502   2019). (a) Three-dimensional reconstruction of the TAcen neuron (Rosner et al., 2019) registered in a

1503   half transparent 3D-atlas with innervated colored neuropils in anterior lateral (right) and posterior

1504   views (left). (b) Anterior projection view of the Neurobiotin-injected TAcen neuron, displaying 100

1505   slices. Inset shows neuron from Rosner et al. (2019). Red arrowhead points at the soma, white arrow

1506   heads to fine arborizations in the antennal mechanosensory and motor center (AMMC), and the

1507   yellow asterisk marks the connection to arborizations in the posterior brain. (c) Three-dimensional

1508   reconstruction of the TMEcen neuron registered in the half transparent 3D-atlas with innervated

1509   neuropils in color, posterior (left) and dorsal (bottom right) view. Inset shows neuron from Rosner et

1510   al. (2019) in anterior view with innervated areas of the OL. (d) Anterior projection view of the

1511   TMEcen neuron from 60 slices showing the arborizations in the OL. (d') Anterior projection view of

1512   the Neurobiotin-injected TMEcen neuron from 115 slices of the central brain. Arrowheads point at

1513   neurites that are stained weakly. a, anterior; CX, central complex; d, dorsal; DAMMC, dorsal AMMC;

1514   GOR, gorget; m, medial; MAMMC, medial AMMC; PS, posterior slope; VES, vest; WED, wedge. Scale

1515   bar = 600 μm (a), 400 μm (b, c), 200 μm (d, d')

Table 1 Ramification areas of visual interneurons in the mantis described in Rosner et al. (2019, 2020).

Neuron	ID[1,2]	Fig.	Ramification areas within the OL						Ramification areas within the central brain											
			ME	ALO-D	ALO-P	DLO	OLO	SLO	AMMC	AVLP	EPA	GOR	ICL	LAL	PLP	PVLP	PS	SLP	VES	WED
TOpro1	160125[2]	2a					x				x				x	x	x		x	x
TOpro2	160301[2]	2c								x					x	x				
TApro_prox1	151013[2]	4a			x					x				x					x	x
COcom	151123[1]	3					x								x	x				x
TAOpro	160427[1]	1c		x			x								x	x			x	
TAcen	170606[1]	4a,b		x					x						x		x			x
TMEcen	161025[1]	4c-e	x									x			x		x		x	x
TOpro3	160503[2]	2d					x			x					x	x				
TApro_prox2	151102[2]	4d			x						x				x	x	x	x	x	x
TApro_prox3	170629[2]	4e			x								x		x	x	x	x		
Spro	170203[2]	4f						x		x						x				
TMeASpro	170605[2]	5b	x					x										x		
TMeOSpro	160216[2]	5a	x				x	x							x	x			x	x
TApro_dist1	151111[2]	3e		x											x		x			x
TADpro	161115[2]	3b		x		x								x	x		x			x

Figure numbers (Fig.) and identification numbers (ID[1,2]) refer to Rosner et al. (2019)[1] and (2020)[2]. The upper box shows neurons registered here, while the lower box lists the remaining types from Rosner et al. (2019, 2020). All neurons were studied in *Hierodula membranacea*, except TApro_prox3 (*Hierodula unimaculata*) and TADpro (*Rhombodera megaera*). The presence of arborizations is indicted by an x. ALO, anterior lobe of the lobula complex; ALO-D, distal ALO; ALO-P, proximal ALO; AMMC, antennal mechanosensory and motor center; AVLP, anterior ventrolateral protocerebrum; DLO, dorsal lobe of the lobula complex; EPA, epaulette; GOR, gorget; ICL, inferior clamp; LAL, lateral accessory lobe; ME, medulla; OLO, outer lobe of the lobula complex; PLP, posterior lateral protocerebrum; PVLP, posterior ventrolateral protocerebrum; PS, posterior slope; SLO, stalk lobe of the lobula complex; SLP, superior lateral protocerebrum; VES, vest; WED, wedge.
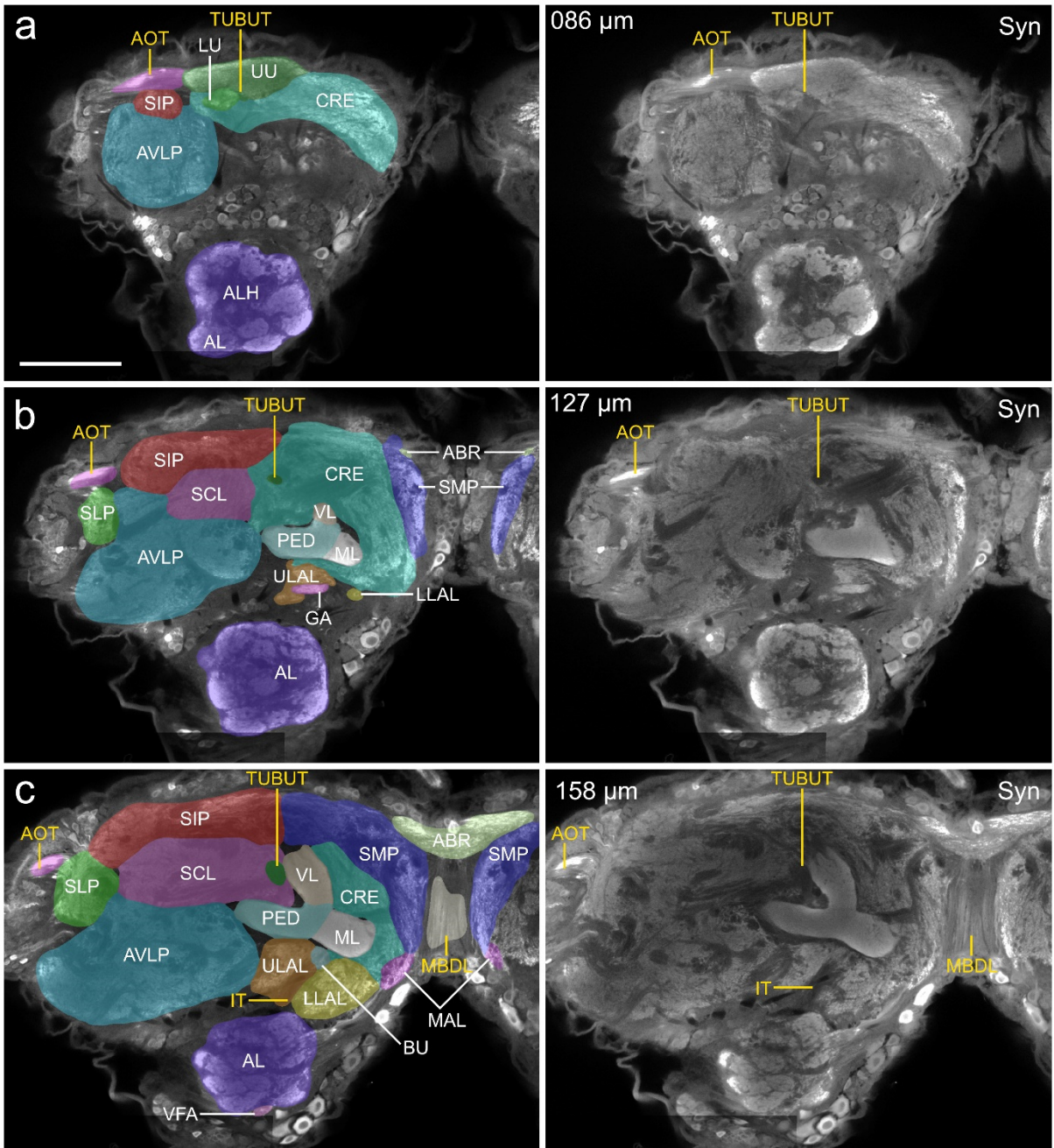
Figure 1
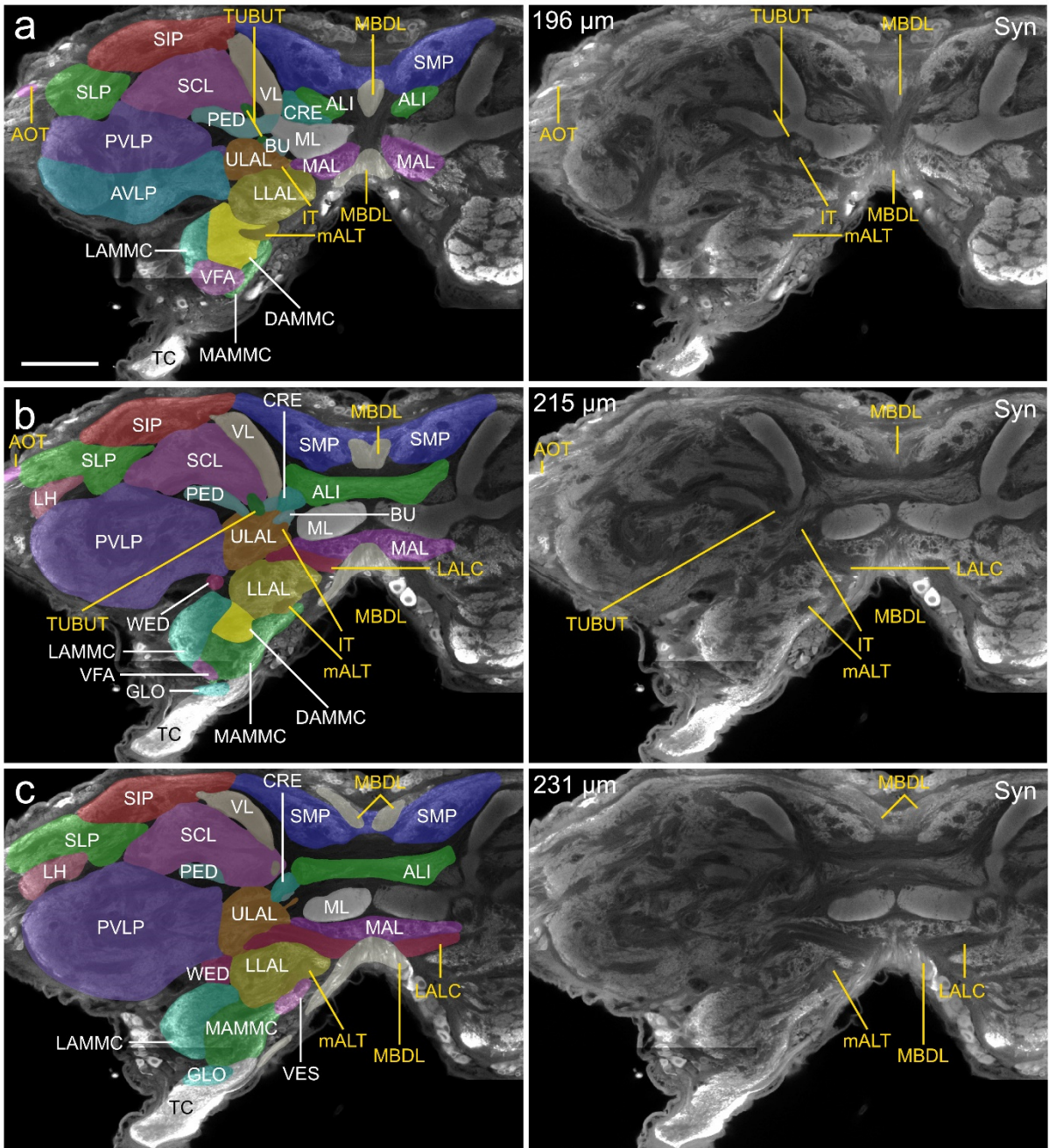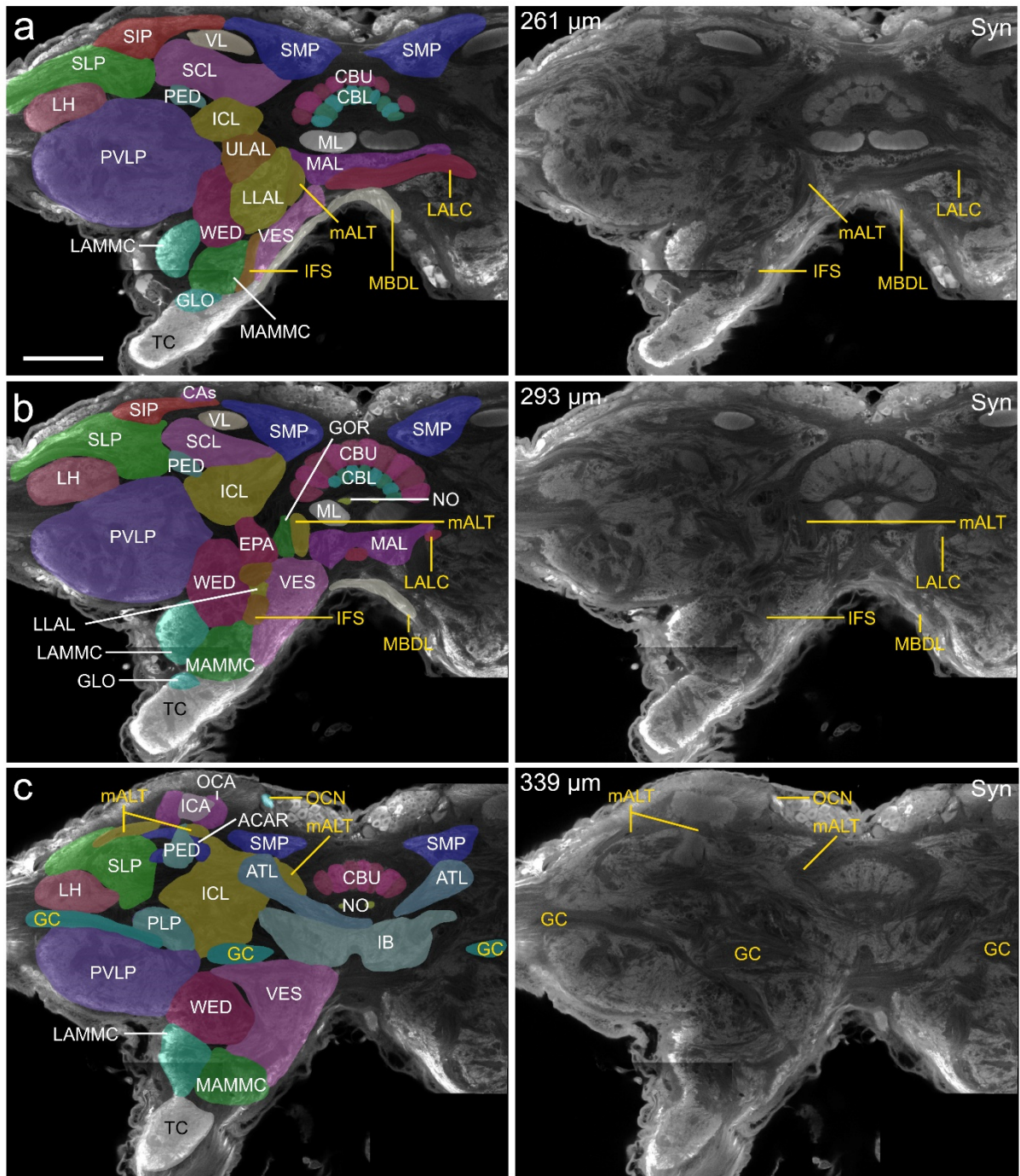
Figure 2

Figure 3

Figure 4
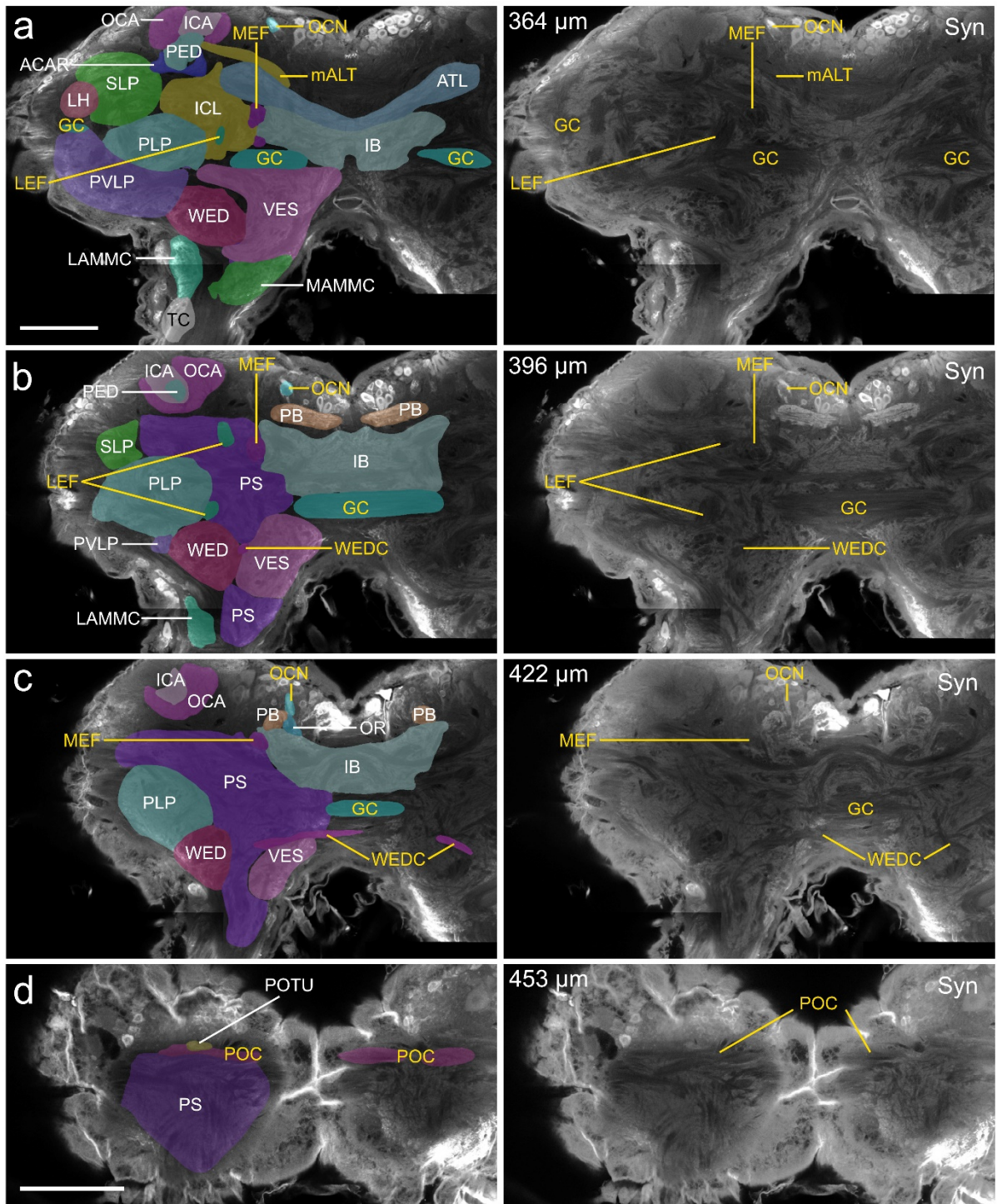
Figure 5
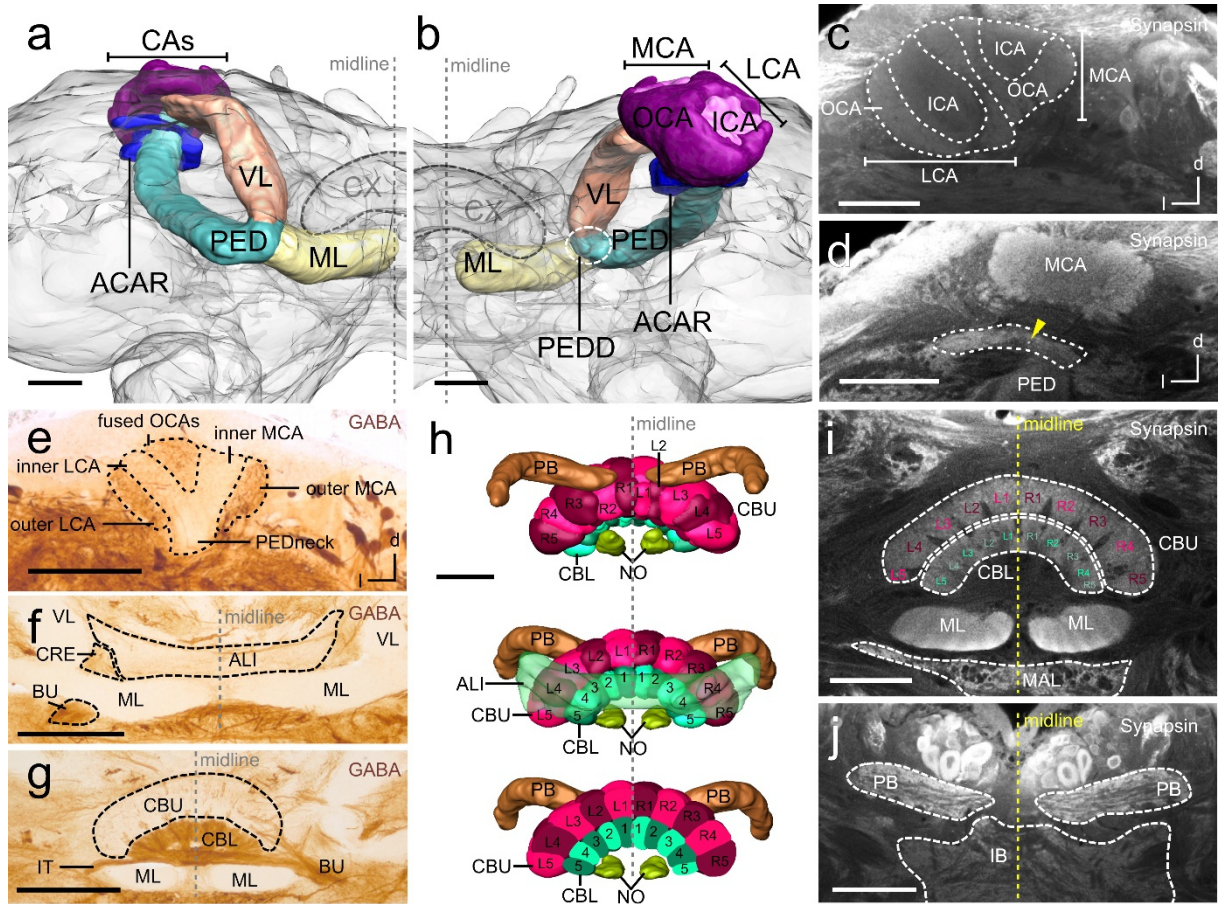
Figure 6
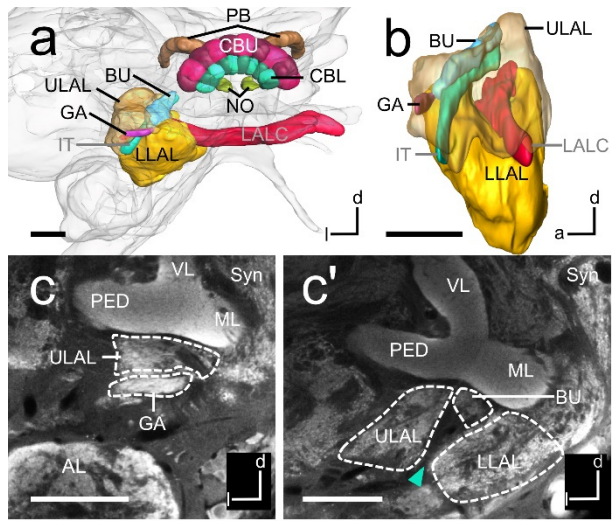
Figure 7
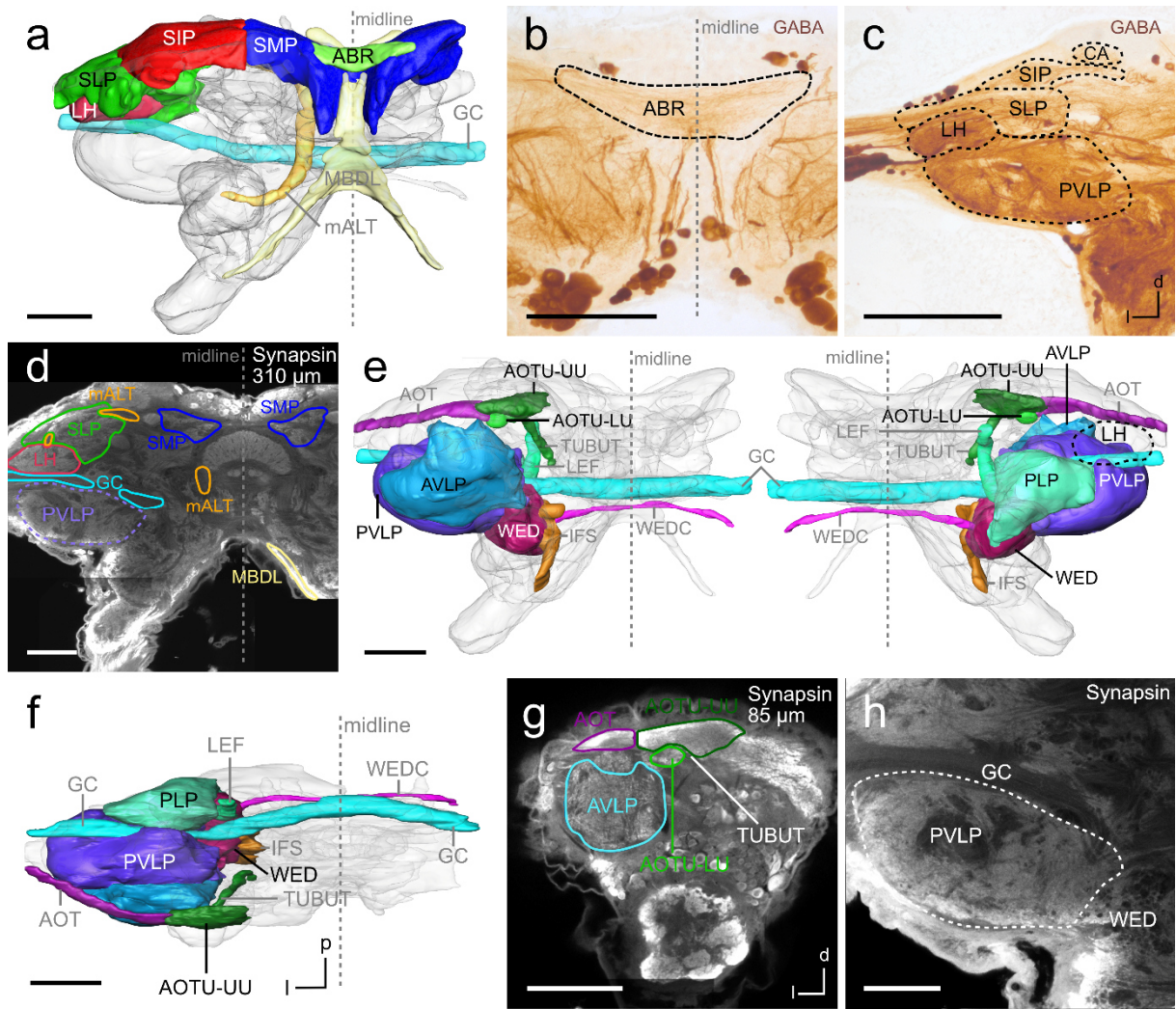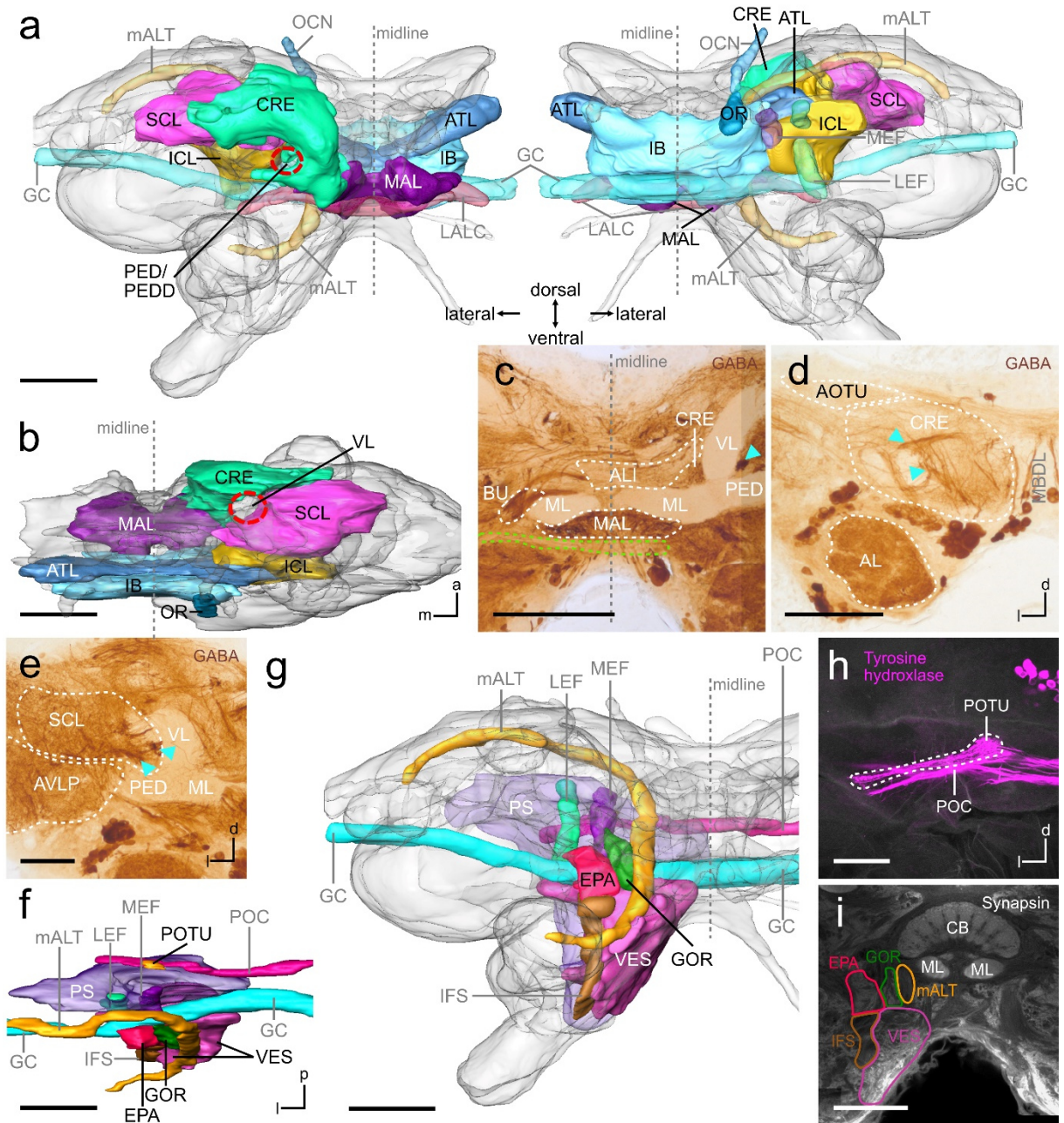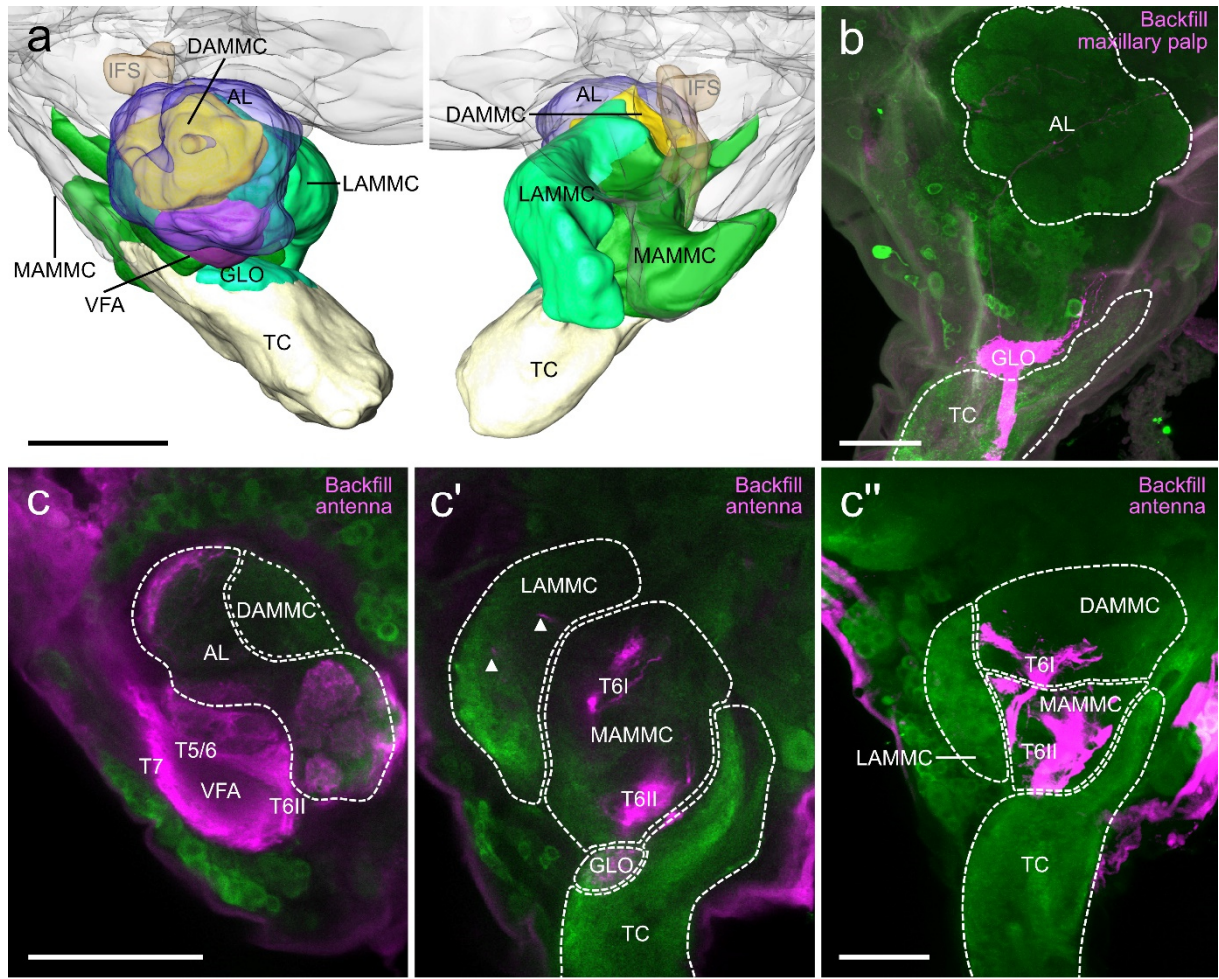
Figure 8

Figure 9

Figure 10
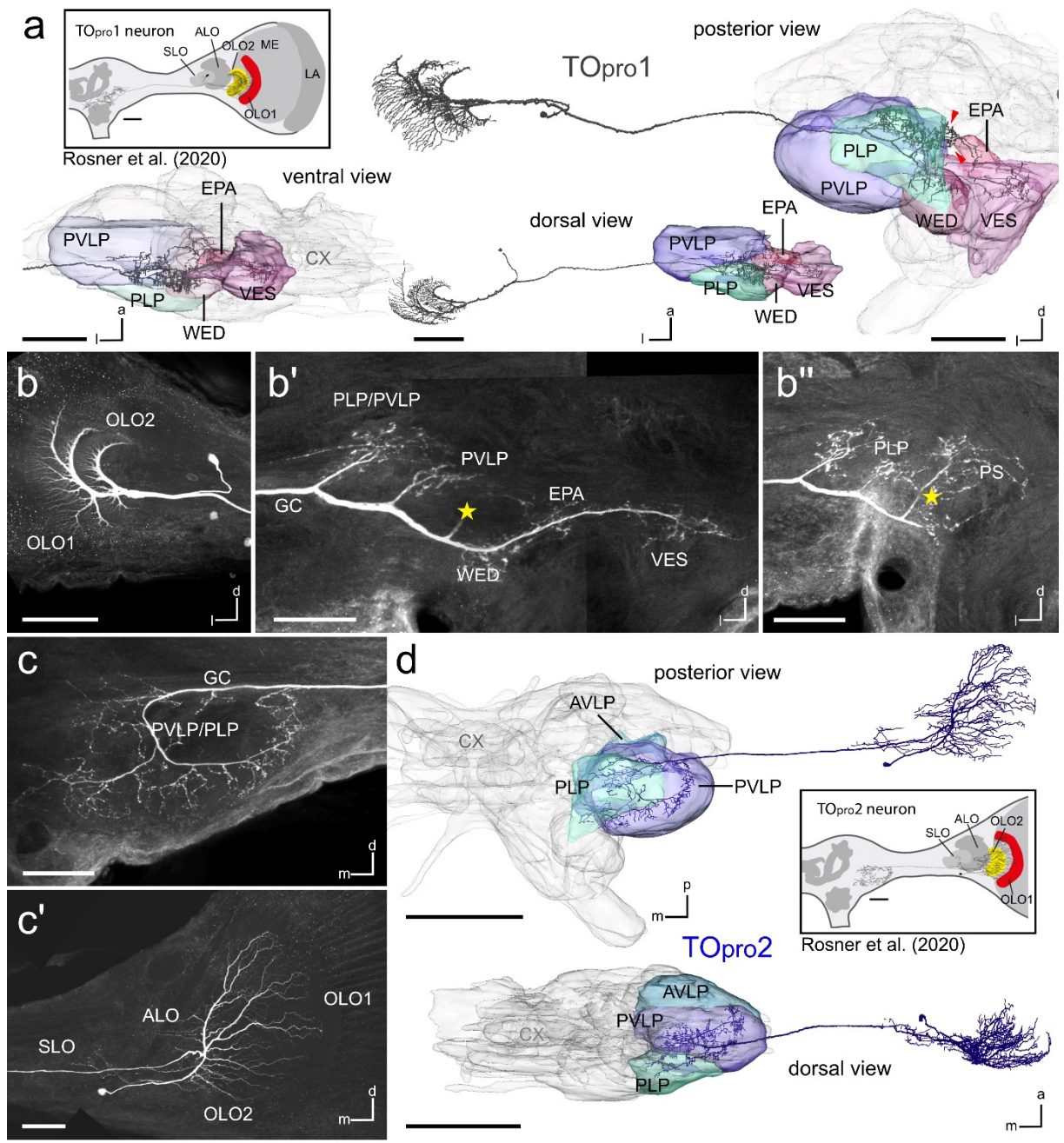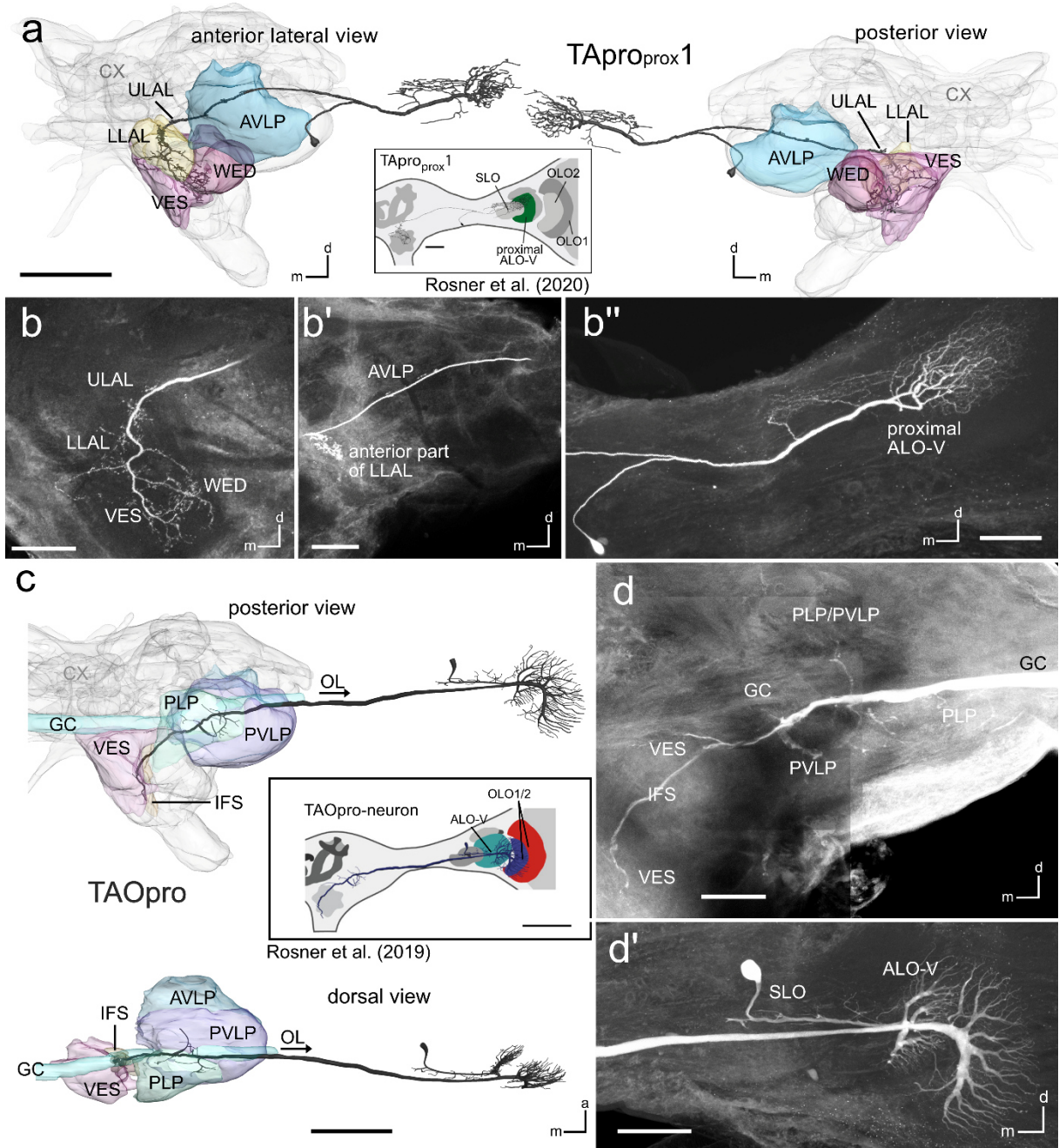
Figure 11

121

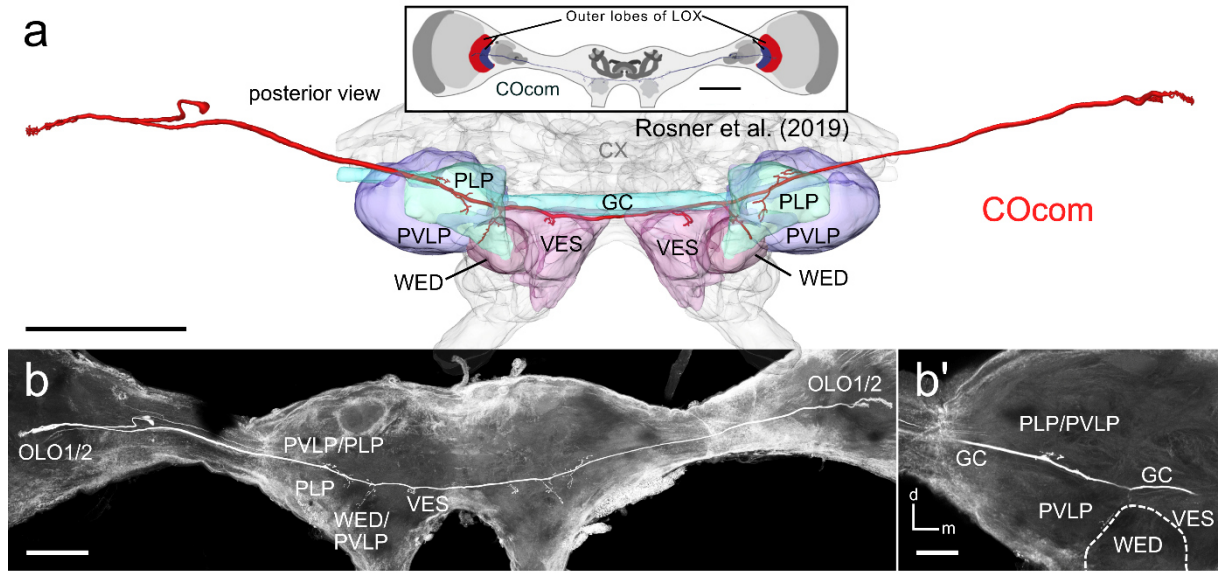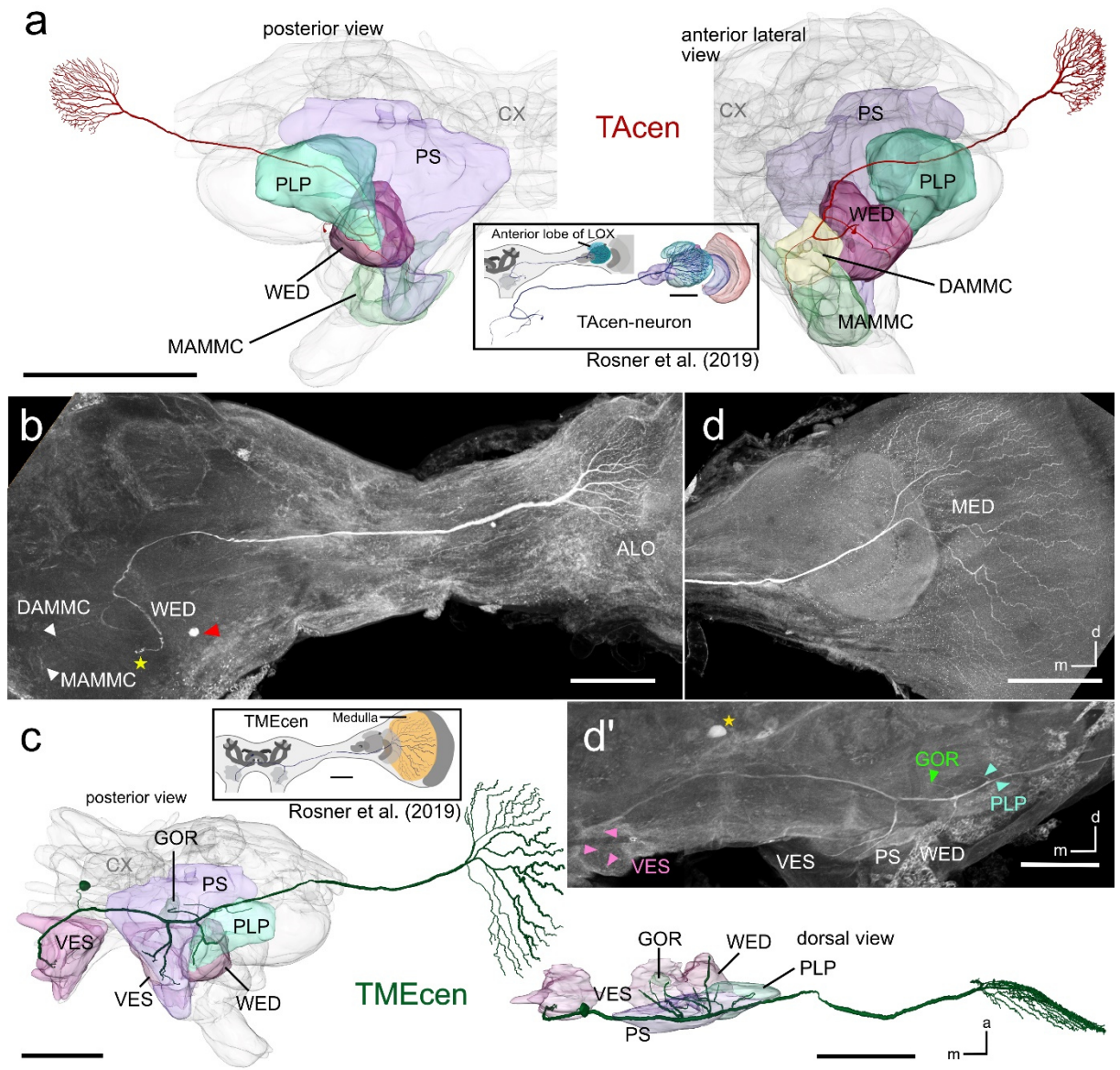Figure 12

Figure 12

Figure 13

123

Figure 14

Kapitel 2   Neuroarchitektur des Zentralkomplexes der Madeiraschabe *Rhyparobia maderae*

Synopsis (Projekt III)

Im Zentrum des Interesses vieler Grundlagenforschungen im Insektengehirn liegt der Zentralkomplex. Er ist involviert in eine Vielzahl von Informationsprozessierungen, gilt als Navigationszentrum des Gehirns und zeigt innerhalb der Insekten eine relativ stark konservierte Neuroarchitektur. Der Zentralkomplex umfasst den Zentralkörper (CB), bestehend aus oberer (CBU*)* und unterer Einheit (CBL), den paarigen Noduli (NO) und der Protozerebralbrücke (PB). Viele funktionelle Untersuchungen konzentrierten sich dabei auf Kopfrichtungskodierung innerhalb der CX Untereinheiten, untersucht in der Fliege, Biene oder Heuschrecke. Jedoch ist wenig über seine Organisation und Funktion bei nachtaktiven Insekten, wie der Schabe *R. maderae*, bekannt. Eine Ausnahme bildet beispielsweise die vergleichende Forschung an dem tag- und nachtaktiven Mistkäfer (el Jundi et al., 2018). Schaben sind agile und stark anpassungsfähige Tiere, deren Orientierung stark auf Informationen antennalen Ursprungs basiert. Sie nutzen ihre langen Antennnen unter anderem für Objekterkennung und Hindernisüberwindung (Harley et al., 2009; Watson et al., 2002), aber auch für geruchsbasierte Orientierung (Willis & Avondet, 2005). Erste Erkenntnisse zeigten, dass diese Fähigkeiten der räumlichen Orientierung und motorischen Kontrolle innerhalb des CX prozessiert werden (Harley & Ritzmann, 2010; Ritzmann et al., 2012; Varga et al., 2017). Der CX in der Madeiraschabe *R. maderae* zeigt eine ähnliche Anatomie wie die anderer bekannter Insektenarten. Seine Neuroanatomie ist besonders geprägt durch kolumnäre, tangentiale und pontine Neurone.

Basierend auf der drei-dimensionalen Rekonstrukion des Schabengehirns konnten die Neurone des CX genaustens analysiert und katalogisiert werden. Mit dieser Arbeit wurde ein Grundstein zur Neuroarchitektur des CX der Schabe gesetzt und kolumnäre und pontine Neurone mit Hilfe von Einzelzellfärbungen und unterschiedlichen Immunfärbungen analysiert und zwei- sowie drei-dimensional rekonstruiert. Ihre Verzweigungsgebiete wurden beschrieben und Verzweigungsmuster wurden, soweit möglich, erarbeitet. Die PB ist einteilbar in 18 vertikale Kolumnen, ähnlich wie die der Hummel *Bombus terrestris* (Sayre et al., 2021), der Fliege *D. melanogaster* (Wolff et al., 2015) oder der Heuschrecke *Schistocerca gregaria* (Hensgen et al., 2022). Auch die CBU in *R. maderea* zeigt eine ähnliche Einteilung mit der von *D. melanogaster* (Hulse et al., 2021) und *B. terrestris* (Sayre et al., 2021), je nach Neuronenset kann diese in 8 oder 9 vertikale Kolumnen eingeteilt werden. Diese werden geformt durch CPU/POU Neurone (8 Scheiben) oder CU Neurone (9 Scheiben). Auffällig in der Schabe ist der unterschiedliche Aufbau der CBL, die sich in 8 stark abgegrenzte Zapfen einteilen lässt, die umschlossen sind durch 9 umliegende Zähne. Unsere Studie zeigt, dass Neurone im CX der Schabe stark mit der anterioren Lippe (ALI) verbunden sind.

Die ALI ist eine bisher wenig erforschte Region, nahe des CX, der in der Schabe sehr prominent ist, dagegen in der Biene reduziert und in der Fliege bisher unbekannt ist. Wir konnten zudem, neben schon bekannten Neuronentypen, 6 neue Typen von Neuronen beschreiben, von denen bisher kein äquivalenter Typ aus anderen Insektenarten bekannt ist.

Durch zukünftige Untersuchungen der tangentialen Neuronentypen in der Schabe, die derzeit in Arbeit sind, sollen die Erkenntnisse über die Neuroanatomie und die Schichtung des CX erweitert werden. Diese Neuronenkatalogisierung und die zukünftig folgende Arbeit über die Neuroarchitektur von tangentialen Neuronen ist eine wichtige Basis zur Erstellung eines vollständigen Konnektoms innerhalb des CX in der Schabe.

Referenzen

el Jundi, B., Warrant, E. J., Pfeiffer, K., & Dacke, M. (2018). Neuroarchitecture of the dung beetle central complex. *Journal of Comparative Neurology 526*, 2612–2630. https://doi.org/10.1002/cne.24520

Harley, C. M., English, B. A., & Ritzmann, R. E. (2009). Characterization of obstacle negotiation behaviors in the cockroach*, Blaberus discoidalis*. *Journal of Experimental Biology 212*, 1463–1476. https://doi.org/10.1242/jeb.028381

Harley, C. M., & Ritzmann, R. E. (2010). Electrolytic lesions within central complex neuropils of the cockroach brain affect negotiation of barriers. *Journal of Experimental Biology 213*, 2851–2864. https://doi.org/10.1242/jeb.042499

Hensgen, R., Dippel, S., Hümmert, S., Jahn, S., Seyfarth, J., & Homberg, U. (2022). Myoinhibitory peptides in the central complex of the locust *Schistocerca gregaria* and colocalization with locustatachykinin-related peptides. *Journal of Comparative Neurology 530*, 2782–2801. https://doi.org/10.1002/cne.25374

Hulse, B. K., Haberkern, H., Franconville, R., Turner-Evans, D., Takemura, S. Y., Wolff, T., Noorman, M., Dreher, M., Dan, C., Parekh, R., Hermundstad, A. M., Rubin, G. M., & Jayaraman, V. (2021). A connectome of the *Drosophila* central complex reveals network motifs suitable for flexible navigation and context-dependent action selection. *Elife 10*. https://doi.org/10.7554%2FeLife.66039

Ritzmann, R. E., Harley, C. M., Daltorio, K. A., Tietz, B. R., Pollack, A. J., Bender, J. A., Guo, P., Horomanski, A. L., Kathman, N. D., Nieuwoudt, C., Brown, A. E., & Quinn, R. D. (2012). Deciding which way to go. How do insects alter movements to negotiate barriers? *Frontiers in Neuroscience 6*, 97. https://doi.org/10.3389/fnins.2012.00097

Sayre, M. E., Templin, R., Chavez, J., Kempenaers, J., & Heinze, S. (2021). A projectome of the bumblebee central complex. *Elife 10*, e68911. https://doi.org/10.7554/eLife.68911

Varga, A. G., Kathman, N. D., Martin, J. P., Guo, P., & Ritzmann, R. E. (2017). Spatial navigation and the central complex: Sensory acquisition, orientation, and motor control. *Frontiers in Behavioral Neuroscience 11*, 4. https://doi.org/10.3389/fnbeh.2017.00004

Watson, J. T., Ritzmann, R. E., Zill, S. N., & Pollack, A. J. (2002). Control of obstacle climbing in the cockroach, *Blaberus discoidalis.* I. Kinematics. *Journal of Comparative Physiology A 188*, 39–53. https://doi.org/10.1007/s00359-002-0277-y

Willis, M. A., & Avondet, J. L. (2005). Odor-modulated orientation in walking male cockroaches *Periplaneta americana*, and the effects of odor plumes of different structure. *Journal of Experimental Biology, 208*, 721–735. https://doi.org/10.1242/jeb.01418

Wolff, T., Iyer, N. A., & Rubin, G. M. (2015). Neuroarchitecture and neuroanatomy of the *Drosophila* central complex: A GAL4-based dissection of protocerebral bridge neurons and circuits. *Journal of Comparative Neurology 523*, 997–1037. https://doi.org/10.1002/cne.23705

Projekt III

Neuroarchitecture of the central complex in the Madeira cockroach *Rhyparobia maderae*: pontine and columnar neuronal cell types

RESEARCH ARTICLE

JCN RESEARCH IN SYSTEMS NEUROSCIENCE
THE JOURNAL OF COMPARATIVE NEUROLOGY

WILEY

Neuroarchitecture of the central complex in the Madeira cockroach *Rhyparobia maderae*: Pontine and columnar neuronal cell types

Stefanie Jahn[1] | Vanessa Althaus[1] | Jannik Heckmann[1] | Mona Janning[1] |
Ann-Katrin Seip[1] | Naomi Takahashi[1] | Clara Grigoriev[1] | Juliana Kolano[1] |
Uwe Homberg[1,2]

[1]Animal Physiology, Department of Biology, Philipps University of Marburg, Marburg, Germany

[2]Center for Mind Brain and Behavior (CMBB), University of Marburg and Justus Liebig University Giessen, Marburg, Germany

Correspondence
Uwe Homberg, Animal Physiology, Department of Biology, Philipps University of Marburg, D-35032 Marburg, Germany.
Email: homberg@staff.uni-marburg.de

Present address
Jannik Heckmann, OEP-Biology c/o Institute for Zoology, Rheinische Friedrich-Wilhelms-Universität Bonn, D-53115 Bonn, Germany.

Naomi Takahashi, Research Center for Integrative Evolutionary Science, SOKENDAI, Shonan Village, Hayama, Kanagawa, 240-0193, Japan.

Abstract

Insects have evolved remarkable abilities to navigate over short distances and during long-range seasonal migrations. The central complex (CX) is a navigation center in the insect brain that controls spatial orientation and directed locomotion. It is composed of the protocerebral bridge (PB), the upper (CBU) and lower (CBL) division of the central body, and a pair of noduli. While most of its functional organization and involvement in head-direction coding has been obtained from work on flies, bees, and locusts that largely rely on vision for navigation, little contribution has been provided by work on nocturnal species. To close this gap, we have investigated the columnar organization of the CX in the cockroach *Rhyparobia maderae*. *Rhyparobia maderae* is a highly agile nocturnal insect that relies largely but not exclusively on antennal information for navigation. A particular feature of the cockroach CX is an organization of the CBU and CBL into interleaved series of eight and nine columns. Single-cell tracer injections combined with imaging and 3D analysis revealed five systems of pontine neurons connecting columns along the vertical and horizontal axis and 18 systems of columnar neurons with topographically organized projection patterns. Among these are six types of neurons with no correspondence in other species. Many neurons send processes into the anterior lip, a brain area highly reduced in bees and unknown in flies. While sharing many features with the CX in other species, the cockroach CX shows some unique attributes that may be related to the ecological niche of this insect.

KEYWORDS
central complex, insect brain, neuroanatomy, neuronal cell types, *Rhyparobia maderae*

129

1 | INTRODUCTION

Insects, like other animals, face the challenge of finding mating partners, food, and shelter in often diverse and unknown environments. Therefore, they must be able to efficiently navigate within their home range and beyond. One insect group in which diverse navigation strategies and their underlying neuronal control have been studied is cockroaches. Research on different cockroach species provided insight into obstacle avoidance (Harley et al., 2009), climbing behavior (Watson, Ritzmann, & Pollack, 2002), goal-directed locomotion (Varga et al., 2017), and escape strategies (Ritzmann, 1984). Cockroaches are particularly agile insects and rely strongly on antennal information for object negotiation (Harley et al., 2009), climbing maneuvers (Watson, Ritzmann, Zill, et al., 2002), odor-guided orientation (Seelinger & Gagel, 1985; Willis & Avondet, 2005), and escape responses. Escape behavior, studied intensely in the American cockroach *Periplaneta americana*, is triggered by multisensory cues, in particular wind direction, and is mediated by receptors on the cerci and antennae. Fast-conducting giant and more slowly conducting nongiant interneurons direct the escape in a preferred set of escape angles away from the threat (Burdohan & Comer, 1990; Camhi & Tom, 1978; Domenici et al., 2008; Stierle et al., 1994). Research on the German cockroach *Blattella germanica* showed that cockroaches are, in addition, formidable navigators during goal-directed orientation (Durier & Rivault, 1999; Rivault & Durier, 2004). They use visual landmarks and olfactory cues for negotiating their return path to a shelter and, even as nymphs, are able to use path integration in complete darkness based exclusively on idiothetic cues to find home (Durier & Rivault, 1999).

A brain area intimately involved in navigational tasks is the central complex (CX). The CX is an assemblage of several highly interconnected neuropils spanning the brain midline, consisting of the protocerebral bridge (PB), the upper (CBU) and lower divisions (CBL) of the central body (CB), also termed fan-shaped body (FB) and ellipsoid body (EB), and, in pterygote insects, a pair of globular-shaped noduli (NO). The PB and CB are subdivided into arrays of 16 or 18 columns and the CB, in addition, into a species-specific number of layers (Homberg et al., 2023; Hulse et al., 2021; Pfeiffer, 2023; Pfeiffer & Homberg, 2014). Studies on several insects including cockroaches showed that the CX transforms navigation-related multisensory inputs into goal-oriented premotor commands depending on behavioral context and internal needs of the animal. Single-cell recordings in locusts, crickets, dung beetles, bees, and butterflies suggest that the CX is involved in sun compass orientation (el Jundi et al., 2014, 2015; Heinze & Homberg, 2007; Heinze & Reppert, 2011; Sakura et al., 2008; Stone et al., 2017). In flies and locusts, it encodes head direction relative to multisensory cues in a topographic compass-like manner (reviewed by Homberg et al., 2023; Honkanen et al., 2019; Pfeiffer, 2023). As shown in *Drosophila melanogaster*, the CX is, in addition, the site of navigation vector memory (Neuser et al., 2008; Strausfeld, 1999; Strauss, 2002). By contacting descending neurons through its outputs in the adjacent lateral complex (LX), it is directly involved in memory-directed steering during flight and walking (Rayshubskiy et al., 2020). Brain lesions as well as multielectrode extracellular recordings in the cockroach *Blaberus discoidalis*, likewise, indicate that the CX plays a crucial role in spatial navigation

and motor control (Ritzmann et al., 2012; Varga et al., 2017). Martin et al. (2015) showed that the CX is involved in adjusting walking speed as well as walking direction in freely moving cockroaches, while lesions in the cockroach CX led to impaired turning behavior (Harley & Ritzmann, 2010).

The cellular architecture of the CX has been studied in several insect species, notably the desert locust (Heinze & Homberg, 2008; Müller et al., 1997; von Hadeln et al., 2020), fruit fly (Hanesch et al., 1989; Hulse et al., 2021; Wolff & Rubin, 2018; Wolff et al., 2015), monarch butterfly (Heinze et al., 2013), dung beetles (el Jundi et al., 2018), honeybee (Hensgen, England, et al., 2021; Homberg, 1985), and bumble bee (Sayre et al., 2021). Three major types of CX neurons were distinguished across species. Tangential neurons connect diverse brain regions to particular horizontal layers and thus are major inputs to the CX (Hanesch et al., 1989; Honkanen et al., 2019; von Hadeln et al., 2020). Columnar neurons connect single vertical slices of the PB and/or the CB with the NO and certain areas in surrounding neuropils. They often but not always form sets of eight or nine neurons per hemisphere and one neuron per vertical slice (Heinze & Homberg, 2008; Sayre et al., 2021). Many types of columnar neurons serve as outputs from the CX navigation network and provide connections to descending pathways. Pontine neurons (hΔ neurons in *D. melanogaster*), the third major cell type, are intrinsic neurons that connect two or more vertical slices of the CBU with each other (Hanesch et al., 1989; Heinze & Homberg, 2008) and, as shown in *D. melanogaster*, contribute to transformation of movements from body- to world-centric space (Lu et al., 2022; Lyu et al., 2022).

In the cockroach *Rhyparobia maderae*, a model organism for research on circadian rhythms (Homberg et al., 2003; Stengl et al., 2015), the gross organization of the CX has been studied recently (Althaus et al., 2022), but no data are available on its cellular composition. By analyzing the morphology of columnar and pontine neurons of the cockroach CX, we aim to broaden our understanding of the variability and evolution of the navigation network in the insect brain. Our analysis, moreover, serves as a basis for physiological work on the cockroach navigation network and will complement an ongoing connectomics analysis of the CX network in *R. maderae*.

2 | MATERIAL AND METHODS

2.1 | Animals

Madeira cockroaches (*Rhyparobia maderae*, formerly termed *Leucophaea maderae*) of both sexes were obtained from crowded colonies at the Department of Biology, Philipps University Marburg. Animals were kept at a temperature of 25–26°C, with a relative humidity of 50%, and reared under a 12:12-h light/dark cycle.

2.2 | Preparation and Neurobiotin injections of single neurons

Animals were cold-anesthetized at 4°C and then fixed with their heads uppermost on a special metal holder using dental wax. The head

capsule of the animal was opened anteriorly for single-cell intracellular tracer application. Fat tissue and trachea were removed above the brain, while it was kept moist with insect saline (4.088 g NaCl, 0.186 g KCl, 0.102 g $MgCl_2 \times 6\,H_2O$, 0.168 g $NaHCO_3$, 0.4125 g NaH_2PO_4, 0.801 g glucose in 0.5 L H_2O; pH 7.25). The neural sheath was removed to allow insertion of a glass electrode. A wire loop was positioned posterior to the brain to reduce movement. Tracer injections were done with sharp glass microelectrodes (Hilgenberg) pulled with a Flaming/Brown horizontal puller (P-97; Sutter Instrument). The tip of the glass electrode was filled with 4% Neurobiotin (Vector Laboratories) in 1 mol·L^{-1} KCl, and the shank was backed up with 1 mol·L^{-1} KCl. Signals were amplified 10× (BA-01X amplifier; npi electronic instruments), visualized with an oscilloscope (Hameg), and displayed acoustically through an audiomonitor. Using a micromanipulator (Scientifica), the electrode was inserted into the brain from a frontal direction to a depth of 100–350 μm. Penetration of neuronal cell membranes was achieved by using the buzzing function of the amplifier and was indicated by the recording of action potentials. Neurobiotin was injected into the neuron by applying a positive current (between 0.5 and 1.5 nA) for 1–10 min. Thereafter, the brains were dissected and fixed in Neurobiotin fixative solution (4% paraformaldehyde, 0.25% glutaraldehyde, and 0.25% saturated picric acid in 0.1 mol·L^{-1} phosphate-buffered saline [PBS]) or 4% paraformaldehyde in sodium phosphate buffer (NaPi; 28.04 g $Na_2HPO_4 \times 2\,H_2O$ and 5.244 g $NaH_2PO_4 \times H_2O$ in 2 L H_2O) overnight at 4°C. For storing up to 2 weeks, the brains could be transferred to 0.1 mol·L^{-1} NaPi.

For visualization of the Neurobiotin tracer, the fixed brains were washed 4 × 15 min in 0.1 mol·L^{-1} PBS (containing 78.8 mmol·L^{-1} $Na_2HPO_4 \times 2\,H_2O$ and 19 mmol·L^{-1} $NaH_2PO_4 \times H_2O$; pH 7.4) and incubated for 3 days in streptavidin-cyanin-3 (Strep-Cy3; Dianova, 1:1000, RRID: AB_2337244) in 0.1 mol·L^{-1} PBT (PBS with 0.3% Triton X-100; TrX; Sigma). After incubation, brains were washed 2 × 30 min in 0.1 mol·L^{-1} PBT followed by 3 × 20 min in 0.1 mol·L^{-1} PBS. They were subsequently dehydrated in an ascending ethanol series (30%, 50%, 70%, 90%, 95%, and 2 × 100% ethanol, 15 min each), transferred to a methyl salicylate:ethanol solution (50:50 for 15 min), and cleared during 30 min incubation in pure methyl salicylate. The brains were finally mounted in Permount medium (Fisher Scientific) between two cover slips. Reinforcement rings were used as spacers.

2.3 | Immunolabeling of rehydrated Neurobiotin-injected brains

To evaluate the morphology of single neurons in more detail, selected brains were rehydrated, sectioned at 130 μm in the frontal plane, and, as needed, immunolabeled with antibodies. For that, Permount-embedded brains from Section 2.2 were transferred to xylene (Roth) for 2–3 h and rehydrated through a descending ethanol series (2 × 100%, 95%, 90%, 70%, 50%, and 30% ethanol, 15 min each). Thereafter, brains were washed 3 × 15 min in 0.1 mol·L^{-1} PBS and frontally embedded in albumin/gelatin (12% ovalbumin, 4.8% gelatin in demineralized water) and again fixed at 4°C in 6% formaldehyde in PBS overnight. The following day, brains were sectioned

with a vibrating-blade microtome (VT 1200 S; Leica Biosystems) in the frontal plane adjusted to 130 μm. The sections were washed 2 × 10 min with 0.1 mol·L^{-1} PBS, 4 × 10 min with PBT and preincubated overnight at 4°C in 5% normal goat serum (NGS; Jackson ImmunoResearch, Cat# 005-000-121, RRID: AB_2336990) and then incubated in primary antibody solutions for 5 days. A rabbit antiserum against locustatachykinin II (LomTK-II; 1:30,000; Jena Bioscience, Cat# ABD-045, RRID: AB_2341129; Table 1) or an antiserum against Pea-MIP-1 (myoinhibitory peptide; 1:12,000; kindly provided by Dr. R. Predel, Cologne, RRID: AB_2314803; Table 1) was used depending on the Neurobiotin-labeled cell type, in combination with an antibody against synapsin (mouse monoclonal, SYNORF1, 1:50; kindly provided by Drs. E. Buchner and C. Wegener, Würzburg, Germany; RRID: AB_2315402; Table 1), to visualize the neuropil borders and layers. Followed by washing steps, 6 × 15 min in PBT, the sections were incubated in the secondary antibodies for 3 days. The solution consisted of Strep-Cy3, goat-anti-mouse IgG antiserum conjugated with cyanin-5 (GaM-Cy5, 1:300; Jackson ImmunoResearch, Cat# 115-175-146, RRID: AB_2338713) for labeling synapsin, and, for double immunolabeling, goat-anti-rabbit IgG antiserum conjugated with cyanin-2 (GaR-Cy2, 1:300; Jackson ImmunoResearch, Cat# 111-225-003, RRID: AB_2307385) with 1% NGS in PBT. After 3 days, the sections were washed 4 × 15 min in PBT and 2 × 15 min in PBS and again dehydrated in an ascending ethanol series (30%, 50%, 70%, 90%, 95%, and 2 × 100% ethanol, 5 min each). Finally, the sections were cleared in a 1:1 methyl salicylate:ethanol solution for 5 min followed by 15 min in pure methyl salicylate. The sections were mounted in Permount medium between two coverslips, using stacks of two reinforcement rings as spacers.

One brain was labeled for serotonin. Here, normal donkey serum (NDS; Jackson ImmunoResearch, Cat# 017-000-121, RRID: AB_2337258) was used in all solutions instead of NGS. The primary antibody solution consisted of a goat antiserum against serotonin (1:10,000; ImmunoStar, Cat# 20079, RRID: AB_572262; Table 1) and the antibody against synapsin. The secondary antibody solution consisted of Strep-Cy3, donkey-anti-mouse IgG antiserum conjugated with cyanin-2 (DaM-Cy2; 1:300; Jackson ImmunoResearch, Cat# 715-225-150; RRID: AB_2340415), and a donkey-anti-goat IgG antiserum conjugated with cyanin-5 (DaG-Cy5; 1:300; Jackson ImmunoResearch, Cat# 705-175-147, RRID: AB_2340415).

2.4 | Immunolabeling on 200-μm sections

For a detailed analysis of the internal organization of the PB, 200-μm sections were labeled for synapsin or double labeled for synapsin and LomTK-II using a LomTK-II antiserum (kindly provided by H.-J. Agricola, Jena) that was biotinylated as described by Vitzthum and Homberg (1998). Reconstructions of the CX and LX are based on 200-μm sections labeled only for synapsin. Animals were cold anesthetized at 4°C. After dissecting, brains were fixed in 4% paraformaldehyde in NaPi overnight. The next day, the brains were washed 3 × 15 min in PBS and embedded in albumin/gelatin. The brains were sectioned with a vibrating-blade microtome in the frontal plane adjusted to 200 μm. The

TABLE 1   Primary antibodies used.

Antibody	Immunogen	Source	Host species	Concentration	Reference
LomTK-II	Locustatachykinin-II coupled to bovine thyroglobulin with glutaraldehyde	Jena Bioscience	Rabbit	1:20,000	Vitzthum & Homberg, 1998; RRID: AB_2341129
LomTK-II (biotinylated)	Locustatachykinin-II coupled to bovine thyroglobulin with glutaraldehyde	H.-J. Agricola	Rabbit	1:30,000	Hensgen et al., 2022; Vitzthum & Homberg, 1998
Mas-AT	Glutaraldehyde conjugates of synthetic *Manduca sexta* allatotropin and thyroglobulin	J. A. Veenstra	Rabbit	1:10,000	Veenstra & Hagedorn, 1993; RRID: AB_2313973
Pea-MIP-1	Conjugates of *Periplaneta americana* myoinhibitory peptide 1 and thyroglobulin	R. Predel	Rabbit	1:12,000	Predel et al., 2001; Schulze et al., 2012; RRID: AB_2314803
Serotonin	Serotonin coupled to bovine serum albumin (BSA) with paraformaldehyde	ImmunoStar	Goat	1:10,000	Althaus et al., 2022; RRID: AB_572262
Synapsin	Fusion proteins of glutathione-S-transferase and *D. melanogaster* SYN1	E. Buchner and C. Wegener	Mouse	1:50	Wei et al., 2010; RRID: AB_2315425

sections were washed 2 × 10 min with 0.1 mol·L^{-1} PBS and 4 × 10 min with PBT. They were preincubated overnight at 4°C in 5% NGS in PBT for the synapsin labeling or for 4 h at room temperature for the LomTK-II/synapsin labeling and then transferred in the primary antibodies together with 1% NGS in PBT for 5 days. Antibodies against biotinylated LomTK-II (1: 30,000) and synapsin (1:50) were used for one brain. A second brain was only labeled with the antibody against synapsin. After washing the sections 6 × 15 min with PBT, they were incubated with the secondary antibodies and 1% NGS for 7 days. Either GaM-Cy5 and GaR-Cy2 (for the double labeling) or only GAM-Cy5 was used. Finally, the sections were washed, dehydrated, cleared, and mounted in Permount as described in Section 2.3 but with three reinforcement rings as spacers.

2.5 | Immunolabeling on 130-μm sections

Sections of 130-μm thickness were stained with the antibody against synapsin to reveal the internal structure of the LX and the position of the CX within the brain. Brains were dissected, fixed, sectioned at 130 μm, and washed as described in Section 2.4. The sections were preincubated for 3 h in 5% NDS or NGS in PBT with 5% TrX at room temperature and incubated with anti-synapsin and 2% NDS or NGS in PBT with 5% TrX for 2 days. After washing 6 × 15 min with PBT, the sections were incubated with a Cy5-conjugated donkey-anti-mouse IgG (DaM-Cy5; 1:300; Jackson ImmunoResearch Labs, Cat# 715-175-150, RRID: AB_2340819) diluted in 1% NDS or Cy5-conjugated goat-anti-mouse IgG (1:300) diluted in 1% NGS in PBT with 5% TrX for 1 day. The sections were further treated as described in Section 2.4.

2.6 | Immunolabeling on 40-μm sections

For analysis of the internal structure of the CBU and CBL, 40-μm sections were triple labeled with a polyclonal antiserum against

allotropin (Mas-AT; kindly provided by J. A. Veenstra, Bordeaux; RRID: AB_2313973; Table 1), serotonin, and anti-synapsin. Brains were dissected as described in Section 2.4 but were only fixed for 2 h. Then, the brains were washed 4 × 10 min in PBS and 1 × 5 min with saline-substituted Tris buffer (SST; 0.1 mol·L^{-1} Tris–HCl/0.3 mol·L^{-1} NaCl, pH 7.4) containing 0.1% TrX and embedded in albumin/gelatin as described above. The brains were sectioned in the frontal or sagittal plane at a thickness of 40 μm. The sections were subsequently washed 5 × 10 min with SST with 0.1% TrX. The sections were preincubated with 5% NDS in SST with 0.5% TrX for 1 h at room temperature followed by incubation with the primary antibodies against synapsin (1:50), serotonin (1:10,000), and Mas-AT (1:10,000) with 2% NDS in SST with 0.5% TrX for 20 h at room temperature. The sections were washed 5 × 10 min with SST with 0.1% TrX and incubated for 2.5 h with Cy2-conjugated donkey-anti-mouse (DaM-Cy2; 1:300; Jackson ImmunoResearch Labs, Cat# 715-225-150, RRID: AB_2340826), Cy3-conjugated donkey-anti-rabbit (1:300), and Cy5-conjugated donkey-anti-goat (1:300) with 2% NDS in SST with 0.5% TrX. After washing the sections 5 × 10 min with SST with 0.1% TrX, they were mounted on chrome alum–gelatin-coated glass slides and left to dry overnight. Finally, they were dehydrated and embedded in Entellan (Merck).

2.7 | Antibody characterization

The polyclonal rabbit antiserum against LomTK-II (K1-50820091; Table 1), kindly obtained from Dr. Hans Agricola (University of Jena, Germany), was biotinylated as described by Vitzthum and Homberg (1998). Staining with the biotinylated and nonbiotinylated antiserum resulted in identical staining patterns on brain sections from the desert locust (Hensgen et al., 2022; Vitzthum & Homberg, 1998).

The polyclonal antiserum against LomTK-II (Jena Bioscience, Cat# ABD-045, RRID: AB_2341129; Table 1) was raised in rabbit against locustatachykinin-II coupled to bovine thyroglobulin with glutaraldehyde (Veenstra et al., 1995). Its specificity was tested by enzyme-linked

immunosorbent assay (ELISA) with synthetic LomTK-I and -II and callitachykinins-I and -II, the LomTK orthologs from the fly *Calliphora vomitoria*, as antigens (Nässel et al., 1995). The antiserum cross-reacted with all four tachykinins but had a slightly higher affinity for the LomTKs. On brain sections of the cockroach *R. maderae*, the pattern of immunostaining using the LomTK-II antiserum was indistinguishable from that obtained with an antiserum against LomTK-I (Muren et al., 1995). Preadsorption of the diluted antiserum with 10 μmol·L^{-1} LomTK-II abolished all immunostaining on brain sections from the cockroach *R. maderae*.

The polyclonal antiserum against Mas-AT (generously provided by Dr. J. A. Veenstra, University of Bordeaux, France; RRID: AB_2313973; Table 1) was raised in rabbit against synthetic *Manduca sexta* allatotropin coupled to glutaraldehyde conjugates of Mas-AT and thyroglobulin. Its specificity and cross-reaction with Lom-AG-MT I, the Mas-AT ortholog from the migratory locust, were tested by ELISA with synthetic Lom-AG-MTI as an antigen (Veenstra & Hagedorn, 1993). Preadsorption of the diluted antiserum with 0.1 μmol·L^{-1} Mas-AT abolished all immunostaining on brain sections from *R. maderae* (Petri et al., 1995).

The polyclonal antiserum against Pea-MIP-1 (generously provided by Dr. R. Predel, University of Cologne, Germany; RRID: AB_2314803; Table 1) was raised in rabbit against conjugates of *Periplaneta americana* MIP-1 and thyroglobulin (Predel et al., 2001). On brain sections from *R. maderae*, immunostaining was abolished after preadsorption of the diluted antiserum with 100 nmol·L^{-1} Pea-MIP-1 (Schulze et al., 2012).

The antiserum against serotonin (ImmunoStar, anti-5-HT, Cat# 20079; RRID: AB_572262; Table 1) was raised in goat against serotonin coupled to bovine serum albumin (BSA) with paraformaldehyde. Labeling is abolished by preadsorption of the diluted antiserum with 100 μg·mL^{-1} serotonin–BSA conjugate (ImmunoStar, product information sheet). In the brain of *R. maderae*, immunostaining with this antiserum and a second anti-serotonin antiserum (Sigma, Cat# S5545, RRID: AB 477522) resulted in identical staining patterns (Althaus et al., 2022).

The monoclonal antibody against synapsin (#3C11, kindly provided by Drs. E. Buchner and C. Wegener, University of Würzburg, Germany; RRID: AB_2315425) was raised in mice against parts of the *D. melanogaster* synaptic vesicle protein SYN1 fused with glutathione-S-transferase (Klagges et al., 1996). The antibody labels synaptic neuropil as shown in various insect species including the cockroach *R. maderae* (Althaus et al., 2022; Wei et al., 2010).

2.8 | Image acquisition

Whole-mount preparations and immunolabeled sections were scanned by a confocal laser scanning microscope (Leica, TCS SP5; Leica Microsystems) with a 20× oil immersion objective (HC PL APO 20×/0.75 Imm Corr CS2). For more detailed images, a 40× objective (HCX PL APO 40×/1.25-0.75 Oil) was used. Images were acquired at a resolution of 1024 × 1024 pixels in the *xy*-plane (pixel size: 0.75 × 0.75 μm) and a step size of 0.5 μm or 1 μm in the *z* direction. Scanning frequency was 400 Hz. Cy2 fluorescence was excited by

an argon laser (488 nm), Cy3 fluorescence by a diode-pumped solid-state laser (561 nm), and Cy5 fluorescence with the helium–neon laser (633 nm). Image stacks were merged with the software AMIRA 6.5 (ThermoFisher Scientific).

2.9 | Anatomical reconstruction and image processing

Three-dimensional (3D) reconstructions of neuropils and further processing of image stacks obtained with the confocal laser scanning microscope were done in AMIRA 6.5. The reconstruction of the outer boundaries of neuropils is based on synapsin staining. In addition, immunolabeling for Mas-AT and serotonin was included to obtain 3D reconstructions of the layering of the neuropils of the CX. By generating a 3D grid, the *Wrap*-module created polygonal surfaces that could be visualized through the *GenerateSurface* and the *SurfaceView* modules. For the 3D reconstruction of single neurons, the skeletonize plugin for AMIRA 5.6 (Evers et al., 2005; Schmitt et al., 2004) was used. Each cell was manually traced by *Snaxels*, and the diameter of each *Snaxel* was fitted automatically. Two-dimensional reconstructions of single neurons were done using Affinity Photo (Serif) by digitally tracing neurites from serial image stacks obtained from AMIRA 6.5. For the presentation of ramification areas, maximum-intensity visualizations of image stacks were produced with the *ImageOrthoProjection* module. Optimization of images and the assembly of final figures were achieved using Affinity Photo (Serif).

3 | RESULTS

The aim of this study was to provide a model of the cockroach CX and LX as well as a catalog of intrinsic and columnar neurons of the CX. The nomenclature for neuropils follows Ito et al. (2014) and, for brain areas specific to the cockroach, Althaus et al. (2022). Based on immunolabeling with antibodies raised against serotonin, Mas-AT, and the presynaptic marker synapsin, we performed 3D reconstructions of the subdivisions of the cockroach CX (Figure 1), the internal organization of the CB (Figure 2), and the neuropils of the LX (Figure 3).

Neurons are termed according to the nomenclature used in the locust *Schistocerca gregaria* (Heinze & Homberg, 2008) and the honeybee *Apis mellifera* (Hensgen, England, et al., 2021). Characterization of columnar neurons showed that the anterior lip (ALI) is closely connected to the CX. We therefore added a 3D reconstruction of the ALI to those of the CX and LX. All axes refer to the body axis of the animal.

3.1 | Nomenclature and neuroarchitecture of the CX and LX

The CX is located in the center of the cockroach brain medial to the pedunculus and dorsal to the medial lobe of the mushroom body. The closely connected LX lies posterior to the medial lobe and pedunculus and dorsomedial to the antennal lobe (Figure 1a). The CX consists of
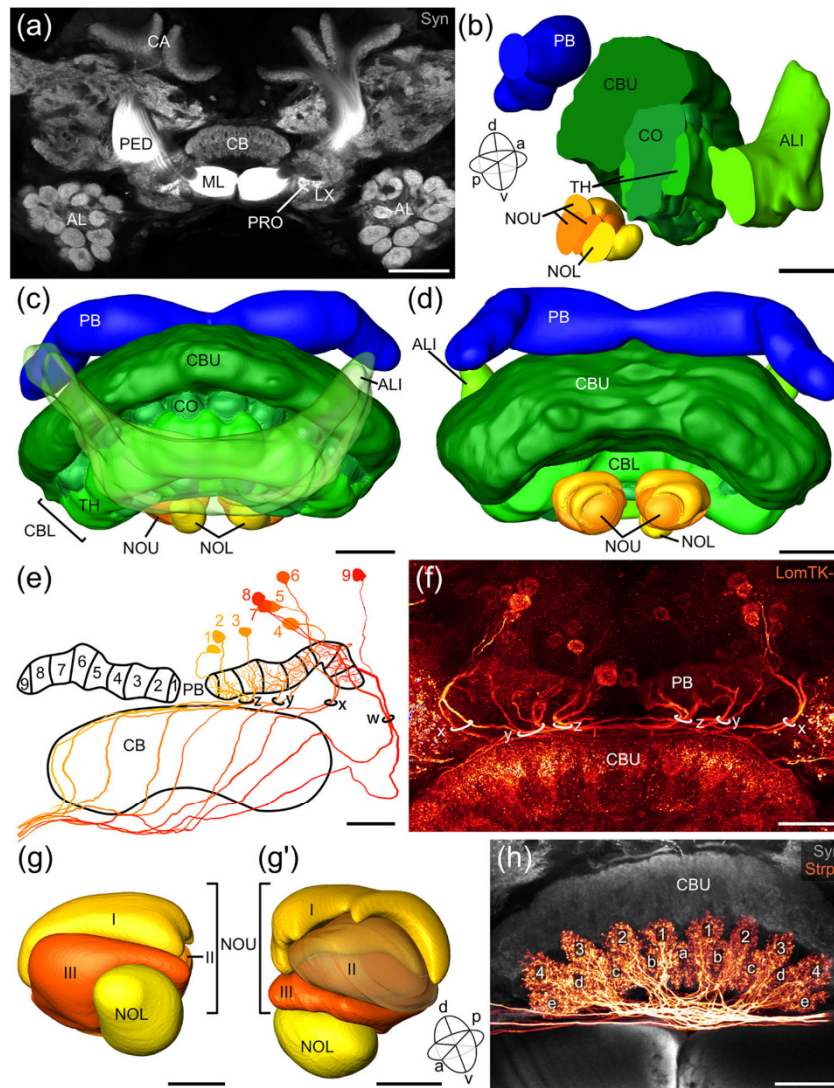
FIGURE 1 Organization of the cockroach central complex (CX) and anterior lip (ALI). (a) Synapsin immunolabeling showing the position of the central body (CB) and the lateral complex (LX) within the cockroach brain, frontal view. The CB is framed laterally by the pedunculi (PED) and ventrally by the medial lobes (ML) of the mushroom bodies. The calyces (CA) are located dorsally and the LX ventrolaterally. The prong (PRO), part of the LX, shows strong synapsin fluorescence. (b) Oblique view of sagittal surface cut of the CX and ALI. CO, cones of the CBL; TH, teeth of the CBL. (c) Three-dimensional reconstruction of the CX with transparent ALI, frontal view; (d) posterior view. (e) Two-dimensional reconstruction of LomTK-II-immunolabeled columnar neurons of the protocerebral bridge (PB). Each neuron innervates one slice of the PB. (f) Maximum projection view of LomTK-II immunolabeling illustrating the x-, y-, and z-bundles between the PB and the upper division of the central body (CBU). (g) Frontal and (g′) oblique 3D reconstruction of a nodulus (NO) illustrating the lower unit (NOL) and the three subunits of the upper unit (NOU). (h) Maximal intensity projection of synapsin immunostaining and mass staining of tangential neurons of the lower division of the central body (CBL) innervating cones 1–4 and teeth a–e. a, anterior; d, dorsal; p, posterior; v, ventral. Scale bars = 200 μm (a); 50 μm (b–f, h); 20 μm (g, g′).

the PB, the CB with CBU and CBL, and the paired NO (Figures 1b-d). Anteriorly, the CB is covered by the large ALI (Figure 1b,c).

The PB is a handlebar-shaped neuropil and the most posterior neuropil of the CX. It lies dorsally to the CB (Figure 1b–d). Its lateral ends are bent posterior-ventrally; both hemispheres are connected across the brain midline through a fiber bundle. The somata of pontine and

columnar neurons of the CX are concentrated dorsally from the PB in the pars intercerebralis. The arborization areas of columnar neurons labeled with the biotinylated antiserum against LomTK-II revealed nine columns, also termed slices, in each hemisphere of the PB that are connected with parts of the LX (Figure 1e,f). Their neurites pass through four fiber bundles, termed w-, x-, y-, and z-bundle (Figure 1e,f)
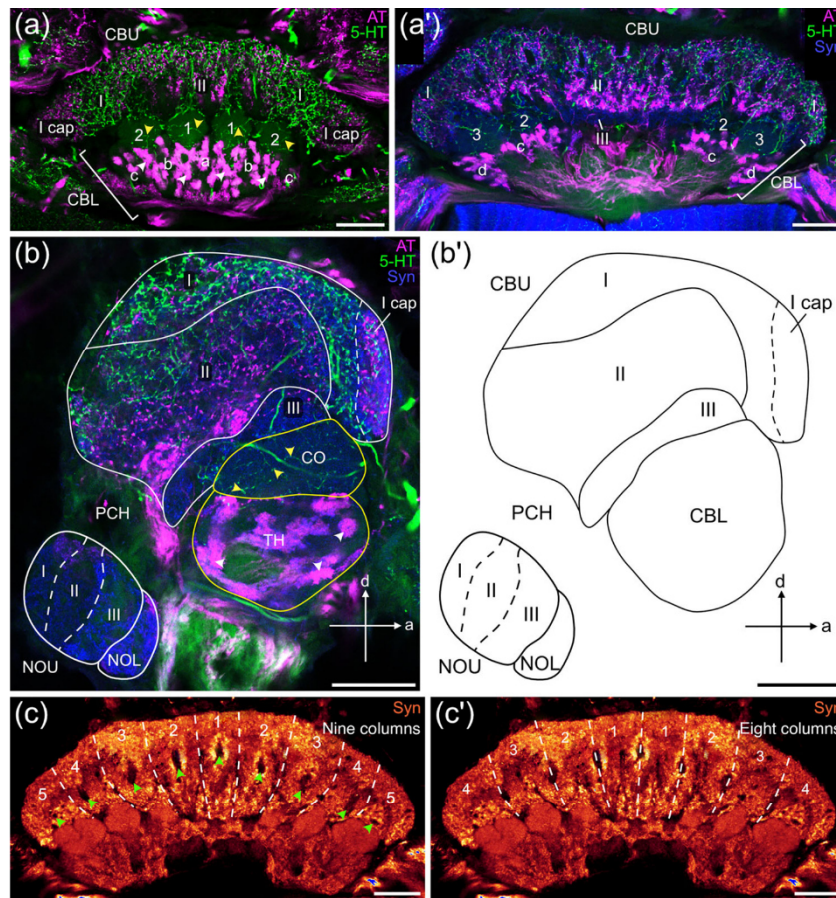
FIGURE 2 Organization of the upper (CBU) and lower (CBL) division of the central body. (a) Single frontal optical section showing Mas-AT (AT; magenta) and serotonin (5-HT; green) immunostaining to illustrate the layering of the CBU. Layer I cap contains only Mas-AT labeling and layer I only serotonin immunostaining. Layer II contains neuronal endings with both immunolabeled substances. (a′) Section at a more posterior level. No fibers that were labeled with one of the antisera exist in layer III. Numbers (1–3) refer to cones (CO) and letters (a–d) to teeth (TH) of the CBL. (b) Sagittal section slightly off the brain midline illustrating the arrangement of layers and sublayers of the CBU and the noduli. Yellow arrowheads in panels (a) and (b) point to serotonin-immunolabeled processes in the cones and white arrowheads to Mas-AT immunostaining in the teeth of the CBL. NOL, lower unit of the nodulus; NOU, upper unit of the nodulus. (b′) Schematic sagittal section through the central body (CB) corresponding to (b). a, anterior; d, dorsal. (c, c′) Combinations of two frontal optical sections immunostained for synapsin showing the columnar organization of the CBU with nine (c) and eight (c′) columns. Nine landmark fiber bundles indicate the column centers (green arrowheads in panel c) or boundaries between the columns (c′). Scale bars = 50 μm.

between the PB and the CB. Each of the w-, x-, and y-bundles contains two LomTK-II immunoreactive fibers, whereas three are located in the z-bundle. The innermost slice 1 of the PB is relatively slim, whereas the outer slice 9 is broader (Figure 1e,f).

The paired NO are located ventroposteriorly from the CBU and are composed of two subunits. The larger upper unit (NOU) consists of three layers (Figure 1g,g′). Only layer II contains orcokinin-immunolabeled arborizations (figure 7e in Althaus et al., 2022). The lower unit (NOL) is smaller, lies anteriorly attached to the NOU (Figure 1c,d,g,g′), and could be distinguished by synapsin staining.

The internal organization of the CBU was unraveled through immunolabeling with antisera against synapsin, serotonin, and Mas-AT

(Figure 2a,b). Thereby, three layers could be distinguished. Their nomenclature is based on a highly similar layering found in the desert locust (Heinze & Homberg, 2008; Homberg, 1991). Layer I contains few Mas-AT-immunostained arborizations, but is innervated by serotonin-immunolabeled fibers. It forms a conspicuous cap-like subdivision at the anterior part of the CBU that contains mostly Mas-AT-immunolabeled arborizations (I cap; Figure 2a,b). Layer II is the largest subunit of the CBU and comprises both serotonin-immunolabeled arborizations in the dorsoposterior part and Mas-AT-rich processes in the ventral part (Figure 2a,b). It occupies the most dorsoposterior volume of the CBU (Figure 2b) and is penetrated by fiber tracts running through the CBU (Figure 2c, green arrowheads). Layer III is the
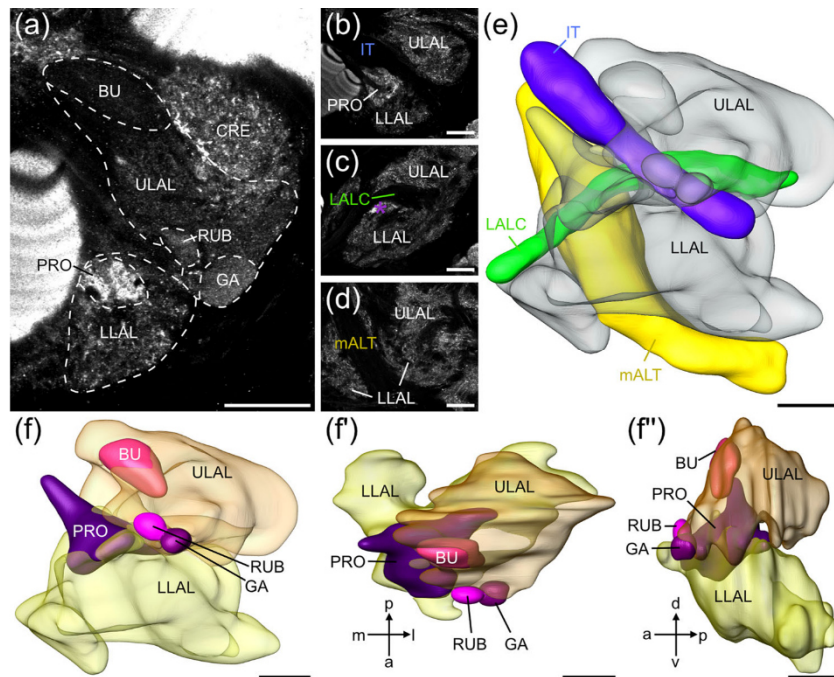
FIGURE 3 Morphology of the lateral complex (LX) and the adjacent rubus (RUB), illustrated by frontal synapsin-immunolabeled optical sections (a–d) and three-dimensional reconstructions (e–f″). (a) The LX is composed of five compartments: the bulb (BU), the upper and lower lateral accessory lobe (ULAL, LLAL), the gall (GA), and the prong (PRO; purple asterisk in panel c). Three fiber tracts, (b) the isthmus tract (IT, blue), (c) the LAL commissure (LALC, green), and (d) the medial antennal lobe tract (mALT; yellow) define the boundaries of the LX. (e) Three-dimensional reconstruction of the LX (light gray) and the three defining tracts IT (blue), LALC (green), and mALT (yellow), frontal view. (f, f″) Three-dimensional reconstruction of all subunits of the LX and the RUB (pink), viewed from frontal (f), dorsal (f′), and lateral (f″) directions. a, anterior; d, dorsal; l, lateral; m, medial; p, posterior; v, ventral. Scale bars = 50 μm.

smallest layer and forms the posterior–ventral sheet of the CBU. It is characterized by the complete absence of serotonin and Mas-AT staining but is rich in synapsin labeling (Figure 2a′,b). In addition to its layered horizontal organization, the CBU comprises two systems of vertical columns that overlap across the whole width of the CBU. They are formed by intertwined sets of different types of columnar neurons (see below). The endings of these cell types are confined to either one or the other system. Nine landmark fiber bundles (Figure 2c, arrowheads) that pass through the CBU served as boundary markers for both systems. The two outermost bundles are thinner than the other ones. One system consists of nine columns with the nine fiber bundles representing the column centers (Figure 2c), and the other system consists of eight columns separated by the bundles (Figure 2c′). In the nine-column system, neuronal endings are located between the fiber bundles, and in the 8-fold system, the endings lie on both sides of the bundles.

The CBL lies ventral to the CBU and consists of eight cone-like and nine tooth-like structures (Figures 1h and 2a; Homberg et al., 2018) that separate the cones. Both teeth and cones show strong GABA immunoreactivity (Homberg et al., 2018) originating from tangential neurons of the CBL (Figure 1h). The cone caps, the most dorsal parts of the cones, contain few fine serotonin-immunolabeled fibers

(Figure 2a,b; yellow arrowheads), while massive Mas-AT labeling with a patchy distribution is located within the teeth and the cone necks, the ventral part of the cones that lie between the teeth (white arrowheads in Figure 2a,b).

The most important input and output area of the CX is the LX (Figures 1a and 3). In the cockroach, it is subdivided into five subunits: the gall, the upper (ULAL) and lower lateral accessory lobe (LLAL), the prong, and the bulb (Althaus et al., 2022). The ULAL and LLAL are mainly defined by three fiber tracts—the isthmus tract (Figure 3b,e), the lateral accessory lobe (LAL) commissure (Figures 3c and 3e), and the medial antennal lobe tract (mALT; Figure 3d,e). Many CX neurons connect a specific subunit of the LX with the CX. The bulb is highly GABA immunoreactive and innervated by tangential neurons of the CBL, the gall is invaded by columnar neurons of the CBL, and the prong is a newly defined neuropil (Althaus et al., 2022) characterized by strong synapsin staining and arborizations of columnar neurons of the CBU and PB (see below). We included the rubus in the reconstruction (Figure 3a,f,f″). It adjoins directly to the LAL but belongs to the dorsally lying crepine. It is also identified by columnar neurons of the CBU (CU neurons).

Columnar and pontine neurons in the cockroach CX are termed following the nomenclature used for CX neurons in the desert locust

TABLE 2   Types of intrinsic and columnar neurons in the cockroach central complex and their arborization areas.

Cell type R. maderae	PB	CBU I cap	I	II	III	CBL CO	TH	NOU I	II	III	NOL IV	ALI	LX ULAL	LLAL	PRO	GA	CRE	RUB	Other	Proposed cell type D. melanogaster[1]
POU1																				hΔD?
POU2a																				hΔE?
POU2b																				/
POU3																				hΔM?
POUv																				vΔ
CP2-1	○													●			○			/
CP2-2	○						○							●			○			/
CL1	○						●									●				EPG/PEG
CL2	○									○										PEN
CPU1a-1	○													●			●			PFL1
CPU1a-3	○				□									●			●			/
CPU2	○			□										●		●				PFL2
CPU4b	○			●										●						
CPU5a	○		●					○						●						] PFN
CPU5d	○									●										
CU1			□											┐						FS1-3
CU2a-1			░				○							●			○			] FC
CU2a-2			░				○							●			○			
CU2c														●			●			FR1?
CU2d														●			●			/
CU3a														┐●						/
CU3b	○						○							●┐			●┐		┐●	/
CU4			░				○				●						●			/

Note: Black dots/bars, varicose arborizations; white dots/bars, fine arborizations; gray dots/bars, mixed arborizations.

Abbreviations: ALI, anterior lip; CBL, lower division of the central body; CBU, upper division of the central body; CO, cone; CRE, crepine; GA, gall; LLAL, lower lateral accessory lobe; LX, lateral complex; NOL, lower unit of the noduli; NOU, upper unit of the noduli; Other, other neuropils in the protocerebrum (further information see Figure 9); PB, protocerebral bridge; PRO, prong; RUB, rubus; TH, tooth; ULAL, upper lateral accessory lobe.

[a] According to Hulse et al. (2021).

(Heinze & Homberg, 2008; Müller et al., 1997). Table 2 summarizes the input (white dots) and output areas (black dots) of all described intrinsic and columnar neuron types investigated here. The right column lists the corresponding neuron names for *D. melanogaster*.

3.2 | Pontine neurons

We found five types of pontine neurons in the cockroach. POU1, POU2, and POU3 neurons connect two different columns of the CBU across the brain midline that are four columns apart and are hence termed pontine neurons of the CBU (Table 2). Their arborizations form eight columns within the CBU. All evaluated POU neurons have their somata in the pars intercerebralis. The cell body fiber of POU1 neurons ($n = 11$, soma diameter: 14–18 μm; Figure 4a) gives rise to fine arborizations confined to a single column on the ipsilateral side of the CBU. The main neurite passes the brain midline posterior to the CBU. It often bifurcates into two arms that enter a column of the CBU from the ventral direction, giving rise to mostly dense arborizations. POU1 neurons are highly variable in the innervated layers in the CBU, suggesting that they consist of several subtypes with distinct innervation domains (Figure 4a, black and magenta reconstructions). Arborizations are concentrated in parts of layer II but, especially on the ipsilateral side, may extend to layer I (Figure 4f).

POU2 neurons can be divided into two subtypes, POU2a and POU2b. Both arborization areas of POU2a neurons ($n = 7$, soma

diameter: 13–17 μm; Figure 4b) are concentrated in the most anterodorsal part of the CBU in layer I (Figure 4c,f). The ipsilateral innervation comprises fine endings, while the contralateral tree of ramifications is denser. The main neurite passes the midline of the brain posterior to the CBU. Unlike POU1 neurons, both innervation areas are entered from the dorsal direction. POU2b neurons ($n = 3$, soma diameter: 14–21 μm; Figure 4d), in contrast, have a main neurite that innervates columns exclusively from the ventral direction (Figure 4d). The main neurite passes the midline dorsoposterior from the CBU, and arborizations are concentrated in layer I of the CBU (Figure 4f). This type is the only one with a wider innervation area on the contralateral side covering two to three columns. Contralateral arborizations have a varicose appearance, while the ramifications on the ipsilateral side are fine (Figure 4d).

POU3 neurons ($n = 8$, soma diameter: 11–20 μm; Figure 4e) are characterized by two parallel arms of dendritic trees extending through a single column of the CBU from layers I to III. The main neurite passes the CBU dorsoposteriorly and innervates mostly layers I and II of the contralateral CBU (Figure 4f).

In contrast to POU1, POU2, and POU3 neurons that connect different columns of the CBU, the vertical POU neuron (POUv, $n = 1$, soma diameter: 13 μm) connects two different layers of the CBU within one CBU column (Figure 5). The soma is located in the pars intercerebralis. The main neurite passes the PB posteriorly before it sends fine processes from the ventral direction into layer III of one column of the CBU (Figure 5a, inset ii, and Figure 5b). The main neurite then continues
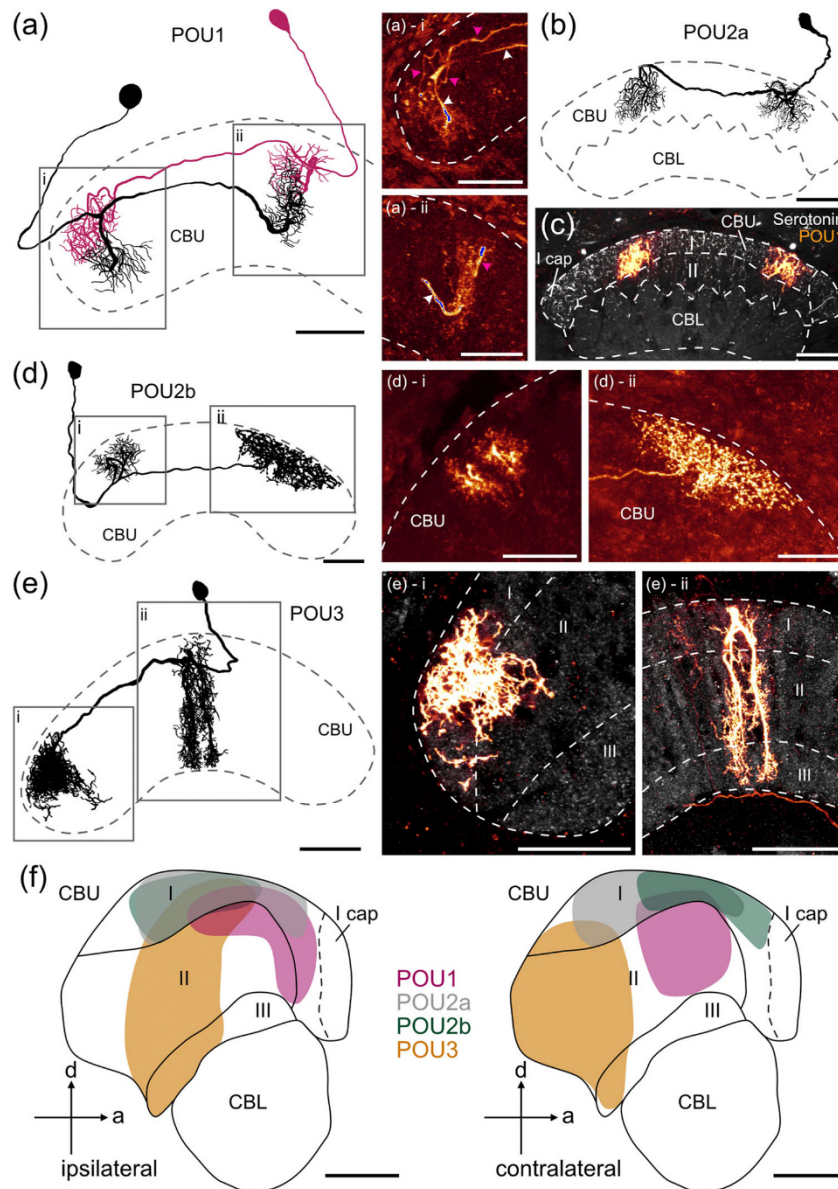
FIGURE 4 Morphology of POU neurons. (a) Two-dimensional reconstruction of two POU1 neurons with fine arborizations on the ipsilateral side (white arrowheads in inset i; magenta arrowhead in inset ii) of the upper division of the central body (CBU) and denser arborizations on the contralateral side (magenta arrowheads in inset i; white arrowhead in inset ii). (b) Two-dimensional reconstruction of a POU2a neuron. Its arborizations are located anterodorsally in the CBU and are concentrated in layer I. (c) Maximal intensity visualization of a POU2a neuron combined with serotonin immunolabeling (gray) to define the layers of the CBU. Ramifications of the POU2a neuron are confined to layer I. (d) POU2b neurons have fine arborizations on the ipsilateral side of the CBU and varicose processes contralaterally. Ramifications extend across two to three columns contralaterally (inset ii), while only one column is innervated on the ipsilateral side (inset i). (e) Two-dimensional reconstruction of a POU3 neuron. Proximal arborizations innervate one column of the CBU. Two narrow dendritic trees extend from layer I to the most ventral part of layer III (inset ii). The contralateral innervation is concentrated in layers I and II (inset i). Some small branches extend to layer III in the posterior CBU. (f) Schematic sagittal sections of the CB with innervated layers of POU1 (magenta), POU2a (gray), POU2b (green), and POU3 neurons (orange) in the ipsilateral (left) and contralateral (right) hemispheres of the CBU. a, anterior; d, dorsal. Scale bars = 50 μm.
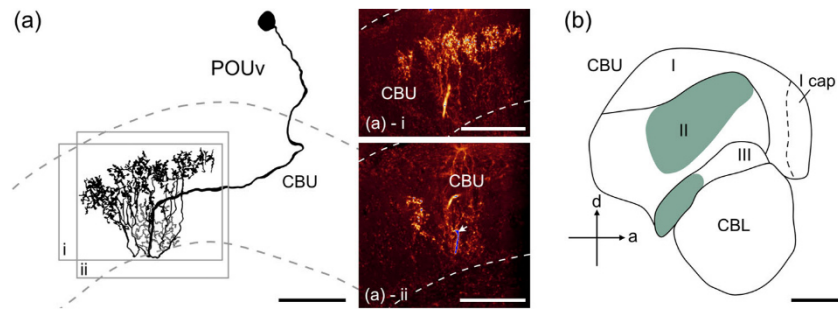
FIGURE 5   Morphology of vertical POU (POUv) neurons. (a) Two-dimensional reconstruction of a POUv neuron innervating layer III (inset ii) of the upper division of the central body (CBU) from the ventral direction. The main neurite then continues dorsally (white arrow in inset ii) and sends processes into layer II (inset i) of the CBU. (b) Schematic sagittal view of the CB illustrating the areas innervated by the neuron in layers III and II (green). a, anterior; CBL, lower division of the central body; d, dorsal. Scale bars = 50 μm.

dorsally and sends varicose processes to several columns of layer II of the CBU (Figure 5a, inset i, and Figure 5b).

3.3 | Columnar neurons

3.3.1 | Columnar neurons of the CBU

Columnar neurons with arborization in the PB and CBU are termed CPU neurons. The most frequently filled neurons were CPU1-type neurons. Several varieties of CPU1 neurons were described in the locust (termed CPU1a, b, and c; Heinze & Homberg, 2008) and the honeybee (CPU1a, type 1 and 2; Hensgen, England, et al., 2021). We found two different subtypes of CPU1a neurons in the cockroach (Figure 6a,c), which were termed CPU1a-1 (n = 4) and CPU1a-3 (n = 3). CPU1a-3 neurons have no obvious correspondence to locust or honeybee CPU1 subtypes. Both subtypes have their somata in the pars intercerebralis (12–20 μm). They connect the PB with the CBU and a distinct area of the LAL, the prong. The CPU1a-3 neurons have additional varicose arborizations in the ALI (Figure 6c, inset iii), which has not been found in any of the CPU1a subtypes of the locust, honeybee, or their counterparts in *D. melanogaster*, the PFL1 neurons. Neurons of both subtypes enter the PB at its anterior surface and arborize in single slices of the ipsilateral half of the PB except for the two innermost slices (R1–R2 or L1–L2) that are innervated together by a single neuron. Slices 3–7 are each invaded by a distinct CPU1a neuron. No CPU1a neurons were encountered in slices 7–9 of the PB (Figure 6d). Arborizations in the PB are smooth (Figure 6c, inset i). The main neurites pass through the posterior chiasma at the dorsal surface of the CBU (Figure 6a,c) and give rise to mostly smooth ramifications except for some beaded processes in one column of the CBU. CPU1a-1 neurons innervate columns of the 8-fold columnar system of the CBU, while CPU1a-3 neurons presumably innervate the 9-fold system. While the ramifications of CPU1a-1 neurons are restricted to layer II and the posterior part of layer III (Figure 6b, orange), CPU1a-3 neurons innervate large parts of layers I, II, and III (Figure 6b, green). The main neurites of the CPU1a neurons run along the anterior surface of the CBU, continue

ventrally, and enter the LAL through the isthmus tract. The neurons innervate a distinct area of the LAL, the synapsin-rich prong in the contralateral hemisphere (Figure 6c, inset iv). Some CPU1a neurons possess two branches that extend beyond the posterior border of the prong. Both branches arborize in the posterior LAL, the upper branch penetrates the ULAL (Figure 6a; upper orange arrowhead) immediately dorsal of the LAL commissure, and the ventral branch runs into the posterior LLAL (Figure 6a; lower orange arrowhead) ventral to the LAL commissure. All processes within the LAL appear varicose. The limited number of stained cells did not allow us to conclusively establish the connectivity between PB and CBU columns. By analyzing all stained CPU1a-1 neurons, we propose a set of five cells per hemisphere. Besides the z-bundle with only one CPU1a-1 neuron, the x- and y-bundles house two neurites each (Figure 6d).

CPU2 neurons (n = 3, soma diameter: 14–20 μm), likewise, connect the PB and CBU. Then, they innervate the ALI and prong bilaterally (Figure 6e). From the prong, a varicose process extends out into the LLAL. We only encountered CPU2 neurons that arborize in slice 2 of the PB and in ipsilateral column 2 of the 8-fold columnar system of the CBU. One neuron showed additional innervations in slice 1 of the PB. The arborizations in the CBU can extend into neighboring columns.

Besides CPU neurons that connect the CBU with the LX, two types of neurons with ramifications in the NO could be distinguished, a subtype of CPU4 neurons corresponding best to CPU4b in the locust and two subtypes of CPU5 neurons (Figure 7). The somata of CPU4b neurons (n = 3) are located in the pars intercerebralis (10–13 μm). After innervating one slice of the PB, the main neurite runs ventrally and ramifies in layer III of the CBU (Figure 7a, insets i and ii). Terminals in the CBU have a bleb-like appearance and span over two columns. The main neurite continues to the contralateral NOU where it arborizes in layer II (Figure 7a, inset iii). The NO arborizations have a mixed fine-beaded appearance.

Two types of CPU5 neurons innervating layer III of the CBU could be distinguished. The somata of both types are located in the pars intercerebralis. The CPU5a neuron (n = 1) has a relatively large soma with a diameter of 19 μm and fine arborizations in one column of the PB. The main neurite runs through the CBU and sends varicose

139
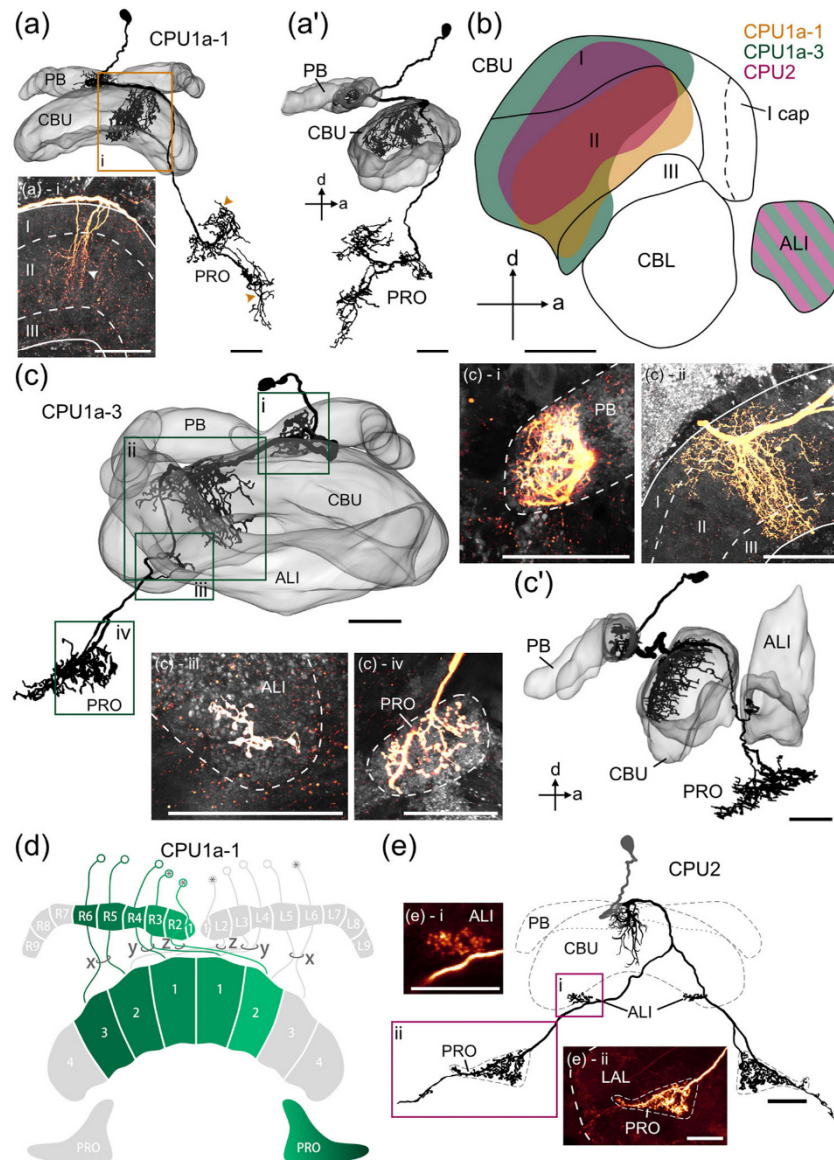
FIGURE 6 Morphology of CPU1a and CPU2 neurons. (a) Three-dimensional reconstruction of a CPU1a-1 neuron with smooth arborizations in the protocerebral bridge (PB) and the upper division of the central body (CBU) and varicose arborizations in the prong (PRO). Two branches extend to the posterior lateral accessory lobe (orange arrowheads). The neuron is shown in a semitransparent CBU and PB in the frontal (a) and sagittal view (a′). Inset i shows the arborization area in layer II (arrowhead) of the CBU. (b) Schematic sagittal section through the CB with innervated layers of CPU1a-1 (orange), CPU1a-3 (green), and CPU2 (magenta) neurons. CPU1a-1 neurons have ramifications in layer II and in the posterior part of layer III. CPU1a-3 neurons innervate large parts of layers I and II and the posterior and ventral part of layer III. The arborizations of CPU2 neurons are located more centrally and cover the inner parts of layers I and II. (c) Three-dimensional reconstruction of a CPU1a-3 neuron with arborizations in the PB (inset i), CBU (inset ii), and PRO (inset iv) and additional ramifications in the anterior lip (ALI, inset iii). Anterior (c) and sagittal view (c′) of the neuron within semitransparent reconstructions of the CBU and PB. (d) Proposed connectivity scheme of CPU1a neurons, based on the injected neurons (asterisks). No CPU1a-1 neurons were encountered in slices 7–9. (e) Two-dimensional reconstruction of a CPU2 neuron with fine ramifications in single columns of the PB and CBU and varicose arborizations in the ALI (inset i) and PRO (inset ii). Scale bars = 50 μm.
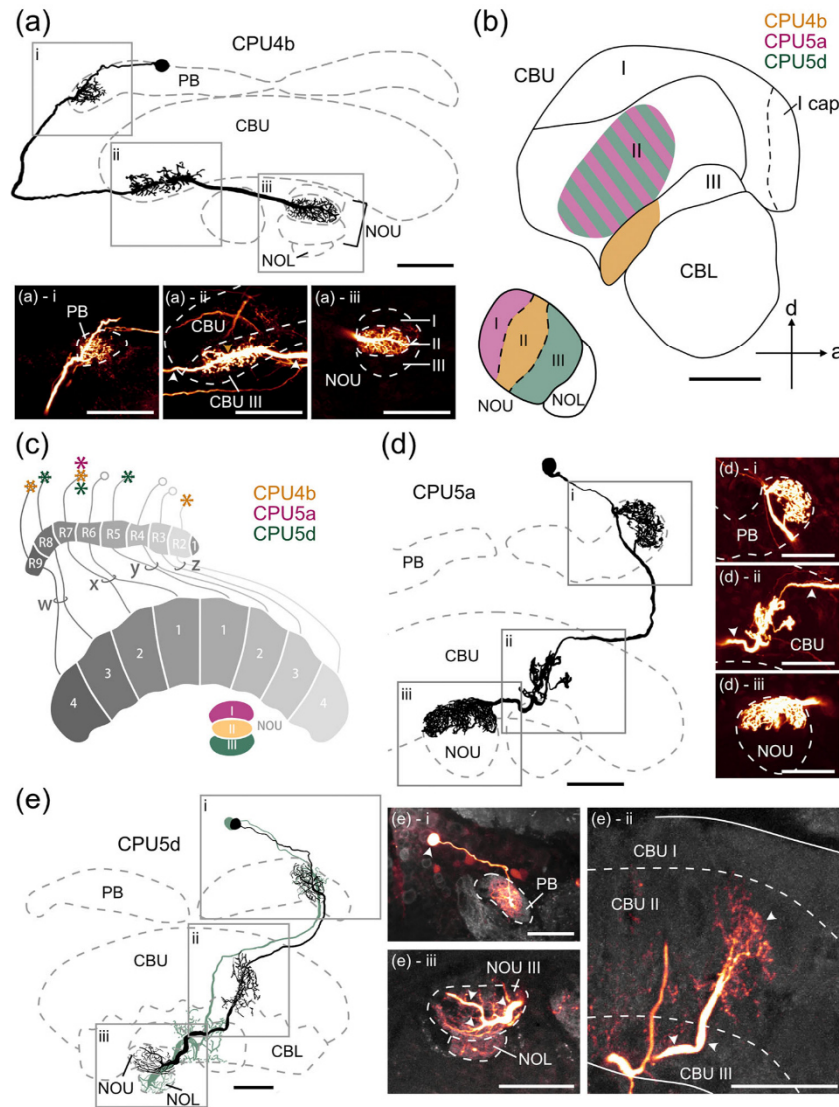
FIGURE 7 Morphology of CPU4 and CPU5 neurons. (a) Two-dimensional reconstruction of a CPU4b neuron with smooth arborizations in the protocerebral bridge (PB, inset i) and varicose ramifications in the upper division of the central body (CBU, inset ii) and layer II of the contralateral upper unit of the nodulus (NOU II, inset iii). (b) Schematic sagittal section through the central body and noduli with innervated layers. The arborizations of CPU4b neurons in the CBU are restricted to layer III (orange). CPU5 neurons connect layer II of the CBU with layer I (CPU5a, magenta) or III (CPU5d, green) of the NOU. (c) Proposed connectivity scheme of CPU4b (orange), CPU5a (magenta), and CPU5d (green) neurons based on the injected neurons (asterisks of respective color). (d) Two-dimensional reconstruction of a CPU5a neuron connecting one column of the PB (inset i) and layer IIb of the CBU (inset ii) with layer I of the contralateral upper unit of the nodulus (NOU, inset iii). The arborizations in the CBU have a bleb-like appearance; the other ramification areas have finer endings. (e) Two-dimensional reconstruction of a CPU5d (black) and CL2 (light green) neuron. The CPU5d neuron arborizes in one column of the PB (inset i), layer IIb of the CBU (inset ii, arrowheads), and layer III of the contralateral NOU (inset iii, arrowheads). The arborizations in the CBU are varicose; the other ramification areas have fine terminals. Scale bars = 50 μm.

141
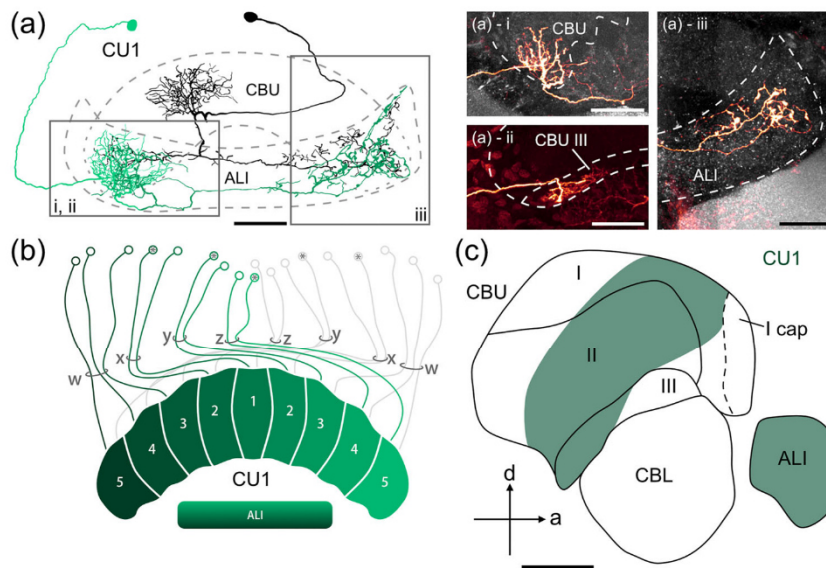
FIGURE 8 Morphology of CU1 neurons. (a) Two-dimensional reconstructions of two CU1 neurons with fine arborizations in the upper division of the central body (CBU) and varicose ramifications in the anterior lip (ALI). Inset i shows ramifications in layer II of the CBU and inset ii in layer III. Inset iii shows a stack of optical slices illustrating arborizations in the contralateral ALI. (b) Proposed connectivity scheme of CU1 neurons, based on the injected neurons (asterisks). (c) Schematic sagittal section of the CB with innervated layers of CU1 neurons (green). a, anterior; CBL, lower division of the central body; d, dorsal. Scale bars = 50 μm.

arborizations dorsally into CBU layer II (Figure 7c and Figure 7d, inset ii) before innervating layer I of the NOU from a dorsal direction (Figure 7d, inset iii). CPU5d neurons ($n = 3$), in contrast, have ramifications in layer III of the contralateral NOU (Figure 7c and Figure 7e, inset iii). This cell type has not been found in the locust (Heinze & Homberg, 2008). CPU5d neurons have small somata with a diameter of about 13 μm. In the CBU, they innervate the same area as the CPU5a neurons (Figure 7b). For the CPU4 and CPU5 neurons, we propose a set of eight neurons per hemisphere that innervate the 8-fold columnar system in the CBU (Figure 7c) with one neuron per slice in the PB except the innermost slice 1. Each of the w-, x-, y-, and z-fiber bundles contains two neurites of each system of neurons.

3.3.2 | Columnar neurons without arborizations in the PB

Seven different types of columnar neurons without a connection to the PB were found. Six of them connect the CBU with the crepine (Table 2). CU1 neurons ($n = 8$) have small somata of approximately 11–14 μm diameter located in the posterior pars intercerebralis. Their main neurites run in the ventral direction, pass the PB posteriorly, and enter the landmark fiber bundles (green arrowheads in Figure 2c) of the CBU. Fine arborizations are located in single columns of the CBU. An exception is neurons that innervate the outermost column 5 of the CBU as they have additional arborizations in the neighboring column 4. Innervation domains extend through layers I, II, and III

(Figure 8a, insets i and ii, and Figure 8c). We propose a set of nine CU1 neurons per hemisphere based on the injected cells (Figure 8b, asterisks). The fiber bundles x, y, and z contain two neurites each, while the three outermost CU1 neurons run through the w-bundle. Primary neurites of neurons arborizing in contralateral columns of the CBU cross the midline in the posterior chiasma. From the CBU, the main neurites run further anteriorly through the CBU and split into two collaterals that innervate the ALI in its full width. All eight injected neurons showed varicose ramifications in the ALI (Figure 8a, inset iii).

CU2a neurons can be divided into two subtypes. The cell bodies of both types (CU2a-1, $n = 8$, Figure 9a, black; CU2a-2, $n = 2$, Figure 9a, green) are located in the pars intercerebralis. The somata of CU2a-1 neurons are similar in size (12–15 μm diameter) to those of CU1 neurons. Most somata of the injected CU2a-1 neurons were located in the posterior and medial parts of the pars intercerebralis. Their main neurites pass the PB anteriorly and enter the CBU from the dorsal direction. Fine arborizations are confined to dorsal parts of layers I and II (Figure 9c, gray). Neurites run further anteriorly through the CBU. When the arborization in the CBU is ipsilateral to the soma, the neurite crosses the midline at the level of the ALI. The axon of the stained CU2a-1 neuron in Figure 9a (black) joins the isthmus tract posterior to the contralateral pedunculus. It arborizes anterior to the rubus within the crepine but, in addition, sends fine processes into the rubus (Figure 9a, inset iv, arrowheads). Overall, the projections of CU2a-1 neurons are somewhat variable. Some cells innervate the rubus with fine processes (Figure 9a, inset iv, arrowheads), while others
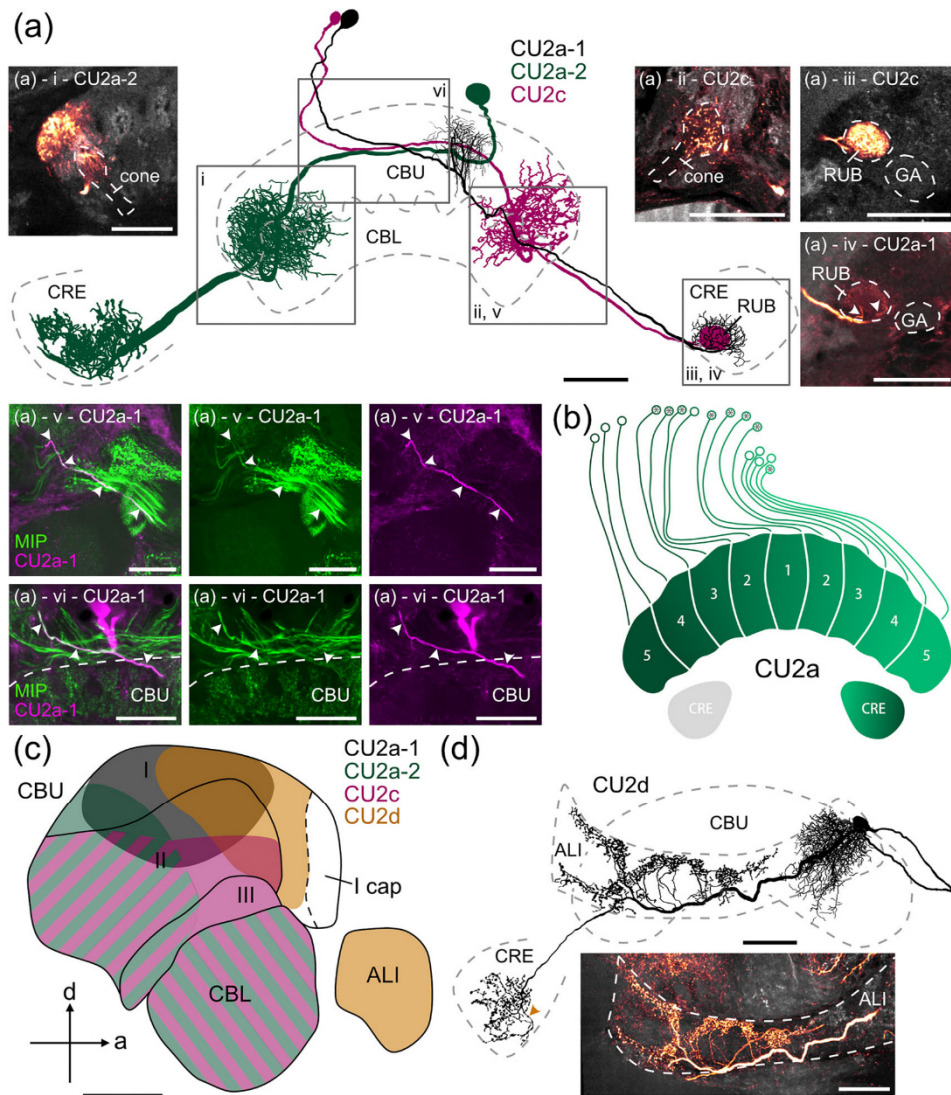
FIGURE 9 Morphology of CU2 neurons. (a) Two-dimensional reconstructions of CU2a-1 (black), CU2a-2 (green), and CU2c (magenta) neurons with arborizations in the upper division of the central body (CBU) and the crepine (CRE). Insets i–iv show arborizations of the different neurons in single optical sections (i–iii) and a maximal intensity projection (iv) with synapsin labeling in gray. In addition to arborizations in the CBU, CU2a-2 and CU2c neurons also ramify in cones of the lower division of the central body (CBL; insets i and ii) corresponding to their CBU domains. The CU2c neuron has fine arborizations in the rubus (RUB, inset iii) and the CU2a-1 neuron around it (inset iv). Inset v and vi show double labeling of a CU2a-1 neuron with an antiserum against the myoinhibitory peptide Pea-MIP-1 (MIP; green). (b) Proposed connectivity scheme of CU2a neurons, based on the injected neurons (asterisks). (c) Schematic sagittal view of the CB with innervated layers of CU2a-1 (gray), CU2a-2 (green), CU2c (magenta), and CU2d (orange) neurons. CU2a-1 neurons have arborizations in the dorsal part of layers I and II, while CU2a-2 neurons arborize in a more ventral area in layers I, II, and III. CU2c neurons arborize in layers II and III. The arborization area of CU2d neurons is located in the dorsal part of layer I and the anterior part of layer II. (d) Two-dimensional reconstruction of a CU2d neuron with fine ramifications in the CBU and varicose terminals in the anterior lip (ALI, inset) and CRE. a, anterior; d, dorsal. Scale bars = 50 μm.

have projections more dorsally into the crepine. Based on the injected CU2a neurons (Figure 9b, asterisks), we propose a set of 16 neurons per hemisphere, with each cell innervating alternately one and two neighboring columns of the CBU (Figure 9b). No cells innervating column 4 or 5 on the ipsilateral side were injected. CU2a-1 neurons can be

double labeled with an antiserum against Pea-MIP-1 (Figure 9a, insets v and vi).

The second type (CU2a-2, $n = 2$) shows the same arborization pattern but has additional ramifications in a cone of the CBL (Figure 9a, inset i). These cells have larger somata (17–22 μm diameter) and denser

and more extensive arborizations in the crepine than CU2a-1 neurons (Figure 9a, green). These innervations are located dorsally to the gall and the rubus. Their varicose endings spread further anteriorly. In contrast to CU2a-1 neurons, the arborizations in the CBU are restricted to a posterior part and innervate layers II and III (Figure 9c).

Although neurons similar to CU2b in the locust (Heinze & Homberg, 2008) with ramifications in anterior parts of CBU layer I were not encountered in the cockroach, two additional types, CU2c and CU2d, were found that have not been described in the locust. While CU2c neurons might correspond to FR1 neurons in *D. melanogaster*, no counterparts to CU2d are present in the fly. CU2c neurons ($n = 2$) have small somata (11–14 μm diameter) in the anterior pars intercerebralis. Their main neurite passes the PB anteriorly and enters the CBU from the posterior direction. Dense arborizations innervate the CBU and CBL (Figure 9a, inset ii). In the CBU, each CU2c neuron innervates two columns. Their main neurites join the isthmus tract and run to the rubus where the neurons form fine and densely packed innervations (Figure 9a, inset iii).

The somata (13-μm diameter) of CU2d neurons ($n = 2$) are located in the pars intercerebralis, near the PB. Their main neurites run lateral to the PB and dorsal to the CBU in a contralateral direction. The neurons send fine arborizations into the dorsalmost part of layers I and II of one column of the CBU (Figure 9c), with a few fibers extending to more posterior parts of layer II. The main neurite passes the CBU and crosses the midline anterior to the CB. It runs further ventrally to the ALI where at least 10 side branches send varicose ramifications into the dorsal part of the ALI (Figure 9d, inset). These innervations have a tree-like shape and are restricted to the contralateral side of the ALI. The main neurite finally joins the isthmus tract and sends further varicose innervations to the crepine. One branch extends around the rubus of the contralateral side (Figure 9d, orange arrowhead).

Two distinct CU3 neurons, termed CU3a and CU3b, with axonal projections to areas in both hemispheres of the cerebrum were encountered. A single CU3a neuron was stained (Figure 10a). Its soma has a diameter of about 11 μm and lies in the posterior pars intercerebralis. The main neurite runs lateral from to the PB through the x-bundle and enters the CBU from the ventroposterior direction. At least one fiber sends fine arborizations to column L2. These arborizations innervate layer I (Figure 10b) but could not be traced further due to poor staining. The neurite runs through the CBU, leaves it on its anterior side, and bifurcates anterior to the ALI without innervating it. Both collaterals join the respective isthmus tract and send varicose arborizations to the crepine (Figure 10a). Whether small arborizations also innervate the LAL cannot be excluded owing to a high background staining.

CU3b neurons ($n = 2$; Figure 10c) innervate several protocerebral neuropils extensively. Their somata (12–15 μm) are located in the posterior pars intercerebralis near the PB. The main neurite of the imaged neuron joins the w-bundle and enters the CBU from the dorsal direction. The other encountered CU3b neuron joins the y-bundle. One side branch innervates two columns of the CBU. Fine arborizations are confined to layer I (Figure 10b). The second arm sends mixed arborizations to the most lateral part of the ALI (Figure 10c, inset iv). A third major

neurite bypasses the CBU anteriorly and splits up into two collaterals that run ventrally and bypass the CBU and ALI. One arm sends out small mixed fibers to the teeth of the CBL (Figure 10c, inset v). Each arm bifurcates again, giving rise to two collaterals in each hemisphere that run along the outer edges of the isthmus tract. On their way, they send varicose arborizations into the crepine, ULAL, and LLAL (Figure 10c, inset iii). In their further course, they innervate the medial antennal mechanosensory and motor center (Figure 10c, inset ii), the wedge, and the dorsal antennal mechanosensory and motor center (Figure 10c, inset i).

The somata of CU4 neurons ($n = 2$, Figure 10d) are located in the anterior pars intercerebralis and have a diameter of 12–13 μm. The main neurite runs dorsally to the CBU and passes it anteriorly. It sends fibers into the CBU and into one cone and tooth of the CBL (Figure 10d, inset i). In the CBU, the innervations are located in two columns. Layer II is only sparsely innervated, most arborizations are located in the cap of layer I and in layer I (Figure 10b). Some branches reach out to the posterior-most part of layers II and III. The neurite continues to the ALI where it forms varicose ramifications (Figure 10d, inset ii). After joining the isthmus tract, the axon gives rise to varicose ramifications in the crepine (Figure 10d).

3.3.3 | Columnar neurons of the PB

Two types of columnar neurons of the PB without major connections to the CB were stained, CP2-1 ($n = 4$) and CP2-2 ($n = 4$) neurons (Figure 11). Their somata are located in the posterior pars intercerebralis and have a diameter of 11–12 μm. Both types show fine arborizations in single columns of the PB (Figure 11a, inset i, and Figure 11b, inset i). Their main neurites pass the CBU dorsally and cross the midline in front of the CBU. Fibers join the isthmus tract and send varicose ramifications into the ULAL (Figure 11a, inset iii, and Figure 11b, inset iii) with fine processes extending into the gall (Figure 11a and Figure 11b, inset iv). Along the anterior face of the CBU, small side branches from the CP2-2 axons give rise to varicose arborizations at the anterior surface of the teeth of the CBL (Figure 11b, inset ii). The neuron reconstructed in Figure 11b innervates two teeth, and three other encountered CP2-2 neurons only ramify in one tooth. CP2-1 neurons are immunoreactive with the antiserum against LomTK-II (Figure 11a, insets i and ii). Based on LomTK-II immunolabeling, we propose a set of nine CP2-1 neurons per hemisphere (Figure 1e). Each CP2-1 neuron innervates one column of the PB and joins one of the four bundles of the posterior chiasma on its way to the LX. While the w-, x-, and y-bundles house two neurites each, the z-bundle contains the neurites of the neurons innervating slices 1–3 of the PB.

### 3.3.4 | Columnar neurons of the CBL

Two types of columnar neurons with arborizations in the CBL could be distinguished. CL1 neurons (Figure 12; $n = 13$) connect the PB and the
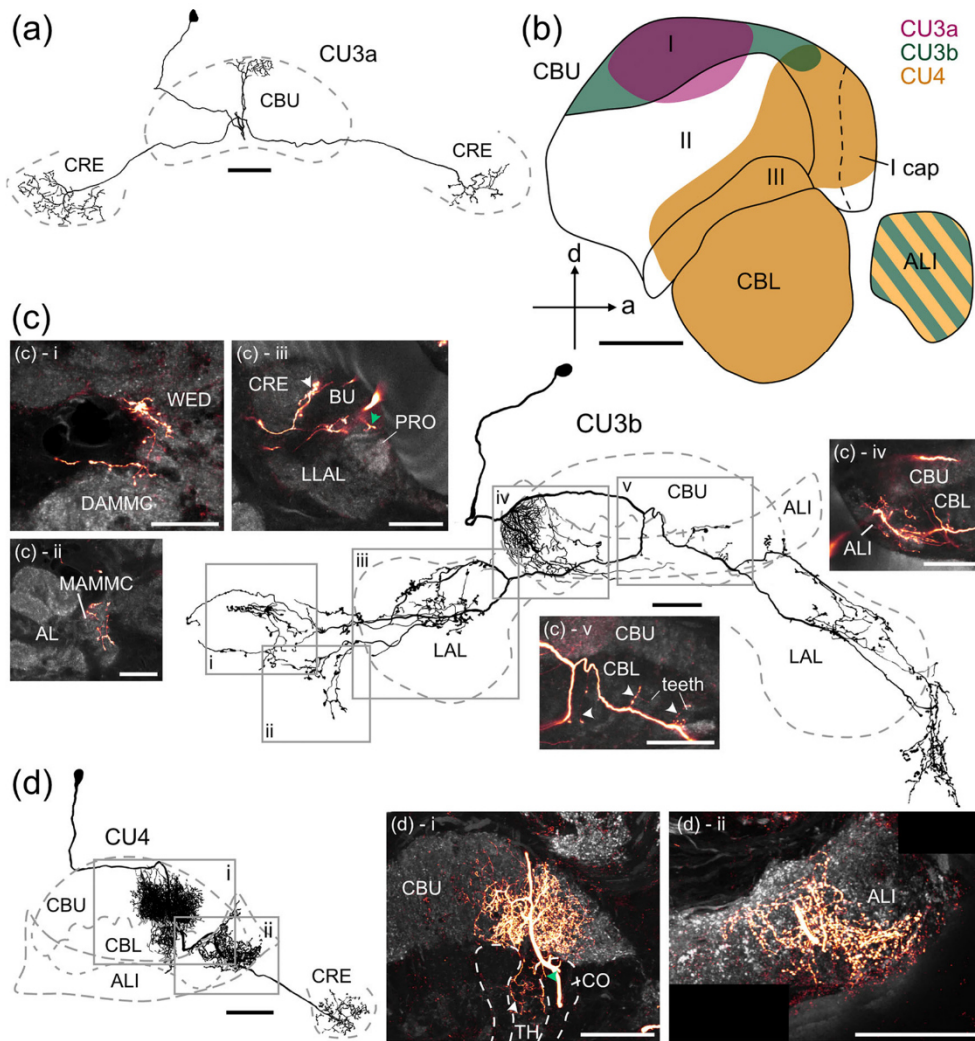
FIGURE 10 Morphology of CU3 and CU4 neurons. (a) Two-dimensional reconstruction of a CU3a neuron with fine arborizations in the upper division of the central body (CBU) and varicose bilateral arborizations in the crepine (CRE). (b) Schematic sagittal section of the CB illustrating the CBU layers innervated by CU3a (magenta), CU3b (green), and CU4 (orange) neurons. CU3a neurons arborize mostly in layer I, CU3b neurons show ramifications in layer I, and CU4 neurons mostly arborize in layer I including the cap region and layer II. Two arms continue to layer III. (c) Two-dimensional reconstruction of a CU3b neuron. Insets i–iv show maximum intensity projections of the different arborization areas combined with synapsin immunolabeling (gray). The neuron has wide ramifications in diverse neuropils. It has fine arborizations in a CBU column and sends out wide, mostly beaded ramifications into the anterior lip (ALI; inset iv), multiple teeth of the lower division of the central body (CBL; inset v), and bilaterally into the lateral accessory lobe (LAL; inset iii), the crepine (CRE; inset iii), the medial antennal mechanosensory and motor center (MAMMC; inset ii), the wedge (WED; inset i), and the dorsal AMMC (inset i). Prong (PRO) and bulb (BU) are free of arborizations (inset iii). (d) Two-dimensional reconstruction of a CU4 neuron connecting the CBU with the CBL (inset i), the ALI (inset ii), and the CRE. In the CBL, it innervates one cone (CO; inset i, green arrowhead) and one tooth (TH; inset i, white arrowhead). Scale bars = 50 μm.

CBL with the gall. Most neurons had beaded ramifications in the PB and mixed fine/beaded processes in the CBL and might, thus, correspond to CL1a neurons in the locust and EPG neurons in *D. melanogaster* (Heinze & Homberg, 2008; Hulse et al., 2021). At least one neuron had fine processes in the PB and beaded ramifications in the CBL, corresponding to CL1b/d neurons in the locust and PEG neurons in the fly. The somata (10–12 μm diameter) of the injected CL1 neurons are located in the

pars intercerebralis. Cell body fibers run ventrally and send arborizations to single columns of the PB. Their main neurites join the *w-*, *x-*, *y-*, or *z-*bundle in the posterior chiasma, continue through the CBU anteroventrally, and send ramifications to a tooth of the CBL. Neurons innervating tooth a and e have additional ramifications in neighboring cones (Figure 12e,g). Axon collaterals join the contralateral isthmus tract, and the neurons finally arborize with small beaded terminals in
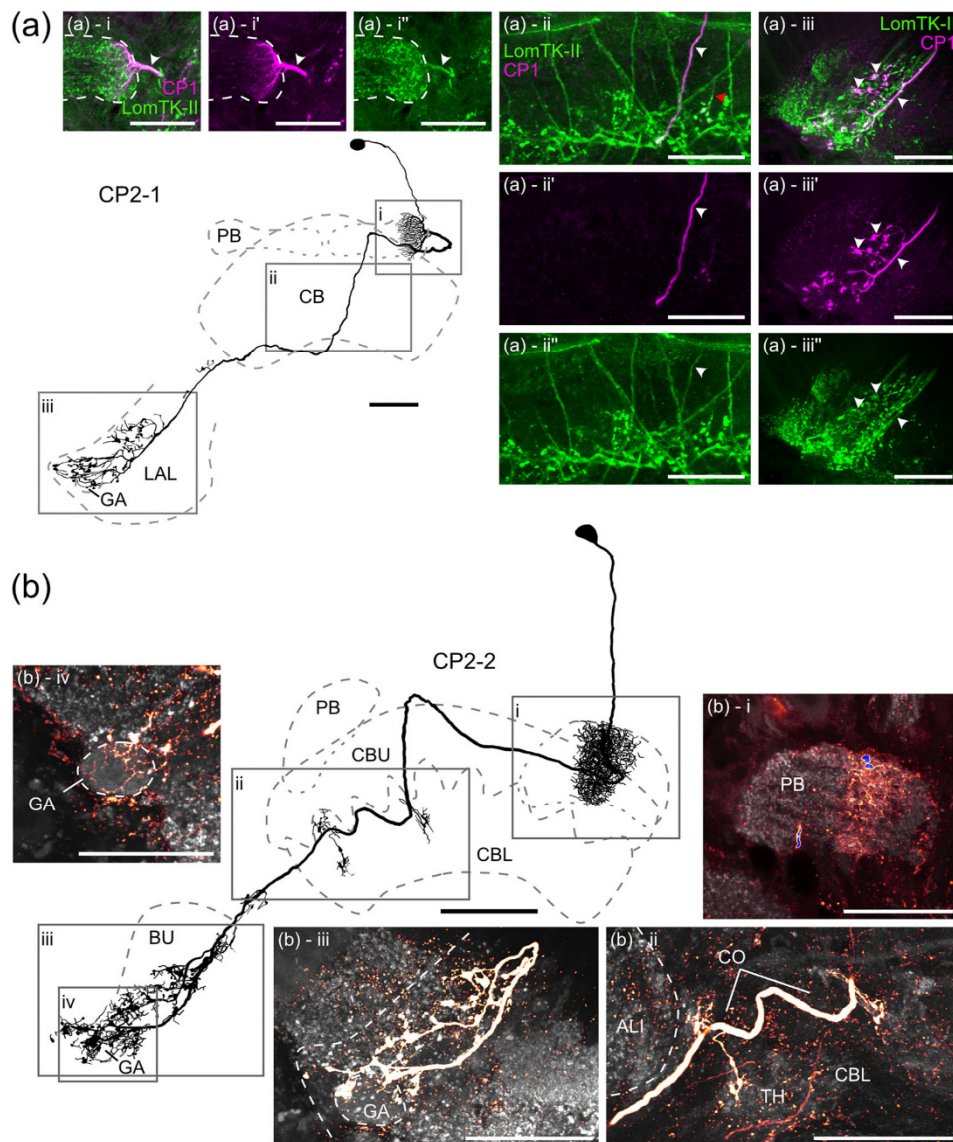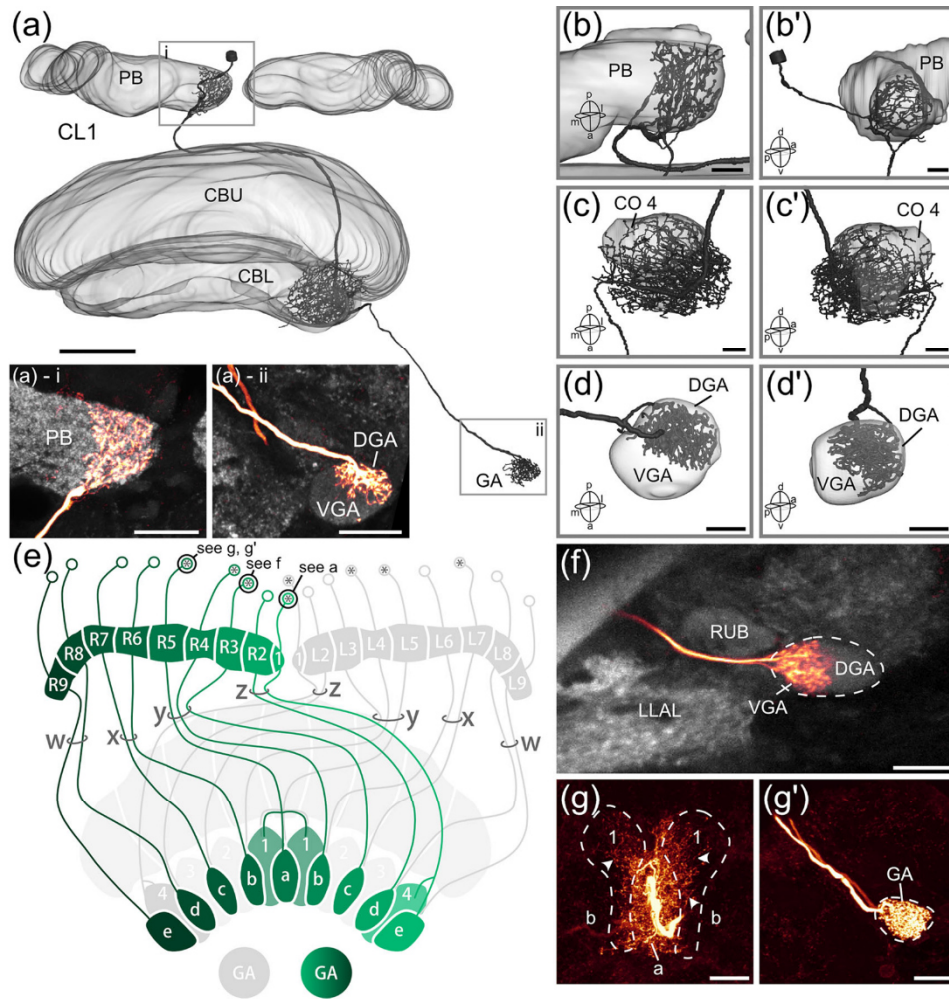
FIGURE 11 Morphology of CP neurons. (a) Two-dimensional reconstruction of a CP2-1 neuron with fine arborizations in the protocerebral bridge (PB; inset i, magenta) and varicose arborizations in the contralateral upper lateral accessory lobe (ULAL) and gall (GA). Insets i–iii show labeling of a CP2-1 neuron (white arrowheads) with an antiserum against LomTK-II (green; inset i, ii, iii). (b) Two-dimensional reconstruction of a CP2-2 neuron. Besides fine arborizations in the PB (inset i) and varicose arborizations in the ULAL (inset iii), this neuron shows fine arborizations in the GA (inset iv) and varicose arborizations in two teeth (TH) of the lower division of the central body (CBL, inset ii). The cones (CO) are free of innervation. ALI, anterior lip; BU, bulb; CB, central body; CBL, lower division of the central body; CBU, upper division of the central body. Scale bars = 50 µm.

either the dorsal (Figure 12a, inset ii) or ventral gall (Figure 12f). We propose sets of nine CL1 neurons per hemisphere. The *w*-, *x*-, and *z*-bundles house two neurons, while the *y*-bundle houses three CL1a neurons (Figure 12e).

CL2 neurons (*n* = 4) connect single columns of the PB with the CBL and the contralateral NOL (Figure 13). Their somata have a diameter of 10–12 µm and are located in the pars intercerebralis. Cell body fibers

pass by the PB posteriorly and send mixed side branches into a column of the PB. No neuron was encountered innervating the innermost columns R1 and L1 of the PB. Neurites join the *w*-, *x*-, *y*-, or *z*-bundle and enter the CBU. Each bundle houses two CL2 neurons (Figure 13b). Fibers continue anteriorly through the CBU, enter the CBL between two adjacent cones, and give rise to a varicose meshwork covering the base and neck of this pair of cones and, in addition, the periphery of

WILEY | 1707

FIGURE 12 Morphology of CL1 neurons. (a) Three-dimensional reconstruction of a CL1 neuron with beaded arborizations in the innermost column of the protocerebral bridge (PB; inset i, b, b') and a distinct area in the gall (GA), the dorsal GA (DGA; inset ii, d, d'). The neuron has mixed fine/beaded endings in tooth e and sparse fine endings in cone 4 (CO) of the lower division of the central body (CBL; c, c'). (b–d) Ramification areas of the neuron in panel (a) viewed from dorsal (b', c', d') and medial directions. (e) Proposed connectivity scheme of CL1a neurons based on the injected neurons (asterisks). Panels showing details of particular neurons (black circles) are indicated. (f) Ramifications of a CL1a neuron in the ventral GA (VGA). (g) Innervation of colabeled CL1 neurons of PB columns R5 (one or two neurons) and L5 (two neurons) in tooth a and both adjacent cones 1 (arrowheads). (g') Ramifications of the two neurons from PB column L5 in panel (g) in the GA. Both subunits of the GA appear to be innervated. a, anterior; CBU, upper division of the central body; d, dorsal; l, lateral; LLAL, lower lateral accessory lobe; m, medial; p, posterior; RUB, rubus; v, ventral. Scale bars = 50 μm (a); 20 μm (inset i and ii in a, f, g'); 10 μm (b–d').

the adjacent teeth (Figure 13a). The CL2 neuron of PB column 9, likewise, gives rise to a mesh of processes largely wrapping around the neck and base of the outermost cone 4 and partly cone 3 in addition to tooth e. Taken together, the data suggest that CL2 neurons of adjacent PB columns invade overlapping pairs of cones in the CBL (Figure 13b). Axonal fibers of all neurons continue posteriorly and arborize with fine processes in the contralateral NOL.

4 | DISCUSSION

Building upon recently established 3D reconstructions of neuropils in the cockroach brain (Althaus et al., 2022), we have analyzed the internal organization of the CX and the attached LX in detail. In addition to novel insights into the neuropil organization of the CX, we have established a catalog of columnar and intrinsic neurons innervating the

147
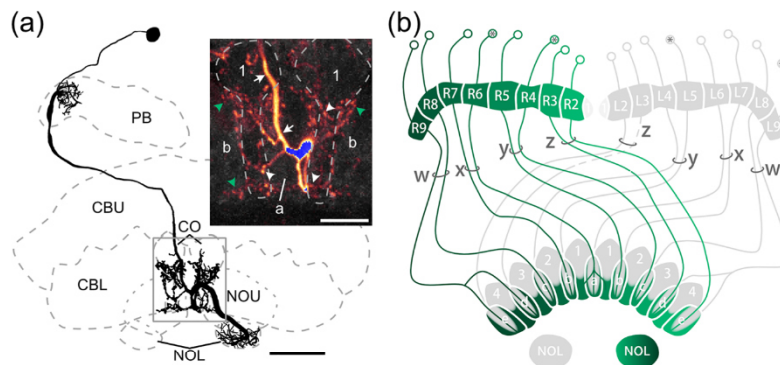
FIGURE 13 Morphology of CL2 neurons. (a) Two-dimensional reconstruction of a CL2 neuron with mixed arborizations in the protocerebral bridge (PB) and the lower unit of the contralateral nodulus (NOL) and varicose ramifications in tooth a and the necks of both neighboring cones (CO; inset, white arrowheads) of the lower division of the central body (CBL). Inset shows the axon of the CL2 neuron (white arrows) and its ramifications extending to tooth b on both sides (green arrowheads). (b) Proposed connectivity scheme of CL2 neurons based on the injected neurons (asterisks). CBU, upper division of the central body. Scale bars = 50 μm (a); 20 μm (inset in a).

CX. Intracellular dye fills revealed five types of pontine neurons and 18 types and subtypes of columnar neurons (Table 2). Many of these cell types appear to have homologs in other insects, for example, *D. melanogaster* (Table 2), but at least six cell types, CPU1a-3, CPU5d, CU2c, CU2d, CU3b, and CU4 neurons, have not been described before. A distinctive feature of the cockroach columnar neurons is their strong connectivity with the ALI and cell-type-specific projections to highly compartmentalized regions of the LX.

4.1 | Internal organization of the CX

In the CX, a characteristic organization into horizontal layers (CBU, CBL, and NO) and vertical slices (PB, CBU, and CBL) is known for many insect species (Heinze & Homberg, 2008; Wolff et al., 2015). Previous immunolabeling studies using antisera against tyrosine hydroxylase (Timm et al., 2021), GABA (Homberg et al., 2018), and the neuropeptides SIFamide (Arendt et al., 2017), Pea-MIP-1 (Schulze et al., 2012), and orcokinin (Hofer & Homberg, 2006) showed that the CBU of the Madeira cockroach is subdivided into three horizontal layers and eight vertical segments. Further insights into the layering of the CBL and CBU require the analysis of individually labeled tangential neurons, planned in an upcoming study on the cockroach CX. As shown here, the PB of the cockroach is composed of nine slices per hemisphere in unison with the PB of the bumblebee *Bombus terrestris* (Sayre et al., 2021), the fly *D. melanogaster* (Lin et al., 2013; Wolff et al., 2015), and the desert locust *S. gregaria* (Hensgen et al., 2022). As in the fly and bee, the innermost columns 1 apparently lack CL2, CPU4, and CPU5 neurons, resulting in systems of eight bilateral pairs of these neurons across the cockroach PB.

Based on sections immunolabeled for synapsin/5-HT/Mas-AT, we identified three layers in the CBU. Three major layers have, likewise, been distinguished in the CBU of the desert locust (Heinze & Homberg, 2008), the bumblebee (Sayre et al., 2021), and the honeybee (Kaiser

et al., 2022), while four layers have been described in the monarch butterfly (Heinze & Reppert, 2012) and the dung beetle (el Jundi et al., 2018), but as many as nine layers in the fruit fly (Wolff et al., 2015). A narrow anterior superficial layer similar to layer I cap in the cockroach is also present in the monarch butterfly (layer I, dorsalmost) and the honeybee (layer Ia). In the monarch butterfly, it shows, like in the cockroach, massive synapsin staining. Beyond that, however, it is at present unclear if and how the layering of the CBU in different species corresponds to each other and how the 3- and 4-fold layering in nondipteran species relates to the nine layers in the fruit fly.

The cockroach CBU can be further subdivided in two interleaved systems of vertical columns, one system composed of nine columns and another system composed of eight columns across the entire width (Figure 2c,c'). CPU and POU neurons are mostly restricted to a column of the 8-fold columnar system (Figures 4 and 6), while many CU neurons follow the 9-fold columnar system. This goes along with neuronal cell types in *D. melanogaster* that divide the FB into different numbers of columns (Hulse et al., 2021). FX neurons subdivide the FB into nine columns like CU neurons in the cockroach. On the other hand, hΔD, hΔE, and hΔM neurons form sets of eight columns in the fly brain that fit the proposed set of eight POU neurons per hemisphere in the cockroach. In the bumblebee and fruit fly, PFL neurons and nearly all types of PFN neurons distribute themselves in sets of nine columns in the FB. This is in contrast to the cockroach CPU neurons that are assumed to innervate eight columns in the CBU.

The composition of the CBL shows the most striking difference to the CBL/EB in other insect species like the locust *S. gregaria* (Heinze & Homberg, 2008; Hensgen, Göthe, et al., 2021; Müller et al., 1997), the honeybee *A. mellifera* (Hensgen, England, et al., 2021), the monarch butterfly *Danaus plexippus* (Heinze et al., 2013), the fly *D. melanogaster* (Hulse et al., 2021), and the dung beetles *Scarabaeus lamarcki* and *Scarabaeus satyrus* (el Jundi et al., 2018). In the cockroach, the CBL consists of nine teeth interleaved with eight cones

but, unlike in all other species studied, apparently no horizontal layering (Homberg et al., 2018). Within the cones, at least two regions can be distinguished, the cone caps and the cone necks. The cone caps refer to the dorsal, broad area of the cones, while the cone necks are the thinner ventral parts. The question of whether these subdivisions correspond to a horizontal layering in other insect species remains unanswered. No columnar neurons that only innervate the cones without innervations in the teeth were found. However, CL2 neurons apparently innervate the boundaries between cones and teeth.

The NO largely share a common organization across insects. A division into an upper unit with three layers and a smaller lower unit as found here is also present in the locust (Heinze & Homberg, 2008), monarch butterfly (Heinze & Reppert, 2012), dung beetle (Immonen et al., 2017), and, slightly modified, also in bees (Hensgen, England, et al., 2021; Sayre et al., 2021). Like in all other species studied, CL2 neurons innervate the NOL (Table 2). CPU neurons have ramifications in the NOU confined to one specific layer (Table 2; Figure 7), which is also the case for CPU4 and CPU5 neurons in the locust (Heinze & Homberg, 2008), monarch butterfly (Heinze et al., 2013), and bumblebee (Sayre et al., 2021). In the fly D. melanogaster, three major subunits have been distinguished, NO1, NO2, and NO3 (Hulse et al., 2021; Wolff & Rubin, 2018; Wolff et al., 2015). NO1 is innervated by PEN/CL2 neurons and therefore corresponds to the NOL. NO2 and NO3 are, like the three NOU layers in the cockroach, invaded by different subtypes of PFN neurons (CPU4 and CPU5 neurons in the cockroach) but, as both subunits are further partitioned into distinct domains, a correspondence to the three NOU layers remains to be established.

The ALI is a prominent neuropil in the brain of the cockroach (Figure 1) and locust, but significantly smaller in the honeybee (Heinze & Homberg, 2008; Hensgen, England, et al., 2021). In D. melanogaster, it has not been recognized as a distinct brain area. Six out of 18 columnar cells found in the cockroach brain have at least some projections into this neuropil. The ALI, therefore, is a prominent output region of the CX. Owing to numerous small side branches of columnar neurons targeting this neuropil, it may also play a modulatory and perhaps recurrent function controlling CX activity.

4.2 | Internal organization of the LX

The LX is the most important input and output area of the CX. It consists of two bilaterally paired neuropils, the LALs and the bulbs. In some species, like the fly D. melanogaster (Hulse et al., 2021) or the locust S. gregaria (Hensgen, Göthe, et al., 2021), further subdivisions of the LX have been established, which contributes substantially to a better understanding of the functional roles of different cell types of the CX.

In the cockroach, the gall and the prong can be distinguished as distinct areas within the LX by synapsin staining (Figure 3). CL1 neurons arborize exclusively in the gall and CPU1 and CPU2 neurons in the prong. While the gall as the target of CL1 neurons is already known from other species (S. gregaria, Hensgen, Göthe, et al., 2021; A. mellifera, Hensgen, England, et al., 2021; S. lamarcki and S. satyrus, el Jundi

et al., 2018; D. melanogaster, Ito et al., 2014; Wolff et al., 2015), the prong is a newly defined neuropil within the LLAL that has not been described in other insect species. In close proximity to the gall, another small structure could be identified, the rubus (Figure 3). This neuropil was first described as part of the crepine in D. melanogaster (Ito et al., 2014; Wolff et al., 2015). In the cockroach, the rubus is densely innervated by CU2c neurons (Figure 9a, magenta) and more sparsely by CU2a-1 neurons (Figure 9a, black). In the fly, the rubus is innervated by FR cells (Hulse et al., 2021) that might, therefore, correspond to CU2c cells in the cockroach. Both FR1 neurons in the fly and CU2c neurons in the cockroach densely innervate the rubus. Hulse et al. (2021) propose that the rubus, unlike the gall, is an output region of the CX and, furthermore, might act as a direct connection to mushroom body neurons via FR1 neurons. If CU2c neurons are homologous to FR1 neurons, they might also have a direct influence on mushroom body neurons and therefore serve a role in memory-guided orientation.

The cockroach gall houses ramifications of four different types of columnar neurons, CP2-1, CP2-2, CL1, and CU2a-2 neurons (Table 2). In D. melanogaster, the gall is innervated by four cell types of the CX, presynaptic EPG and PEG cells (CL1a and CL1b in locust) and postsynaptic ER and ExR (TL in locust) neurons that largely form CX-to-CX connections. In the dung beetle and the desert locust, CP neurons, termed CP1 in the dung beetle and CP2 in the locust, likewise, innervate the gall (el Jundi et al., 2018; Hensgen, Göthe, et al., 2021). In the locust, the endings of CP1 neurons are restricted to the ovoid body (Hensgen, Göthe, et al., 2021), which has not been found in the cockroach brain. In contrast to the cockroach CP2-2 neurons, the locust CP2 neurons lack additional innervations in the CBL. CP neurons are completely lacking in the D. melanogaster brain. Besides CP neurons, one type of columnar neuron without arborizations in the PB innervates the gall, namely, CU2a-2 neurons. Cockroach CU2a-2 neurons might correspond to a certain type of FC neuron in the fly, although CU2a-2 neurons have additional ramifications in the CBL (Figure 9). CL1 neurons in the cockroach divide the gall into two subunits, the dorsal and the ventral gall (Figure 12). These subcompartments also exist in the fruit fly (Hulse et al., 2021; Lin et al., 2013) and the dung beetle (el Jundi et al., 2018). In the fly, EPG and PEG neurons selectively ramify in only one of these units. The dorsal gall houses ramifications of EPG and PEG neurons that arborize only in EB wedges with odd numbers, and the ventral gall houses ramifications of EPG/PEG neurons from even-numbered EB wedges. A similar connectivity pattern has not been observed in the cockroach, but owing to poor staining in several preparations it cannot be excluded that two types of different CL1 neurons were combined in the connectivity pattern in Figure 12e and accordingly, alternated innervation remained undetected.

The gall surround in the fly houses terminals from EL and PFGs neurons. Those neuron types have no clear homologs in the cockroach, but the CP neurons (Figure 11) show innervations within the close surrounding of the gall. Whether this area corresponds to the fly gall surround remains unclear as D. melanogaster lacks the CP cell types.

In many insect species, certain columnar neurons of the CX are sensitive to sky compass cues (el Jundi et al., 2015; Hardcastle et al., 2021; Heinze & Homberg, 2009; Heinze & Reppert, 2012;

Pegel et al., 2018; Stone et al., 2017), namely, CL1, CL2, CPU1, CPU2, and CP neurons. These neurons belong to the core compass network that is involved in directed navigation with respect to idiothetic and celestial cues. Neurons of this network appear to be highly conserved. CL1 and CL2 neurons (EPG and PEN neurons in the fly) form the basis of this head direction circuit by generating an activity bump in the CBL/EB and PB that tracks the rotation of the insect through input signaling, specifically self-rotation via CL2 neurons (Green et al., 2017; Turner-Evans et al., 2017; Zittrell et al., 2023). A requirement for this network is a one-column offset between CL1 and CL2 innervations in the CBL, demonstrated in the fly, desert locust, and bumblebee (Heinze & Homberg, 2008; Sayre et al., 2021; Turner-Evans et al., 2017). A corresponding offset is, likewise, present in the cockroach (Figures 12e and 13b), with the exception that cockroach CL2 neurons do not exclusively innervate the teeth but rather the border between cones and teeth. This innervation scheme might connect CL2 neurons not only to CL1 neurons but also to other neurons of the CBL, such as tangential neurons that have not been investigated yet.

4.3 | Pontine neurons

Pontine neurons connect different columns of the CBU with each other or, as illustrated by vΔ neurons in *D. melanogaster*, arborization domains of different layers within the same column (Hulse et al., 2021). We encountered five different types of pontine neurons of the CBU (Table 2). One of these, the POUv neuron, is the first encounter of a vΔ neuron outside *D. melanogaster*. Like most vΔ neurons in the fly, it appears to take input in a lower CBU layer (layer III) and output in an upper layer (layer II). As only a single POUv neuron was encountered, it remains to be seen how entire systems of these neurons are organized in the cockroach. The remaining four types of POU neurons differ in the layers they innervate. They have input regions in one column and output regions in the contralateral hemisphere of the CBU four columns apart. In *D. melanogaster*, pontine cells are called hΔ cells as their proposed function is to horizontally shift the activity to the other hemisphere. Hulse et al. (2021) describe 13 different types of hΔ cells in the fly, whereas at least five different types were found in the bumblebee (Sayre et al., 2021). In the cockroach, pontine neurons form eight columns in the CBU. The encountered POU1 neurons are highly variable in their morphology and might comprise several subtypes. We propose a homology to hΔD cells in the fly owing to their similar morphology (Hulse et al., 2021). hΔD cells also form eight columns in the fly FB. POU2a neurons have their arborizations at the anterodorsal surface of the CBU (Figure 4b) similar to the POU2 neurons in the locust (Heinze & Homberg, 2008) and hΔ Type 1 neurons in the bumblebee (Sayre et al., 2021). In *D. melanogaster*, hΔE cells might correspond to the POU2a neurons in the cockroach as they share the anterodorsally concentrated innervation pattern. POU2b neurons are, besides the POUv neuron, the only cell type in the cockroach that covers two to three columns of the CBU (Figure 4d). No clear homologs in other insect species are obvious. POU3 neurons in the cockroach are characterized by a large proximal innervation area. They are the only pontine

neurons that innervate layer III of the CBU (Figure 4f), corresponding to POU3 neurons in the locust. In the bumblebee, hΔ Type 3 and 4 neurons show the same characteristic long processes extending from the dorsal to the ventral surface of the CBU (Sayre et al., 2021). In the fly, hΔM cells have large arborization domains on the proximal side. Their main neurite runs dorsoposteriorly along the CBU, similar to the axon of POU3 neurons in the cockroach. Both neuronal types, POU3 in the cockroach and hΔM in the fly, divide the CBU into eight columns. Although interspecies morphological homologies may exist, no conclusion about the function of pontine neurons in the cockroach brain can be drawn yet.

4.4 | Columnar neurons of the CBU

In the cockroach, six different types of CPU neurons were encountered (Table 2). Three types connect the PB and CBU with the LX, while three others form connections between the PB, CBU, and NO. While most of these neurons are already known from other insect species, CPU1a-3 and CPU5d neurons are described here for the first time.

As shown in the locust (Heinze & Homberg, 2007, 2009; Pegel et al., 2018, 2019), the monarch butterfly (Heinze & Reppert, 2012), dung beetles (el Jundi et al., 2015), and sweat bees (Stone et al., 2017), CPU1 and CPU2 neurons are sensitive to visual stimuli mimicking skylight cues. They connect the PB and CBU with specific regions in the LAL. In the monarch butterfly (Heinze et al., 2013), the honeybee (Hensgen, England, et al., 2021), and the Bogong moth (de Vries et al., 2017), two subtypes of CPU1a neurons were described, CPU1a-type-1 and CPU1a-type-2, differing in the extent of their axonal arborizations. In the cockroach, CPU1a-1 neurons show an innervation pattern like CPU1a neurons in the locust (Heinze & Homberg, 2008), with the difference that the cockroach CPU1a-1 neurons restrict their endings in the LX to the prong. No homologs to the CPU1a-type-2 in the butterfly or bee were found in the cockroach but a new variant of CPU1a neurons, termed CPU1a-3. These neurons have side branches in the ALI. The same is true for CPU2 neurons (Figure 6e). CPU1a-1 and CPU1a-3 neurons innervate different layers of the CBU (Figure 6b) and thus might transfer different information to the prong. In the cockroach, we encountered only CPU2 neurons with arborizations in slice 2 of the PB. Judging from its projection to ipsilateral column 1 of the CBU, the entire system fits well to the pattern of CPU2 neurons in the locust (Heinze & Homberg, 2008) and PFL2 neurons in the fly (Hulse et al., 2021), but not to the strikingly different pattern of these neurons in the bumblebee (Sayre et al., 2021).

In the cockroach, like in the locust, different subtypes of CPU4 and CPU5 neurons connect specific layers in the CBU with distinct layers of the NOU (Heinze & Homberg, 2008). Corresponding neurons in the bumblebee, termed PFN and PFNc (Sayre et al., 2021), likewise show layer-specific innervations of the NO.

CPU4 and CPU5 neurons (PFN neurons in *D. melanogaster*; Hulse et al., 2021; Wolff & Rubin, 2018) have not been considered part of the core compass network, although at least CPU4 neurons in the locust

may be sensitive to polarized light depending on the internal state of the animal (Heinze & Homberg, 2009; Pegel et al., 2018). Several subtypes of PFN neurons in the fly show responses not only to visual cues but also to air flow (Currier et al., 2020). Furthermore, these neurons are sensitive to specific heading directions and translational velocity and, together with hΔ neurons, play a role in transforming egocentric directions into world-centric space (PFNv and PFNd; Lu et al., 2022; Lyu et al., 2022; Pfeiffer, 2023). As the arborization pattern of CPU4b neurons in the cockroach brain resembles the organization of PFN neurons in *D. melanogaster*, they might fulfill a similar function in the cockroach brain.

4.5 | Columnar neurons without arborizations in the PB

CX neurons without arborizations in the PB are termed FX neurons in *D. melanogaster* and CU neurons in other insect species. In the locust, three different types of CU neurons have been found. CU1 neurons connect CBU and ALI, CU2 neurons have arborizations in CBU and crepine, and CU3 neurons show broad bilateral ramifications in the LAL (Heinze & Homberg, 2008). In the bee *A. mellifera* (Hensgen, England, et al., 2021), the bumblebee (Sayre et al., 2021), and the dung beetle (el Jundi et al., 2018), no CU neurons were found. In the monarch butterfly *D. plexippus*, CU1 neurons arborize in a special region of the anterior inferior protocerebrum that might resemble the ALI (Heinze et al., 2013). In *D. melanogaster,* the corresponding FX neurons encompass FC, FS, and FR neurons (Hulse et al., 2021). FS neurons connect the CBU with regions in the superior medial protocerebrum. They show close similarity to CU1 neurons in cockroach, locust, and monarch butterfly as they innervate the superior medial protocerebrum suggesting that the ALI is fused with this neuropil in the fly brain.

FC neurons connect the CBU with the crepine and thus might be homologs to CU2a neurons (Figure 9). In the fly, FC neurons provide input to PFL2 and PFL3 neurons. Hulse et al. (2021) suggest that they may maintain a vector in the working memory and are involved in modulating behavior for self-orientation.

Cockroach CU2 neurons that innervate the rubus were named CU2c and CU2d (Figure 9). Homologs of CU2d neurons are unknown in other insect species, but CU2c neurons may correspond to a subtype of FR neurons in *D. melanogaster*. FR neurons comprise two types— FR1 and FR2. FR1 neurons show dense arborizations within the rubus, and ramifications of FR2 neurons are less dense and also spread to the surrounding crepine. CU2c neurons show the same dense innervation pattern in the rubus as FR1 neurons. In *D. melanogaster*, FR neurons influence the mushroom bodies as they connect to mushroom body output neurons (Hulse et al., 2021).

In the cockroach, three types of CU neurons form CBU–CBL connections (CU2a-2, CU2c, and CU4; Table 2). In the bumblebee, PF1 cells are the only cell type that forms these connections (Sayre et al., 2021). In contrast, columnar neurons with CBU–CBL connections were not found in the honeybee (Hensgen, England, et al., 2021), the desert locust (Heinze & Homberg, 2008), and the dung beetle (el Jundi et al.,

2018). In *D. melanogaster*, EL neurons show at least small innervations in the FB, but their function is unknown (Hulse et al., 2021).

4.6 | Functional considerations

The neuroarchitecture of the cockroach CX shares many features with the CX organization in other species, notably the locust *S. gregaria* and the fly *D. melanogaster*. It is, therefore, likely that it serves a similar key role in the control of spatial orientation and spatial vector memory as in other species. While no functional studies on the CX exist so far in *R. maderae*, considerable research has been done on the CX in a closely related species of blaberid cockroaches, the discoid cockroach *Blaberus discoidalis* (reviewed by Ritzmann et al., 2012; Varga et al., 2017). Through extracellular wire-bundle tetrodes, the authors recorded neural activity from the area of the CX, partly in freely walking animals, although without being able to identify the neurons under study morphologically. The authors showed that many neurons of the CX receive mechanosensory input from the antennae as well as visual input (Ritzmann et al., 2008, 2012). Most units responded to lateral displacement of one or both antennae. Visual inputs were characterized more specifically as responses to optomotor stimuli (stripe pattern) again predominantly moving in horizontal directions (Kathman et al., 2014). Passive rotation of cockroaches on a platform relative to a fixed landmark revealed units that encoded the animal's heading relative to the landmark (Varga & Ritzmann, 2016). Some units maintained directional tuning even in the absence of visual cues, similar to head direction tuning by CX neurons in the fly (Seelig & Jayaraman, 2015). Finally, and perhaps most importantly, electrolytic lesions (Harley & Ritzmann, 2010), recordings, and electrical stimulations in stationary (Bender et al., 2010; Guo & Ritzmann, 2013) and freely walking cockroaches (Martin et al., 2015) showed that the CX controls the initiation and speed of forward walking, left and right turns, as well as various aspects of climbing behavior.

Taken together, these data provide a strong case for a key role of the cockroach CX in multisensory control of walking and spatial orientation during walking. The columnar architecture of the CX uncovered here supports this role and provides a solid basis for future analysis of neural computations underlying goal-directed locomotion in the cockroach at the cellular level.

DATA AVAILABILITY STATEMENT

Three-dimensionally reconstructed models and images of all labeled neurons are freely available from the InsectBrainDatabase (https:// insectbraindb.org/app/; Heinze et al., 2021). All data that support the findings of this study are available from the corresponding author.

ORCID

Stefanie Jahn https://orcid.org/0000-0002-1151-2875
Vanessa Althaus https://orcid.org/0000-0001-8018-0555
Juliana Kolano https://orcid.org/0000-0001-7677-6401
Uwe Homberg https://orcid.org/0000-0002-8229-7236

REFERENCES

Althaus, V., Jahn, S., Massah, A., Stengl, M., & Homberg, U. (2022). 3D-atlas of the brain of the cockroach *Rhyparobia maderae*. *Journal of Comparative Neurology*, *530*(18), 3126–3156. https://doi.org/10.1002/cne.25396

Arendt, A., Baz, E.-S., & Stengl, M. (2017). Functions of corazonin and histamine in light entrainment of the circadian pacemaker in the Madeira cockroach, *Rhyparobia maderae*. *Journal of Comparative Neurology*, *525*(5), 1250–1272. https://doi.org/10.1002/cne.24133

Bender, J. A., Pollack, A. J., & Ritzmann, R. E. (2010). Neural activity in the central complex of the insect brain is linked to locomotor changes. *Current Biology*, *20*(10), 921–926. https://doi.org/10.1016/j.cub.2010.03.054

Burdohan, J. A., & Comer, C. M. (1990). An antennal-derived mechanosensory pathway in the cockroach: Descending interneurons as a substrate for evasive behavior. *Brain Research*, *535*(2), 347–352. https://doi.org/10.1016/0006-8993(90)91623-o

Camhi, J. M., & Tom, W. (1978). The escape behavior of the cockroach *Periplaneta americana*. *Journal of Comparative Physiology A*, *128*(3), 193–201. https://doi.org/10.1007/BF00656852

Currier, T. A., Matheson, A. M., & Nagel, K. I. (2020). Encoding and control of orientation to airflow by a set of *Drosophila* fan-shaped body neurons. *eLife*, *9*, e61510. https://doi.org/10.7554/eLife.61510

de Vries, L., Pfeiffer, K., Trebels, B., Adden, A. K., Green, K., Warrant, E., & Heinze, S. (2017). Comparison of navigation-related brain regions in migratory versus non-migratory noctuid moths. *Frontiers in Behavioral Neuroscience*, *11*, 158. https://doi.org/10.3389/fnbeh.2017.00158

Domenici, P., Booth, D., Blagburn, J. M., & Bacon, J. P. (2008). Cockroaches keep predators guessing by using preferred escape trajectories. *Current Biology*, *18*(22), 1792–1796. https://doi.org/10.1016/j.cub.2008.09.062

Durier, V., & Rivault, C. (1999). Path integration in cockroach larvae, *Blattella germanica* (L.) (insect: Dictyoptera): Direction and distance estimation. *Animal Learning & Behavior*, *27*(1), 108–118. https://doi.org/10.3758/BF03199436

el Jundi, B., Pfeiffer, K., Heinze, S., & Homberg, U. (2014). Integration of polarization and chromatic cues in the insect sky compass. *Journal of Comparative Physiology A*, *200*(6), 575–589. https://doi.org/10.1007/s00359-014-0890-6

el Jundi, B., Warrant, E. J., Byrne, M. J., Khaldy, L., Baird, E., Smolka, J., & Dacke, M. (2015). Neural coding underlying the cue preference for celestial orientation. *Proceedings of the National Academy of Sciences of the United States of America*, *112*(36), 11395–11400. https://doi.org/10.1073/pnas.1501272112

el Jundi, B., Warrant, E. J., Pfeiffer, K., & Dacke, M. (2018). Neuroarchitecture of the dung beetle central complex. *Journal of Comparative Neurology*, *526*(16), 2612–2630. https://doi.org/10.1002/cne.24520

Evers, J. F., Schmitt, S., Sibila, M., & Duch, C. (2005). Progress in functional neuroanatomy: Precise automatic geometric reconstruction of neuronal morphology from confocal image stacks. *Journal of Neurophysiology*, *93*(4), 2331–2342. https://doi.org/10.1152/jn.00761.2004

Green, J., Adachi, A., Shah, K. K., Hirokawa, J. D., Magani, P. S., & Maimon, G. (2017). A neural circuit architecture for angular integration in *Drosophila*. *Nature*, *546*(7656), 101–106. https://doi.org/10.1038/nature22343

Guo, P., & Ritzmann, R. E. (2013). Neural activity in the central complex of the cockroach brain is linked to turning behaviors. *Journal of Experimental Biology*, *216*(Pt. 6), 992–1002. https://doi.org/10.1242/jeb.080473

Hanesch, U., Fischbach, K.-F., & Heisenberg, M. (1989). Neuronal architecture of the central complex in *Drosophila melanogaster*. *Cell and Tissue Research*, *257*(2), 343–366. https://doi.org/10.1007/BF00261838

Hardcastle, B. J., Omoto, J. J., Kandimalla, P., Nguyen, B.-C. M., Keleş, M. F., Boyd, N. K., Hartenstein, V., & Frye, M. A. (2021). A visual pathway for skylight polarization processing in *Drosophila*. *eLife*, *10*, e63225. https://doi.org/10.7554/eLife.63225

Harley, C. M., English, B. A., & Ritzmann, R. E. (2009). Characterization of obstacle negotiation behaviors in the cockroach, *Blaberus discoidalis*. *Journal of Experimental Biology*, *212*(Pt. 10), 1463–1476. https://doi.org/10.1242/jeb.028381

Harley, C. M., & Ritzmann, R. E. (2010). Electrolytic lesions within central complex neuropils of the cockroach brain affect negotiation of barriers. *Journal of Experimental Biology*, *213*(Pt. 16), 2851–2864. https://doi.org/10.1242/jeb.042499

Heinze, S., el Jundi, B., Berg, B. G., Homberg, U., Menzel, R., Pfeiffer, K., Hensgen, R., Zittrell, F., Dacke, M., Warrant, E., Pfuhl, G., Rybak, J., & Tedore, K. (2021). A unified platform to manage, share, and archive morphological and functional data in insect neuroscience. *eLife*, *10*, e65376. https://doi.org/10.7554/eLife.65376

Heinze, S., Florman, J., Asokaraj, S., el Jundi, B., & Reppert, S. M. (2013). Anatomical basis of sun compass navigation II: The neuronal composition of the central complex of the monarch butterfly. *Journal of Comparative Neurology*, *521*(2), 267–298. https://doi.org/10.1002/cne.23214

Heinze, S., & Homberg, U. (2007). Maplike representation of celestial *E*-vector orientations in the brain of an insect. *Science*, *315*(5814), 995–997. https://doi.org/10.1126/science.1135531

Heinze, S., & Homberg, U. (2008). Neuroarchitecture of the central complex of the desert locust: Intrinsic and columnar neurons. *Journal of Comparative Neurology*, *511*(4), 454–478. https://doi.org/10.1002/cne.21842

Heinze, S., & Homberg, U. (2009). Linking the input to the output: New sets of neurons complement the polarization vision network in the locust central complex. *Journal of Neuroscience*, *29*(15), 4911–4921. https://doi.org/10.1523/JNEUROSCI.0332-09.2009

Heinze, S., & Reppert, S. M. (2011). Sun compass integration of skylight cues in migratory monarch butterflies. *Neuron*, *69*(2), 345–358. https://doi.org/10.1016/j.neuron.2010.12.025

Heinze, S., & Reppert, S. M. (2012). Anatomical basis of sun compass navigation I: The general layout of the monarch butterfly brain. *Journal of Comparative Neurology*, *520*(8), 1599–1628. https://doi.org/10.1002/cne.23054

Hensgen, R., Dippel, S., Hümmert, S., Jahn, S., Seyfarth, J., & Homberg, U. (2022). Myoinhibitory peptides in the central complex of the locust *Schistocerca gregaria* and colocalization with locustatachykinin-related peptides. *Journal of Comparative Neurology*, *530*(15), 2782–2801. https://doi.org/10.1002/cne.25374

Hensgen, R., England, L., Homberg, U., & Pfeiffer, K. (2021). Neuroarchitecture of the central complex in the brain of the honeybee: Neuronal

cell types. *Journal of Comparative Neurology*, *529*(1), 159–186. https://doi.org/10.1002/cne.24941

Hensgen, R., Göthe, J., Jahn, S., Hümmert, S., Schneider, K. L., Takahashi, N., Pegel, U., Gotthardt, S., & Homberg, U. (2021). Organization and neural connections of the lateral complex in the brain of the desert locust. *Journal of Comparative Neurology*, *529*(15), 3533–3560. https://doi.org/10.1002/cne.25209

Hofer, S., & Homberg, U. (2006). Orcokinin immunoreactivity in the accessory medulla of the cockroach *Leucophaea maderae*. *Cell and Tissue Research*, *325*(3), 589–600. https://doi.org/10.1007/s00441-006-0155-y

Homberg, U. (1985). Interneurones of the central complex in the bee brain (*Apis mellifera*, L.). *Journal of Insect Physiology*, *31*(3), 251–264. https://doi.org/10.1016/0022-1910(85)90127-1

Homberg, U. (1991). Neuroarchitecture of the central complex in the brain of the locust *Schistocerca gregaria* and *S. americana* as revealed by serotonin immunocytochemistry. *Journal of Comparative Neurology*, *303*(2), 245–254. https://doi.org/10.1002/cne.903030207

Homberg, U., Hensgen, R., Jahn, S., Pegel, U., Takahashi, N., Zittrell, F., & Pfeiffer, K. (2023). The sky compass network in the brain of the desert locust. *Journal of Comparative Physiology A*, *209*, 641–662. https://doi.org/10.1007/s00359-022-01601-x

Homberg, U., Humberg, T.-H., Seyfarth, J., Bode, K., & Quintero Pérez, M. (2018). GABA immunostaining in the central complex of dicondylian insects. *Journal of Comparative Neurology*, *526*(14), 2301–2318. https://doi.org/10.1002/cne.24497

Homberg, U., Reischig, T., & Stengl, M. (2003). Neural organization of the circadian system of the cockroach *Leucophaea maderae*. *Chronobiology International*, *20*(4), 577–591. https://doi.org/10.1081/CBI-120022412

Honkanen, A., Adden, A., da Silva Freitas, J., & Heinze, S. (2019). The insect central complex and the neural basis of navigational strategies. *Journal of Experimental Biology*, *222*(1), jeb188854. https://doi.org/10.1242/jeb.188854

Hulse, B. K., Haberkern, H., Franconville, R., Turner-Evans, D., Takemura, S.-Y., Wolff, T., Noorman, M., Dreher, M., Dan, C., Parekh, R., Hermundstad, A. M., Rubin, G. M., & Jayaraman, V. (2021). A connectome of the *Drosophila* central complex reveals network motifs suitable for flexible navigation and context-dependent action selection. *eLife*, *10*, e66039. https://doi.org/10.7554/eLife.66039

Immonen, E.-V., Dacke, M., Heinze, S., & el Jundi, B. (2017). Anatomical organization of the brain of a diurnal and a nocturnal dung beetle. *Journal of Comparative Neurology*, *525*(8), 1879–1908. https://doi.org/10.1002/cne.24169

Ito, K., Shinomiya, K., Ito, M., Armstrong, J. D., Boyan, G., Hartenstein, V., Harzsch, S., Heisenberg, M., Homberg, U., Jenett, A., Keshishian, H., Restifo, L. L., Rössler, W., Simpson, J. H., Strausfeld, N. J., Strauss, R., & Vosshall, L. B. (2014). A systematic nomenclature for the insect brain. *Neuron*, *81*(4), 755–765. https://doi.org/10.1016/j.neuron.2013.12.017

Kaiser, A., Hensgen, R., Tschirner, K., Beetz, E., Wüstenberg, H., Pfaff, M., Mota, T., & Pfeiffer, K. (2022). A three-dimensional atlas of the honeybee central complex, associated neuropils and peptidergic layers of the central body. *Journal of Comparative Neurology*, *530*(14), 2416–2438. https://doi.org/10.1002/cne.25339

Kathman, N. D., Kesavan, M., & Ritzmann, R. E. (2014). Encoding wide-field motion and direction in the central complex of the cockroach *Blaberus discoidalis*. *Journal of Experimental Biology*, *217*(Pt. 22), 4079–4090. https://doi.org/10.1242/jeb.112391

Klagges, B. R., Heimbeck, G., Godenschwege, T. A., Hofbauer, A., Pflugfelder, G. O., Reifegerste, R., Reisch, D., Schaupp, M., Buchner, S., & Buchner, E. (1996). Invertebrate synapsins: A single gene codes for several isoforms in *Drosophila*. *Journal of Neuroscience*, *16*(10), 3154–3165. https://doi.org/10.1523/JNEUROSCI.16-10-03154.1996

Lin, C.-Y., Chuang, C.-C., Hua, T.-E., Chen, C.-C., Dickson, B. J., Greenspan, R. J., & Chiang, A.-S. (2013). A comprehensive wiring diagram of the protocerebral bridge for visual information processing in the *Drosophila* brain.

Cell Reports, *3*(5), 1739–1753. https://doi.org/10.1016/j.celrep.2013.04.022

Lu, J., Behbahani, A. H., Hamburg, L., Westeinde, E. A., Dawson, P. M., Lyu, C., Maimon, G., Dickinson, M. H., Druckmann, S., & Wilson, R. I. (2022). Transforming representations of movement from body- to world-centric space. *Nature*, *601*(7891), 98–104. https://doi.org/10.1038/s41586-021-04191-x

Lyu, C., Abbott, L. F., & Maimon, G. (2022). Building an allocentric travelling direction signal via vector computation. *Nature*, *601*(7891), 92–97. https://doi.org/10.1038/s41586-021-04067-0

Martin, J. P., Guo, P., Mu, L., Harley, C. M., & Ritzmann, R. E. (2015). Central-complex control of movement in the freely walking cockroach. *Current Biology*, *25*(21), 2795–2803. https://doi.org/10.1016/j.cub.2015.09.044

Muren, J. E., Lundquist, C. T., & Nässel, D. R. (1995). Abundant distribution of locustatachykinin-like peptide in the nervous system and intestine of the cockroach Leucophaea maderae. *Philosophical Transactions of the Royal Society of London Series B*, *348*, 423–444. https://doi.org/10.1098/rstb.1995.0079

Müller, M., Homberg, U., & Kühn, A. (1997). Neuroarchitecture of the lower division of the central body in the brain of the locust (*Schistocerca gregaria*). *Cell and Tissue Research*, *288*(1), 159–176. https://doi.org/10.1007/s004410050803

Nässel, D. R., Passier, P. C., Elekes, K., Dircksen, H., Vullings, H. G., & Cantera, R. (1995). Evidence that locustatachykinin I is involved in release of adipokinetic hormone from locust corpora cardiaca. *Regulatory Peptides*, *57*(3), 297–310. https://doi.org/10.1016/0167-0115(95)00043-B

Neuser, K., Triphan, T., Mronz, M., Poeck, B., & Strauss, R. (2008). Analysis of a spatial orientation memory in *Drosophila*. *Nature*, *453*(7199), 1244–1247. https://doi.org/10.1038/nature07003

Pegel, U., Pfeiffer, K., & Homberg, U. (2018). Integration of celestial compass cues in the central complex of the locust brain. *Journal of Experimental Biology*, *221*(Pt. 2), jeb171207. https://doi.org/10.1242/jeb.171207

Pegel, U., Pfeiffer, K., Zittrell, F., Scholtyssek, C., & Homberg, U. (2019). Two compasses in the central complex of the locust brain. *Journal of Neuroscience*, *39*(16), 3070–3080. https://doi.org/10.1523/JNEUROSCI.0940-18.2019

Petri, B., Stengl, M., Würden, S., & Homberg, U. (1995). Immunocytochemical characterization of the accessory medulla in the cockroach *Leucophaea maderae*. *Cell and Tissue Research*, *282*(1), 3–19. https://doi.org/10.1007/BF00319128

Pfeiffer, K. (2023). The neuronal building blocks of the navigational toolkit in the central complex of insects. *Current Opinion in Insect Science*, *55*, 100972. https://doi.org/10.1016/j.cois.2022.100972

Pfeiffer, K., & Homberg, U. (2014). Organization and functional roles of the central complex in the insect brain. *Annual Review of Entomology*, *59*, 165–184. https://doi.org/10.1146/annurev-ento-011613-162031

Predel, R., Rapus, J., & Eckert, M. (2001). Myoinhibitory neuropeptides in the American cockroach. *Peptides*, *22*(2), 199–208. https://doi.org/10.1016/S0196-9781(00)00383-1

Rayshubskiy, A., Holtz, S. L., D'Alessandro, I., Li, A. A., Vanderbeck, Q. X., Haber, I. S., Gibb, P. W., & Wilson, R. I. (2020). *Neural circuit mechanisms for steering control in walking* Drosophila. bioRxiv. https://doi.org/10.1101/2020.04.04.024703

Ritzmann, R. E. (1984). The cockroach escape response. In R. C. Eaton (Ed.), *Neural mechanisms of startle behavior* (pp. 93–131). Springer. https://doi.org/10.1007/978-1-4899-2286-1

Ritzmann, R. E., Harley, C. M., Daltorio, K. A., Tietz, B. R., Pollack, A. J., Bender, J. A., Guo, P., Horomanski, A. L., Kathman, N. D., Nieuwoudt, C., Brown, A. E., & Quinn, R. D. (2012). Deciding which way to go. How do insects alter movements to negotiate barriers? *Frontiers in Neuroscience*, *6*, 97. https://doi.org/10.3389/fnins.2012.00097

Ritzmann, R. E., Ridgel, A. L., & Pollack, A. J. (2008). Multi-unit recording of antennal mechano-sensitive units in the central complex of the cockroach, *Blaberus discoidalis*. *Journal of Comparative Physiology A*, *194*(4), 341–360. https://doi.org/10.1007/s00359-007-0310-2

Rivault, C., & Durier, V. (2004). Homing in German Cockroaches, *Blattella germanica* (L.) (Insecta: Dictyoptera): Multi-channelled orientation cues. *Ethology*, *110*(10), 761–777. https://doi.org/10.1111/j.1439-0310.2004.01018.x

Sakura, M., Lambrinos, D., & Labhart, T. (2008). Polarized skylight navigation in insects: Model and electrophysiology of e-vector coding by neurons in the central complex. *Journal of Neurophysiology*, *99*(2), 667–682. https://doi.org/10.1152/jn.00784.2007

Sayre, M. E., Templin, R., Chavez, J., Kempenaers, J., & Heinze, S. (2021). A projectome of the bumblebee central complex. *eLife*, *10*, e68911. https://doi.org/10.7554/eLife.68911

Schmitt, S., Evers, J. F., Duch, C., Scholz, M., & Obermayer, K. (2004). New methods for the computer-assisted 3-D reconstruction of neurons from confocal image stacks. *Neuroimage*, *23*(4), 1283–1298. https://doi.org/10.1016/j.neuroimage.2004.06.047

Schulze, J., Neupert, S., Schmidt, L., Predel, R., Lamkemeyer, T., Homberg, U., & Stengl, M. (2012). Myoinhibitory peptides in the brain of the cockroach *Leucophaea maderae* and colocalization with pigment-dispersing factor in circadian pacemaker cells. *Journal of Comparative Neurology*, *520*(5), 1078–1097. https://doi.org/10.1002/cne.22785

Seelig, J. D., & Jayaraman, V. (2015). Neural dynamics for landmark orientation and angular path integration. *Nature*, *521*(7551), 186–191. https://doi.org/10.1038/nature14446

Seelinger, G., & Gagel, S. (1985). On the function of sex pheromone components in *Periplaneta americana*: Improved odour source localization with periplanone-A. *Physiological Entomology*, *10*(2), 221–234. https://doi.org/10.1111/j.1365-3032.1985.tb00038.x

Stengl, M., Werckenthin, A., & Wei, H. (2015). How does the circadian clock tick in the Madeira cockroach? *Current Opinion in Insect Science*, *12*, 38–45. https://doi.org/10.1016/j.cois.2015.09.007

Stierle, I. E., Getman, M., & Comer, C. M. (1994). Multisensory control of escape in the cockroach *Periplaneta americana*. I. Initial evidence from patterns of wind-evoked behavior. *Journal of Comparative Physiology A*, *174*, 1–11. https://doi.org/10.1007/BF00192001

Stone, T., Webb, B., Adden, A., Weddig, N. B., Honkanen, A., Templin, R., Wcislo, W., Scimeca, L., Warrant, E., & Heinze, S. (2017). An anatomically constrained model for path integration in the bee brain. *Current Biology*, *27*(20), 3069.e11–3085.e11. https://doi.org/10.1016/j.cub.2017.08.052

Strausfeld, N. J. (1999). A brain region in insects that supervises walking. *Progress in Brain Research*, *123*, 273–284. https://doi.org/10.1016/S0079-6123(08)62863-0

Strauss, R. (2002). The central complex and the genetic dissection of locomotor behaviour. *Current Opinion in Neurobiology*, *12*(6), 633–638. https://doi.org/10.1016/S0959-4388(02)00385-9

Timm, J., Scherner, M., Matschke, J., Kern, M., & Homberg, U. (2021). Tyrosine hydroxylase immunostaining in the central complex of dicondylian insects. *Journal of Comparative Neurology*, *529*(12), 3131–3154. https://doi.org/10.1002/cne.25151

Turner-Evans, D., Wegener, S., Rouault, H., Franconville, R., Wolff, T., Seelig, J. D., Druckmann, S., & Jayaraman, V. (2017). Angular velocity integration in a fly heading circuit. *eLife*, *6*, e23496. https://doi.org/10.7554/eLife.23496

Varga, A. G., Kathman, N. D., Martin, J. P., Guo, P., & Ritzmann, R. E. (2017). Spatial navigation and the central complex: Sensory acquisition, orientation, and motor control. *Frontiers in Behavioral Neuroscience*, *11*, 4. https://doi.org/10.3389/fnbeh.2017.00004

Varga, A. G., & Ritzmann, R. E. (2016). Cellular basis of head direction and contextual cues in the insect brain. *Current Biology*, *26*(14), 1816–1828. https://doi.org/10.1016/j.cub.2016.05.037

Veenstra, J. A., & Hagedorn, H. H. (1993). Sensitive enzyme immunoassay for *Manduca* allatotropin and the existence of an allatotropin-immunoreactive peptide in *Periplaneta americana*. *Archives of Insect Biochemistry and Physiology*, *23*(3), 99–109. https://doi.org/10.1002/arch.940230302

Veenstra, J. A., Lau, G. W., Agricola, H. J., & Petzel, D. H. (1995). Immunohistological localization of regulatory peptides in the midgut of the female mosquito *Aedes aegypti*. *Histochemistry and Cell Biology*, *104*(5), 337–347. https://doi.org/10.1007/BF01458127

Vitzthum, H., & Homberg, U. (1998). Immunocytochemical demonstration of locustatachykinin-related peptides in the central complex of the locust brain. *Journal of Comparative Neurology*, *390*(4), 455–469. https://doi.org/10.1002/(SICI)1096-9861(19980126)390:4⟨455::AID-CNE1⟩3.0.CO;2-%23

von Hadeln, J., Hensgen, R., Bockhorst, T., Rosner, R., Heidasch, R., Pegel, U., Quintero Pérez, M., & Homberg, U. (2020). Neuroarchitecture of the central complex of the desert locust: Tangential neurons. *Journal of Comparative Neurology*, *528*(6), 906–934. https://doi.org/10.1002/cne.24796

Watson, J. T., Ritzmann, R. E., & Pollack, A. J. (2002). Control of climbing behavior in the cockroach, *Blaberus discoidalis*. II. Motor activities associated with joint movement. *Journal of Comparative Physiology A*, *188*(1), 55–69. https://doi.org/10.1007/s00359-002-0278-x

Watson, J. T., Ritzmann, R. E., Zill, S. N., & Pollack, A. J. (2002). Control of obstacle climbing in the cockroach, *Blaberus discoidalis*. I. Kinematics. *Journal of Comparative Physiology A*, *188*(1), 39–53. https://doi.org/10.1007/s00359-002-0277-y

Wei, H., el Jundi, B., Homberg, U., & Stengl, M. (2010). Implementation of pigment-dispersing factor-immunoreactive neurons in a standardized atlas of the brain of the cockroach *Leucophaea maderae*. *Journal of Comparative Neurology*, *518*(20), 4113–4133. https://doi.org/10.1002/cne.22471

Willis, M. A., & Avondet, J. L. (2005). Odor-modulated orientation in walking male cockroaches *Periplaneta americana*, and the effects of odor plumes of different structure. *Journal of Experimental Biology*, *208*(Pt. 4), 721–735. https://doi.org/10.1242/jeb.01418

Wolff, T., Iyer, N. A., & Rubin, G. M. (2015). Neuroarchitecture and neuroanatomy of the *Drosophila* central complex: A GAL4-based dissection of protocerebral bridge neurons and circuits. *Journal of Comparative Neurology*, *523*(7), 997–1037. https://doi.org/10.1002/cne.23705

Wolff, T., & Rubin, G. M. (2018). Neuroarchitecture of the *Drosophila* central complex: A catalog of nodulus and asymmetrical body neurons and a revision of the protocerebral bridge catalog. *Journal of Comparative Neurology*, *526*(16), 2585–2611. https://doi.org/10.1002/cne.24512

Zittrell, F., Pabst, K., Carlomagno, E., Rosner, R., Pegel, U., Endres, D. M., & Homberg, U. (2023). Integration of optic flow into the sky compass network in the brain of the desert locust. *Frontiers in Neural Circuits*, *17*, 338. https://doi.org/10.3389/fncir.2023.1111310

Danksagung

Ich möchte mich von ganzem Herzen bei euch allen bedanken. Ohne eure Unterstützung, euer Verständnis und eure endlose Geduld wäre meine Reise zur Promotion nicht möglich gewesen. Obwohl ich während dieser Zeit einige unkonventionelle Wege eingeschlagen habe, habt ihr mich stets ermutigt und unterstützt.

Der erste Dank gilt Uwe, du hast mich bereits seit meiner Bachelorarbeit begleitet und unterstützt. Ich danke dir für die Möglichkeit, meine Doktorarbeit überhaupt durchzuführen. Deine ruhige und immer hilfsbereite Art, kombiniert mit deinem geballten Wissen, haben mich maßgeblich geprägt und mir geholfen mich immer weiter zu entwickeln.

Danke an Ronny, mit dessen Hilfe das letzte Manuskript fertig werden konnte. Danke auch an das ein oder andere (manchmal auch etwas verwirrte), aber immer hilfreiche Telefonat.

Martina, du bist seit jeher der tragende KERN unserer Arbeitsgruppe gewesen. Ohne dich hätte das Labor nicht funktioniert. Danke für alles, was du für uns getan hast. Von lustigen Gesprächen bis hin zu ernsten Diskussionen – du warst immer da und hast dein Bestes gegeben um uns bei allen Problemen weiterzuhelfen. Du bist mir wirklich ans Herz gewachsen, auch wenn ich dich manchmal in den Wahnsinn getrieben habe.

Danke an Dr. Erich Staudacher, du magst ein alter störrischer Bayer sein, aber du hast einen großen Einfluss auf mich gehabt. Ich bin dankbar für die Zeit, die ich mit dir verbringen durfte und für alles, was ich von dir lernen konnte. Die vielen auch oft tiefgründigeren Gespräche, Dinge einmal von anderen Blickpunkten anzugehen und deine große Hilfsbereitschaft mir gegenüber. Danke.

Steffi, das letzte Einhorn, danke für die Zeit im Büro, die uns zu Freunden hat werden lassen. Wir haben gemeinsam Höhen und Tiefen durchlebt, mehr als ich uns und vor allem dir gewünscht hätte. Danke für deine grenzenlose Hilfsbereitschaft, Unterstützung und die wunderbare Zusammenarbeit. Ich glaube fest an dich und weiß, dass du mehr erreichen kannst, als du dir selbst zutraust.

Großen Dank auch an Simon, ohne deine Unterstützung hätte ich niemals den Mut gehabt, eine Schreinerlehre zu absolvieren und gleichzeitig zu promovieren. Danke, dass du die Rolle als mein Lebensmanager in allen Belangen erfüllt hast. Ich kann gar nicht in Worte fassen, wie tief ich dafür in deiner Schuld stehe. Du bist ein wundervoller Mensch, und ich bin dankbar, dass du mich schon so lange erträgst.

Danke an meine tolle Familie, eine bessere könnte ich mir nicht aussuchen. Ihr seid die, die mich immer verstehen und unterstützen. Ihr seid die, mit denen ich vor Lachen Weinen kann. Ihr seid die, vor denen ich keine Rechtfertigung brauche. Ihr seid die, mit denen 1 oder 2 Fläschchen Wein am Besten schmecken. Danke, dass ihr immer da seid!

Und natürlich möchte ich mich bei all meinen Freunden bedanken: Die Bauchs mit kleinem Clemens äääh Elias, Michelle und Tom mit der kleinen Marie Flora, Fred und Janine, Tete, Lena, Ronja, Joss und alle die ich namentlich nicht genannt habe, aber genauso wichtig sind. Danke für alle schönen Moment, Unterstützung und Liebe die ihr mir schenkt. **Ihr seid super!**

Danke auch an meine neue Werkstatt-Crew. Ich schätze euch und die Zusammenarbeit wirklich sehr und bin dankbar, dass ihr mich so liebevoll aufgenommen habt. Ich hätte nicht erwartet, dass ich mich in so kurzer Zeit so pudelwohl fühlen kann. Das ist euer Verdienst.

Curriculum vitae

The content of this page was removed as it contains personal information.